



ADAPTION OF SCHOTTEL INSTREAM TURBINES FOR RIVER-APPLICATIONS

Markus Ernst Rupp

Dissertação de Mestrado apresentada ao Programa de Pós-graduação em Engenharia Oceânica, COPPE, da Universidade Federal do Rio de Janeiro, como parte dos requisitos necessários à obtenção do título de Mestre em Engenharia Oceânica.

Orientador: Antonio Carlos Fernandes

Rio de Janeiro

Março de 2018

ADAPTION OF SCHOTTEL INSTREAM TURBINES FOR RIVER-APPLICATIONS

Markus Ernst Rupp

DISSERTAÇÃO SUBMETIDA AO CORPO DOCENTE DO INSTITUTO ALBERTO LUIZ COIMBRA DE PÓS-GRADUAÇÃO E PESQUISA DE ENGENHARIA (COPPE) DA UNIVERSIDADE FEDERAL DO RIO DE JANEIRO COMO PARTE DOS REQUISITOS NECESSÁRIOS PARA A OBTENÇÃO DO GRAU DE MESTRE EM CIÊNCIAS EM ENGENHARIA OCEÂNICA.

Examinada por:

Prof. Antonio Carlos Fernandes, Ph.D.

Prof. Geraldo Lúcio Tiago Filho, Ph.D.

Prof. Carlos Antônio Levi da Conceição, Ph.D.

Prof. Marco Aurélio dos Santos, Ph.D.

Dr. Joel Sena Sales Junior, D.Sc.

RIO DE JANEIRO, RJ - BRASIL

MARÇO DE 2018

Rupp, Markus Ernst

Adaption of Schottel Instream Turbines for River-Applications/ Markus Ernst Rupp. – Rio de Janeiro: UFRJ/COPPE, 2018.

XV, 197 p.: il.; 29,7 cm.

Orientador: Antonio Carlos Fernandes

Dissertação (mestrado) – UFRJ/ COPPE/ Programa de Engenharia Oceânica, 2018.

Referências Bibliográficas: p. 132-134.

1. River Hydrokinetic Energy. 2. Hydrokinetic Turbines. 3. River Resources. 4. Levelized Cost of Energy
I. Fernandes, Antonio Carlos. II. Universidade Federal do Rio de Janeiro, COPPE, Programa de Engenharia Oceânica. III. Título.

To my wonderful daughter Isabella.

Acknowledgements

This work was created due to the wish to apply today's common engineering concepts, in particular from the field of fluid mechanics and data analysis, to contribute to solutions with regards to real existing problems in the Ocean Renewable Energy Industry. From the beginning the intention was to carry out this thesis work in cooperation with a partner from the industry which could have been realized thanks to the opportunity given by the management team of SCHOTTEL Hydro GmbH, a leading tidal energy technology developer, headquartered in Spay am Rhein, Germany.

Therefore my first thank you is due to Mr. Niels Lange, Managing Director, and to Dr.-Ing. Ralf Starzmann, head of hydrodynamics and sales in the company for providing the opportunity to carry out this work in cooperation with a leading industry pioneer.

Special thanks are due to Dr.-Ing. Ralf Starzmann who supported me during the development of this thesis in the function as supervisor during my stay in the company.

As I was greatly welcomed and supported by Prof. Antonio Carlos Fernandes (UFRJ) from the very beginning after I displayed my intention of developing my thesis in cooperation with an industry partner, throughout various surveys of progress via skype meetings until the final evaluation of the obtained results, I would like to express my sincerest thanks to him for his consistently constructive support in every way possible related to this work.

I would also like to thank Prof. Geraldo Lúcio Tiago Filho (Unifei), as a leading expert on Small Hydropower in Brazil, for following the invitation of being a member of the examination committee. He gave numerous helpful advice in the beginning of this work which formed significant parts of the direction this work took.

Furthermore I would like to thank the Brazilian National Water Agency (ANA) for providing extensive river data, publically accessible, on their Hidroweb online platform which made large parts of this work possible in the first place.

Finally, I want to thank my marvelous family and friends because few of the results would have been possible without their support, motivation and enthusiasm.

Resumo da Dissertação apresentada à COPPE/UFRJ como parte dos requisitos necessários para a obtenção do grau de Mestre em Ciências (M.Sc.)

ADAPTAÇÃO DE UMA TURBINA SCHOTTEL PARA APLICAÇÃO EM RIOS

Markus Ernst Rupp

Março/2018

Orientador: Antonio Carlos Fernandes

Programa: Engenharia Oceânica

No presente trabalho é apresentado o estado da arte do aproveitamento da Energia Hidrocinética de Rios, assim como os desafios para o uso desta tecnologia. Foram analisados os recursos fluviais de mais de quinze rios brasileiros, para então desenvolver um método analítico de categorização do regime de fluxo destes. Diversas simulações em CFD foram realizadas para conceitualizar uma Usina de Aproveitamento Hidrocinético de 1 MW no rio Amazonas, Brasil. O estudo de caso revelou que existem lugares do rio com recursos para operacionalizar comercialmente este tipo de aproveitamento da Energia.

Abstract of Dissertation presented to COPPE/UFRJ as a partial fulfillment of the requirements for the degree of Master of Science (M.Sc.)

ADAPTION OF SCHOTTEL INSTREAM TURBINES FOR RIVER-APPLICATIONS

Markus Ernst Rupp

March/2018

Advisor: Antonio Carlos Fernandes

Department: Ocean Engeneering

In the present thesis paper today's state of the art of River Hydrokinetic Energy as a potential emerging renewable source of energy is presented as well as challenges regarding the establishment of the technology. River resources have been analyzed investigating flow data of over 15 Brazilian rivers and an analytical method which categorizes a river's flow regime been developed. Several CFD-Simulations have been carried out to conceptualize a 1-MW River Hydrokinetic Power Plant in the Amazon, Brazil. The case study revealed that there exist river sites which from a resource perspective allow a commercial operation of hydrokinetic energy extraction devices at market competitive costs.

Contents

ACKNOWLEDGEMENTS	V
LIST OF FIGURES	X
LIST OF TABLES	XV
1 INTRODUCTION	1
1.1 GENERAL	1
1.2 OBJECTIVES OF THE ON HAND THESIS	4
2 HYDROKINETIC ENERGY	6
2.1 CONCEPT	6
2.2 CHARACTERISTICS/ WORKING PRINCIPLES OF HYDROKINETIC TURBINES	11
2.2.1 Hydrodynamic Forces	12
2.2.1.1 Lift/Drag	12
2.2.1.2 Thrust	14
2.2.1.3 Torque	14
2.3 HYDROKINETIC TURBINES	15
2.3.1 Horizontal Axis Turbines	17
2.3.1.1 SCHOTTEL SIT-250	20
2.3.2 Vertical Axis Turbines	23
2.3.2.1 VAACT	24
2.4 HYDROKINETIC ENERGY IN BRAZIL	29
2.4.1 Current and Future Brazilian Electricity Supply	29
2.4.2 Current State: River Hydrokinetic Energy in Brazil	31
3 RIVER RESOURCES	35
3.1 RENEWABLE FRESHWATER RESOURCES WORLDWIDE	36
3.2 RIVER FLOW CHARACTERISTICS	40
3.2.1 Discharge Fluctuation	41
3.2.2 Flow Duration Curve	43
3.2.3 Estimation of River Flow Velocity	46
3.2.3.1 Volumetric Flow Rate Approach	46
3.2.3.2 Hydraulic Geometry Relationships	47
3.2.3.3 Manning Equation	48
3.3 BRAZILIAN RIVER RESOURCE STUDY	49
3.3.1 Initial Intention	50
3.3.2 Extended Data Acquisition	53
3.3.3 River Data Processing	55
3.3.3.1 Determining monthly averaged data points	55
3.3.3.2 Creating dimensionless Flow Duration Curves (FDCs)	58
3.3.3.3 Creating dimensionless Cross-Sectional Area Duration Curves (CDCs)	61
3.3.3.4 Creating dimensionless River Flow Speed Duration Curves (SDCs)	62
3.3.3.5 Creating Flow Speed Histograms out of SDCs	63

3.3.3.6	Comparison of River vs. Tidal Resources (part 1)	65
3.3.3.7	Comparison of River vs. Tidal Resources (part 2)	69
3.4	DIMENSIONING OF A RIVER HYDROKINETIC TURBINE	71
3.4.1	The Importance of the Speed Class for the Annual Energy Production (AEP)	72
3.4.2	Calculating mechanical AEPs for different rotor sizes	75
3.4.3	Thrust as Limiting Factor	81
4	NUMERICAL ANALYSIS OF OPERATING SIT-250 TURBINES IN RIVER FLOW	83
4.1	TIDEMODELLER	84
4.2	SIMULATION SET-UP	86
4.2.1	Simulation Domain and Numerical Grid	89
4.2.2	Boundary Conditions	91
4.3	SIMULATION OF VARIOUS FLOWS USING CFX-TIDEMODELLER	94
4.3.1	One Plat-I	94
4.3.2	Two Plat-I, Distance: 126 m (20 x D)	96
4.3.3	Two Plat-I, Distance:441 m (70 x D)	98
4.4	CFD POST-PROCESSING	99
5	CASE STUDY: 1 MW RHK POWER PLANT IN THE AMAZON	107
5.1	CONDITIONS AT SITE AND PLATFORM POSITIONING	107
5.2	ARRAY LAYOUT AND YIELD STUDY	110
5.2.1	Array Layout	111
5.2.2	Yield Study	114
5.3	LCOE CONSIDERATION	116
5.3.1	LCoE Model (DECC – UK)	117
5.3.2	LCoE Estimation of the 1 MW RHK Case Study	119
5.3.3	Comparison of LCoEs for several power generating technologies in Brazil	124
6	CONCLUSION AND OUTLOOK	128
	REFERENCES	132
	APPENDIX I – RIVER SITES, BASIC DATA	135
	APPENDIX II – RIVER SITES, DISCHARGE CLASSIFICATION	150
	APPENDIX III – FLOW SPEED DISTRIBUTION (1)	158
	APPENDIX IV – FLOW SPEED DISTRIBUTION (2)	166
	APPENDIX V – CODE: MAIN CALCULATIONS	174

List of Figures

Figure 1.1	History of Energy Consumption in the United States (1776-2015) in quadrillion Btu(British thermal units, 1 Btu \approx 1055 J) [2]	2
Figure 1.2	World Energy Consumption Increasing 56% by 2040 in comparison to 2010 projected by the EIA [2]	3
Figure 1.3	New installed electricity capacity by fuel, 2016 [3]	3
Figure 1.4	Renewable electricity capacity growth by technology and periods [3]	4
Figure 2.1	Flow through an ideal Betz Turbine [4]	8
Figure 2.2	c_P over v^3/v_1	10
Figure 2.3	Development of velocity and static pressure p along the stream tube [4]	11
Figure 2.4	Lift force L and drag force D of an airfoil with upcoming apparent velocity w [4]	12
Figure 2.5	Lift and drag coefficients versus angle of attack α_A from wind tunnel measurements for profiles NACA 4412 to 4424 [4]	13
Figure 2.6	Forces acting on blade element [5]	15
Figure 2.7	Power coefficients of wind rotors of different design [6]	16
Figure 2.8	Torque extracted by different wind turbines [4]	16
Figure 2.9	Sketch of experimental conditions	18
Figure 2.10	Buckingham table: P , v , μ being expressed by ρ , N , D	18
Figure 2.11	Typical Power and Thrust coefficients vs. tip speed ratio for a hydrokinetic turbine [8]	20
Figure 2.12	SCHOTTEL Hydro Instream Turbine – 250 [9]	21
Figure 2.13	c_P and c_T vs. tip speed ratio of the SIT-250 – 6.30 m rotor [9]	22
Figure 2.14	Performance Curves of the SIT-250 turbine with rotor diameter 6.30 m, illustrated: mechanical power at turbine shaft, absorbed thrust and torque at turbine shaft [9]	23
Figure 2.15	Schematic illustration of VAACT operating in channel, [10]	25
Figure 2.16	Vortices at backside of plate [11]	26
Figure 2.17	VAACT rotation pattern depending on I^* and current velocity (Re_y) [12]	27
Figure 2.18	Torque coefficient of VAACT without flapped tips at $\lambda = 0,65$ [12]	27
Figure 2.19	Torque coefficient of VAACT with flapped tips at $\lambda = 0,65$ [12]	28
Figure 2.20	c_P over λ of flapped plate at optimum I^* [12]	28
Figure 2.21	Brazil's Electric Energy capacity by sources, December 2014 [13]	30
Figure 2.22	Estimated Brazil's Electric Energy Capacity by source, December 2024 [13]	31
Figure 3.1	Total Renewable Freshwater Supply by Region, 2013 [16]	36
Figure 3.2	Total Renewable Freshwater Supply by country, 2013 [16]	37
Figure 3.3	Total Renewable Freshwater Supply by Country, 2013 – Top 30 [16]	37

Figure 3.4	Variation of monthly discharge over two years of Amazon River at Óbidos, Brazil. Black line: measurements, blue and red line: discharge prediction models developed by the University of Tokyo [18]	42
Figure 3.5	Variation of monthly discharge over two years of Bramaputra River at Bahadurabad, Pakistan. Black line: measurements, blue and red line: discharge prediction models developed by the University of Tokyo [18]	43
Figure 3.6	Seasonal runoff and corresponding monthly flow duration curve of the Danube at Vienna [19]	44
Figure 3.8	Flow Duration Curve constructed of daily records over 10 years of the Bouie River near Hattiesburg, State of Mississippi [21], with added lines and commentaries (red) by the author	45
Figure 3.9	Hydrographic regions in Brazil, Source: IBGE (www.ibge.gov.br)	50
Figure 3.10	Hydrograph, built out of monthly averaged flow velocity data points of site (Table 3.6), Amazon River at Itacoatiara, AM, Brazil	57
Figure 3.11	Defined Reference Flow Duration Curves	59
Figure 3.12	Dimensionless FDC of the Amazon River at São Paulo de Olivença, AM, Brazil (Discharge Class 1 site)	59
Figure 3.13	Dimensionless FDC of the Rio Negro at Manaus, AM, Brazil (Discharge Class 2 site)	60
Figure 3.14	Dimensionless FDC of the Rio Tocantins, downstream of the Tucuruí hydropower plant, PA, Brazil	60
Figure 3.15	Defined Reference Cross-sectional Area Duration Curves	62
Figure 3.16	Defined Reference River Speed Duration Curves	63
Figure 3.17	Dimensional SDC for Amazon at Itacoatiara (compare v_{min} , v_{max} with those of Table 3.6)	64
Figure 3.18	Flow speed distribution of site (step size: 0,1 m/s) created out of dimensional SDC (Figure 3.17)	65
Figure 3.19	Tidal Speed Classes established by SCHOTTEL HYDRO (step size: 0,4 m/s) representing tidal sites worldwide; each Speed Class is allocated to a different rotor diameter and ideal tip speed ratio for the point of operation	66
Figure 3.20	Tidal Speed Classes established by SCHOTTEL HYDRO (step size: 0,1 m/s) representing tidal sites worldwide; each Class is allocated to a different rotor diameter and ideal tip speed ratio for the point of operation	67
Figure 3.21	Comparison of Tidal Speed Classes with flow speed distribution of Amazon River at Itacoatiara, AM, Brazil	67
Figure 3.22	Flow speed histogram of Amazon at Itacoatiara, based on monthly averaged data points (Appendix I)	70
Figure 3.23	Flow Speed Histograms for Itacoatiara, under the assumption that the site could be also a Class 2 or 3 resource (blue and red histogram bars)	73
Figure 3.24	Flow Speed Histograms for Óbidos, under the assumption that the site could be also a Class 2 or 3 resource (blue and red histogram bars)	74

Figure 3.25	Flow Speed Histograms for Itacoatiara, under the assumption that the site could be also a Class 2 or 3 resource (blue and red graphs), as line plot (cubic splines between data points)	74
Figure 3.26	Flow Speed Histograms for Óbidos, under the assumption that the site could be also a Class 2 or 3 resource (blue and red graphs), as line plot (cubic splines between data points)	75
Figure 3.27	Flow Speed Histogram of Itacoatiara with power curves of different rotor sizes	76
Figure 3.28	Flow Speed Histogram of Óbidos with power curves of different rotor sizes	77
Figure 3.29	AEPs for Itacoatiara under consideration of all Speed Classes (1, 2 and 3) and for different rotor diameters	77
Figure 3.30	AEPs for Óbidos under consideration of all Speed Classes (1, 2 and 3) and for different rotor diameters	78
Figure 3.31	Capacity Factors for Itacoatiara under consideration of all Speed Classes (1, 2 and 3) and for different rotor diameters (4 m, 6.30 m, 8 m and 10 m)	79
Figure 3.32	Capacity Factors for Óbidos under consideration of all Speed Classes (1, 2 and 3) and for different rotor diameters (4 m, 6.30 m, 8 m and 10 m)	80
Figure 3.33	Flow Speed Histogram of Itacoatiara with thrust curves of different rotor diameters	81
Figure 3.34	Flow Speed Histogram of Óbidos with thrust curves of different rotor diameters	82
Figure 3.35	Maximum occurring thrust over rotor diameter for three selected sites	82
Figure 4.1	Schematic illustration of the calculation process using an actuator disk model	83
Figure 4.2	Plat-I Platform in operating modus mounting four SCHOTTEL Instream Turbines	87
Figure 4.3	Plat-I Platform in operating modus, front view	87
Figure 4.4	Plat-I Platform in operating modus, side view	88
Figure 4.5	Plat-I Platform in operating modus, top view	88
Figure 4.6	Modelled tank	89
Figure 4.7	Top view simulation domain (X-Y-Plane)	90
Figure 4.8	Top view (X-Y-Plane), zoomed-in, to illustrate the transition from the coarse mesh to the refined mesh	90
Figure 4.9	Side view on simulation domain (X-Z-Plane), zoomed in	91
Figure 4.10	Mesh refinement around turbine for one (left), two (middle), and five (right) refinement steps	91
Figure 4.11	Definition of tank walls in Tidemodeller	92
Figure 4.12	Graphical illustration of Plug flow, Seventh Power Law flow and Log Law flow over depth	93

Figure 4.13	1 Plat-I, cut through turbine center X-Y-plane, top view, length of tank: 700 m	94
Figure 4.14	1 Plat-I, cut through center of turbine 3, side view, length of tank: 700 m	94
Figure 4.15	1 Plat-I, cut through turbine center X-Y-plane, top view, zoomed, length of tank: 700 m	95
Figure 4.16	1 Plat-I, cut through center of turbine 3, side view, zoomed, length of tank: 700 m	95
Figure 4.17	2 Plat-I, distance: 20 D, cut through turbine center X-Y-plane, top view, length of tank: 850 m	96
Figure 4.18	2 Plat-I, distance: 20 D, cut through center of turbine 3, side view, length of tank: 850 m	96
Figure 4.19	2 Plat-I, distance: 20 D, cut through turbine center X-Y-plane, top view, zoomed, length of tank: 850 m	97
Figure 4.20	2 Plat-I, distance: 20 D, cut through center of turbine 3, side view, zoomed, length of tank: 850 m	97
Figure 4.21	2 Plat-I, distance: 70 D, cut through turbine center X-Y-plane, top view, length of tank: 1400 m	98
Figure 4.22	2 Plat-I, distance: 70 D, cut through center of turbine 3, side view, length of tank: 1400 m	98
Figure 4.23	2 Plat-I, distance: 70 D, cut through turbine center X-Y-plane, top view, zoomed, length of tank: 1400 m	99
Figure 4.25	Velocity measurement lines throughout tank, height: turbine center, Y and Z- coordinate fix	100
Figure 4.26	Flow velocity throughout tank on hub height of all turbines	101
Figure 4.27	Previous figure transformed in non-dimensional illustration: udeficit over x/D	101
Figure 4.28	udeficit on hub height, 2 platforms, distance: 10 D	102
Figure 4.29	udeficit on hub height, 2 platforms, distance: 20 D	102
Figure 4.30	udeficit on hub height, 2 platforms, distance: 30 D	103
Figure 4.31	udeficit on hub height, 2 platforms, distance: 40 D	103
Figure 4.32	udeficit on hub height, 2 platforms, distance: 50 D	104
Figure 4.33	udeficit on hub height, 2 platforms, distance: 60 D	104
Figure 4.34	udeficit on hub height, 2 platforms, distance: 70 D	105
Figure 5.1	Flow Speed Distribution of Amazon at Óbidos and Power Curves (mechanical and electric) of 6.30 m rotor	108
Figure 5.2	ADCP measurement of Amazon river at Óbidos [14], compare flow speeds with that of Figure 5.1	109
Figure 5.3	Satellite view on site with cross section of ADCP measurement (yellow line), viewing height: 16.97 km	109
Figure 5.4	Satellite view on site with cross section of ADCP measurement (yellow line), viewing height: 5.15 km	110

Figure 5.5	5 Plat-I, distance: 2 x 25 D, cut through turbine center X-Y-plane, top view, length of tank: 1500 m	111
Figure 5.6	5 Plat-I, distance: 2 x 25 D, cut through turbine center X-Y-plane, top view, zoomed, length of tank: 1500 m	111
Figure 5.7	5 Plat-I, distance: 2 x 25 D, cut through center of turbine 3, side view, zoomed, length of tank: 1500 m	112
Figure 5.8	5 Plat-I, distance: 2 x 25 D, cut through Y-Z-planes 10 m behind turbines, side view, length of tank: 1500 m	112
Figure 5.9	Óbidos site with 1 MW Plat-I Array placement, true-to-scale representation	113
Figure 5.10	Medium AEPs for several rotor diameters	115
Figure 5.11	Sensitivity of LCoE to changes in CapEx (OpEx const.), note: y-axis logarithmic	122
Figure 5.12	Sensitivity of LCoE to Changes in CapEx within pursued operation range	123
Figure 5.13	Sensitivity of LCoE to changes in OpEx (CapEx const.), note: y-axis logarithmic	123
Figure 5.14	Sensitivity of LCoE to Changes in OpEx within pursued operation range	124
Figure 5.15	Estimated Brazil's Electric Power Generation Capacity by source for 2024 [13]	125
Figure 5.16	LCoE of different generating facilities and technologies including also social, environmental and transmission system costs under the assumption of a discount rate of 10 % [26]	125
Figure 5.17	Solar versus Peaking Capacity (Global Markets) [27]	126
Figure 5.18	LCoE comparison of different alternative and conventional power generating technologies operating in the US with sensitivity to fuel prices: dark areas correspond to $\pm 25\%$ fuel price fluctuation [27]	127

List of Tables

Table 2.1	Recent events regarding the Development of River Hydrokinetic Energy Technology in Brazil, part 1	33
Table 2.2	Continuation of Table 2.1	34
Table 3.1	Original data set of measurement records of the Amazon River at Itacoatiara, Brazil, provided by the ANA	40
Table 3.2	List of hydropower plants investigated for downstream data (part 1)	52
Table 3.3	List of hydropower plants investigated for downstream data (part 2)	53
Table 3.4	List of investigated free-streaming river sites	54
Table 3.5	Re-sorted and monthly averaged measurement data sheet, Itacoatiara, Amazon River, Brazil	56
Table 3.6	Monthly averaged recordings for discharge („Vazao“), cross sectional area (“AreaMolhada”), width at free surface (“Largura”), average flow speed (“VelMedia”), and depth (“Profundidade”)	57
Table 3.7	Mathematical formulation of the Reference Discharge Classes	58
Table 3.8	Mathematical formulations of the Reference Cross-sectional Area Classes	62
Table 3.9	Annual average flow speed of the 15 investigated river sites determined with two different methods	71
Table 3.10	AEP Calculations for all 15 sites considering different rotor diameters	78
Table 3.11	CF Calculations for all 15 sites considering different rotor diameters	80
Table 4.1	Input parameters for simulations (some vary, some are fix), varying are those which figures include ranges	93
Table 5.1	Mechanical power extracted by each Plat-I platform (rig), calculated by ANSYS CFX POST	113
Table 5.2	Summary of AEP cases with percentage change to base case	116
Table 5.3	Input data for Project Configuration	119
Table 5.4	Input data for single cost positions	120
Table 5.5	Input data to determine the WACC	120
Table 5.6	Calculation of year by year discounted characteristics	120
Table 5.7	Summed up discounted characteristic	121
Table 5.8	Extention of Table 13 with LCoE column	121

1 INTRODUCTION

1.1 GENERAL

The demand for cheap and sustainable renewable energy is increasing on a worldwide basis as current and previous conventional resources for power generation – still based over 80% on the combustion of fossil fuels [1], [2] such as oil, coal and natural gas – on the one hand, due to high demand and production, are depleting faster than they recover and on the other hand are amplifying one of the significant problems today's and future humanity is facing: global warming. The latter observation, meaning the contribution to climate change through the combustion of fossil fuels over the last approximately 150 years, by now, is practically undoubted among researchers, politicians and citizens around the world.

Although the benefits of energy production from renewable sources are obviously versatile to practically everybody involved in the energy cycle (producers, consumers, environment), the transformation of the current energy mix into a more sustainable is more likely to be at the beginning than at the end. This has mainly to do with the significant decrease in costs at which energy produced from renewable sources, today, is coming to the market in comparison to that a few years ago. This breakthrough in cost efficiency over recent years is responsible for more and more renewable production facilities coming online around the world without subsidies.

The in nowadays for power generation in use renewable sources are mainly: wind, solar, hydroelectric power plants, bio thermal and bio gas plants, and geothermal power plants. Energy generated from hydrokinetic resources, such as ocean tides/currents/waves or river currents, is yet small and overall still in testing phases. Given the fact that roughly 70% of the earth's surface is covered by water, it seems reasonable to analyze the potential as well as available technologies for future energy production coming from oceans and rivers in order to contribute to the process of transforming today's energy mix into a more renewable based one in the future.

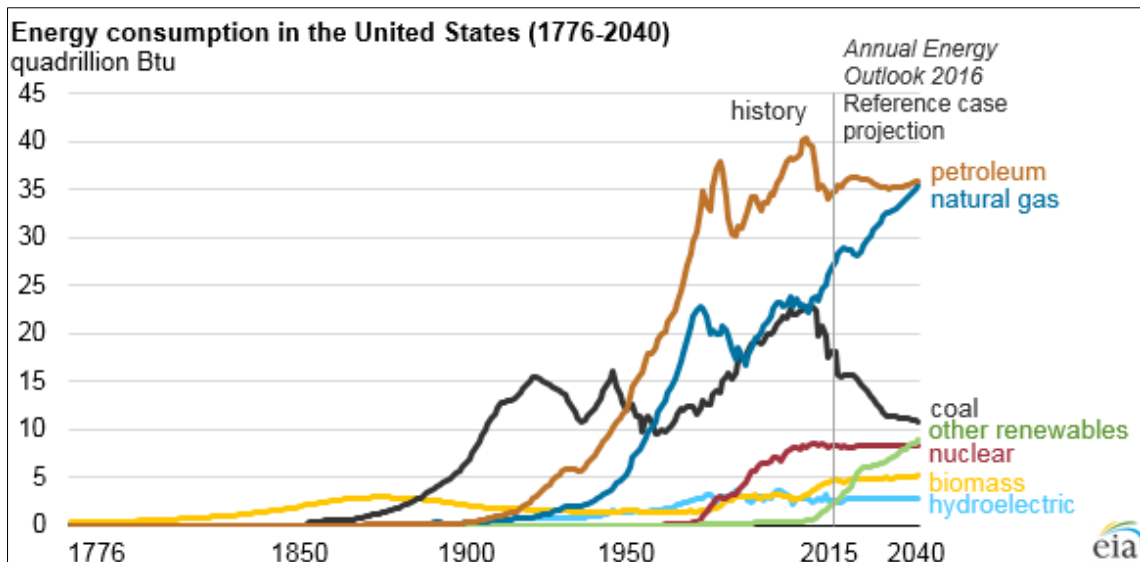


Figure 1.1 History of Energy Consumption in the United States (1776-2015) in quadrillion Btu (British thermal units, 1 Btu \approx 1055 J) [2]

As the EIA states in its report from 2013 with regards to the worldwide energy consumption, the appetite for energy on a global basis is expected to increase by 56 % by the year 2040 taking 2010 as the year of reference. The largest share of that increase is expected to come from non-OECD countries as Figure 1.2 illustrates. Even though the EIA projects rising consumption of practically all energy resources, a 30-years outlook is a far prediction and prone to errors. However, there is reason to assume that renewables play a significantly stronger role in the world's energy mix 30 years from now than currently projected. This is not only due to serious changes in political agendas (e.g. recent Chinese, Indian environmental/air protection policies) and the awareness of the global public of the issue but also due to major technological and cost breakthroughs in the entire renewable energy industry.

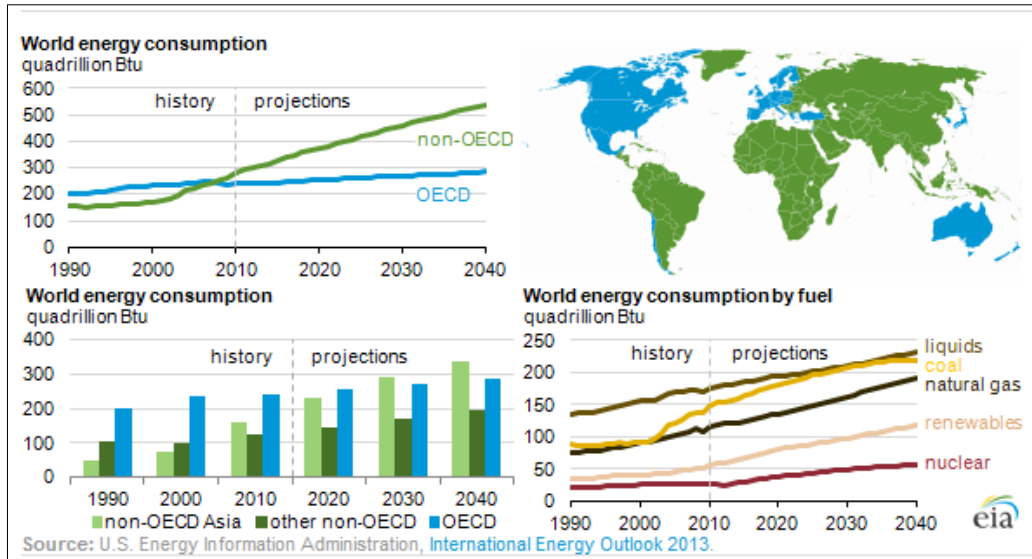


Figure 1.2 World Energy Consumption Increasing 56% by 2040 in comparison to 2010 projected by the EIA [2]

The International Energy Agency (IEA) for instance reports that in 2016 alone 165 GW new installed global power capacity came from renewable sources which account for two-thirds of the total new installed capacity in that year [3].

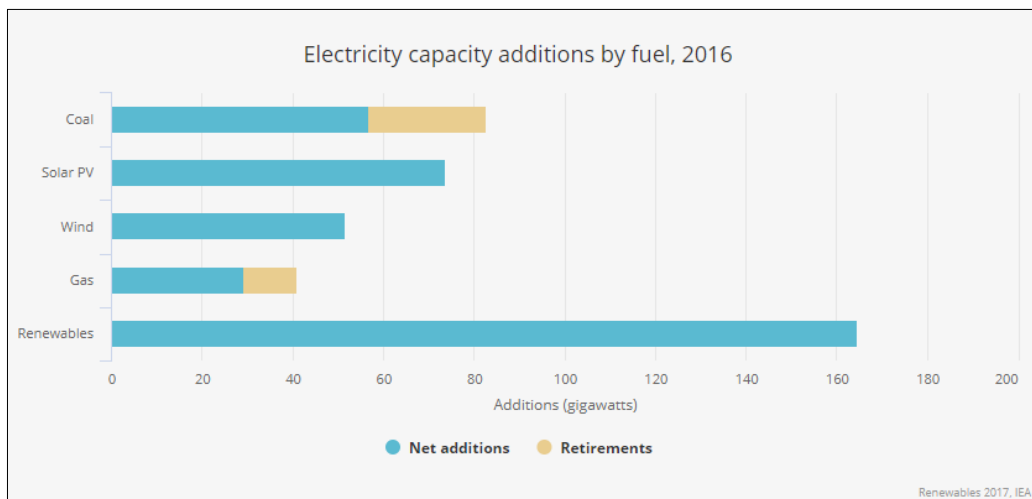


Figure 1.3 New installed electricity capacity by fuel, 2016 [3]

According to the IEA not only the future installed capacity will grow strongly but the growth rates itself will increase over the years, see Figure 1.4

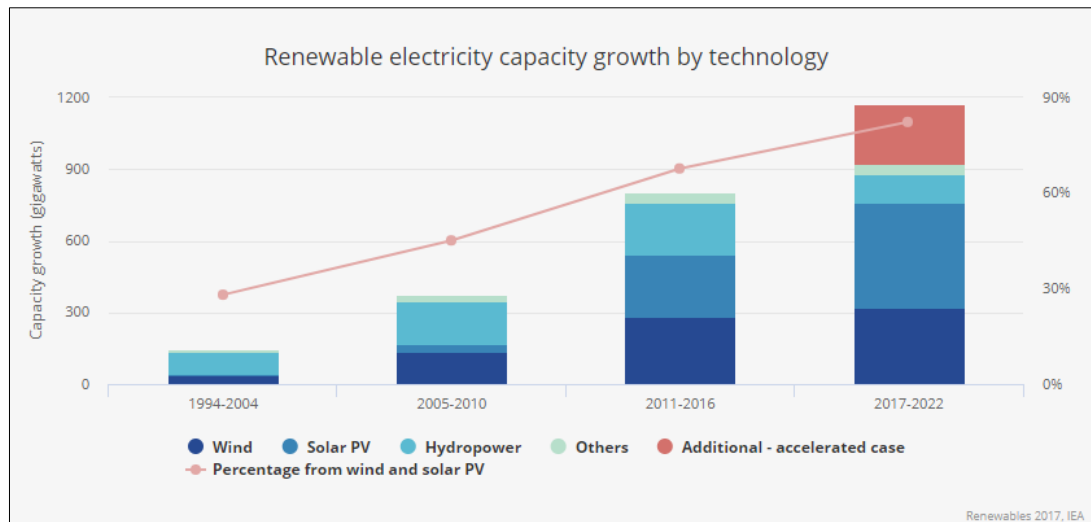


Figure 1.4 Renewable electricity capacity growth by technology and periods [3]

On the basis of these data renewable energy technologies will play a more important role for future global electric power generation than ever before. This justifies the interest in the development of additional renewable energy technologies such as hydrokinetic energy generation form waves, tides, and ocean or river currents.

1.2 OBJECTIVES OF THE ON HAND THESIS

This work aims to fully and accurately describe:

- (1) today's state of the art of hydrokinetic river energy extraction devices,
- (2) a methodology to characterize river resources with regards to their potential for hydrokinetic power generation,
- (3) the application of nowadays available technology to a real existing, feasible river site, determining:
 - (a) extracted power and annual energy production,
 - (b) achieved efficiencies,
 - (c) evaluate the economic viability of a real set-up power plant project.

This thesis is structured chronologically starting with an introduction to the technology and its underlying physical principles, continuing with a comprehensive analysis on river resources, and finally combining the technology with the resource by conceptualizing a 1-MW hydrokinetic power plant operating at a river section of the Amazon in the State of Para, Brazil.

Questions answered in this work will be:

- (1) Are rivers principally capable to power hydrokinetic energy extraction devices?
- (2) Which characteristics define a river resource to be suitable for hydrokinetic power generation?
- (3) In case of existing feasible resources what are requirements to the extraction devices for an efficient operation?
- (4) How economically viable could a potential river hydrokinetic power plant be operating? Can the technology be cost competitive to peer groups (e.g. wind or solar)?

2 HYDROKINETIC ENERGY

The object of this chapter is to discuss what hydrokinetic energy is, where it occurs and what physical principles are determining its nature.

2.1 CONCEPT

Hydrokinetic Energy is the energy coming from moving water. Different from hydrostatic energy which potential roots in its pressure head, a hydrostatic pressure difference derived from a difference in altitude of two reservoirs, hydrokinetic energy is just of kinetic characteristic and therefore has no pressure head. Regarding this fact, some literature is referring to hydrokinetic energy extraction devices as “zero-head” turbines.

Hydrokinetic energy sources can be:

- (1) ocean tides and currents
- (2) waves
- (3) river currents and man-made channels.

In particular Hydrokinetic River Energy is demonstrating competitive strengths in comparison with all electric power generation technologies in its applicability for clean and reliable energy generation. It has no GHG emission and can reach high capacity factors of 65-90% which makes it a possible provider for base-load power.

The power which is carried by any current is defined as mass flow times kinetic energy, eq. (2.1), it applies for a tidal, ocean and river current as well as for a wind current.

$$P_{current} = \frac{1}{2} \dot{m} v_1^2 = \frac{1}{2} \rho A v_1^3 \quad (2.1)$$

where:

$P_{current}$	<i>Power of current in Watts</i>	[kg m ² /s ³]
\dot{m}	<i>mass flow</i>	[kg/s]

v_1	<i>incident (undisturbed) current velocity</i>	[m/s]
ρ	<i>density of fluid</i>	[kg/m ³]
A	<i>area perpendicular to current velocity</i>	[m ²]

Equation (2.1) represents the intrinsic power of a current but not the possible extractable power by a turbine or any other power extracting device. For a turbine theoretically extracting 100% of the power stated in eq. (2.1) the velocity of the incident flow (v_1) had to drop to zero after passing the rotor of the turbine which subsequently would affect the incident flow by causing blockage. In practice one cannot reduce the current speed to zero, so a power coefficient c_p is defined as the ratio between the actual power obtained and the maximum available power as defined by eq. (2.1).

$$c_p = \frac{P_{turbine}}{P_{current}} = \frac{M \cdot \omega}{\frac{1}{2} \rho A v_1^3} \quad (2.2)$$

where:

M	<i>mechanical torque at turbine shaft</i>	[Nm]
ω	<i>angular velocity of rotor</i>	[rad/s]

This ratio, eq. (2.2), equals the usually as efficiency η used term for turbo machines. However, for wind turbines and hydrokinetic turbines the term “ c_p ” has been established.

All kinetic energy extracting devices which are generating power by taking out momentum of a stationary or non-steady flow have a theoretical limit of the power they can possible extract from the kinetic energy carrying current. It is called the “Betz-Limit”, named after the physicist Albert Betz who postulated it during his research on wind mills in 1919.

Betz stated that the flow is reduced in velocity the closer it gets to the rotor and thus through the conservation of mass, eq. (2.3), the area of the flow widens which causes some of the incident flow not to pass the turbine but flowing “around” of it and not offering its kinetic energy to be extracted by the turbine.

$$\dot{m}_{in} = \dot{m}_{out} \quad (2.3)$$

$$\rho A_1 v_1 = \rho A v_2 = \rho A_3 v_3 \quad (2.3a)$$

Figure 2.1 is showing the concept of the flow reducing its velocity and as a consequence widening in area.

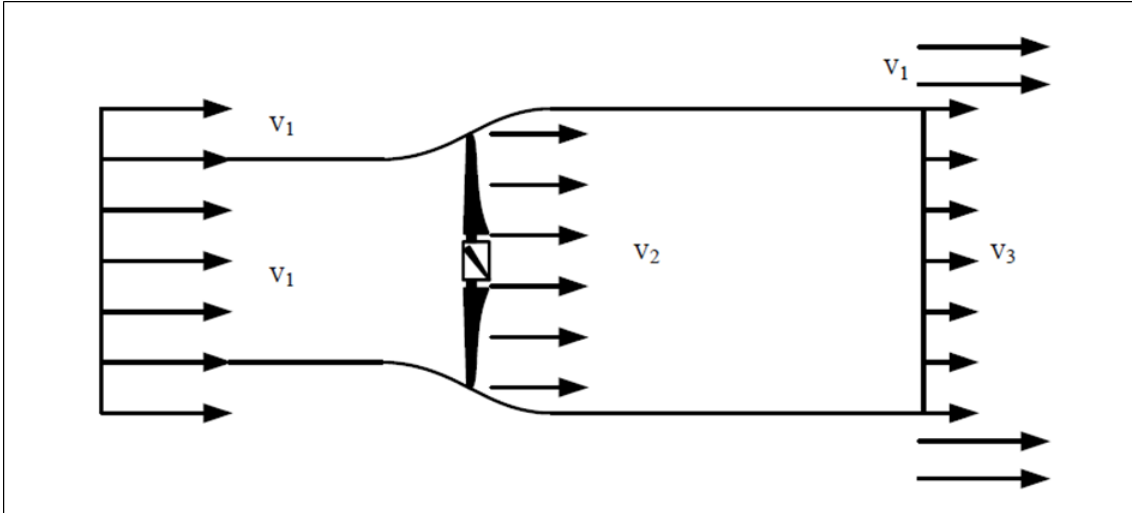


Figure 2.1 Flow through an ideal Betz Turbine [4]

The extracted energy by the turbine is defined as upstream energy minus downstream energy:

$$E_{ex} = \frac{1}{2} \dot{m} (v_1^2 - v_3^2) \quad (2.4)$$

The extracted power by the turbine then is:

$$P_{ex} = \dot{E}_{ex} = \frac{1}{2} \dot{m} (v_1^2 - v_3^2) = \frac{1}{2} \rho A v_2 (v_1^2 - v_3^2) \quad (2.5)$$

In order the turbine can achieve maximum power extraction the optimum speed ratio between v_1 and v_3 has to be determined. This can be achieved if v_2 is known. It is assumed:

$$v_2 = \frac{v_1 + v_3}{2} \quad (2.6)$$

This assumption is correct, as proved by the Froude-Rankine Theorem. Now, the mass flow equation (2.3) and the velocity direct at the rotor (2.6) will be inserted in the power extraction function, eq. (2.5):

$$\begin{aligned} P_{ex} &= \frac{1}{2} \rho A v_2 (v_1^2 - v_3^2) = \frac{1}{2} \rho A \frac{v_1 + v_3}{2} (v_1^2 - v_3^2) \\ &= \frac{1}{2} \rho A v_1^3 \left[\frac{1}{2} \left(1 + \frac{v_3}{v_1} \right) \left(1 - \left(\frac{v_3}{v_1} \right)^2 \right) \right] \end{aligned} \quad (2.7)$$

Power in flow power coefficient c_P

As shown in eq. (2.7) c_P can be also written as:

$$c_P = \frac{1}{2} \left(1 + \frac{v_3}{v_1} \right) \left(1 - \left(\frac{v_3}{v_1} \right)^2 \right) \quad (2.8)$$

Calculating the maximum value for c_P in the range from 0 to 1 reveals to:

$$c_{P,max} = \frac{16}{27} = 0.593 \quad \text{at} \quad \frac{v_3}{v_1} = \frac{1}{3}. \quad \text{This maximum } c_P\text{-value is called the Betz-Limit.}$$

Figure 2.2 is illustrating the result.

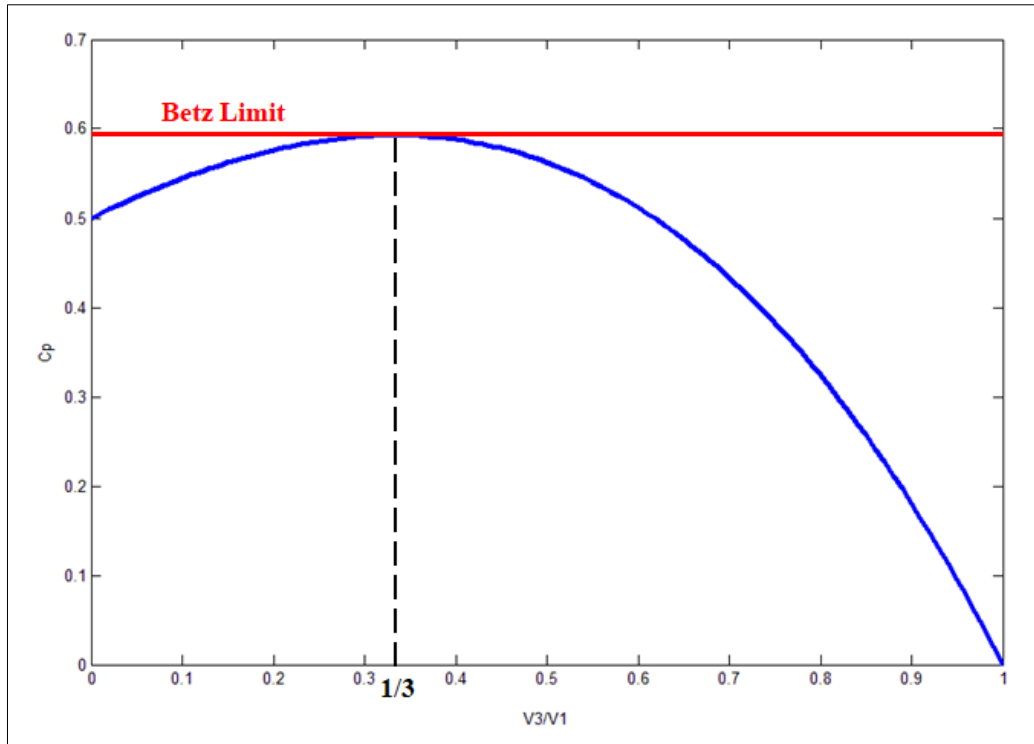


Figure 2.2 c_p over v_3/v_1

So for maximum power extraction it has to be: $v_3 = \frac{1}{3}v_1$ and $v_2 = \frac{2}{3}v_1$.

Tip Speed Ratio:

An important dimensionless turbine property is the so called tip speed ratio λ . It is defined as the ratio between the tangential speed at the tip of the blade and the upcoming current speed v_1 . The tip speed ratio is related to efficiency, with its optimum varying with blade design. In most performance charts it represents the x-axis (c_p over λ , c_Q over λ , c_T over λ).

$$\lambda = \frac{\omega R}{v_1} \quad (2.9)$$

where:

ω	<i>angular velocity of rotor</i>	[rad/s]
R	<i>radius of rotor (D/2)</i>	[m]

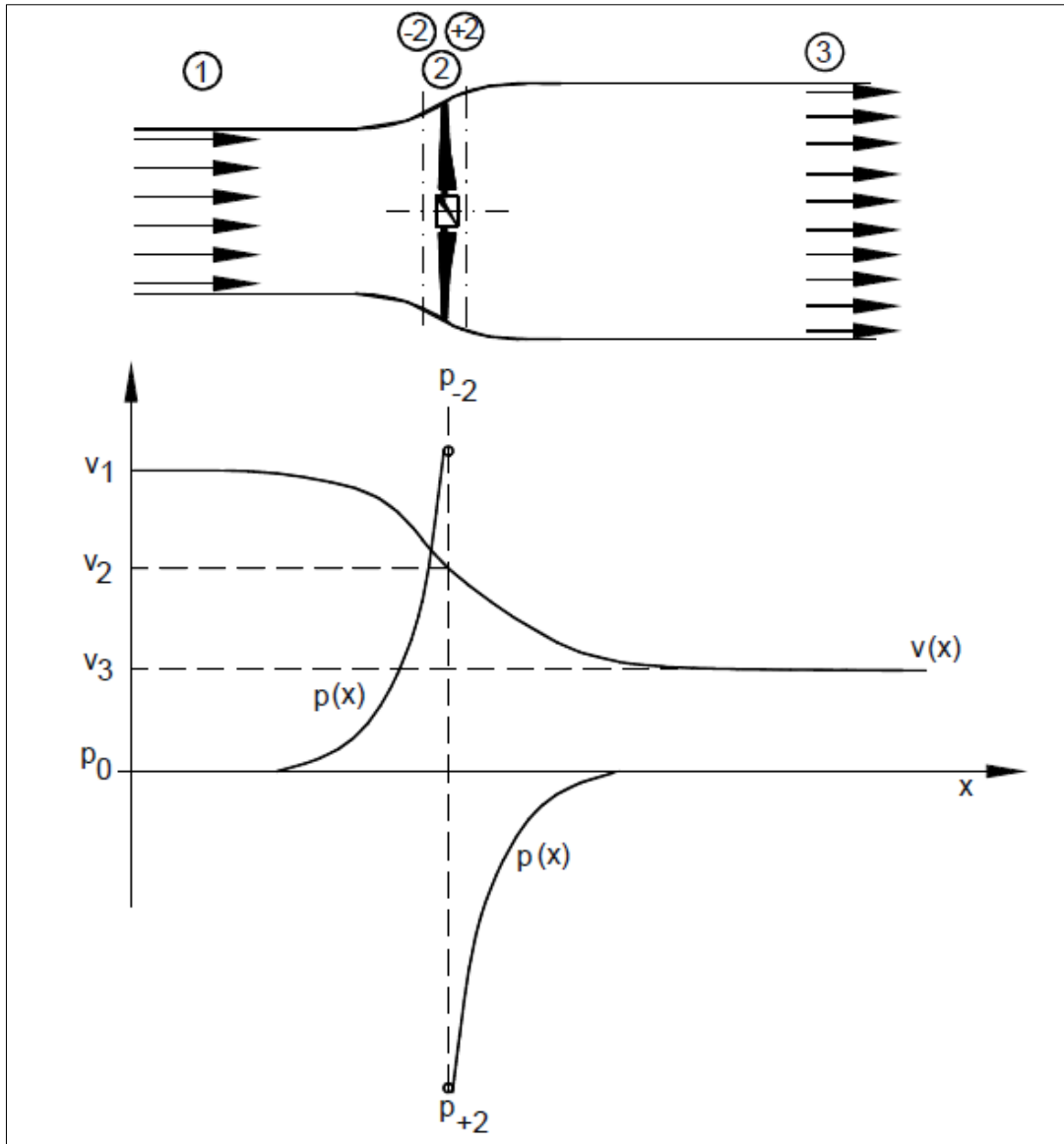


Figure 2.3 Development of velocity and static pressure p along the stream tube [4]

2.2 CHARACTERISTICS/ WORKING PRINCIPLES OF HYDROKINETIC TURBINES

The cause of any massed body changing its velocity is the result of acting forces on it. This law is also valid for any turbine part which is moving, meant is the rotor. It is moving due to resulting forces acting on the rotor blades. Those forces will be analyzed quickly.

2.2.1 Hydrodynamic Forces

2.2.1.1 Lift/Drag

Lift:

Lift is the force perpendicular to the apparent velocity (\vec{w}) which an airfoil or hydrofoil is experiencing when fluid passes around it. It is a function of the angle of attack (α_A).

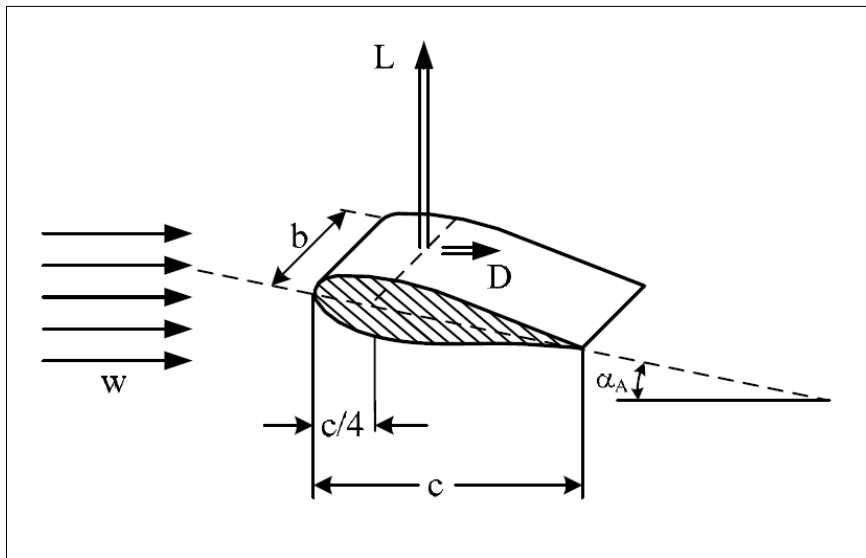


Figure 2.4 Lift force L and drag force D of an airfoil with upcoming apparent velocity w [4]

The dimensionless coefficient for lift, the lift coefficient (c_L), is a function of the angle of attack and the geometric shape of the blade. For small angles of attack ($0 < \alpha_A < 10^\circ$) c_L and α_A are proportional to each other.

$$c_L(\alpha_A) = \frac{L}{\frac{1}{2} \rho A w^2} \quad (2.10)$$

where:

L	lift force	[kg m/s ²]
ρ	density of fluid	[kg/m ³]
A	foil area: $c \cdot b$	[m ²]
\vec{w}	apparent velocity: wind speed (\vec{v}) – tip speed (\vec{u})	[m/s]
α_A	angle of attack	[-]

Drag:

Drag is the force in the same direction of the apparent velocity (\vec{w}) which an airfoil or hydrofoil is experiencing when fluid passes around it. It is also a function of the angle of attack (α_A).

$$c_D(\alpha_A) = \frac{D}{\frac{1}{2}\rho A w^2} \quad (2.11)$$

where:

D	<i>drag force</i>	[kg m/s ²]
ρ	<i>density of fluid</i>	[kg/m ³]
A	<i>foil area: $c \cdot b$</i>	[m ²]
\vec{w}	<i>apparent velocity: wind speed (\vec{v}) – tip speed (\vec{u})</i>	[m/s]
α_A	<i>angle of attack</i>	[1]

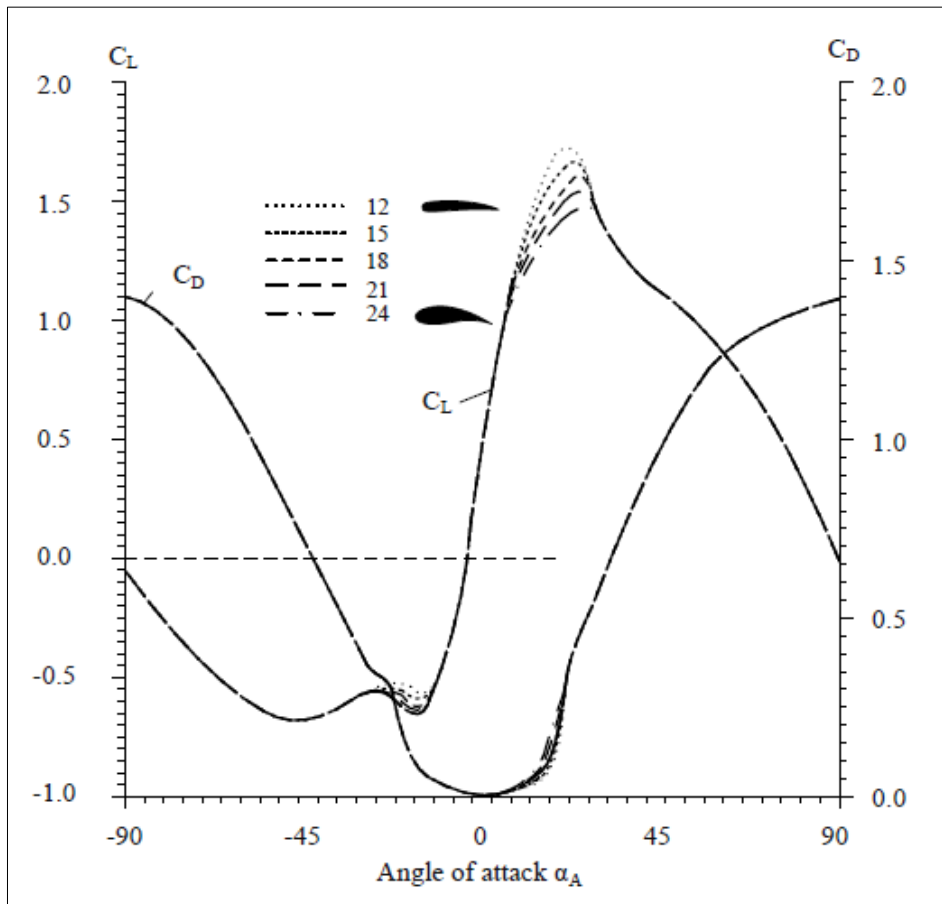


Figure 2.5 Lift and drag coefficients versus angle of attack α_A from wind tunnel measurements for profiles NACA 4412 to 4424 [4]

2.2.1.2 Thrust

Thrust is the force which is for example generated in jet engines to move an aircraft. Regarding jet engines as high as possible thrust forces are desirable as it is the parameter which characterizes the power of such an engine. Whereas it is wished in thrust engines it is undesired in hydrokinetic or wind turbines because it is the force which is bending the blades and subsequently demands the blades to resist structural stresses. Its direction is the same as the incident flow velocity v_1 . Like in a jet engine it is described as the difference of the velocities of the surpassing fluid mass flow.

$$T = \dot{m}(v_1 - v_3) = \rho A v_2 (v_1 - v_3) \quad (2.12)$$

$$T = \rho A v_2 (v_1 - v_3) \quad (2.12a)$$

It can also be described using the pressure drop of the static pressure directly before and after the rotor. Using the terms of Figure 2.3, we have:

$$T = \dot{m}(p_{-2} - p_{+2}) \quad (2.13)$$

Its dimensionless coefficient, the thrust coefficient (c_T), is described by:

$$c_T = \frac{T}{\frac{1}{2} \rho A (v_1)^2} \quad (2.14)$$

2.2.1.3 Torque

$$M = \frac{P}{\omega} \quad (2.15)$$

$$c_M = \frac{M}{\frac{1}{2} \rho A (v_1)^2 R} \quad (2.16)$$

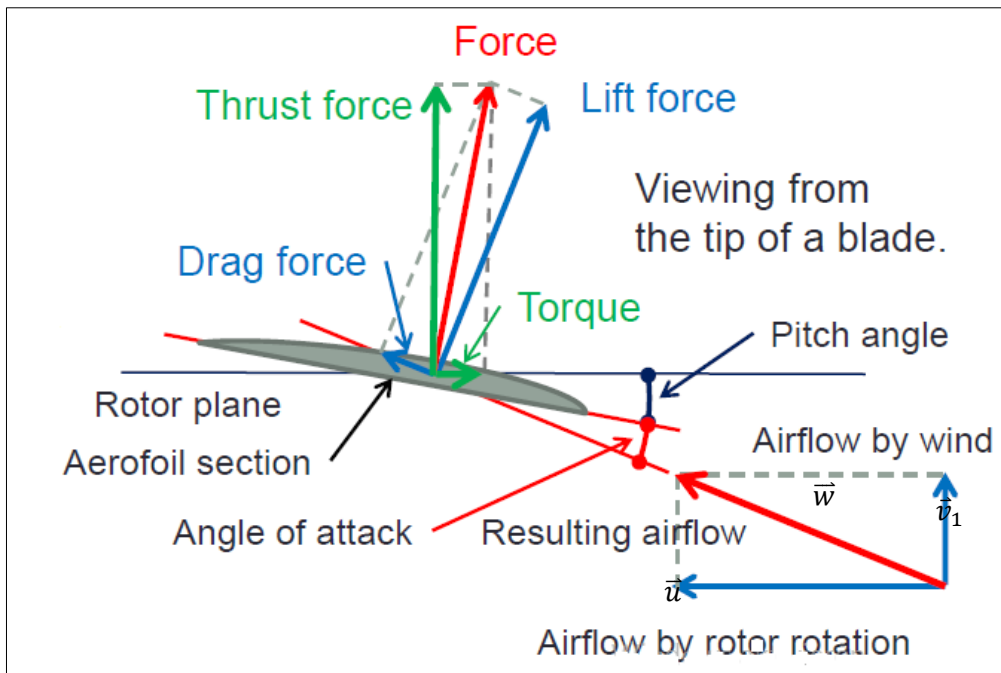


Figure 2.6 Forces acting on blade element [5]

2.3 HYDROKINETIC TURBINES

Hydrokinetic turbines are energy converting devices which extract kinetic energy of the fluid flow they are placed into and convert it into mechanical and subsequent electric energy. The physics of hydrokinetic power extraction and its limits are described in chapter 2.1 and 2.2.

There are three main types of turbine designs which differ from each other through their main axis position to the flow. These are:

- (1) horizontal axis turbines (straight axis, inclined axis)
- (2) vertical axis turbines (Darrieus, Savonius, Gorlov, VAACT)
- (3) cross-flow turbines

The hydrodynamic principle which is driving those devices is whether lift or drag or a combination of the two (e.g. VAACT). Figure 2.7 illustrates the c_p over λ performance curves of different wind rotors. The three-blade horizontal axis design shows highest efficiency (c_p) which is one among other reasons why it is today's most common wind

turbine design. Even though the c_p of vertical axis and multiblade horizontal axis turbines are lower than those of two and three-blade horizontal axis turbines, they show a significant higher torque coefficient c_Q (Figure 2.8). The curves are also applicable for hydrokinetic turbines.

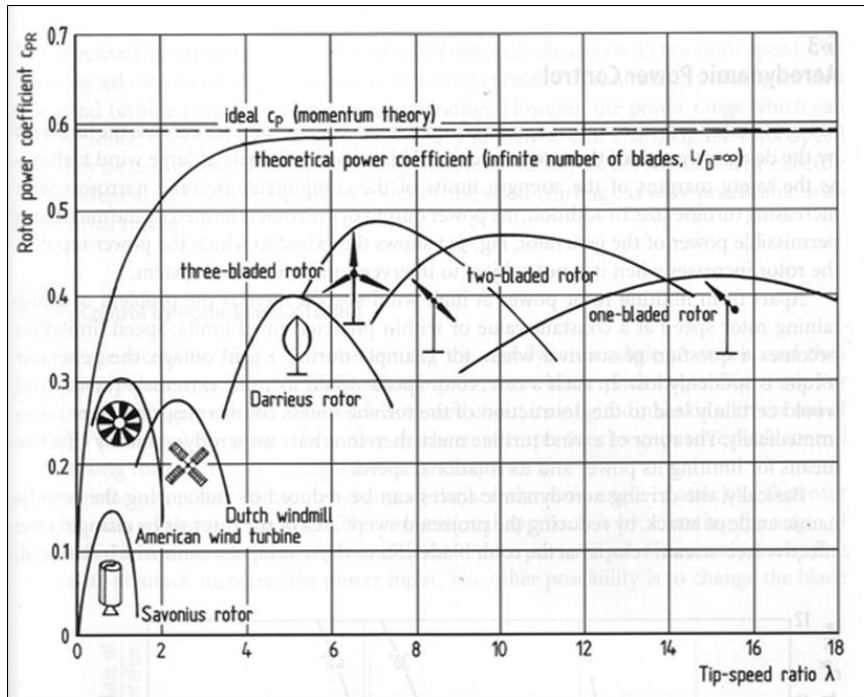


Figure 2.7 Power coefficients of wind rotors of different design [6]

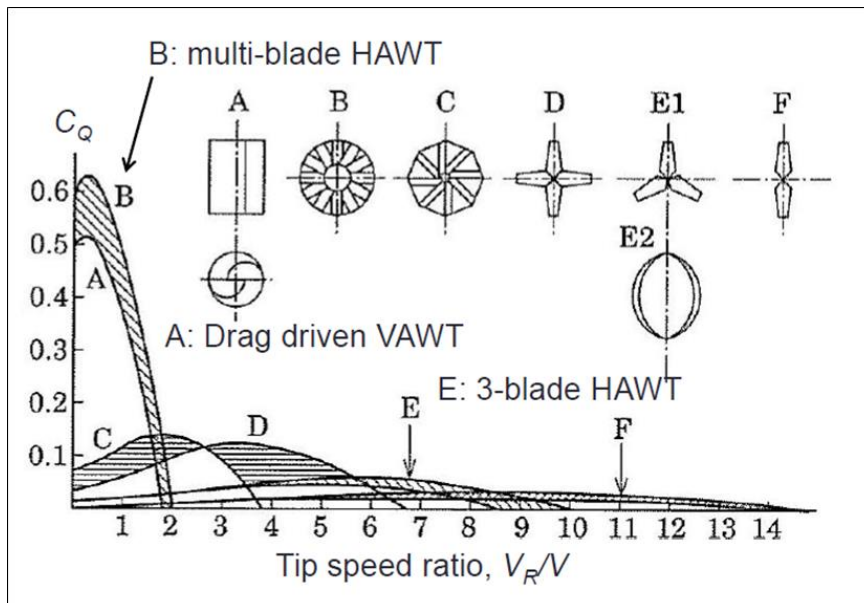


Figure 2.8 Torque extracted by different wind turbines [4]

2.3.1 Horizontal Axis Turbines

Horizontal axis turbines make up the majority of all built hydrokinetic turbine designs. This is mainly due to their efficiency which is generally higher than that achieved by vertical axis or cross-flow turbines. A main focus designing a horizontal axis turbine is laid on the blade design which is responsible for the lift (and drag) generated by the rotor operating in moving fluid. However, in the context of this work blade design cannot be discussed in more detail as it would go beyond the scope of this work. It is mentioned that blade design is an entire scientific branch within the field of turbo machinery and there are a variety of scientific works carried out on the topic.

Dimensional Analysis for a horizontal axis turbine:

Dimensional analysis is a method for reducing the number and complexity of experimental variables which affect a given physical phenomenon by using a sort of compacting technique. If a phenomenon depends upon n dimensional variables, dimensional analysis will reduce the problem to only k *dimensionless* variables, where the reduction $n - k = 1, 2, 3,$ or 4 , depending upon the problem complexity. Generally $n - k$ equals the number of different dimensions (sometimes called basic or primary or fundamental dimensions) which govern the problem. In fluid mechanics the four basic dimensions are usually taken to be mass M , length L , time T , and temperature Θ , or an $MLT\Theta$ system for short [7].

A dimensional analysis will be performed for a horizontal axis turbine placed in an incident flow with velocity v .

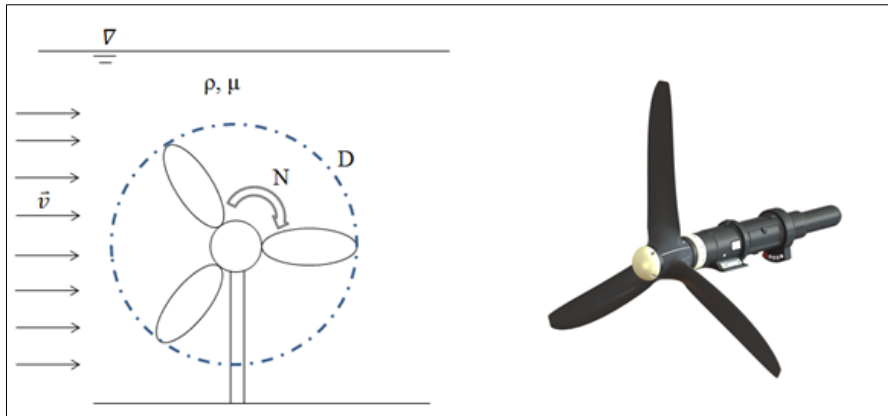


Figure 2.9 Sketch of experimental conditions

- Characteristic of interest: Power $P = f(\rho, N, D, v, \mu)$

where:

P	<i>power</i>	$[W] = [kg\ m^2/s^3]$
ρ	<i>fluid density</i>	$[kg/m^3]$
N	<i>angular velocity</i>	$[1/s]$
D	<i>rotor diameter</i>	$[m]$
v	<i>incident current velocity</i>	$[m/s]$
μ	<i>dynamic viscosity</i>	$[kg/(m \cdot s)]$

- applying the Buckingham Π -Theorem:

$P = f(\rho, N, D, v, \mu)$

		P	ρ	N	D	v	μ
ρ	M	1	1	0	0	0	1
D	L	2	-3	0	1	1	-1
N	T	-3	0	-1	0	-1	-1

$n' - k'' = 6 - 3 = 3 \quad \rightarrow \quad \underline{\underline{3\ \Pi's}}$

$\Pi_1 = \frac{P}{\rho N^3 D^5} \quad \Pi_2 = \frac{v}{ND} \quad \Pi_3 = \frac{\mu}{\rho ND^2}$

Figure 2.10 Buckingham table: P, v, μ being expressed by ρ, N, D

The initially determined Π s (illustrated in Figure 2.10) will now be arranged slightly different, all in accordance with the Buckingham Theorem, to demonstrate the dimensionless performance parameters behind them and display how they are connected to each other.

The single calculus operations are the following:

- (1) $\Pi'_2 := \frac{1}{2 \Pi_2} \rightarrow \frac{ND}{2v} = \frac{NR}{v} =: \lambda$ *tip speed ratio*
- (2) $\Pi'_3 := \frac{1}{\Pi_3} \rightarrow \frac{\rho ND^2}{\mu} =: Rey$ *Reynolds number*
- (3) hypothesis: $c_P = f(\lambda, Rey)$ *c_P is function of λ and Rey*
- (4) $c_P \sim \frac{\Pi_1}{(\Pi_2)^3} \rightarrow \frac{\frac{P}{\rho N^3 D^5}}{\left(\frac{v}{ND}\right)^3} = \frac{P}{\rho D^2 v^3} =: \Pi_4$ *$c_P \sim \Pi_4$*
- (5) $c_P := \frac{8}{\pi} \Pi_4 \rightarrow \frac{P}{\frac{1}{2} \rho \frac{\pi}{4} D^2 v^3} = \frac{P}{\frac{1}{2} \rho A v^3} =: c_P$ *proof of hypothesis from (3)*
- (6) $c_M := \frac{c_P}{\lambda} \rightarrow \frac{P}{\frac{1}{2} \rho A v^3} \cdot \frac{v}{\omega R} = \frac{M}{\frac{1}{2} \rho A v^2 R} =: c_M$ *torque coefficient*

The dimensional analysis revealed that the power coefficient (c_p) only is depending on the tip speed ratio and the Reynolds Number.

Performance Curves of a horizontal axis turbine:

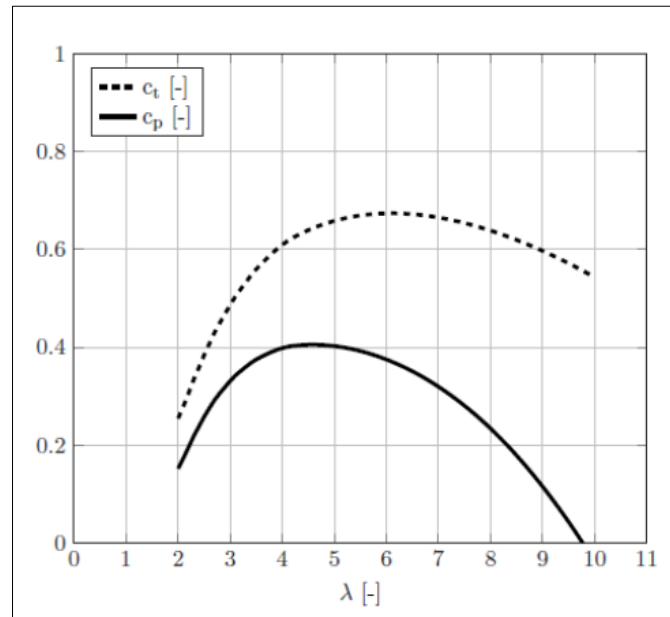


Figure 2.11 Typical Power and Thrust coefficients vs. tip speed ratio for a hydrokinetic turbine [8]

2.3.1.1 SCHOTTEL SIT-250

The SCHOTTEL Instream Turbine (SIT) – 250 is a horizontal axis hydrokinetic turbine designed for tidal power generation. It has been developed between 2011 and 2018 by SCHOTTEL Hydro GmbH, a company based in Germany. The SCHOTTEL Group's actual core business is the development and fabrication of ship propulsion systems. In addition of promoting their own hydrokinetic turbine system, the company is assigned to construct parts for competing companies in the tidal energy industry. The effort and achievements within the tidal energy sector put the company in a leading position in the hydrokinetic energy market.

In contrast to turbines with nacelle weights of up to 130 t or more, a single SIT weights about 1 t which keeps its cost per installed power capacity comparatively low. SCHOTTEL Hydro aims to provide hydrokinetic energy at maximum competitive costs.

Currently the turbines of the SIT-250 generation are available in four designs each accounting for one rotor size: 3 m, 4 m, 5 m, and 6.30 m (in diameter). This allows the turbine to operate in a wider range of flow speeds compared to a turbine which comes

with only one rotor size allowing principally all turbine parts with exception of the rotor to stay the same. This concept is owed to the fact that different resources (tidal as well as river resources) show different flow speed distributions. In order to be able to operate the turbine at as many different places as possible the machine need to be able to adapt to a as wide as possible range of flow conditions. This is why currently four rotor sizes are in existence.

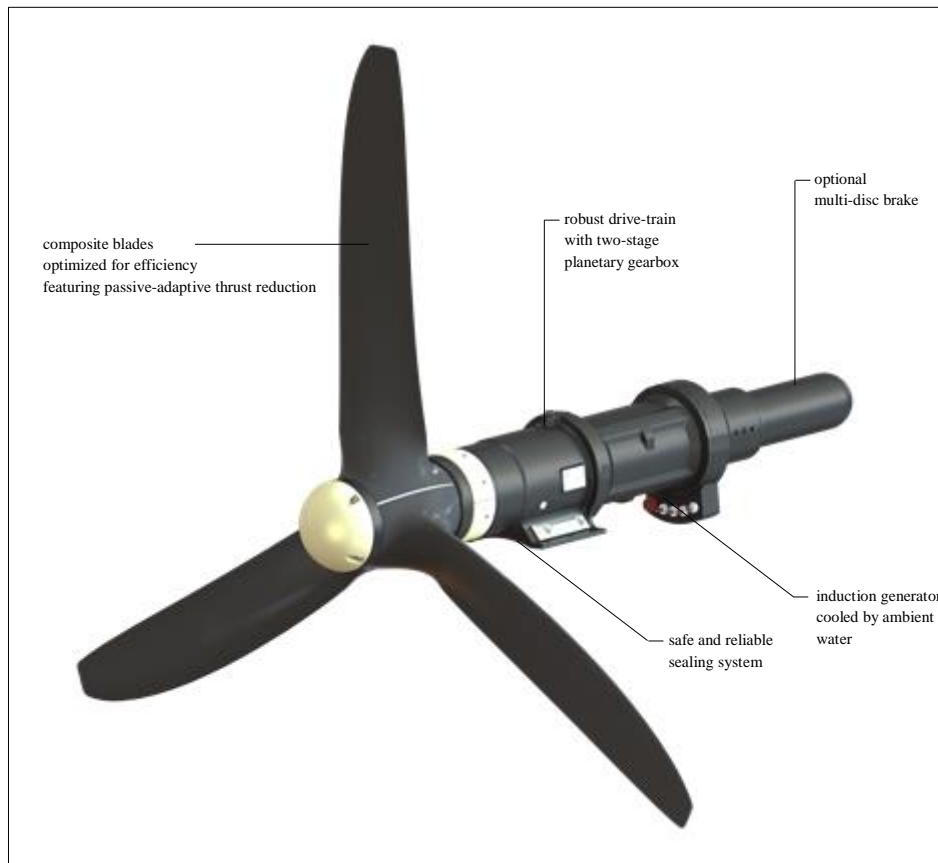


Figure 2.12 SCHOTTEL Hydro Instream Turbine – 250 [9]

The three bladed rotor is turning the rotor shaft which then, over a planetary gearbox, drives the asynchronous generator through a transmission ratio of 1:28. Both the planetary gearbox as well as the generator is being cooled by the ambient water. There is no active pitch mechanism, in case overload thrust forces occur the blades deform themselves elastically so that acting thrust on the rotor diminishes.

The following performance curves have been derived for the 6.30 m turbine of the SIT-250 series. The performance characteristics of this particular design has been chosen to

be illustrated due to the fact that its operational range fits best for the majority of river flow speeds (which will be discussed in detail in chapter 3).

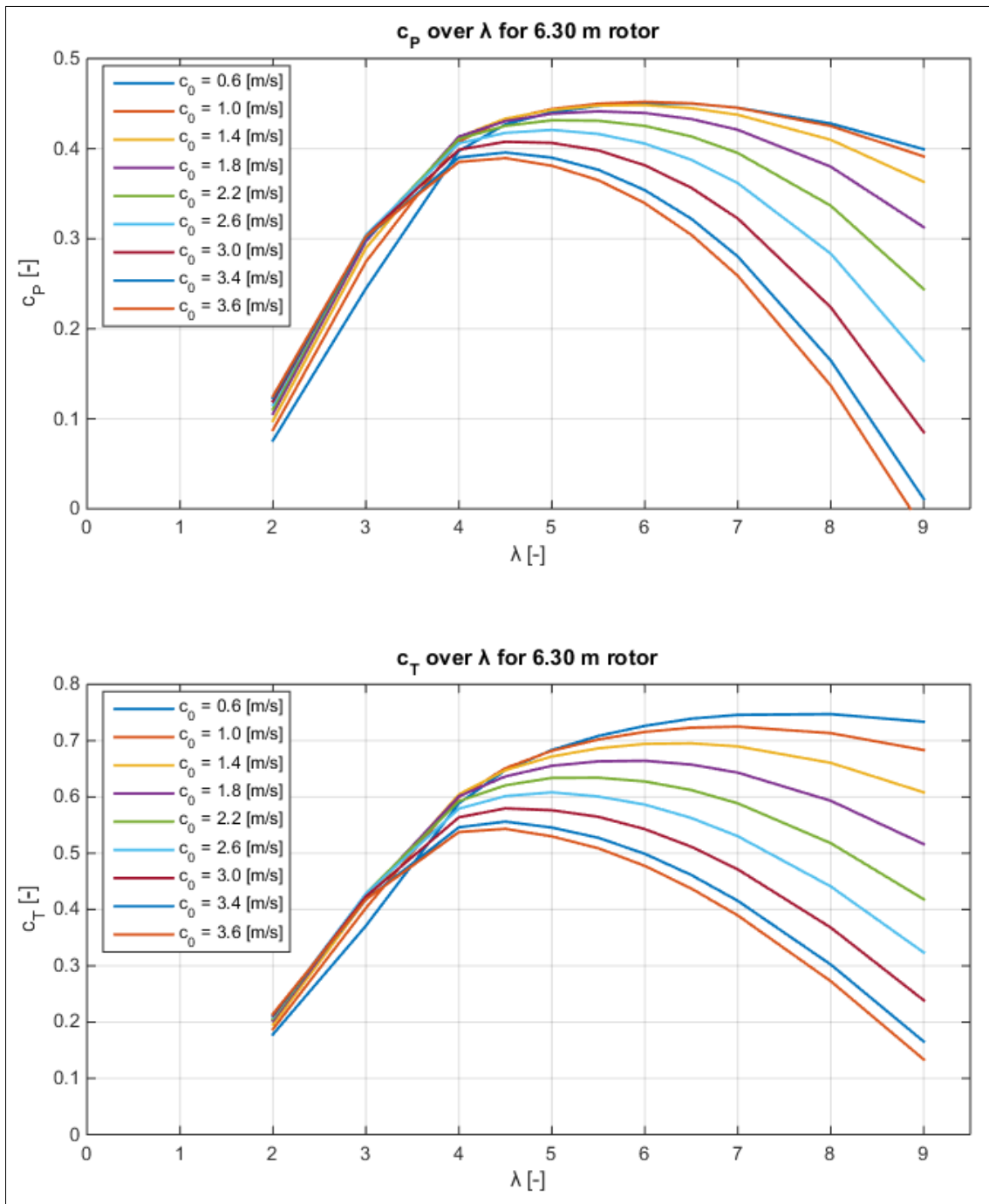


Figure 2.13 c_p and c_T vs. tip speed ratio of the SIT-250 – 6.30 m rotor [9]

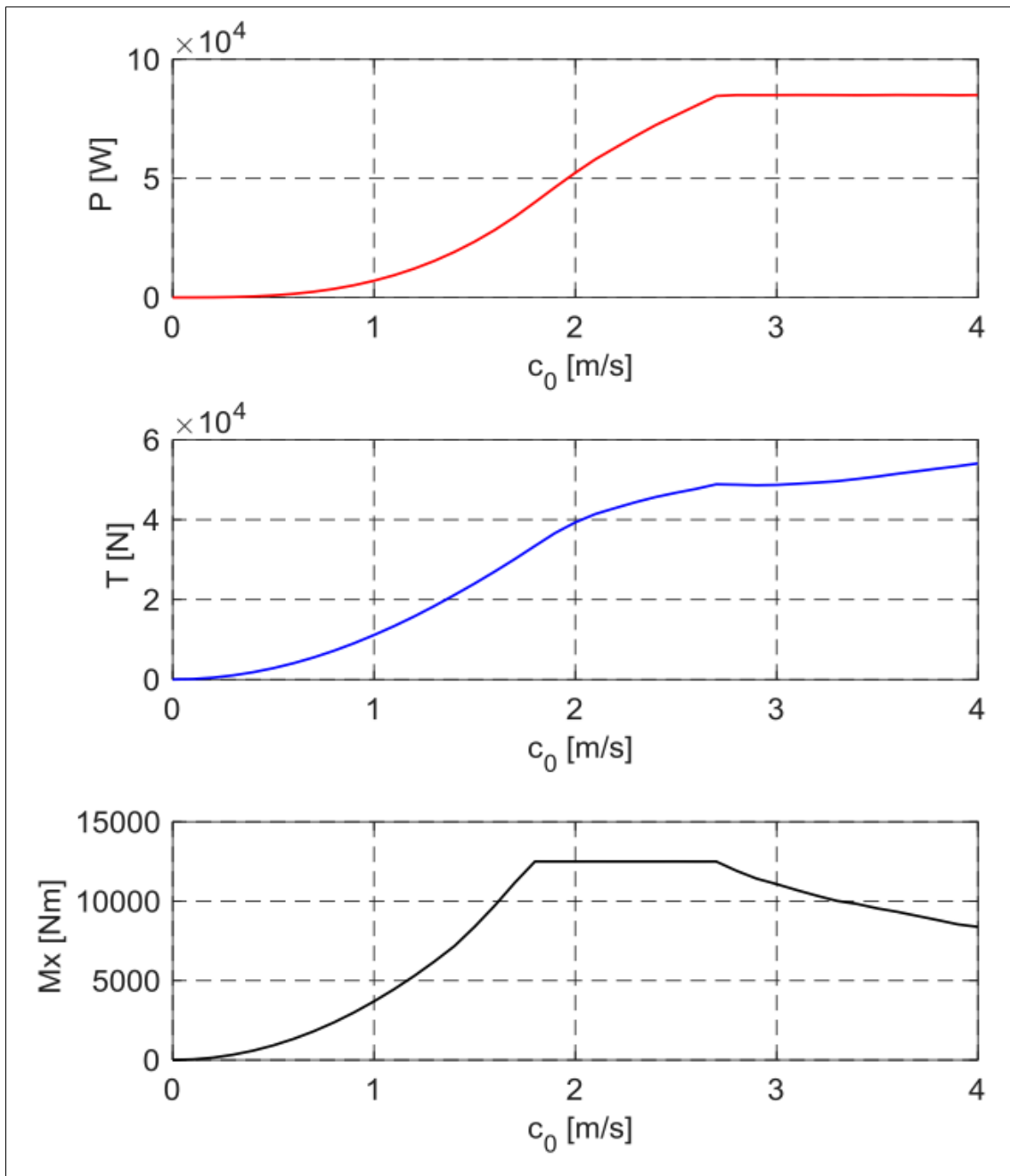


Figure 2.14 Performance Curves of the SIT-250 turbine with rotor diameter 6.30 m, illustrated: mechanical power at turbine shaft, absorbed thrust and torque at turbine shaft [9]

2.3.2 Vertical Axis Turbines

Vertical Axis Turbines are principally cheaper in development and production costs in comparison to horizontal axis turbines. This fact does not make them products of lower quality or less suitable for power production. Their ideal usage ranges in a different resource spectrum than that of horizontal axes turbines. Essentially they can operate in

low flow speeds achieving high efficiencies. So one can conclude that for low flow speed resources vertically axes turbines are the better choice for energy generation than horizontal axes turbines which have a minimum speed threshold, the cut-in speed, which has to be surpassed in order they start to turn themselves. Vertical axes turbines do not have this threshold and thus start to produce energy in any slow moving fluids. However, the maximum efficiency vertical axes turbines achieve are lower than those of horizontal axes turbines.

2.3.2.1 VAACT

The Vertical Axis Autorotation Current Turbine (VAACT) developed by researchers of LOC¹ (COPPE/UFRJ) origins out of the study of a flat plate placed in a uniform flow. The study revealed that three rotational patterns could be stated:

- (1) *fluttering*, which describes the oscillation of the plate within angle of attacks $< \pm 90^\circ$,
- (2) *chaotic fluttering-autorotation*, where the plate flutters as well as rotates partially around its own axis (in both directions), and
- (3) *autorotation*, where the plate rotates stable around its own axis without fluttering.

For energy extracting applications the autorotation pattern is desired and thus the plate was optimized to ensure stable autorotation. Therefore the plate tips were flapped and the mass moment of inertia artificially increased by installing additional weights relatively far from the center of rotation. The application of the extra mass moment of inertia is improving all operational characteristics such as rotational velocity, tip-speed ratio, torque and subsequently: performance.

¹ LOC: Laboratório de Ondas e Correntes, engl: Laboratory for Waves and Currents (Federal University of Rio de Janeiro)

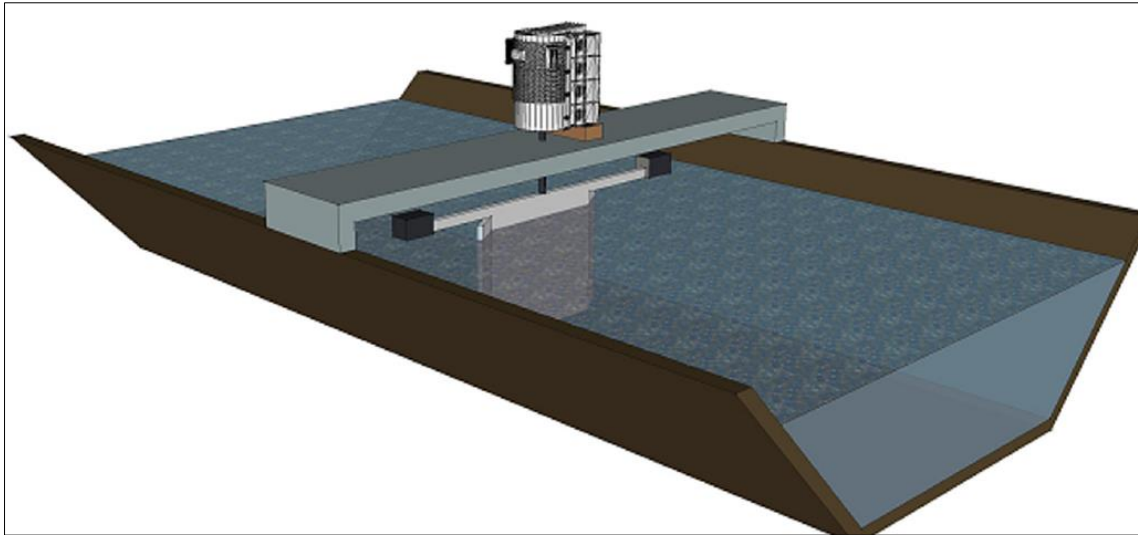


Figure 2.15 Schematic illustration of VAACT operating in channel [10]

Hydrodynamics:

The VAACT is driven by lift and drag forces. For small angles of attack, the lift force is predominant and for higher angles of attack drag mainly causes the yaw motion. There are also vortices produced on the backside of the plate so that areas of different pressures are surrounding the moving plate. The vortex formed at the retreating face is larger than the one of the advance face leading to a sucking effect of the plate towards the low pressure area at the retreating face which drives the yaw motion.

In each cycle of rotation there are four crucial positions (parallel and perpendicular to the current) where the hydrodynamic moment vanishes (lift and drag forces disappear). That is where sufficient mass moment of inertia (I) can help the turbine to overcome these critical situations.

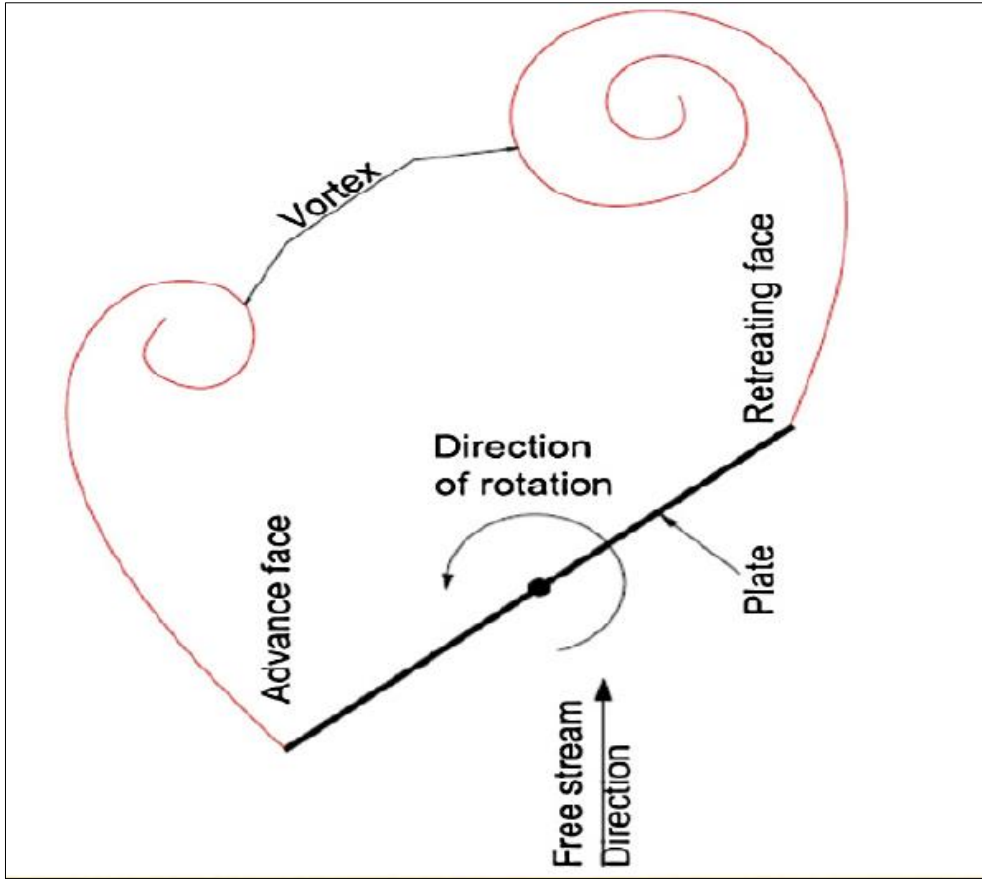


Figure 2.16 Vortices at backside of plate [11]

Rostami and Fernandes [3] showed that the power coefficient c_P for VAACT is a function of the dimensionless mass moment of inertia I^* , the tip-speed ratio λ , and the Reynolds-Number Re_y .

$$c_P = f(I^*, \lambda, Re) \quad (2.17)$$

where:

I^*	dimensionless mass moment of inertia	$I^* = \frac{I}{\rho c^5}$
λ	Tip Speed Ratio	$\lambda = \frac{\omega R}{v}$
Re_y	Reynolds Number	$Re_y = \frac{\rho c v}{\mu}$

Further, it was experimentally determined that with increasing I^* the autorotation becomes more stable and that independent of the current velocity (Figure 2.17).

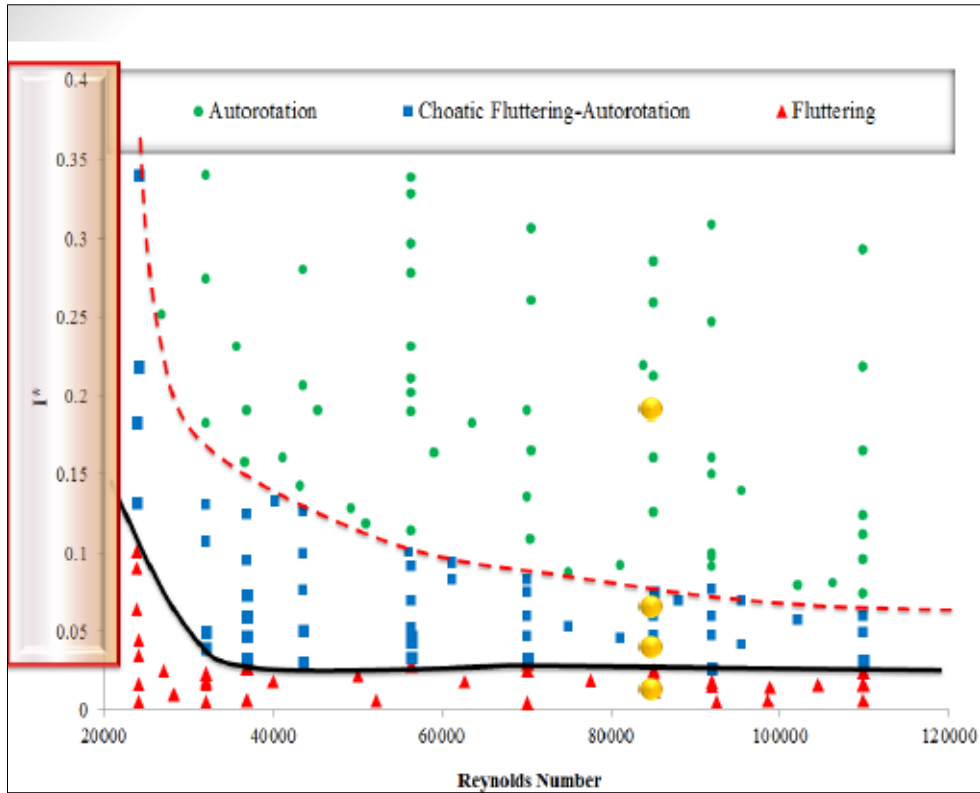


Figure 2.17 VAECT rotation pattern depending on I^* and current velocity (Rey) [12]

There are also significant differences in the performances of the two types of VAECT (with and without flapped tips).

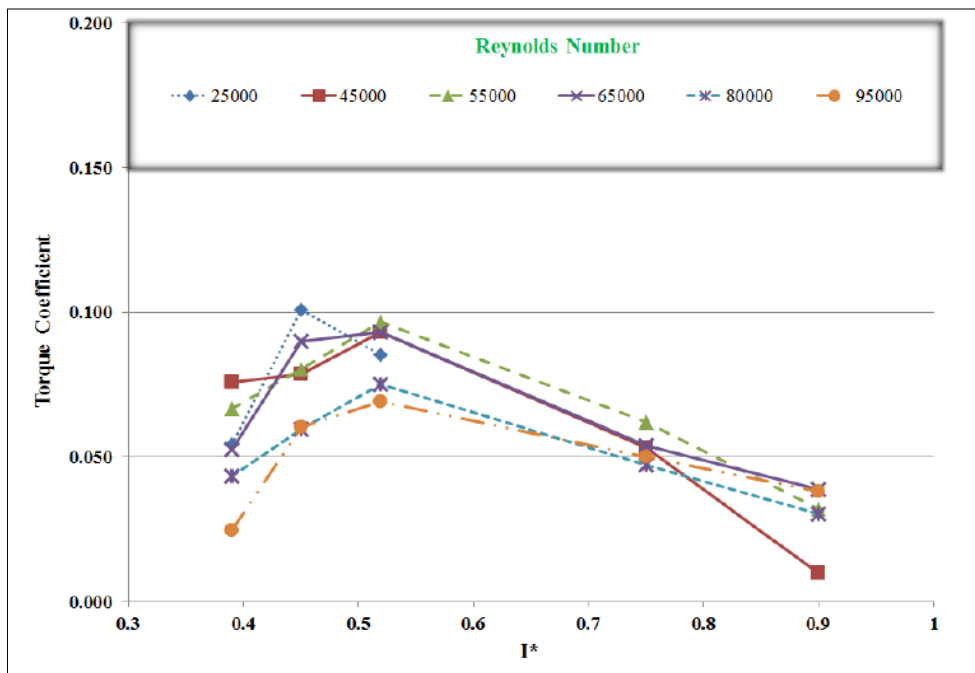


Figure 2.18 Torque coefficient of VAECT without flapped tips at $\lambda = 0,65$ [12]

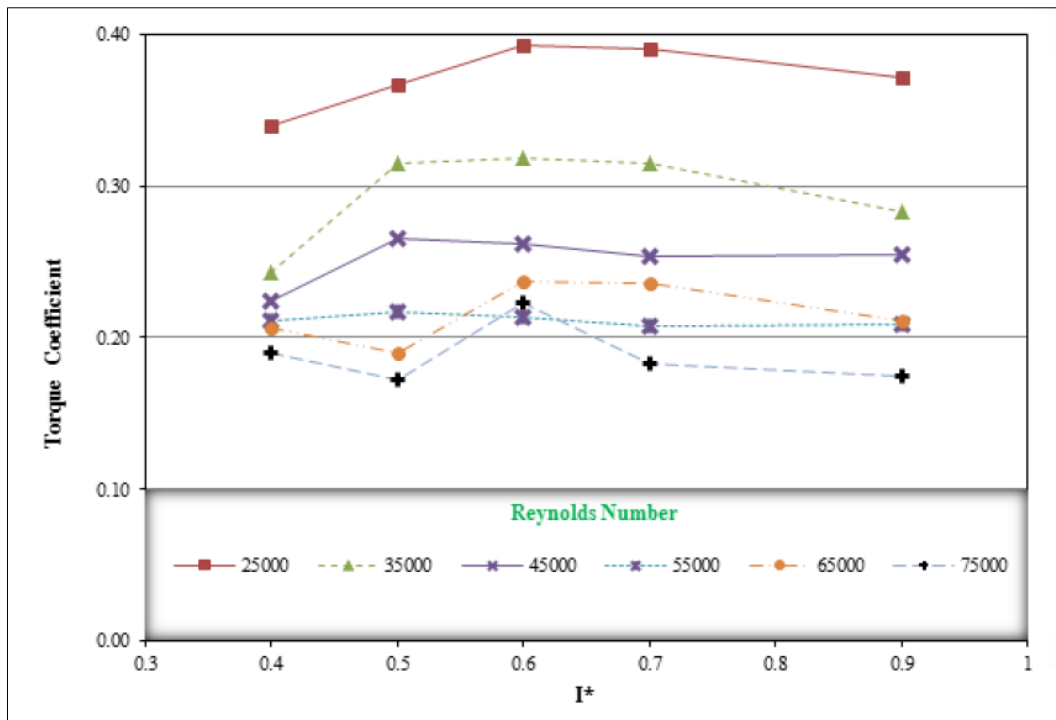


Figure 2.19 Torque coefficient of VAACT with flapped tips at $\lambda = 0,65$ [12]

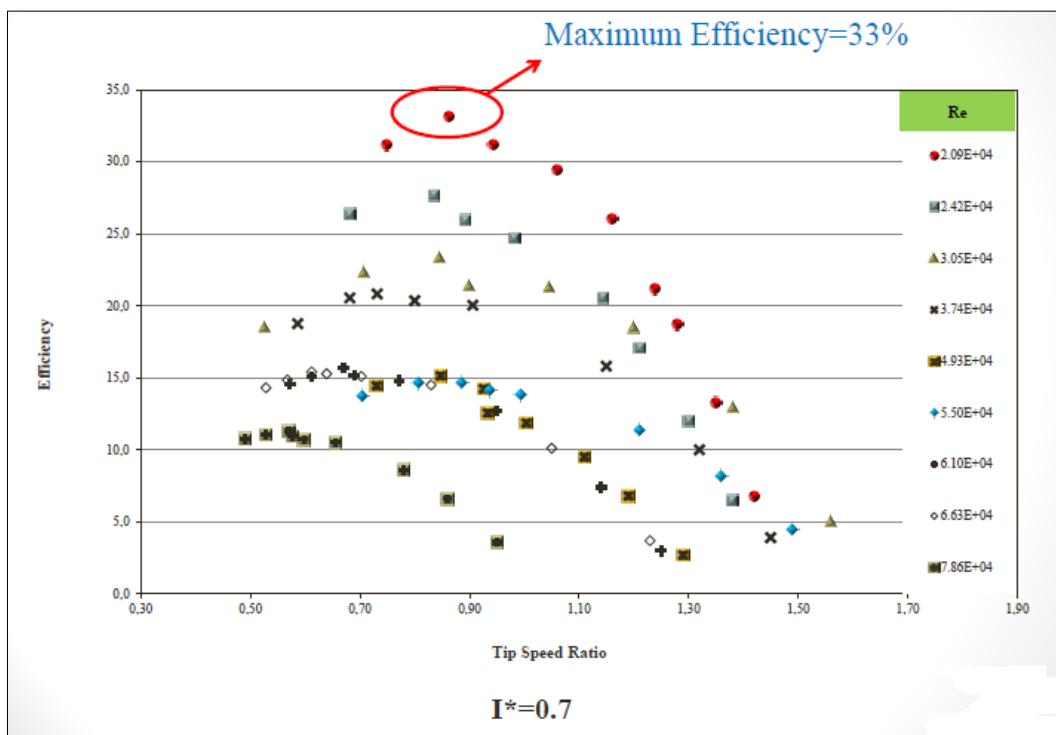


Figure 2.20 c_P over λ of flapped plate at optimum I^* [12]

It can be concluded that the VAACT is a low current speed turbine (low λ , high efficiency at low Re_y). Its optimum range of operation is estimated to be between 0.07 to 0.5 m/s. Its efficiency (c_p) of 0,33 in flapped form at the optimum mass moment of inertia and optimum λ is remarkable for a vertical axis turbine.

It seems reasonable to assume that performance could be further enhanced finding a more optimized plate geometry. Another interesting question would be to determine the ideal aspect ratio with regards to efficiency.

However, these two questions cannot be answered within the scope of this thesis. Adequate answering of those questions may require the focus and work scope of another thesis or research project.

2.4 HYDROKINETIC ENERGY IN BRAZIL

Before it will be discussed where within the Brazilian Electricity Matrix River Hydrokinetic Energy (RHK) may be established in the future, the current Brazilian electricity generating structure and its future projection being displayed. Following, recent efforts and events towards the development of the technology in Brazil being deliberated.

2.4.1 Current and Future Brazilian Electricity Supply

Brazil currently is generating over 80% of its electricity from renewable sources and will continue so in the future. By December 2014 Brazil's total installed capacity for electric power generation was 126 GWs, importing just 7 GWs, so that total demand of 133 GW was matched by 95% domestic production (see Figure 2.21).

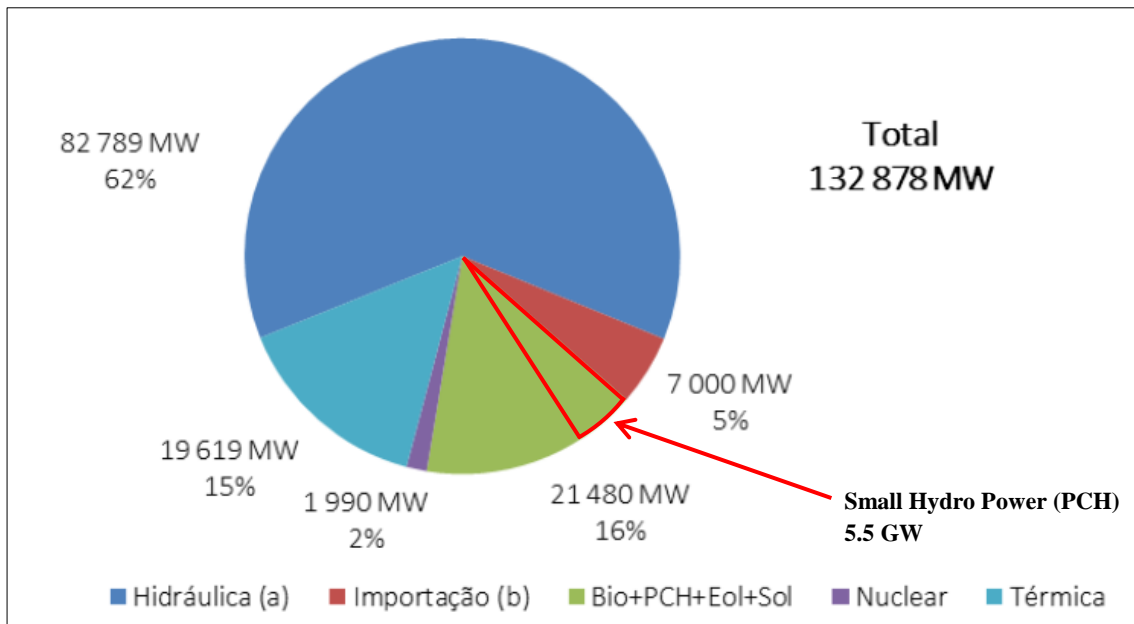


Figure 2.21 Brazil's Electric Energy capacity by sources, December 2014 [13]

By 2024 the Brazilian government is expecting the capacity for electric energy to grow by another 74 GWs so that by December 2024 the total installed electric energy capacity will be at 207 GWs. This corresponds to a growth of 55 % over 10 years or an annual growth rate of 4.5 %. It is worth mentioning that almost all that growth in capacity is coming from renewable sources so that by the end of 2024, 84.1 % of the total installed capacity is coming from renewable sources. This lists Brazil among the most sustainable countries in the world with regards to electric power generation.

Whereas all energy sources mentioned in Figure 2.21 will grow in capacity over the 10 year projected time frame (Figure 2.22) it is assumed that River Hydrokinetic Energy can be a part of the “Small Hydro Power” (port.: “Pequenas Centrais Hidrelétricas (PCH)”) share with its today installed capacity of 5,5 GW, according to the Nacional Agency of Electric Energy (port. “Agencia Nacional de Energia Elétrica (ANEEL)”). Small Hydro Power refers to hydro power plants with an installed capacity between 1-30 MW. This power capacity range seems to be reasonable to reach for potential future River Hydrokinetic Power Plants.

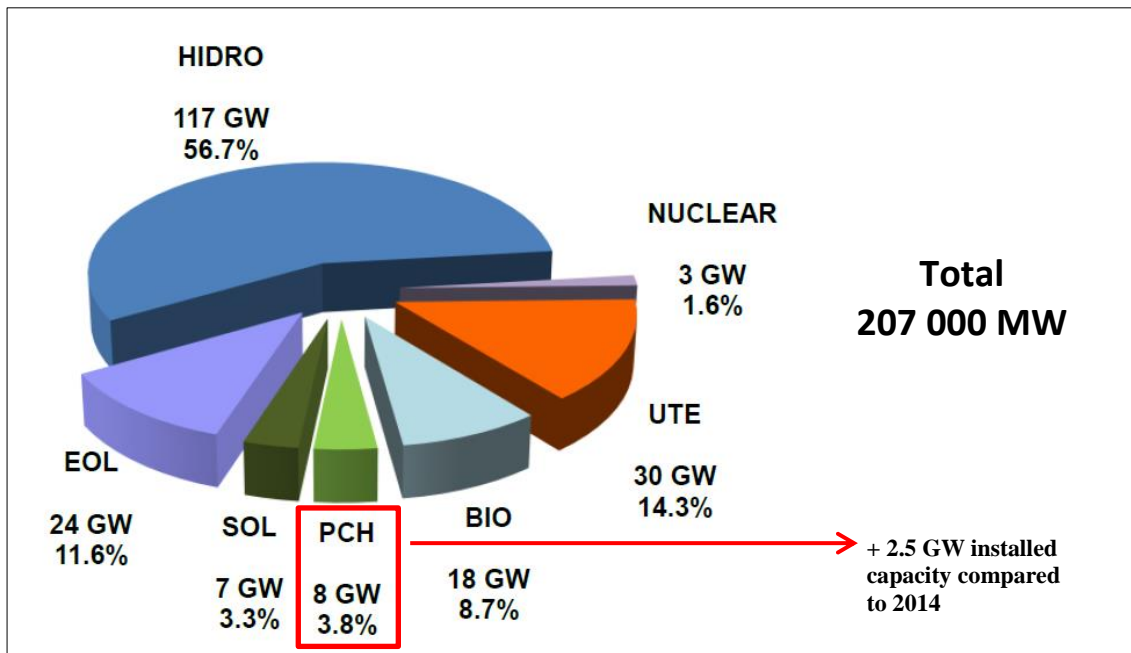


Figure 2.22 Estimated Brazil's Electric Energy Capacity by source, December 2024 [13]

2.4.2 Current State: River Hydrokinetic Energy in Brazil

In Brazil the potential of generating electric power from rivers (in-stream) without building a dam has gained stronger attention in recent years. Not just due to the significant smaller social and environmental impact or due to the fact that it is not possible to build dams everywhere but also due to the wish to provide clean and renewable energy for rural areas located close by rivers which do not have grid access yet.

The technology seems to have reasonable chances to be applied in Brazil's Northern Region which is generally very sparsely populated and diesel fuel still plays an important role as primary source for electric power generation.

According to the Inter-American Development Bank study (2015) "*Preliminary Analysis of Potential River Hydrokinetic Energy Technologies in the Amazon Basin*" there are over 10 million inhabitants living along mainstream Amazon River and its tributaries where the electrification rates are the lowest among the country (lower than 25%) compared with the national rate of 70% [14].

Having briefly stated the most likely area of operation for hydrokinetic river technology applications in the future, the phase of the development of the technology as well as major protagonists in developing the technology and planning hydrokinetic parks will be mentioned.

Currently the technology is in the advanced development phase. Significant research has been carried out mainly by universities, in particular by the Federal University of Itajubá (Unifei), the University of Brasília (UNB), the Federal University of Pará (UFPA) and the Federal University of Amazon (UFAM). These universities carried out research and development on the elevation of the resource potential, studying and quantifying the kinetic energy potential of several rivers, as well as designing river turbine prototypes.

From the industrial side Eletronorte and Itaipu Binacional did efforts on the elevation of Brazil's river resource potential. Eletronorte beyond that in 2014 planned to install the first Hydrokinetic Energy Park in Brazil, called "Tucunaré" located downstream of the Tucuruí Hydropower plant. By today there is no hydrokinetic river energy park in operation in Brazil yet, however it seems reasonable for that to happen in the near to mid-term future.

Following a table stating relevant "Recent events" regarding the development of hydrokinetic river technology and its application is illustrated. It covers events from November 2014 until today.

Table 2.1 Recent events regarding the Development of River Hydrokinetic Energy Technology in Brazil, part 1

Recent events: Hydrokinetic River Energy Development in Brazil					
#	Date	Type	Initiator	Subject	Results
1	03.11.2014	Seminar	Eletronorte, Itaipu Binacional, University of Brasília, Federal University of Pará	1st Seminar on Hydrokinetic Power Generation Parks (I Seminário sobre Parques Hidrelétricos Hidrocinéticos Fluviais) - discussing the hydrokinetic energy potential and its possible future development in Brazil	(1) Downstream of the Tucuruí Dam the first hydrokinetic energy park in Brazil will be opened (approx. timeframe: 5 years), power: min. 5 MW (2) Eletronorte and Itaipu Binacional signing an agreement on technical cooperation regarding the installation of the park as well as on the "mapping" of the hydrokinetic potential of Brazilian rivers (3) Professors of UFPA, UnB and engineers from Eletronorte present the Tucunare project [name of the park described in (1)] which focuses on the turbine requirements for the park: turbines of 500 KW at 2,5 m/s flow speed, rotor diameter: 10 m, mass: 17 tons, cost per turbine: 10 million R\$ [Turbine requirements estimated in (3) will be revised in further project development]
<p><u>Sources:</u></p> <p>(1) http://agencia.eletronorte.gov.br/site/2014/10/31/pioneirismo-eletronorte-promove-o-i-seminario-sobre-parques-hidreletricos-hidrocineticos-fluviais/</p> <p>(2) https://www.ambienteenergia.com.br/index.php/2014/11/primeiro-parque-hidrocinetico-sera-implantado-brasil/24745</p> <p>(3) http://www.pgintegridade.unb.br/2-pagina-inicial/48-tucunare-turbinas-hidrocineticas-para-o-aproveitamento-do-potencial-remanescente-em-usinas-hidreletricas</p> <p>(4) https://energiahidrocinetica.blogspot.com.br/2015/07/projeto-tucunare.html</p>					
2	11/2014	Public Tendering	British Government (Foreign & Commonwealth Office) - Strategic Programme Fund, Eletronorte, Federal University of Itajubá (Unifei)	Development and implementation of procedures for developing a hydrokinetic park and the survey of applicable technologies downstream hydropower plants. Case studies: Samuel and Curuá-Una Hydropower plants - analyzing flow speed distribution, depth profile and the potential of generating power over 5 km along the two rivers (Jamari and Curuá-Una) downstream of the dams	(1) UK Embassy spent ~1 million R\$ financing the project (2) Data acquisition carried out by researchers from Unifei (3) Results of project presented at "Workshop on hydrokinetic energy studies in the North Region" [Brasília, 27.04.2016]
<p><u>Sources:</u></p> <p>(1) http://www1.folha.uol.com.br/mercado/2015/08/1674115-projetos-na-regiao-norte-buscam-gerar-energia-com-a-correnteza-dos-rios.shtml</p> <p>(2) https://cerpch.unifei.edu.br/wp-content/uploads/2016/05/WCN-003.pdf</p>					
3	11/2015	Survey, Resource Analysis	Inter-American Development Bank, Federal University of Amazon (UFAM)	Preliminary Analysis of Potential for River Hydrokinetic Energy Technologies in the Amazon Basin - general analysis on the potential of hydrokinetic power generation in the Amazon basin - detailed study on 8 sites (4 Peruvian, 3 Brazilian, 1 Equadorian) for potential hydrokinetic power takeoff with flow speed analysis and depth profile	(1) >10 million people along Amazon river do not have appropriate electricity access from grid (growth rate: ~6% /year) (2) hydrokinetic energy parks could be installed at various sites (especially in Brazil) in the magnitude of GW (3) installation of parks would have massive positive impact on population close by the rivers (potential projects could be enforced at the cities of: Óbidos (50.000 inhabitants), Manacapuru (93.000 inhabitants), Itacoatiara (96.000 inhabitants))
<p><u>Source:</u></p> <p>(1) https://publications.iadb.org/handle/11319/7292</p>					

Table 2.2 Continuation of Table 2.1

#	Date	Type	Organizer(s) / Host(s)	Subject	Results
4	17.03.2016	Public Tendering	Eletronorte	<p>Public tendering 001/2016</p> <p>(Chamada Pública 001/2016)</p> <p>Compilation of R&D Projects - Development of a Hydrokinetic Turbine Unit for the use of the potential downstream of a Hydropowerplant (dam)</p>	<p>(1) Find a turbine of minimum 100 kW to be installed downstream of Tucuruí dam, nominal flow: 2,5 m/s, turbine being able to operate between 1 and 3 m/s, rotor diameter: 5m</p> <p>(2) The selected contractor should be able to fabricate such turbines and install them at the specific sites chosen by Eletronorte, a solution for mooring/positioning the turbine system in the river should be offered, define breaking system, development of an energy dissipating system to run tests at site, development of a diffusor system with mounting concept on turbine</p> <p>(3) Publicly known applicants as by 27/04/2016: Andritz, Delp, Hubz, Fox Oil, Enersud, Aero Alcool, BBEng Engenheiros Associados</p>
<p><u>Sources:</u></p> <p>(1) http://www.eletronorte.gov.br/opencms/export/sites/eletronorte/pilares/tecnologia/pepd/Chamada_01_2016/Chamada_Pxblica_001_2016_Final.pdf</p> <p>(2) http://www.eletronorte.gov.br/opencms/opencms/pilares/tecnologia/pepd/Chamada_01_2016/index.html</p>					
5	27.04.2016	Workshop	British Government (Foreign & Commonwealth Office) - Strategic Programme Fund, Eletronorte, Federal University of Itajubá (Unifei)	<p>Workshop on hydrokinetic energy studies in the North Region</p> <p>(Workshop sobre estudos de energia hidrocinética na Região Norte)</p> <p>- presentation of the studies about the hydrokinetic potential downstream of the Samuel and Curuá-Una Hydropower plant</p>	<p>(1) Potential identified within 5 km downstream of Curuá-Una: 2,4 MW which results in 13,2 GWh/year</p> <p>(2) Further steps about dimensioning adequate machinery for average flow speed of 2,5 m/s as well as mooring systems and grid connection solutions</p> <p>(3) Implement partnerships and exchange with institutions which are doing research and develop hydrokinetic energy harvesting technology</p>
<p><u>Sources:</u></p> <p>(1) http://agencia.eletronorte.gov.br/site/2016/04/25/brasil-e-reino-unido-promovem-workshop-sobre-estudos-de-energia-hidrocinetica-na-regiao-norte/</p> <p>(2) http://agencia.eletronorte.gov.br/site/2016/04/30/hidrocinetica-estudos-identificam-aproveitamento-em-curuá-una/</p> <p>(3) https://cerpch.unifei.edu.br/wp-content/uploads/2016/05/WCN-003.pdf</p>					
6	03.05.2016	Workshop	University of Brasília, Eletronorte	<p>Workshop Tucunaré</p> <p>(Workshop Tucunaré: Resultados de P&D - Turbinas Hidrocinéticas para o aproveitamento do potencial remanescente em usinas hidroelétricas)</p> <p>- presentation of results for turbine requirements/development issued in the public tendering ("Chamada Pública") 001/2016 from Eletronorte published on 17/03/2016</p>	<p>(1) Eletronorte looking for an industrial partner for the development of a 100 KW (5m diameter) turbine which went already through testing, commissioning and installed operation (at 1 m/s flow speed or higher)</p> <p>(2) no suitable turbine design found yet</p>
<p><u>Sources:</u></p> <p>(1) http://agencia.eletronorte.gov.br/site/2016/05/02/workshop-tucunare-apresenta-resultados-de-pesquisas-sobre-turbinas-hidrocineticas/</p> <p>(2) http://agencia.eletronorte.gov.br/site/2016/05/05/energia-hidrocinetica-projeto-tucunare-apresenta-resultados-e-busca-parceria-para-desenvolver-prototipo-de-turbina/</p> <p>(3) http://www.eletronorte.gov.br/opencms/opencms/pilares/tecnologia/pepd/</p> <p>(4) http://www.eln.gov.br/opencms/export/sites/eletronorte/pilares/tecnologia/pepd/Chamada_01_2016/Chamada_Pxblica_001_2016_Final.pdf</p>					
7	05.08.2016	Public announcement	Eletronorte	<p>Cancelling of the Public Tendering 001/2016</p>	<p>(1) Cancelling due to receiving R&D projects disaccoring with requirements established in Public Tendering 001/2016</p>
<p><u>Sources:</u></p> <p>(1) http://www.eletronorte.gov.br/opencms/export/sites/eletronorte/pilares/tecnologia/pepd/Chamada_01_2016/Resultado__Chamada001.pdf</p> <p>(2) http://www.eletronorte.gov.br/opencms/opencms/pilares/tecnologia/pepd/Chamada_01_2016/index.html</p>					
8	01.05.2017	Publication	ANEEL (Agencia Nacional de Energia Elétrica)	<p>ANEEL releases new rules for small hydropower operators in Brazil</p> <p>- Nacional Agency of Electric Energy (ANEEL) published new rules governing operators of small hydropower plants in Brazil</p>	<p>(1) Normative Resolution No. 765/2017 defines the procedures</p> <p>(2) changes affect power plants from 5 - 50 MW</p>
<p><u>Source:</u></p> <p>(1) http://www.hydroworld.com/articles/2017/05/aneel-releases-new-rules-for-small-hydropower-operators-in-brazil.html</p>					

3 RIVER RESOURCES

Data on freshwater resources are usually published by research institutes, governments or international institutions such as the United Nations. For this particular research all information on freshwater resources are coming from either one or several of the following institutes:

- (1) AQUASTAT, FAO (Food and Agricultural Organization, UN)
- (2) Pacific Institute (USA)
- (3) ANA (Agência Nacional de Águas, Brazil)
- (4) Stockholm International Water Institute

In particular the FAO and the Pacific Institute (full name: Pacific Institute for Studies in Development, Environment, and Security) provide comprehensive studies on global freshwater resources regarding its regional (current and future) demand and supply. Researchers from the Pacific Institute introduced and established concepts such as “Peak Water²” or the “Soft Water Path³” which are receiving broad acceptance among experts and researchers around the world. Their biennial report entitled “The World’s Water” contains a table entitled “Total Renewable Freshwater Supply by Country” which comprises both renewable surface water and groundwater supplies including surface inflows from neighboring countries.

Definitions by the FAO [15]:

- Renewable water resources are computed on the basis of the water cycle. In this report they represent the long-term average annual flow of rivers (surface water) and ground water.
- Non-renewable water resources are groundwater bodies (deep aquifers) that have a negligible rate of recharge on the human time-scale and thus can be considered non-renewable.

² Peak Water – in analogy to „Peak Oil“, a peaking and then decline in water production, with far-reaching consequences; for detailed information see: [34]

³ Soft Water Path – “new” approach to managing water resources; for detailed information see: [36]

As rivers form a major part of a countries renewable freshwater resources, the numbers from The World’s Water report are important to quantify countries and regions which have suitable river resources for potential river hydrokinetic energy applications. Principally, regions/countries which have high renewable freshwater resources are more likely to have suitable river sites for potential RHK applications than those with small renewable freshwater resources. This is due to the fact that rivers with higher discharges normally having a larger cross sectional area and therefore sufficient depth to place turbines with rotor diameters that allow power extraction in the magnitude of approximately 50 kW or higher (rotor diameter > 4 m).

3.1 RENEWABLE FRESHWATER RESOURCES WORLDWIDE

Following, several figures displaying the distribution of the world’s total renewable freshwater resources are illustrated.

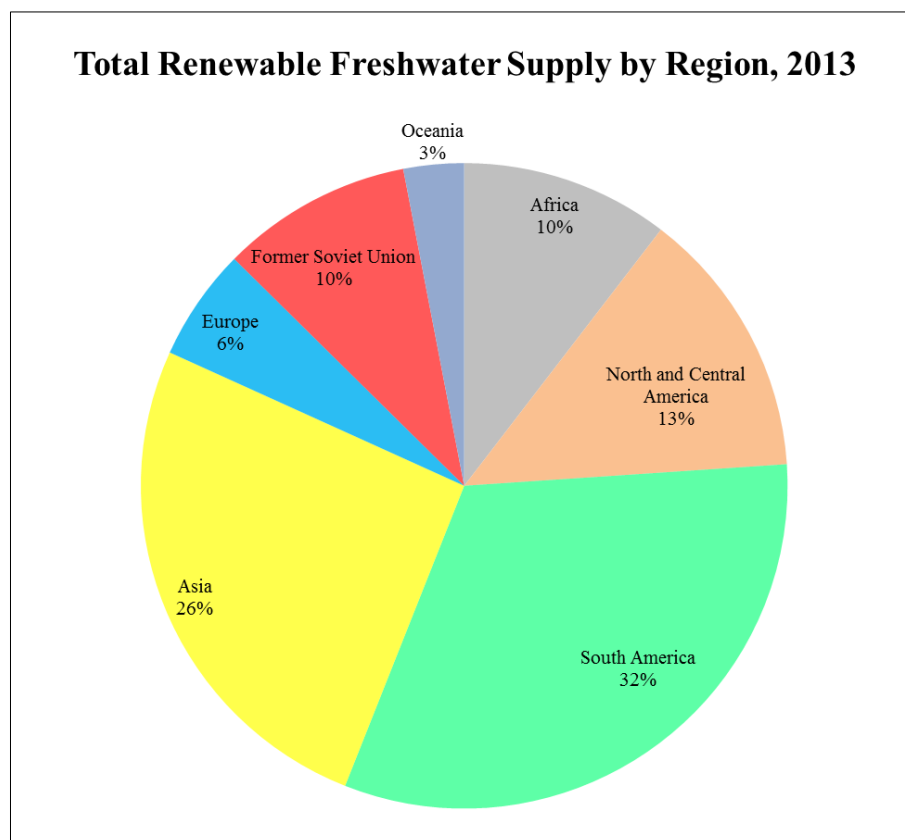


Figure 3.1 Total Renewable Freshwater Supply by Region, 2013 [16]

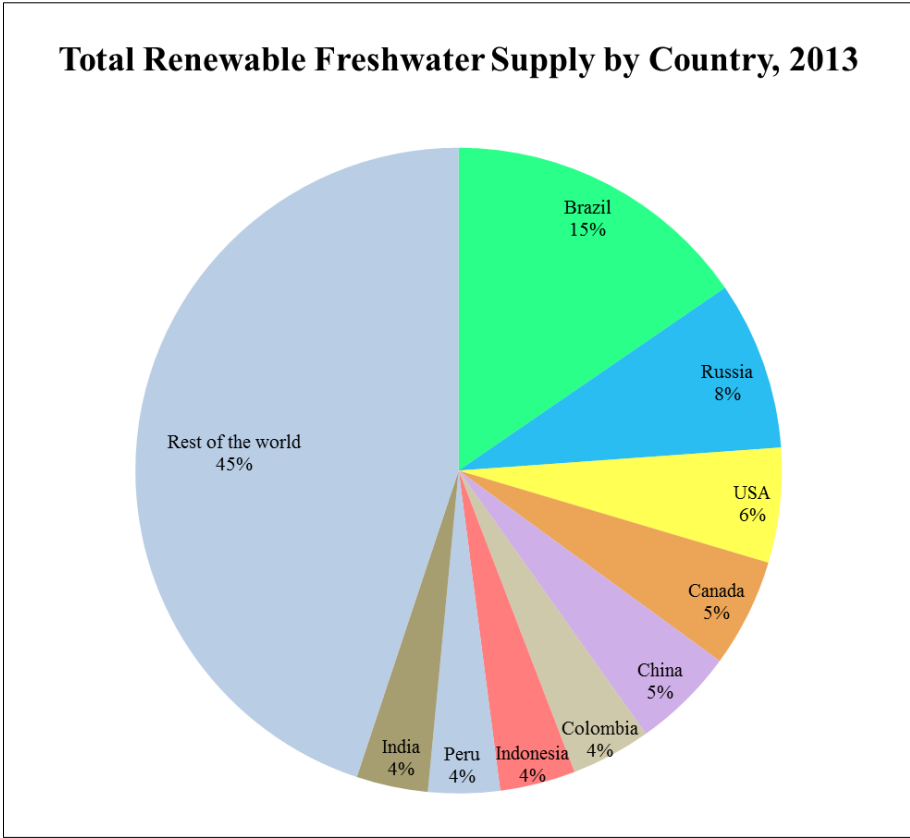


Figure 3.2 Total Renewable Freshwater Supply by country, 2013 [16]

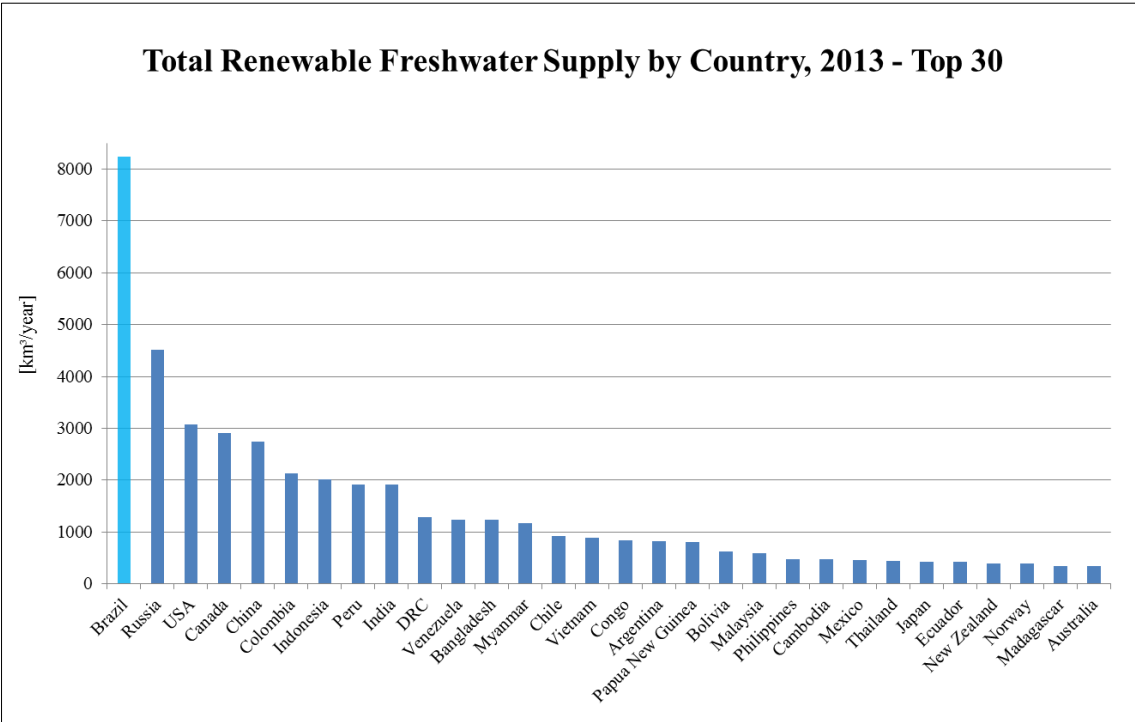


Figure 3.3 Total Renewable Freshwater Supply by Country, 2013 – Top 30 [16]

As the above presented figures show, Brazil has the largest renewable freshwater resources among all countries and therefore is predestinated for its river resources being studied more in depth regarding the potential for hydrokinetic power extraction. The attempt to provide a comprehensive river resource analysis consisting of the study of 20 Brazilian Rivers has been carried out to evaluate a principal feasibility of major Brazilian rivers for hydrokinetic river energy applications. All river data for the in this work carried out analyses are coming from the Brazilian National Water Agency: Agência Nacional de Águas (ANA). Their publicly accessible database “Hidroweb” provides comparatively extensive river data (discharge, cross sectional area, flow speed, etc.) on most Brazilian rivers to carry out the intended river resource evaluation.

Challenges with regional water resource estimations/studies:

Even though river data is existent for a specific site or section there are several difficulties regarding the creation of a reliable water resource estimation of a certain region or water system. This is due to several circumstances, amongst others: (1) lack of data, meaning the nonexistence or non-accessibility of data bases which contain river data; (2) inconsistent/fragmentary data records, meaning that existent data often is only available in fragmentary data points, e.g. time between two performed measurements being months or even years; and (3) accuracy of recorded data, meaning that for several data sets precision of the recorded data is partly or in total questionable, for instance when comparing two data sets of the same site with significant distance in time between their records or when comparing datasets of the same site by different surveyors.

A leading hydrologist from the University of Bologna, Italy, states it as following:

“The most relevant challenge when assessing water resources is lack of data. This is a widespread problem in hydrology, as observations of climate and hydrology started relatively recently. Moreover, even when data are available it is not always easy to have access at them, for the institutional fragmentation that usually affects water resources management, especially in Europe.”

Alberto Montanari, Professor of Hydraulic Works and Hydrology, University of Bologna [16]

Table 3.1 exemplary shows a data set of recorded measurements of the Amazon River close to the city of Itacoatiara, AM, Brazil. This data set can be evaluated as a comparatively well consistent and accurate data set; even though it reveals fragmentary recordings. Data has been recorded over a period of 10 years (2008-2017) with the number of records for each year varying from one to eight measurements, so that in the end 38 measurements were carried out which are covering all 12 months of a hydrologic year with one to seven data points per month. It will be responded more in depth to the “data problem” later in this work (chapter 3.3). The short introduction to this subject however is considered to be reasonable at this point.

Table 3.1 Original data set of measurement records of the Amazon River at Itacoatiara, Brazil, provided by ANA

ITACOATIARA, Original										

//										
// Sistema de Informações Hidrológicas										
// Versão Web 3.0										
// \$ 2001 Agência Nacional de Águas (ANA)										
//										
// NívelConsistencia: 1 = Bruto, 2 = Consistido										
//										
// Restrições da consulta:										
// Código da Estação: 16030000										
//										

//EstacaoCodigo	NivelConsistencia	Data	Hora	NumMedicao	Cota	Vazao	AreaMolhada	Largura	VelMedia	Profundidade
16030000	1	21.03.2008	01.01.1900 15:07	1	1245	187340	127658	3898,89	1,468	32,74
16030000	1	19.05.2008	01.01.1900 13:13	2	1386	186471	135295	3970	1,378	34,08
16030000	1	17.06.2008	01.01.1900 11:11	3	1410	195080	131960	3863	1,478	34,16
16030000	1	24.07.2008	01.01.1900 05:59	4	1305	182755	130785	3823	1,398	34,21
16030000	1	23.08.2008	01.01.1900 09:24	5	1116	151421	121140	3757	1,25	32,24
16030000	1	08.11.2008	01.01.1900 11:15	6	793	98026	95323	3631	1,028	26,25
16030000	1	18.03.2009	01.01.1900 16:54	7	1311	190832	127638	3491	1,496	36,57
16030000	1	07.07.2009	01.01.1900 07:23	8	1490	203136	132378	4082	1,535	32,43
16030000	1	07.10.2009	01.01.1900 15:35	9	724	110133	104953	3352,36	1,049	31,31
16030000	1	07.02.2010	01.01.1900 14:35	10	928	149309	111847	3460,21	1,335	32,32
16030000	1	14.05.2010	01.01.1900 12:57	11	1319	210165	127662	3538,9	1,646	36,07
16030000	1	30.08.2010	01.01.1900 06:08	12	885	130096,4	110892,7	3503,35	1,173	31,65
16030000	1	27.01.2011	01.01.1900 14:42	13	731	123250,9	106933,6	3311,19	1,153	32,29
16030000	1	18.05.2011	01.01.1900 14:50	14	1357	181403	139576	3732	1,303	37,4
16030000	1	04.08.2011	01.01.1900 13:27	15	1264	174180	128724	3597,68	1,353	35,78
16030000	1	14.12.2011	01.01.1900 15:11	16	551	105892,7	101386,5	3333,86	1,044	30,41
16030000	1	12.03.2012	01.01.1900 11:40	17	1294	213151	127923	3495	1,67	36,61
16030000	1	26.06.2012	01.01.1900 06:56	18	1447	227328,5	132991,7	3811,22	1,71	34,89
16030000	1	27.10.2012	01.01.1900 10:49	19	388	81826,66	94150,83	3298,08	0,869	28,55
16030000	1	04.02.2013	01.01.1900 07:39	20	911	153876	117373	3631,56	1,311	32,32
16030000	1	05.09.2013	01.01.1900 12:00	22	1104	180322	132291	4003	1,363	33,04
16030000	1	18.02.2014	01.01.1900 08:16	23	1570	0,881	130202,7	3717,97	1,28	35,02
16030000	1	21.05.2014	01.01.1900 07:00	1	1483	229795	140509	3761,42	1,635	37,36
16030000	1	05.06.2014	01.01.1900 11:45	24	1503	195510,6	142090,5	3677,87	1,376	31,8
16030000	1	21.09.2014	01.01.1900 13:17	25	1073	159570,3	126015,4	3776,48	1,267	33,37
16030000	1	09.02.2015	01.01.1900 08:02	26	1050	172519,2	122384,3	3488,77	1,98	35,08
16030000	1	11.05.2015	01.01.1900 07:38	27	1439	223822	138849	3704,55	1,612	37,48
16030000	1	11.05.2015	01.01.1900 11:31	28	1439	220809	137671	3713,61	1,604	37,07
16030000	1	24.11.2015	01.01.1900 11:41	29	358	81378	100325	3405,11	0,811	29,46
16030000	1	19.03.2016	01.01.1900 07:24	31	890	155273	114392	3557,48	1,357	32,16
16030000	1	19.03.2016	01.01.1900 08:23	30	697	123764	110375	3470,16	1,121	31,81
16030000	1	15.04.2016	01.01.1900 06:32	32	1097	174720,2	121242,5	3547,36	1,441	34,18
16030000	1	16.05.2016	01.01.1900 07:15	31	1223	203070,7	126723,2	3550,18	1,602	35,69
16030000	1	02.06.2016	01.01.1900 06:44	34	1248	206532	129064	3589,99	1,6	35,95
16030000	1	17.07.2016	01.01.1900 13:49	35	1218	198291,2	132174,1	3731,53	1,5	35,42
16030000	1	19.10.2016	01.01.1900 06:16	34	477	93341	101971	3482,25	0,959	29,28
16030000	1	03.11.2016	01.01.1900 09:22	35	482	96498,73	102307,7	3485,71	0,943	29,35
16030000	1	11.02.2017	01.01.1900 07:00	36	1085	171467	123252	3603	1,39	34,2

3.2 RIVER FLOW CHARACTERISTICS

As stated above, Brazilian river data is comparatively well documented and monitored. Discharge measurements as well as cross sectional area surveys for most Brazilian rivers do exist for specific sites. River data is collected in publicly accessible databases such as Hidroweb or ORE-Hybam. This fact distinguishes Brazil from many other countries which either do not have detailed river data of their rivers or do not provide

them publicly. Therefore a data-driven analysis regarding the evaluation of the hydrokinetic river power potential of major Brazilian rivers is assumed to be possible.

For the purpose of this work, river characteristics of interest are those which make a statement about a river's flow regime at a specific site, mainly:

- (1) *discharge, Q* [m³/s],
 - (2) *cross-sectional area, A* [m²],
 - (3) *average flow speed, v* [m/s]
- over a particular cross-sectional area: Q/A

River data acquisition is principally subject to hydrologists and, more rarely, to geologists. For their work, additional data such as water levels, sediment transport and mineral solution are of interest, too. However, those data are not of interest for this particular work. For the purpose to evaluate a river site regarding its potential to deliver hydrokinetic energy, physical space (mainly related to cross-sectional area) and the river's flow speed are of utmost importance. Therefore rivers with high discharges ($Q = A v$) are principally more feasible for a RHK energy application than those with comparatively low discharges.

3.2.1 Discharge Fluctuation

The physical quantity that combines cross-sectional area and flow speed is the discharge. It is therefore the first property to analyze, more precisely: the variation of the discharge over time (usually one year), which is called 'hydrograph' when visualized in a graphic. Generalizing discharge characteristics is difficult, as different rivers have different discharge fluctuations over time. Where there are rivers such as for example the Amazon, which have a comparatively low discharge fluctuation (maximum monthly averaged discharge within one year, Q_{max} , is about twice or tripple as high as its minimum monthly averaged discharge, Q_{min}) there are other rivers, such as for example the Mekong or Ganges (both located in Asia) where their Q_{max} is 10, 20 or even 40 times as high as their Q_{min} (e.g. during monsoon season).

The annual pattern of a river's discharge is the response to the region's climate within the area of its basin: amount/distribution of rain fall, rates of evaporation, snowmelt, floods and droughts. Figure 3.4 and 3.5 are illustrating continuous discharge records (hydrographs) over two years of two sites from different rivers which show differences in the variation of seasonal discharge.

Whereas the discharge fluctuation of the Amazon at Óbidos (Brazil) varies almost harmonically sinusoidal from about 90.000 m³/s during dry season to about 240.000 m³/s at the peak of the rain season ($Q_{max}/Q_{min} = 2.67$), the discharge fluctuation of the Brahmaputra at Bahadurabad (Pakistan) varies from about 3.000 m³/s in the dry season to over 70.000 m³/s during monsoon season ($Q_{max}/Q_{min} = 23$).

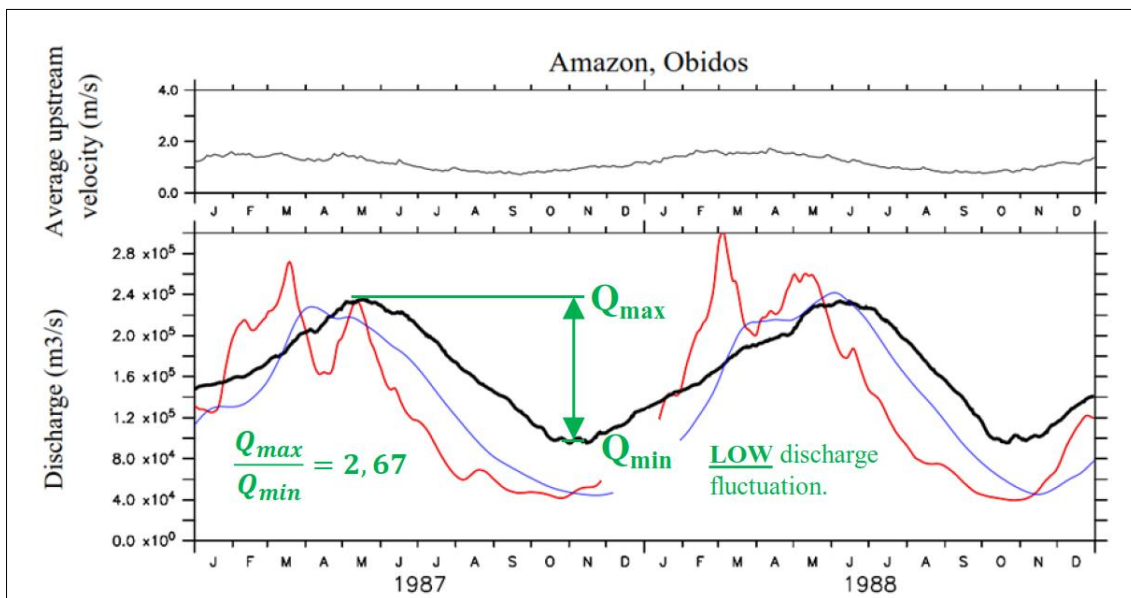


Figure 3.4 Variation of monthly discharge over two years of Amazon River at Óbidos, Brazil. Black line: measurements, blue and red line: discharge prediction models developed by the University of Tokyo [18]

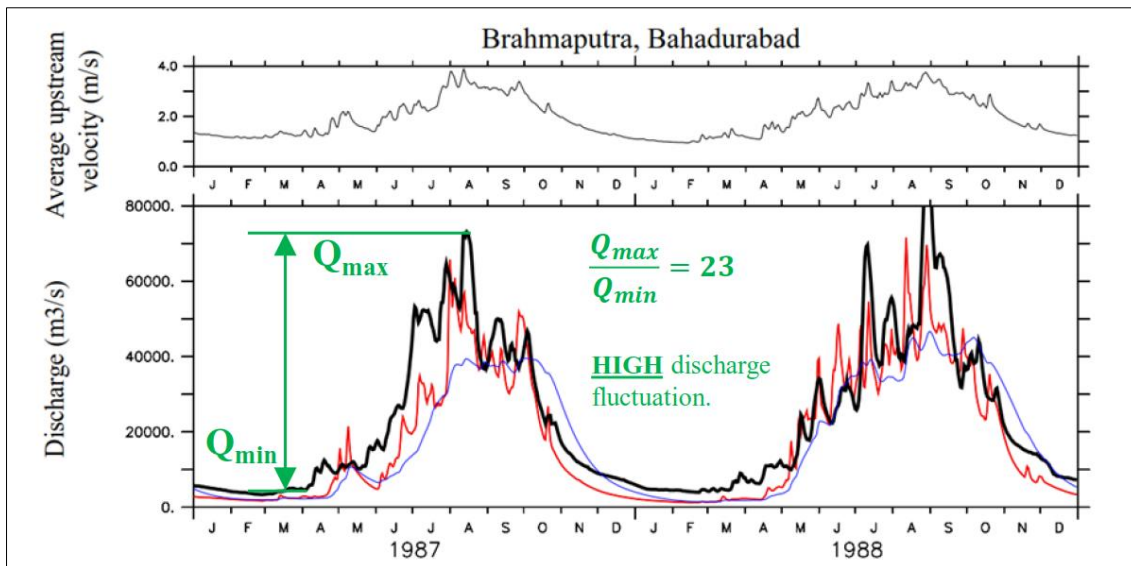


Figure 3.5 Variation of monthly discharge over two years of Bramaputra River at Bahadurabad, Pakistan. Black line: measurements, blue and red line: discharge prediction models developed by the University of Tokyo [18]

The comparison of the two above illustrated discharge records reveals that each river has its unique annual discharge variation pattern that has to be determined by continuous measurements over time.

Nevertheless, continuous discharge records (like Fig.3.4 and 3.5) have not become the characteristic curve to characterize a river's discharge behavior. The established concept to do so is by illustrating its Flow Duration Curve (FDC).

3.2.2 Flow Duration Curve

Flow Duration Curves (FDCs) are generated out of many years of continuously recorded discharge measurements by illustrating the duration exceedance in percentage of a certain discharge over a certain investigated period of time (usually many years); see right part of Figure 3.6. FDCs therefore carry information about extreme discharge events such as floods and droughts in the very low and very high percentage regions respectively.

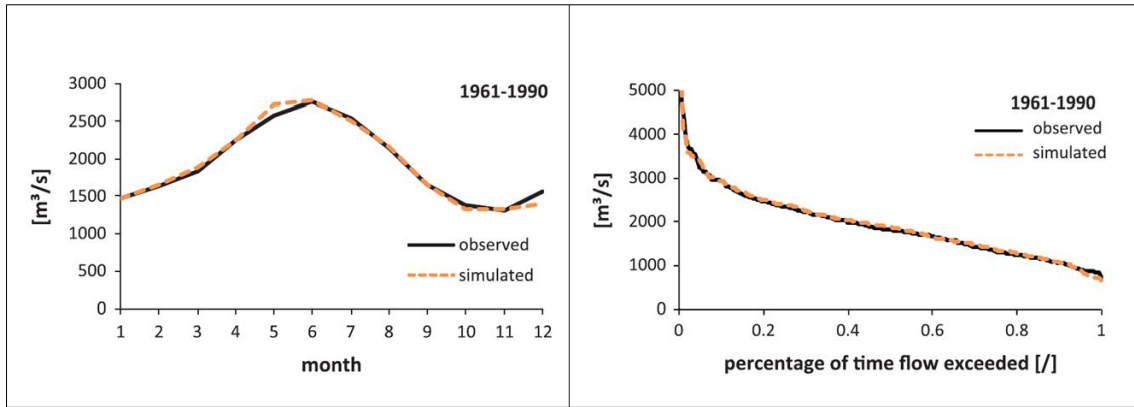


Figure 3.6 Seasonal runoff and corresponding monthly flow duration curve of the Danube at Vienna [19]

FDCs are being used to describe the flow regime of a river. An empirical flow duration curve (FDC) graphically represents the percentage of time (or duration) in which the stream flow has been equaled or exceeded over a historical period of time [20]. It combines in one curve the flow characteristics of a stream throughout the range of discharge, without regard to the sequence of occurrence. If the period upon which the curve is based represents the long term flow of a stream, the curve may be used to predict the distribution of future flows for water power, water supply, and pollution studies [21]. Flow Duration Curves can be displayed in several forms regarding the scaling of the x- and y-axis, see Figure 3.7.

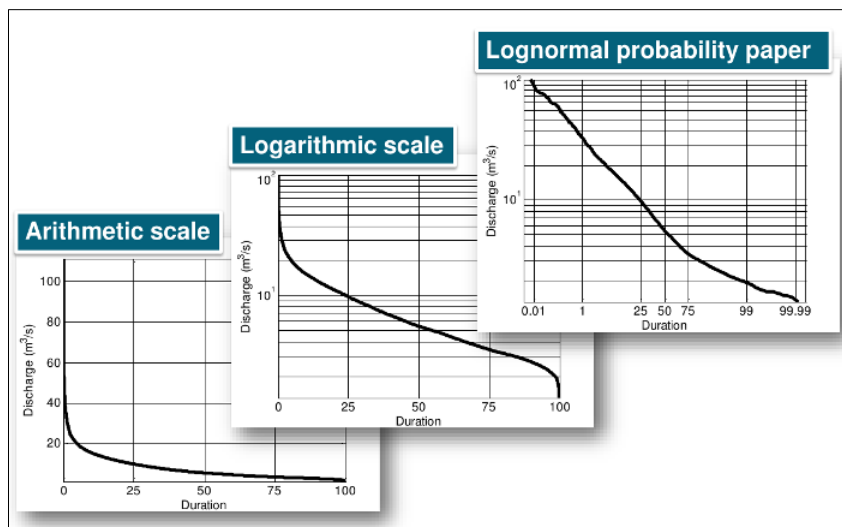


Figure 3.7 Graphical representations of Flow Duration Curves from an observed hydrograph [20]

Flow Duration Curves, depending on the time discharge measurements have been recorded, contain extreme flow regimes such as floods and droughts. These events occur rarely but have a significant influence on the shape of the curves, see Figure 3.8.

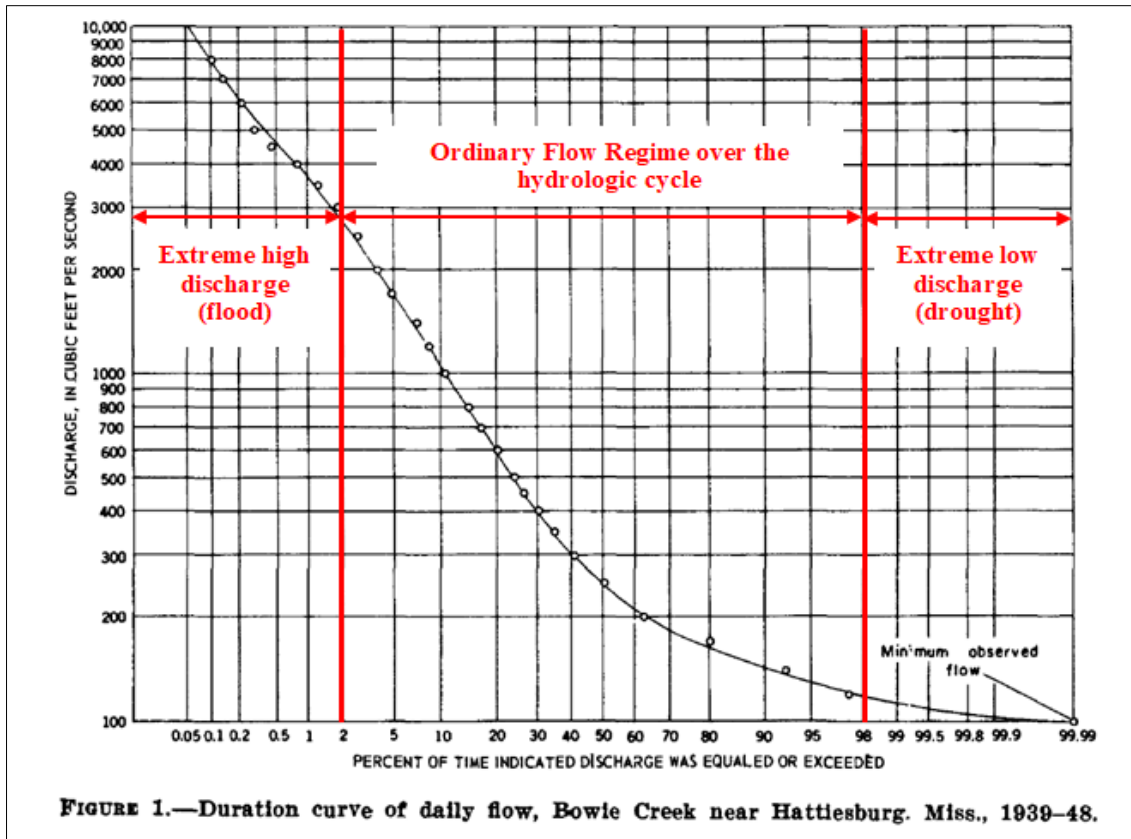


Figure 3.8 Flow Duration Curve constructed of daily records over 10 years of the Bowie River near Hattiesburg, State of Mississippi [21], with added lines and commentaries (red) by the author

Extreme flow regimes of a river do play an important role for issues such as flood control or water scarcity but have a low impact on the annual energy production on any hydropower facility as a consequence to the short period of time those states last within a year. Due to fragmentary river data recordings, which are present for most sites, the extreme flow regimes for the majority of river sites cannot be represented in Flow Duration Curves. The scarcity of recorded data leads to other approaches regarding the creation of FDCs for given sites. A common method uses monthly averaged discharge data points to build the FDCs. This approach will be applied and explained in detail in the carried out river resource study (Chapter 3.3).

3.2.3 Estimation of River Flow Velocity

In hydrology, there are many ways to describe a flow and the velocity of such. However, three concepts are dominant to estimate the average river flow speed present in a certain defined river or channel section. These are:

- (1) the Volumetric Flow Rate Approach;
- (2) Hydraulic Geometry Relationships
- (3) the Manning Equation.

All concepts relate the average flow velocity v to other properties and thus all methods vary in their results. In this work, Hydraulic Geometry Relationships as well as the Manning Equation will just be discussed superficially, as they will not be further applied in this thesis. They are mentioned and recognized for the purpose of completeness.

3.2.3.1 Volumetric Flow Rate Approach

In fluid mechanics and hydrometry the volumetric flow rate (\dot{V}) or discharge (Q) is defined as the volume of fluid which passes per unit of time through a certain cross-sectional area/surface (A), eq. (3.1), (3.2).

$$Q = \dot{V} = \lim_{\Delta t \rightarrow 0} \frac{\Delta V}{\Delta t} = \frac{dV}{dt} \quad (3.1)$$

For plane, flat cross-sectional areas or surfaces, it is defined by:

$$Q = v \cdot A \quad (3.2)$$

where:

v	<i>averaged river flow velocity</i>	[m/s]
Q	<i>discharge</i>	[m ³ /s]
A	<i>cross-sectional area</i>	[m ²]

Out of equation (3.2), the averaged river flow speed (v) can be determined as: $v = \frac{Q}{A}$.

For curved surfaces, eq. (3.2) is written in integral form:

$$Q = \iint_A v \cdot dA \quad (3.3)$$

This simple relationship, eq. (3.2), describes the general flow through a given river section well.

However, among some researchers and experts a drive towards a deeper scientification to determine river flow speed can be observed with the result of more complex formulations describing river flow velocity. (Two of the most common among those approaches are stated in the following two sections: 3.2.3.2 and 3.2.3.3.)

3.2.3.2 Hydraulic Geometry Relationships

Leopold and Maddock [21] established the concept of hydraulic geometry. They defined a set of equations in which hydraulic variables were primarily a function of river discharge [22]. A subset of these variables was related to each other through continuity.

$$w = aQ^b \quad (3.4)$$

$$d = cQ^f \quad (3.5)$$

$$v = kQ^m \quad (3.6)$$

Continuity results in:

$$Q = w d v = aQ^b \cdot cQ^f \cdot kQ^m \quad (3.7)$$

and therefore:

$$b + f + m = 1 \quad (3.8)$$

$$a \cdot c \cdot k = 1 \quad (3.9)$$

where:

w	<i>stream width</i>	[m]
d	<i>average depth</i>	[m]
v	<i>average velocity</i>	[m/s]
Q	<i>flow, discharge</i>	[m ³ /s]
a, c, k	<i>empirical coefficients</i>	[-]
b, f, m	<i>empirical exponents</i>	[-]

Hydraulic geometry estimations have some difficulties regarding their accurate application due to the various coefficients which are involved in their formulations. If the coefficients are not exactly determined, results are of low accuracy. This makes their proper application more difficult than for example the volumetric flow rate approach.

3.2.3.3 Manning Equation

The so called Manning Equation, or sometimes also cited as the Gauckler-Manning-Strickler Equation, is a flow formula coming from the Irish Engineer Robert Manning and was published first in 1891 in the “Transactions of the Institution of Civil Engineers”, Ireland [24]. Manning at the time studied seven existing river/channel flow formulas with the goal to simplify them and at the same time exceed their accuracy. He came up with the following conclusion, the Manning Formula:

$$v = k_{St} \sqrt[3]{(HR)^2} \sqrt{s} \quad (3.10)$$

where:

v	<i>average river flow velocity</i>	[m/s]
k_{St}	<i>river bed roughness (Strickler)</i>	[m ^{1/3} /s]
HR	<i>hydraulic radius of river channel, with: $HR = A/U$ $A =$ cross-section area, and $U =$ circumference of cross section <u>without</u> the free surface</i>	[m]
s	<i>river bed slope</i>	[m/m]

Similar to the hydraulic geometry formulas, the Manning Equation consists of various variables which have to be determined as exactly as possible to achieve an accurate result for the flow velocity. However estimations for the river bed roughness or the slope are often not as simple as they may seem to be. This is why for further flow speed estimations in this work the simple volumetric flow rate approach ($v = \frac{Q}{A}$) will be applied, especially because for many sites there are existing data recordings for Q and A and it is assumed that these measurements were properly recorded.

3.3 BRAZILIAN RIVER RESOURCE STUDY

In this chapter a river resource analysis consisting of 15 real existing river sites is presented. For each site discharge and flow speed characteristics are illustrated and their potential regarding hydrokinetic power extraction (based on the available flow data) is evaluated. The process of how this resource study has been carried out is documented step by step from the initial intention throughout adaptations during the process until the final results (comparison with established tidal flow speed distributions).

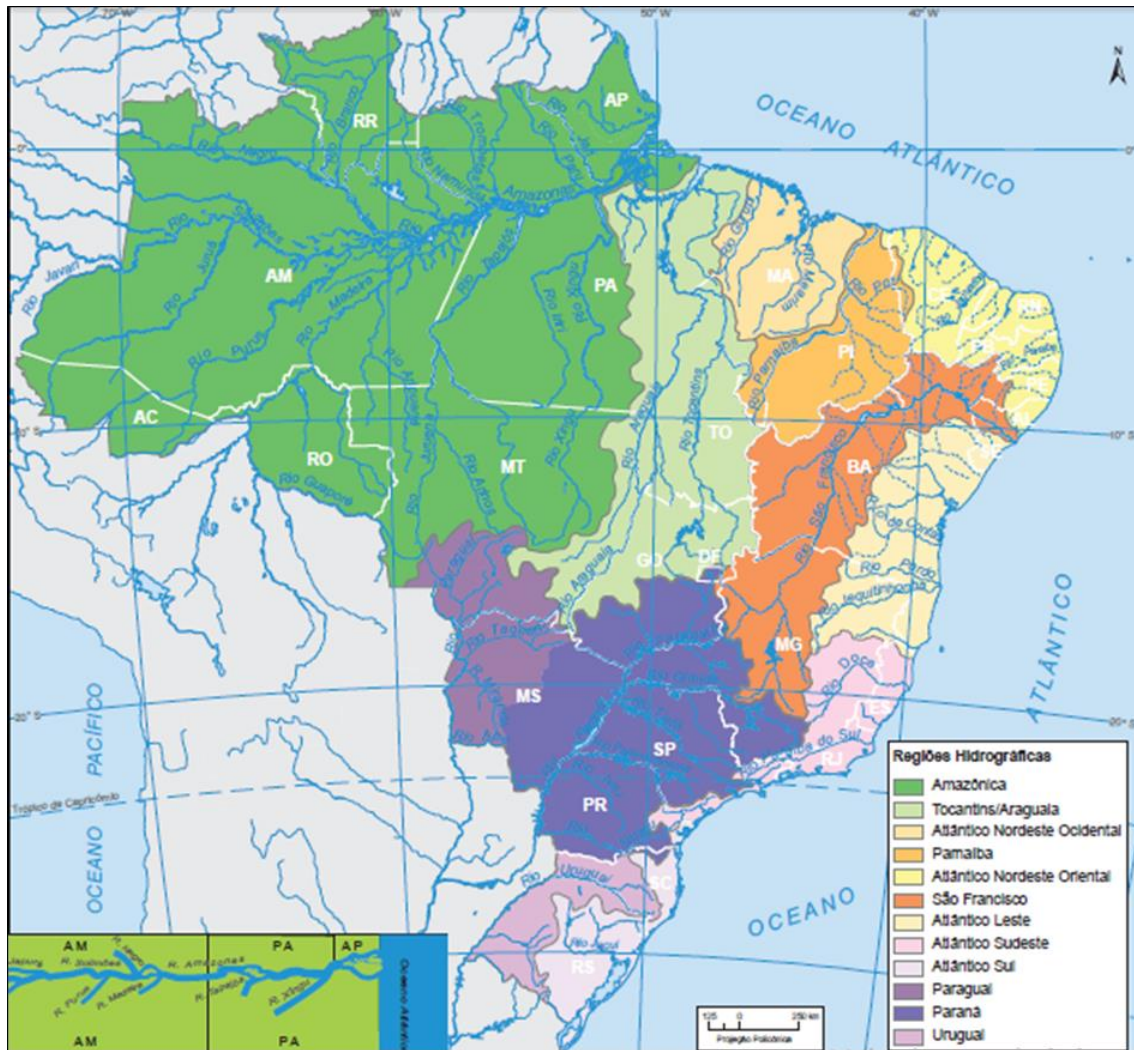


Figure 3.9 Hydrographic regions in Brazil, Source: IBGE (www.ibge.gov.br)

3.3.1 Initial Intention

Initially the objective of this study was the identification of suitable river sites for potential hydrokinetic power extraction downstream of existing large hydropower plants. The idea behind that approach results from the fact that the positioning of a hydrokinetic turbine downstream of a hydropower plant would guarantee some for such operation convenient conditions:

- (1) water cleanness (no debris which may could damage turbines),
- (2) existing grid infrastructure (produced electricity could be fed into the hydropower plants power supply system),
- (3) predictable power extraction (discharge which passes through hydropower plant is always known).

However, this approach did not result in the desired outcome, as flow data downstream of hydropower plants in most cases are either not accessible or existent in the Hidroweb database. However, extinct dam discharge data is available through the Nacional Electricity System Operator (port.: Operador Nacional do Sistema Elétrico – ONS) who published discharge data on most Brazilian Dams on its website (<http://ons.org.br/>). Yet, this data does not include any information on the flow speed downstream of the dam as the cross-sectional area is not known.

Nethertheless 43 hydropower plants located along major Brazilian rivers throughout the entire country have been investigated. Table 3.2 and 3.3 are listing information about the hydropower plants which have been investigated. The data listed there is exclusively from Hidroweb.

Table 3.2 List of hydropower plants investigated for downstream data (part 1)

	general information	averaged annual discharge [m³/s]	width at site [m]	depth at site [m]	averaged annual flow speed [m/s]	Comments
• Paranaíba River (tributary of Rio Paraná)	MG, GO	796				
- UHE Emborcação	1,19 GW; Δh = 85 m	DOWNSTREAM DATA NOT ACCESSIBLE OR NOT EXISTING				Downstream data worth knowing
- UHE Itumbiara	2,08 GW; Δh = 81 m	DOWNSTREAM DATA NOT ACCESSIBLE OR NOT EXISTING				Downstream data worth knowing
- UHE Cachoeira Dourada	0,65 GW; Δh = 30 m	DOWNSTREAM DATA NOT ACCESSIBLE OR NOT EXISTING				Downstream data worth knowing
- UHE São Simão	1,71 GW; Δh = 71 m	DOWNSTREAM DATA NOT ACCESSIBLE OR NOT EXISTING				Downstream data worth knowing
- UHE Davinópolis	0,21 GW; Δh = 81 m	DOWNSTREAM DATA NOT ACCESSIBLE OR NOT EXISTING				-
• Rio Grande (tributary of Rio Paraná)	MG, SP	2.400				
- UHE de Furnas	1,22 GW; Δh = 127 m	1687	240	8,28	0,77	Low flow speed
- UHE de Camargos	46 MW; Δh = 36 m	DOWNSTREAM DATA NOT ACCESSIBLE OR NOT EXISTING				Downstream data seems interesting
- UHE Itutinga	52 MW; Δh = 23 m	DOWNSTREAM DATA NOT ACCESSIBLE OR NOT EXISTING				Downstream data seems interesting
- UHE Funil	180 MW; Δh = 50 m	DOWNSTREAM DATA NOT ACCESSIBLE OR NOT EXISTING				-
- UHE Mascarenhas de Moraes	476 MW; Δh = 51 m	DOWNSTREAM DATA NOT ACCESSIBLE OR NOT EXISTING				Downstream data seems interesting
- UHE Luís Carlos Barreto de Carvalho	1,05 GW; Δh = 92 m	DOWNSTREAM DATA NOT ACCESSIBLE OR NOT EXISTING				Downstream data worth knowing
- UHE Jaguará	424 MW; Δh = 40 m	DOWNSTREAM DATA NOT ACCESSIBLE OR NOT EXISTING				Downstream data seems interesting
- UHE Igarapava	210 MW; Δh = unknown	DOWNSTREAM DATA NOT ACCESSIBLE OR NOT EXISTING				Downstream seems slow
- UHE Volta Grande	380 MW; Δh = 56 m	DOWNSTREAM DATA NOT ACCESSIBLE OR NOT EXISTING				Downstream seems interesting
- UHE Porto Colômbia	320 MW; Δh = 40 m	DOWNSTREAM DATA NOT ACCESSIBLE OR NOT EXISTING				Downstream seems slow
- UHE Marimbondo	1,44 GW; Δh = 91 m	DOWNSTREAM DATA NOT ACCESSIBLE OR NOT EXISTING				Downstream data worth knowing
- UHE Água Vermelha	1,39 GW; Δh = 57 m	DOWNSTREAM DATA NOT ACCESSIBLE OR NOT EXISTING				Downstream data worth knowing
• Rio Tietê (tributary of Rio Paraná)	SP	2.500				
- UHE Três Irmaos	807 MW; Δh = 82 m	DOWNSTREAM DATA NOT ACCESSIBLE OR NOT EXISTING				Downstream data seems interesting
• Rio Paranapanema (tributary of Rio Paraná)	SP, PR					
- UHE Capivara	619 MW; Δh = 60 m	1.463	361	3,69	0,88	Low flow speed
- UHE Rosana	372 MW; Δh = 17 m	DOWNSTREAM DATA NOT ACCESSIBLE OR NOT EXISTING				Downstream data seems interesting
- UHE Chavantes	414 MW; Δh = 83 m	336	170	3,65	0,53	Low flow speed
- UHE Taquarucu	554 MW; Δh = 23 m	DOWNSTREAM DATA NOT ACCESSIBLE OR NOT EXISTING				Downstream seems slow
- UHE Jurumirim	100 MW; Δh = 55 m	DOWNSTREAM DATA NOT ACCESSIBLE OR NOT EXISTING				Downstream seems slow
• Rio Iguaçu (tributary of Rio Paraná)	PR, SC	1.413				
- UHE Foz do Areia	1,67 GW; Δh = 120 m	585,95	115,59	3,44	1,26	on the ground site assessment maybe interesting
- UHE Governador Ney Aminithas	1,26 GW; Δh = 145 m	DOWNSTREAM DATA NOT ACCESSIBLE OR NOT EXISTING				Downstream data seems interesting
- UHE de Salto Santiago	1,42 GW; Δh = 106 m	DOWNSTREAM DATA NOT ACCESSIBLE OR NOT EXISTING				Downstream data seems interesting
- UHE de Salto Osório	1,08 GW; Δh = 72 m	894,28	257,44	6,10	0,58	Downstream seems slow
- UHE de Salto Caxias	1,24 GW; Δh = 67 m	1887,70	326,38	9,45	0,54	on the ground site assessment maybe interesting
• Rio Paraná	SP, MS, PR	17.290				
- UHE Ilha Solteira	3,44 GW; Δh = 41 m	DOWNSTREAM DATA NOT ACCESSIBLE OR NOT EXISTING				Downstream seems slow
- UHE Engenheiro Souza Dias (Jupú)	1,55 GW; Δh = 21 m	7.299,45	866,05	8,46	0,89	on the ground site assessment maybe interesting
- UHE Porto Primavera	1,54 GW; Δh = 19 m	DOWNSTREAM DATA NOT ACCESSIBLE OR NOT EXISTING				Downstream data seems interesting
- UHE Itaipú	14 GW; Δh = 118 m	DOWNSTREAM DATA NOT ACCESSIBLE OR NOT EXISTING				Downstream data seems interesting
• Rio São Francisco	MG, BA, PE, AL, SE	2.943				
- UHE de Xingó	3,16 GW; Δh = 140 m	DOWNSTREAM DATA NOT ACCESSIBLE OR NOT EXISTING				Downstream data seems interesting
- UHE de Paulo Afonso	4,28 GW; Δh = 80 m	DOWNSTREAM DATA NOT ACCESSIBLE OR NOT EXISTING				Downstream data seems interesting

Table 3.3 List of hydropower plants investigated for downstream data (part 2)

• Rio Sao Francisco	MG, BA, PE, AL, SE	2,943				
- UHE de Xingó	3,16 GW; Δh = 140 m	DOWNSTREAM DATA NOT ACCESSIBLE OR NOT EXISTING		Downstream data seems interesting		
- UHE de Paulo Afonso	4,28 GW; Δh = 80 m	DOWNSTREAM DATA NOT ACCESSIBLE OR NOT EXISTING		Downstream data seems interesting		
• Rio Tocantins	GO, TO, MA, PA	13,598				
- UHE de Cana Brava	450 MW; Δh = unknown	DOWNSTREAM DATA NOT ACCESSIBLE OR NOT EXISTING		Downstream data seems interesting		
- UHE de Serra da Mesa	1,27 GW; Δh = unknown	DOWNSTREAM DATA NOT ACCESSIBLE OR NOT EXISTING		Downstream seems slow		
- UHE de Sao Salvador	243 MW; Δh = unknown	DOWNSTREAM DATA NOT ACCESSIBLE OR NOT EXISTING		Downstream seems slow		
- UHE de Luiz Eduardo Magalhaes	902 MW; Δh = unknown	DOWNSTREAM DATA NOT ACCESSIBLE OR NOT EXISTING		Downstream seems slow		
- UHE de Estreito	1,08 GW; Δh = unknown	DOWNSTREAM DATA NOT ACCESSIBLE OR NOT EXISTING		-		
- UHE de Tucuruí	8,3 GW; Δh = 65 m	10,559,66	1,378,34	8,85	0,74	on the ground assessment maybe interesting
• Rio Araguaia (tributary of Rio Tocantins)	GO, MT, TO, PA	5,400				NO MENTIONABLE HYDRO POWER PLANTS
• Rio Xingú (tributary of Amazon)	MT, PA	9,700				
- UHE Belo Monte	11,23 GW; Δh = 89 m	DOWNSTREAM DATA NOT ACCESSIBLE OR NOT EXISTING				
• Rio Tapajós (tributary of Amazon)	PA, AM	13,540				NO HYDRO POWER PLANTS PERMITTED (YET)
• Rio Madeira (tributary of Amazon)	RO, AM	31,200				
- UHE Jirau	3,75 GW; Δh = 62 m	DOWNSTREAM DATA NOT ACCESSIBLE OR NOT EXISTING				
- UHE Santo Antonio	3,57 GW; Δh = 13,5 m	DOWNSTREAM DATA NOT ACCESSIBLE OR NOT EXISTING				

Due to the low rate of accessible and therefore analyzable downstream data regarding flow speed, the investigation for potential suitable sites has been decided to be extended. It was searched subsequently for data of free-streaming river sites of major Brazilian rivers. This second approach of investigation was rather more promising than the first attempt. Data could have been extracted for 14 new river sites (see section 3.3.2 below).

3.3.2 Extended Data Acquisition

The investigation for free-streaming river sites revealed data available for additional 14 chosen sites all located in Brazil's Northern Region. These sites are located either directly at the Amazon or at tributaries of it. Table 3.4 illustrates the results for the investigated free-streaming river sites.

Table 4 reveals that the Amazon sites all show averaged annual flow speeds of over 1,25 m/s which positively distinguished them from the other free-streaming sites. Even

though half of the 14 sites show lower annual flow speeds than 1,25 m/s their discharge and flow speed variation over the year has been analyzed, too. So that finally 15 sites (all free-streaming river sites with the exception of “Parintins” plus two downstream hydropower plant sites: “UHE Jupia” and “UHE Tucuru”) were analyzed and compared with regards to their annual discharge fluctuation and consequently flow speed variation and distribution over the year.

Table 3.4 List of investigated free-streaming river sites

	general information	averaged annual discharge [m ³ /s]	width at site [m]	depth at side [m]	averaged annual flow speed [m/s]	Comments
• Amazon River	AM, PA, AP	209.000				
- Teresina	Population: N/A	44.135	2098,38	14,81	1,38	on the ground site assessment maybe interesting
- São Paulo de Olivença	Population: 14.267	46.996	1503,28	19,61	1,56	on the ground site assessment maybe interesting
- Manacapuru	Population: 95.000	104.518	3176,53	24,37	1,32	on the ground site assessment maybe interesting
- Itacoatiara	Population: 98.000	154.785	3589,47	32,82	1,29	on the ground site assessment maybe interesting
- Parintins	Population: 112.000	~ 170.000	3276,12	40,52	~ 1,3	on the ground site assessment maybe interesting
- Óbidos	Population: 50.000	180.000	2600,00	50-60	1,7	on the ground site assessment maybe interesting
• Rio Madeira (tributary of Amazon)	RO, AM	31.200				
- Manicoré	Population: 53.000	24754,21	845,24	20,25	1,31	on the ground site assessment maybe interesting
- Foz do Madeira	Population: N/A	30308,40	1138,93	24,31	1,07	
• Rio Purus (tributary of Amazon)	AC, AM	11.000				GENERALLY LOW FLOW SPEED
- Beruri	Population: 18.579	13.066,84	1115,43	18,52	0,58	Interesting site maybe 2 km downstream
• Rio Juruá (tributary of Amazon)	AC, AM	8.440				
- Gavião	Population: N/A	4.750	335	13,21	0,93	-
• Rio Negro (tributary of Amazon)	AM	28.400				GENERALLY LOW FLOW SPEED
- Curicuriari	Population: N/A	12077,96	1287,84	12,46	0,91	-
- Manaus	Population: 2.100.000	34421,25	2570,03	32,79	0,39	-
- Tatu	Population: N/A	29233,14	2647,07	32,03	0,33	-
• Rio Japurá (tributary of Amazon)	AM	18.620				NO SITES IDENTIFIED
• Rio Branco (tributary of Amazon)	RR	5.400				GENERALLY LOW FLOW SPEED
- Caracaraí	Population: 20.000	2.934,78	556,8	6,73	0,67	-

3.3.3 River Data Processing

In order to make river data of different recording quality comparable, a common denominator with which all river data sets could cope with has to be determined. This means that a form of representing all the data sets under the same criteria has to be defined. Ideally, a hydrograph is constructed of as many data points as possible (e.g. daily records at site over one year) and the ideal flow duration curve is built also out of as many continuously recorded data points over several years. Unfortunately, in reality, data recordings of such quality are rare. Most times, recorded site data consists of few single recordings taken over a certain year (at randomly chosen points in time in that year) over a period of several years. This fact leads to the decision that the representative data points out of which further hydrographs and flow duration curves for the each site being generated will be arithmetically monthly averaged values.

3.3.3.1 Determining monthly averaged data points

Following, the above explained approach is illustrated (see Tables 3.5, 3.6, and Figure 3.10).

First, the data of the original data measurement sheet (compare Table 3.1) is re-sorted into a monthly sequence, meaning that first all recordings from January are listed (regardless of the year of recording) then the recordings of February and so forth.

Second, the re-sorted recordings are arithmetically averaged for each month (Table 3.5).

Third, the monthly averaged values are compiled in a separate table (Table 3.6).

Finally, the monthly averaged flow speeds (in Table 3.6 expressed as “VelMedia”, from Portuguese “Velocidade Media”, meaning “average velocity”) is plotted over 24 months (repeating itself after 12 month) to visualize the flow speed fluctuation over the hydrologic cycle (Figure 3.10) at a particular site.

Table 3.5 Re-sorted and monthly averaged measurement data sheet, Itacoatiara, Amazon River, Brazil

//----- // // Sistema de Informações Hidrológicas Itacoatiara // Versão Web 3.0 // S 2001 Agencia Nacional de Águas (ANA) // // NivelConsistencia: 1 = Bruto, 2 = Consistido // // Restrições da consulta: // Código da Estação: 16030000 //-----											
month	//EstacaoCodigo	NivelConsistencia	Data	Hora	NumMedicao	Cota	Vazao	AreaMolhada	Largura	VelMedia	Profundidade
1	16030000	1	27.01.2011	14:42:00	13	731	123250,9	106933,6	3311,19	1,153	32,29
							123250,90	106933,60	3311,19	1,15	32,29
2	16030000	1	07.02.2010	14:35:00	10	928	149309	111847	3460,21	1,335	32,32
2	16030000	1	04.02.2013	07:39:00	20	911	153876	117373	3631,56	1,311	32,32
2	16030000	1	18.02.2014	08:16:00	23	1570	0,881	130202,7	3717,97	1,28	35,02
2	16030000	1	09.02.2015	08:02:00	26	1050	172519,2	122384,3	3488,77	1,98	35,08
2	16030000	1	11.02.2017	07:00:00	36	1085	171467	123252	3603	1,39	34,2
							161792,80	121011,80	3580,30	1,46	33,79
3	16030000	1	21.03.2008	15:07:00	1	1245	187340	127658	3898,89	1,468	32,74
3	16030000	1	18.03.2009	16:54:00	7	1311	190832	127638	3491	1,496	36,57
3	16030000	1	12.03.2012	11:40:00	17	1294	213151	127923	3495	1,67	36,61
3	16030000	1	19.03.2016	07:24:00	31	890	155273	114392	3557,48	1,357	32,16
3	16030000	1	19.03.2016	08:23:00	30	697	123764	110375	3470,16	1,121	31,81
							174072,00	121597,20	3582,51	1,42	33,98
4	16030000	1	15.04.2016	06:32:00	32	1097	174720,2	121242,5	3547,36	1,441	34,18
							174720,20	121242,50	3547,36	1,44	34,18
5	16030000	1	19.05.2008	13:13:00	2	1386	186471	135295	3970	1,378	34,08
5	16030000	1	14.05.2010	12:57:00	11	1319	210165	127662	3538,9	1,646	36,07
5	16030000	1	18.05.2011	14:50:00	14	1357	181403	139576	3732	1,303	37,4
5	16030000	1	21.05.2014	07:00:00	1	1483	229795	140509	3761,42	1,635	37,36
5	16030000	1	11.05.2015	07:38:00	27	1439	223822	138849	3704,55	1,612	37,48
5	16030000	1	11.05.2015	11:31:00	28	1439	220809	137671	3713,61	1,604	37,07
5	16030000	1	16.05.2016	07:15:00	31	1223	203070,7	126723,2	3550,18	1,602	35,69
							207933,67	135183,60	3710,09	1,54	36,45
6	16030000	1	17.06.2008	11:11:00	3	1410	195080	131960	3863	1,478	34,16
6	16030000	1	26.06.2012	06:56:00	18	1447	227328,5	132991,7	3811,22	1,71	34,89
6	16030000	1	05.06.2014	11:45:00	24	1503	195510,6	142090,5	3677,87	1,376	31,8
6	16030000	1	02.06.2016	06:44:00	34	1248	206532	129064	3589,99	1,6	35,95
							206112,78	134026,55	3735,52	1,54	34,20
7	16030000	1	24.07.2008	05:59:00	4	1305	182755	130785	3823	1,398	34,21
7	16030000	1	07.07.2009	07:23:00	8	1490	203136	132378	4082	1,535	32,43
7	16030000	1	17.07.2016	13:49:00	35	1218	198291,2	132174,1	3731,53	1,5	35,42
							194727,40	131779,03	3878,84	1,48	34,02
8	16030000	1	23.08.2008	09:24:00	5	1116	151421	121140	3757	1,25	32,24
8	16030000	1	30.08.2010	06:08:00	12	885	130096,4	110892,7	3503,35	1,173	31,65
8	16030000	1	04.08.2011	13:27:00	15	1264	174180	128724	3597,68	1,353	35,78
							151899,13	120252,23	3619,34	1,26	33,22
9	16030000	1	05.09.2013	12:00:00	22	1104	180322	132291	4003	1,363	33,04
9	16030000	1	21.09.2014	13:17:00	25	1073	159570,3	126015,4	3776,48	1,267	33,37
							169946,15	129153,20	3889,74	1,32	33,21
10	16030000	1	07.10.2009	15:35:00	9	724	110133	104953	3352,36	1,049	31,31
10	16030000	1	27.10.2012	10:49:00	19	388	81826,66	94150,83	3298,08	0,869	28,55
10	16030000	1	19.10.2016	06:16:00	34	477	93341	101971	3482,25	0,959	29,28
							95100,22	100358,28	3377,56	0,96	29,71
11	16030000	1	08.11.2008	11:15:00	6	793	98026	95323	3631	1,028	26,25
11	16030000	1	24.11.2015	11:41:00	29	358	81378	100325	3405,11	0,811	29,46
11	16030000	1	03.11.2016	09:22:00	35	482	96498,73	102307,7	3485,71	0,943	29,35
							91967,58	99318,57	3507,27	0,93	28,35
12	16030000	1	14.12.2011	15:11:00	16	551	105892,7	101386,5	3333,86	1,044	30,41
							105892,70	101386,50	3333,86	1,04	30,41

Table 3.6 Monthly averaged recordings for discharge („Vazao“), cross sectional area („AreaMolhada“), width at free surface („Largura“), average flow speed („VelMedia“), and depth („Profundidade“)

month	Monthly Averaged Data (Itacoatiara)				
	Vazao [m³/s]	AreaMolhada [m²]	Largura [m]	VelMedia [m/s]	Profundidade [m]
1	123251	106933,60	3311,19	1,15	32,29
2	161793	121011,80	3580,30	1,46	33,79
3	174072	121597,20	3582,51	1,42	33,98
4	174720	121242,50	3547,36	1,44	34,18
5	207934	135183,60	3710,09	1,54	36,45
6	206113	134026,55	3735,52	1,54	34,20
7	194727	131779,03	3878,84	1,48	34,02
8	151899	120252,23	3619,34	1,26	33,22
9	169946	129153,20	3889,74	1,32	33,21
10	95100	100358,28	3377,56	0,96	29,71
11	91968	99318,57	3507,27	0,93	28,35
12	105893	101386,50	3333,86	1,04	30,41
Average (year)	154784,63	118520,26	3589,47	1,29	32,82

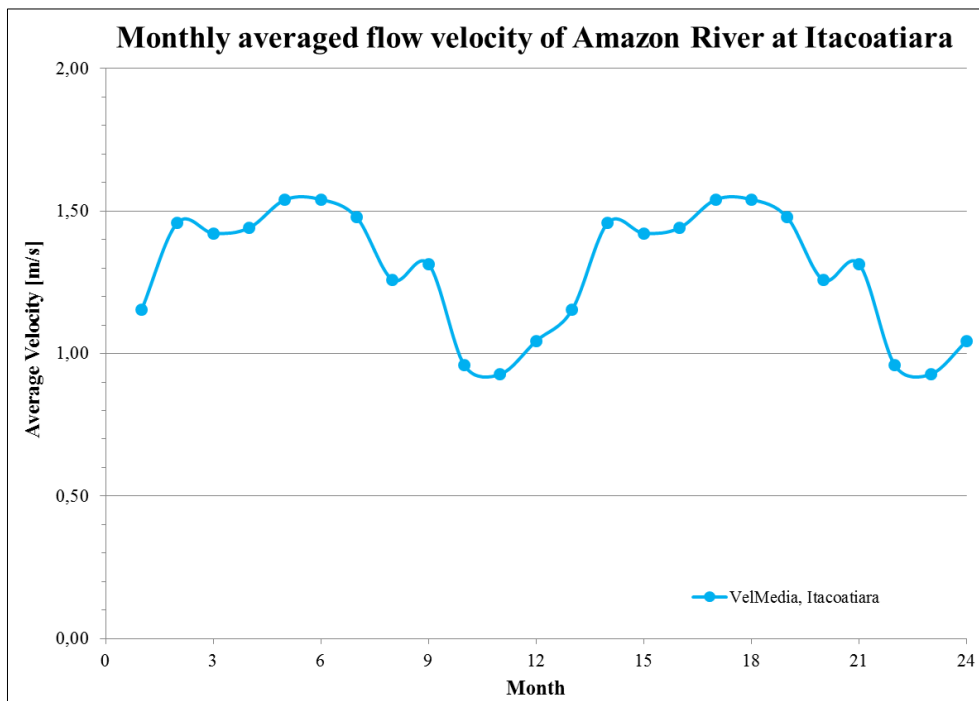


Figure 3.10 Hydrograph, built out of monthly averaged flow velocity data points of site (Table 3.6), Amazon River at Itacoatiara, AM, Brazil

This process has been performed for all 15 sites (see Appendix I).

In order to follow the goal of comparison of the each river sites to each other, additional data manipulation had to be carried out.

3.3.3.2 Creating dimensionless Flow Duration Curves (FDCs)

What characterizes a river's flow regime is the discharge fluctuation over the hydrologic cycle (one year). As discussed in chapter 3.2, different rivers show different discharge fluctuations (over time). Their differences become noticeable when illustrating the each flow duration curve in dimensionless form. Therefore the monthly averaged discharge values were plotted in the form of a dimensionless flow duration curve. This curve illustrates Q/Q_{\max} over the percentage of time the flow equals or exceeds a certain Q/Q_{\max} ratio, so that the y-axis ranges from 0 to 1 and the x-axis from 0 to 100 %. Further, so called discharge classes have been defined based on the comparison of the flow duration curves of the investigated sites (empirical process). The analyses of the different dimensionless flow duration curves revealed that rivers do show similarities regarding their discharge variation behavior. This is exhibited through the illustration of the values of Q_{\min}/Q_{\max} and the shape the curve shows between the two points: Q_{\max}/Q_{\max} and Q_{\min}/Q_{\max} . This is exemplary showed in Figure 3.11. The dimensionless flow duration curves for each site has been created using a self-programmed Matlab application. Figure 3.12, 3.13, and 3.14 are showing dimensionless FDCs for three analyzed sites (each allocated to one of the defined Discharge Classes).

The Reference Curves have been defined out of empirical analyses. Following, mathematical relations have been defined to describe the several discharge variations (Table 3.7):

Table 3.7 Mathematical formulation of the Reference Discharge Classes

Discharge Class 1				Discharge Class 2				Discharge Class 3			
x	0	0.4	1	x	0	0.5	1	x	0	0.4	1
y	1	0.8	0.4	y	1	0.6	0.2	y	1	0.5	0.125
$y = -0.1667 x^2 - 0.4333 x + 1$				$y = -0.8 x + 1$				$y = 0.625 x^2 - 1.5 x + 1$			

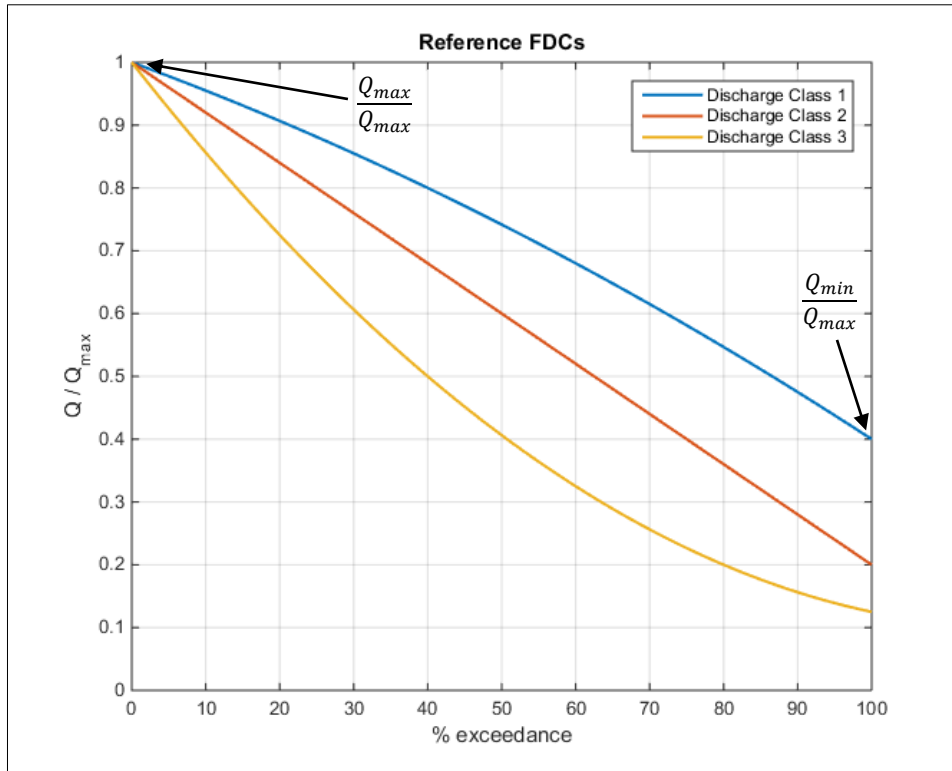


Figure 3.11 Defined Reference Flow Duration Curves

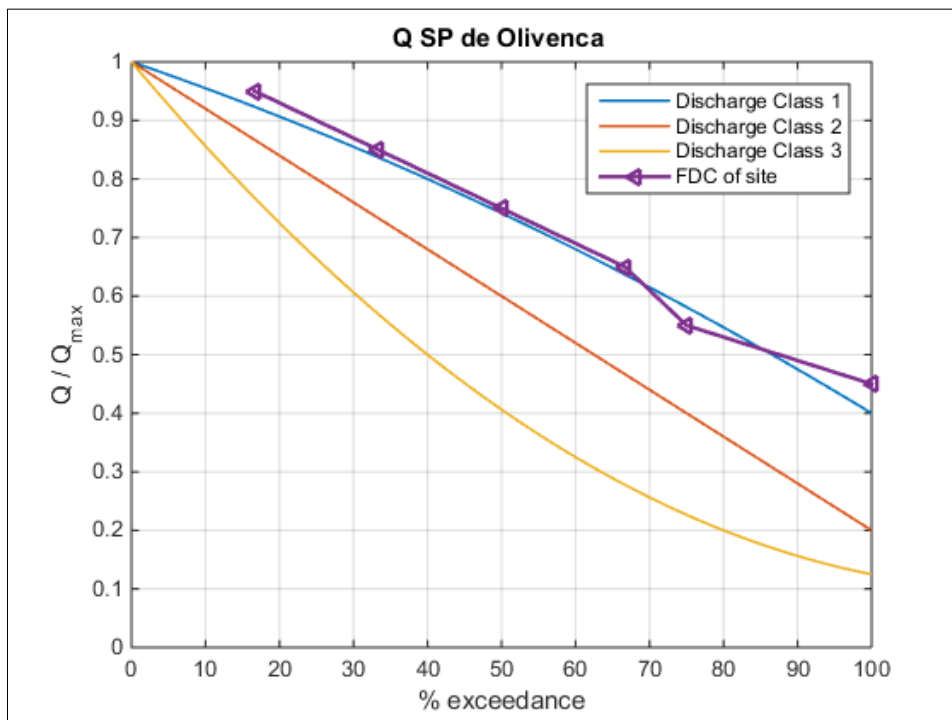


Figure 3.12 Dimensionless FDC of the Amazon River at São Paulo de Olivença, AM, Brazil (Discharge Class 1 site)

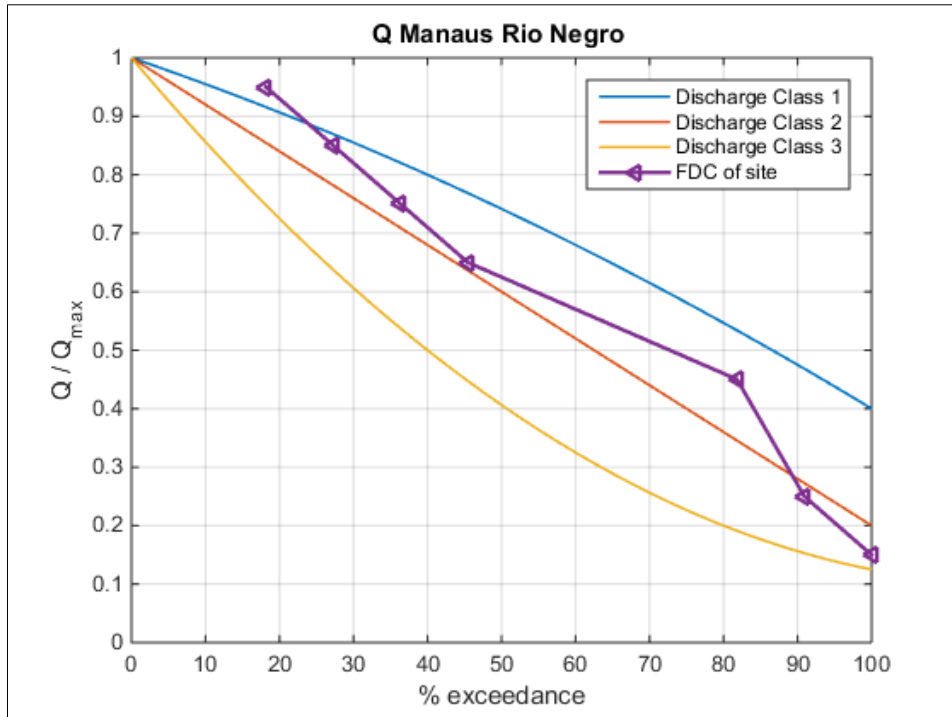


Figure 3.13 Dimensionless FDC of the Rio Negro at Manaus, AM, Brazil (Discharge Class 2 site)

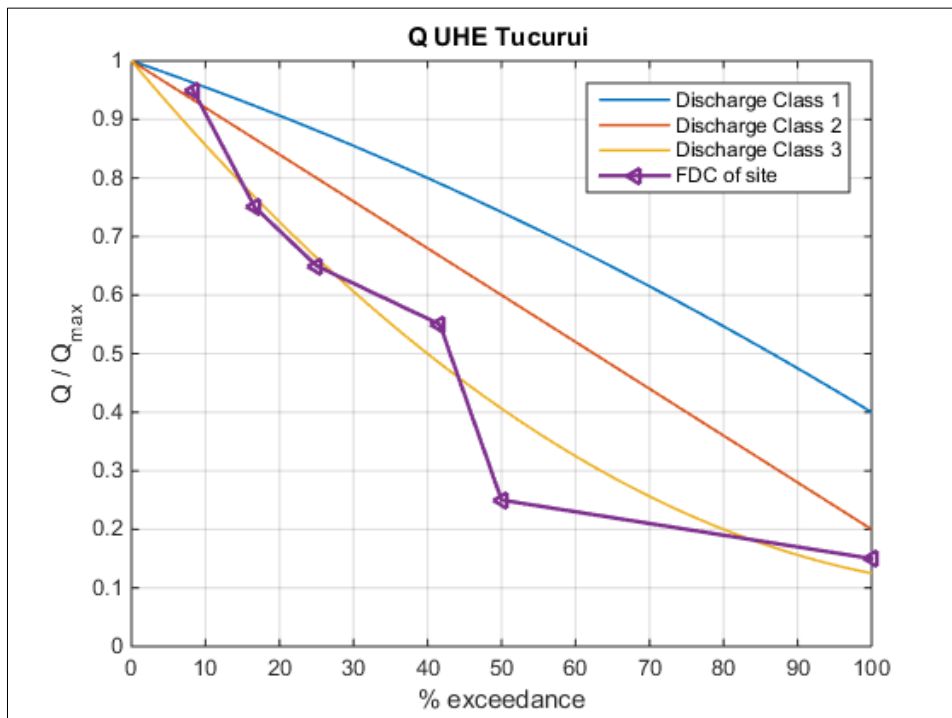


Figure 3.14 Dimensionless FDC of the Rio Tocantins, downstream of the Tucuruí hydropower plant, PA, Brazil (Discharge Class 3 site)

This process has been performed for all 15 investigated sites (see Appendix II).

As the final goal of this resource analysis is to determine the occurrence and distribution of the flow speed at all investigated sites, continuous data processing has to be carried out.

3.3.3.3 Creating dimensionless Cross-Sectional Area Duration Curves (CDCs)

In order to apply the volumetric flow rate approach ($v = \frac{Q}{A}$) to estimate the flow speed at any site, not only the discharge variation but also the change in cross-sectional area over a hydrological cycle has to be known. In analogy to the defined discharge classes (3.3.3.2), the variation of the cross-sectional area of the investigated sites has to be examined as well. The approach to determine the variation of the cross-sectional area is identically to the approach to determine the discharge variation: an empirical analysis of the maximum and minimum values for the cross-sectional areas (over a hydrologic cycle) in combination with the study of the trend of these curves. The result of this approach revealed the curves displayed in Figure 3.15. Two main observations could be stated:

- (1) the variation of the cross-sectional area of a river site over a hydrologic cycle is smaller than its discharge variation (compare Figure 3.15 to Figure 3.11);
- (2) the shape of a cross-sectional area variation curve of a specific site strongly correlates with the shape of its discharge variation curve. Thus, sites whose discharge variations were allocated to for instance Discharge Class 1, show cross-sectional area variation behavior of similar form so that they be allocated to the corresponding Cross-sectional Area Class 1.

The Reference Curves have been defined out of empirical analyses. Following, mathematical relations have been defined to describe the several cross-sectional area variations (Table 3.8):

Table 3.8 Mathematical formulations of the Reference Cross-sectional Area Classes

Cross-sectional Area Class 1				Cross-sectional Area Class 2				Cross-sectional Area Class 3			
x	0	0.4	1	x	0	0.5	1	x	0	0.4	1
y	1	0.9	0.7	y	1	0.77	0.54	y	1	0.7	0.44
$y = -0.0833 x^2 - 0.2167 x + 1$				$y = -0.46 x + 1$				$y = 0.3167 x^2 - 0.8767 x + 1$			

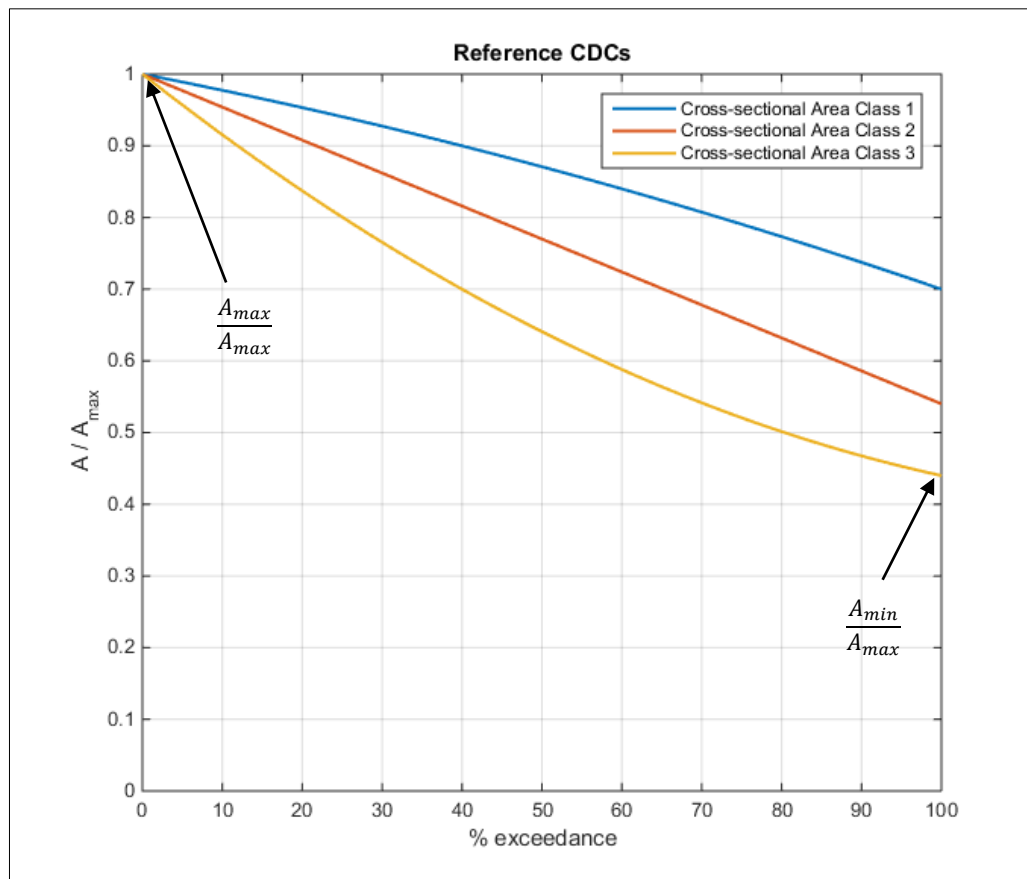


Figure 3.15 Defined Reference Cross-sectional Area Duration Curves

3.3.3.4 Creating dimensionless River Flow Speed Duration Curves (SDCs)

When discharge and cross-sectional area variation of a specific site are known the volumetric flow rate equation ($v = \frac{Q}{A}$) allows determining the flow speed variation of that site by dividing the discharge through the cross-sectional area at each point in time. Performing this calculation leads to the curves displayed in Figure 3.16.

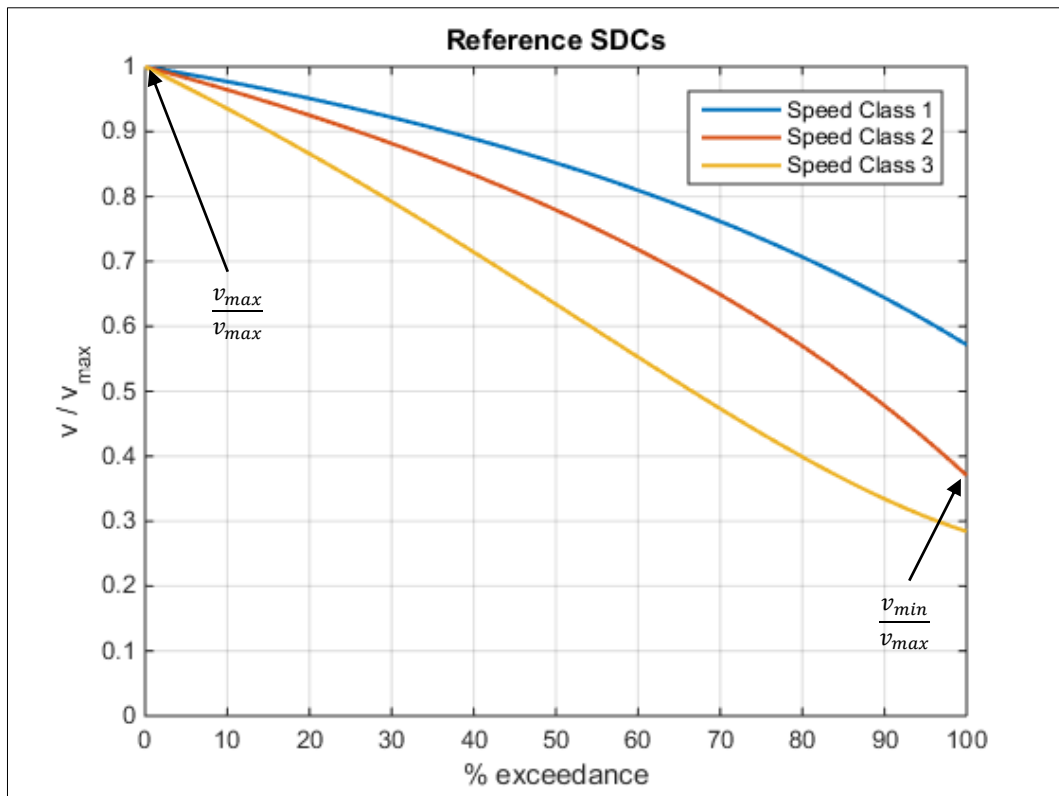


Figure 3.16 Defined Reference River Speed Duration Curves

3.3.3.5 Creating Flow Speed Histograms out of SDCs

As mentioned before, the ultimate goal of this river resource analysis is to predict the flow speed distribution of any given river site throughout a whole year so that energy yields as well as suitable turbines for the present resource could be predicted adequately and defined, respectively. Therefore, the dimensional River Flow Speed Duration Curve of a site is transformed into a histogram which illustrates occurrence over flow speed intervals. The sequence of this process works as follows:

- (1) *creation of dimensional flow speed duration curve*, by multiplying the appropriate river speed duration curve (1,2, or 3) for the specific site with its $v_{max} = \frac{Q_{max}}{A_{max}}$, see Figure 3.17
- (2) *transforming dimensional flow speed duration curve into flow speed histogram*, by applying a self-programmed Matlab code (Appendix V), see Figure 3.18

In a next step (chapter 3.3.3.6) the river flow speed histograms are compared with established tidal flow speed distributions. Those tidal speed classes have been defined by SCHOTTEL HYDRO out of empirical data acquisition analyzing several tidal sites around the world. In continuation to point (1) and (2) it is done the following:

- (3) *plot created flow speed histograms together with established SCHOTTEL Tidal Speed Classes (the SCHOTTEL Tidal Speed Classes (1-4) correspond to a specific rotor diameter)*
- (4) *plot monthly averaged flow speed data points (Appendix I) together with Tidal Speed Classes, see Figure 3.22*

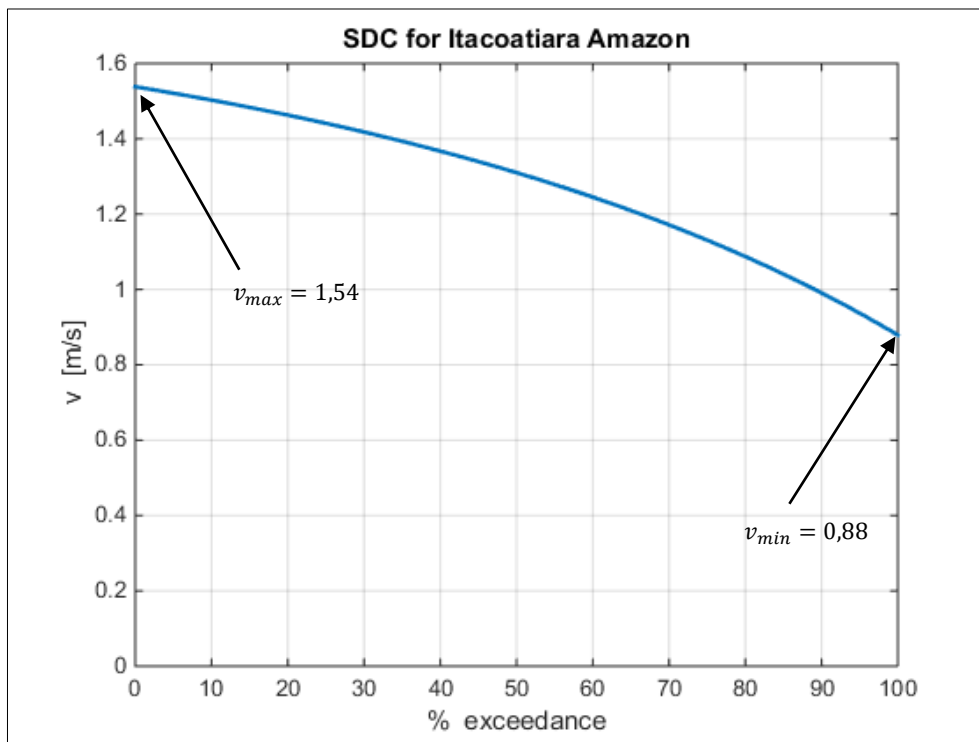


Figure 3.17 Dimensional SDC for Amazon at Itacoatiara (compare v_{min} , v_{max} with those of Table 3.6)

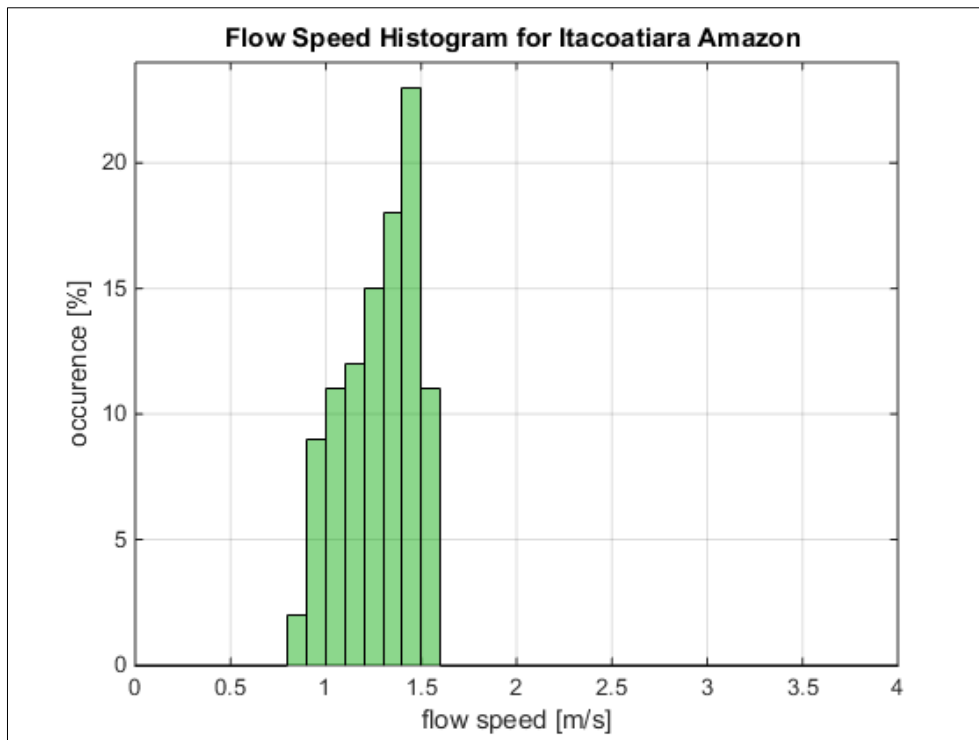


Figure 3.18 Flow speed distribution of site (step size: 0,1 m/s) created out of dimensional SDC (Figure 3.17)

This process has been performed for all 15 investigated sites and the each distribution is illustrated together with the by SCHOTTEL HYDRO defined tidal speed classes for the purpose of comparison (see Appendix III). It is recommended to first read chapter 3.3.3.6 before going through Appendix III.

3.3.3.6 Comparison of River vs. Tidal Resources (part 1)

Tidal sites show flow speed distributions similar to those of wind speeds at a specific site. Their flow speed occurrences can be illustrated using a Weibull distribution model. Out of comprehensive tidal resource analyses carried out by SCHOTTEL HYDRO, four different Speed Classes representing a wide range of worldwide tidal resources have been defined (Figure 3.19).

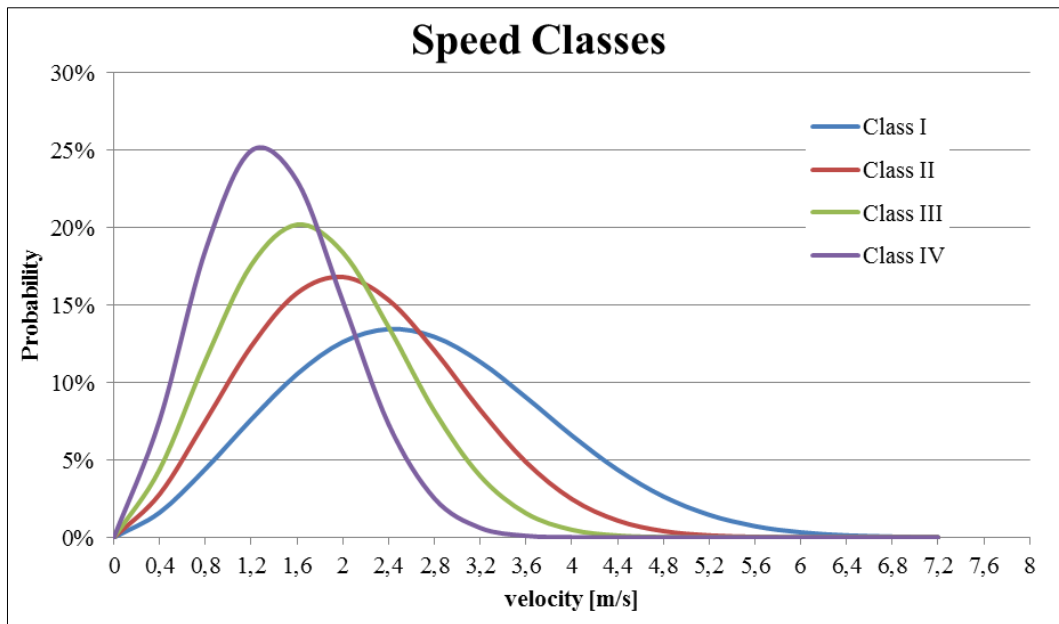


Figure 3.19 Tidal Speed Classes established by SCHOTTEL HYDRO (step size: 0,4 m/s) representing tidal sites worldwide; each Speed Class is allocated to a different rotor diameter and ideal tip speed ratio for the point of operation

In order to make any tidal energy extraction application as efficient and economically viable as possible, the extraction devices have to be designed for the resource present at the location of intended power generation. This is why before any concrete planning of a tidal energy facility comprehensive resource analyses being carried out so that if turbines being installed they are well adapted to the existing resource.

The objective of this comparison between river and tidal flow speed distributions is to figure out if the existing turbine models (with their rotor diameters of 3 m, 4 m, 5 m and 6.30 m which are allocated to the Speed Classes I, II, III, and IV respectively) could be used for river hydrokinetic energy applications, too, or if there has to be new turbines designed to match river resources.

Figure 3.21 shows exemplary such comparison. In order to make the comparison possible one by one, the tidal speed classes had to be adjusted to the same step sizes as the river speed distribution step sizes: 0,1 m/s. This flattens the tidal speed classes curves, making them not achieving the high values for their probability of occurrence like them in Figure 3.19 where the step size is 0,4 m/s.

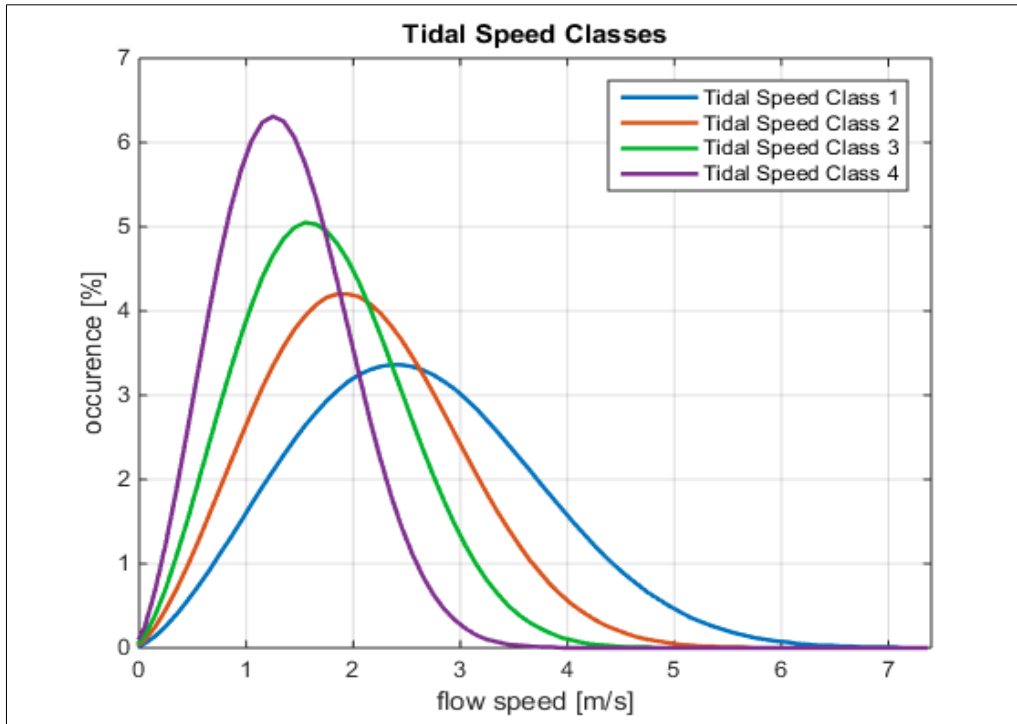


Figure 3.20 Tidal Speed Classes established by SCHOTTEL HYDRO (*step size: 0,1 m/s*) representing tidal sites worldwide; each Class is allocated to a different rotor diameter and ideal tip speed ratio for the point of operation

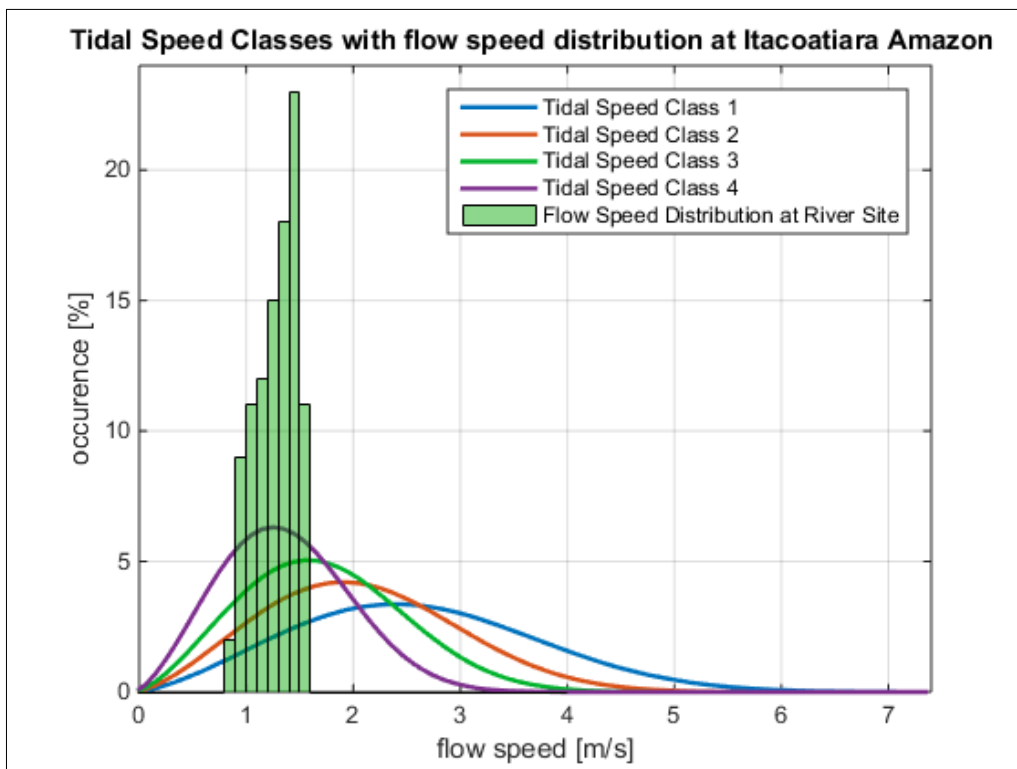


Figure 3.21 Comparison of Tidal Speed Classes with flow speed distribution of Amazon River at Itacoatiara, AM, Brazil

This process has been performed for all 15 investigated sites (see Appendix III).

The comparison of the river flow speed distributions with the tidal speed classes reveals two major observations:

- (1) the flow speed range of river sites are significantly smaller than those of tidal sites,
- (2) the fast river sites (all located along the Amazon River) whose speed distribution is centered where Speed Class 3 and Speed Class 4 are having their maximum, thus which have broad overlapping with a tidal speed class around its top, could be served with the equivalent rotors like the corresponding tidal speed class (here: mainly Tidal Speed Class 4 which corresponds to rotor diameter of 6.30 m).

Other sites would theoretically require bigger rotor diameters to achieve similar capacity factors. However, larger rotor diameters require larger depths which fewer rivers can provide. It is mentioned that the rivers which were investigated in this study are all listed among the top 30 rivers in the world regarding their annual average discharge figure. This means that river dimensions (width, depth, cross-sectional area) presented in this study are not representative for most rivers. For example Germany's biggest and economically most important river, the Rhine, has an annual discharge of $\sim 2.300 \text{ m}^3/\text{s}$ ($\sim 1\%$ of Amazon) at its highest discharge section, Rees. Over the most part of its course it has an average depth of 2.5 m to 4.3 m. Despite of its compare to major Brazilian rivers shallow water depth it has very frequent shipping traffic and is used for cooling of several power plants (nuclear and coal), in short: it is of high relevance for transportation and other economic factors of the country. Due to its relevance and comparison to other rivers in Europe, the Rhine is considered a "big" river in Europe (which in contrast to high discharge Brazilian rivers may appear amusing but still can be stated like that). Concluding, it is not representative to use the biggest Brazilian rivers as a scale for average river dimensions or discharge measures where water depth practically never is a limiting factor for turbine placement. However, most country's largest rivers (with regards to discharge) have an average annual discharge within the range of 1.000 to 2.000 m^3/s with average depth levels similar to that of the Rhine or

even shallower. This fact is limiting turbine size and has to be considered when designing a river hydrokinetic turbine. This issue will be discussed more in detail in chapter 3.4.

3.3.3.7 Comparison of River vs. Tidal Resources (part 2)

In this section, again flow speed histograms of the investigated river sites will be illustrated in a similar way they have been illustrated in the previous chapter (3.3.3.6). This time however, the data out of which the histograms are generated are the monthly averaged flow speeds from the each sites (see Appendix I). Figure 3.22 is illustrating this approach exemplary.

This process has been performed for all 15 investigated sites (see Appendix IV).

The purpose of this activity is to validate the results which were generated in chapter 3.3.3.6, by comparing the two histograms for the same site (Appendix III and IV), here: compare Figure 3.21 with Figure 3.22, two major observations can be made:

- (1) the flow speed range, meaning the flow speed interval in which occurrence is different from 0, matches very well with each other, so that the method introduced in chapter 3.3.3.5 is carrying out reasonable results,
- (2) the distribution of the histogram bars for most sites slightly differ from each other, which addresses: (a) the continuity of the speed flow occurrence interval (it is always continuous for the histogram generated out of the speed flow duration curve, chapter 3.3.3.5, and sometimes discontinuous for the monthly averaged method, current chapter), and (b) the difference in magnitude for the each histogram bars which correspond amongst others to the difference in the amount of data points out of which the two histograms are generated.

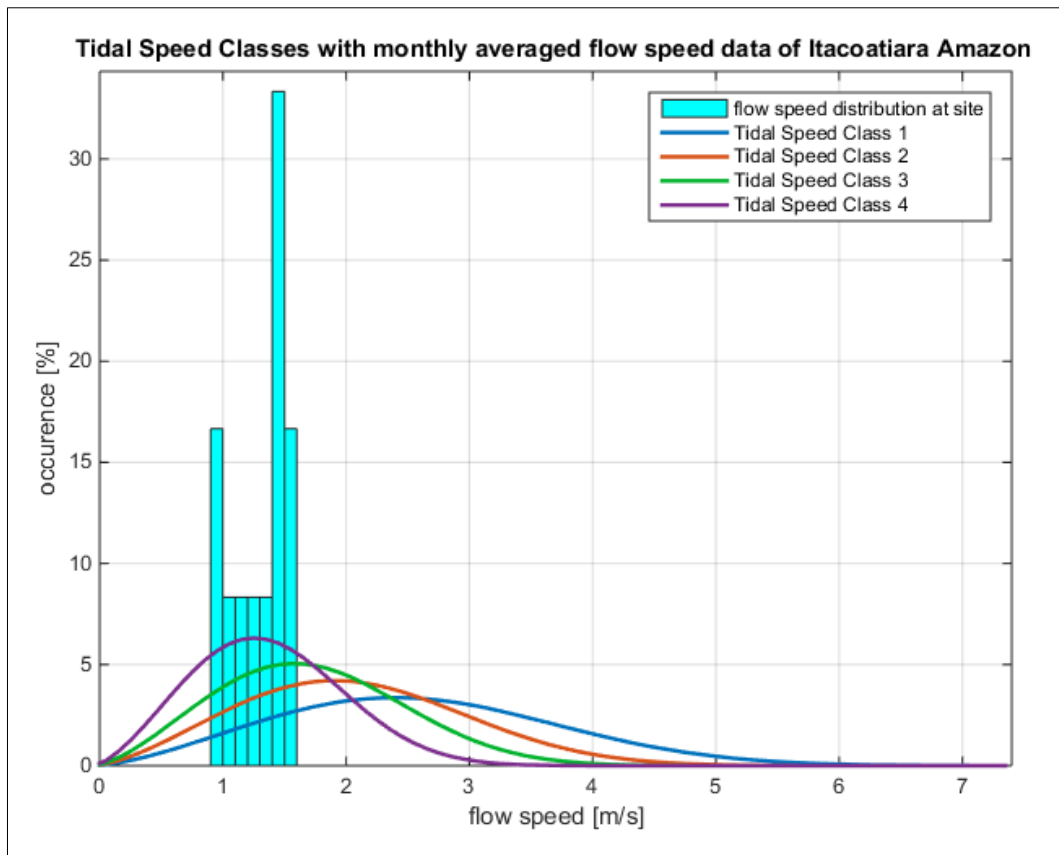


Figure 3.22 Flow speed histogram of Amazon at Itacoatiara, based on monthly averaged data points (Appendix I)

The histogram introduced in chapter 3.3.3.5 is created out of 100 data points which are arranged in continuous form ranging from v_{\min} to v_{\max} . The histogram generated out of the monthly averaged data is constructed out of only 12 data points, each accounting subsequently for 8.33 % for the time of occurrence and thus the histograms coming from that approach are more erratic and discontinuous than those which were generated in 3.3.3.5.

Nevertheless, a comparison of the annual mean velocity calculated for both methods (see Table 3.9) reveals that the two methods over the year determine similar results. The averaged deviation of the two methods regarding the determination of the mean velocity for all 15 sites is 11.4 % which shows that both methods reflect the distribution of the flow speed well considering that the data which the analysis relies on is not ideal.

Table 3.9 Annual average flow speed of the 15 investigated river sites determined with two different methods

Comparison annual v_{mean}				
Site	Monthly Averaged Data (3.3.3.6) [m/s]	Speed Duration Curve Data (3.3.3.5) [m/s]	Difference in flow speed [m/s]	Difference in flow speed [%]
1) Beruri, Rio Purus	0,58	0,64	0,06	10,3
2) Caracaraí, Rio Branco	0,67	0,83	0,16	23,9
3) Curicuirari, Rio Negro	0,91	0,89	-0,02	-2,2
4) Foz do Madeira, Rio Madeira	1,07	1,11	0,04	3,7
5) Gaviao, Rio Juruá	0,93	1,02	0,09	9,7
6) Itacoatiara, Rio Amazonas	1,29	1,29	0,00	0,0
7) Manacapuru, Rio Amazonas	1,32	1,30	-0,02	-1,5
8) Manaus, Rio Negro	0,39	0,46	0,07	17,9
9) Manicoré, Rio Madeira	1,31	1,51	0,20	15,3
10) Óbidos, Rio Amazonas	1,78	1,97	0,19	10,7
11) Sao Paulo de Olivenca, Rio Amazonas	1,56	1,61	0,05	3,2
12) Tatu, Rio Negro	0,33	0,46	0,13	39,4
13) Teresina, Rio Amazonas	1,38	1,41	0,03	2,2
14) Downstream UHE Jupia, Rio Paraná	0,88	1,01	0,13	14,8
15) Downstream UHE Tucuruí, Rio Tocantins	0,74	0,86	0,12	16,2
Average Deviation:				11,4

A statement regarding which method describes more exact the real flow speed distribution over one year is considered to be difficult as both methods use interpolation techniques within their data structure. The monthly averaged method interpolates from month to month, the Speed Duration Curve Method supposes a certain development of the flow speed between its maximum and minimum value. When analyzing the flow speed distribution of a given site, it is recommended to use the two approaches in order to have broader information on how the exact flow speed distribution is likely to be.

3.4 DIMENSIONING OF A RIVER HYDROKINETIC TURBINE

Turbine machine dimensions such as the rotor diameter, the electric capacity of the generator or the rotational speed under which the turbine will operate all depend on the resource present at the site intended for the turbine to operate. This means that the resource is determining the size of the rotor, the size of the generator, and the tip speed ratio the turbine ideally will be operating, the platform system on which the turbines will be mounted, the design of the mooring system and so forth.

As discussed in the previous chapter, 15 sites have been investigated and analyzed with regards to their flow speed and its distribution over one year, this chapter aims to describe the process of dimensioning a river turbine for a particular river resource. This process will be demonstrated for two promising sites along the Amazon:

- (1) Amazon river at Itacoatiara, AM, Brazil, and
- (2) Amazon river at Óbidos, PA, Brazil.

Those two sites were chosen for a variety of reasons. First, the resource at both locations is a Class 1 resource as classified in the previous chapter. Second, there is extensive data on hand for those two sites provided by the ANA so it is assumed that the data for those two sites is of high reliability and therefore particularly suitable for real project dimensioning. And third, both sites show additional favorable conditions regarding a potential realization of a hydrokinetic river power plant project: they have existing energy demand close by the site as well as existing infrastructure and sufficient space in their river sections, which all favors a potential commercial application of hydrokinetic river energy technology.

The following sections of this chapter will look on key aspects which have to be taken in consideration when dimensioning a turbine for river applications.

3.4.1 The Importance of the Speed Class for the Annual Energy Production (AEP)

We know that both sites (Itacoatiara and Óbidos) are Class 1 resources, meaning that they are allocated to Discharge Class 1 and subsequently Cross-Sectional Area Class 1 and Speed Class 1. To demonstrate the difference for the Annual Energy Production (AEP) which results for one and the same resource when classified into a different discharge and speed class, respectively, AEPs for both sites will be calculated under the consideration that both sites could also be a Class 2 or Class 3 resource.

Annual Energy Production (AEP):

The AEP is defined as the sum of all products between the Power Curve of a specific turbine and the time of occurrence of a specific flow speed over the year. However, it has to be stated in advance what power curve is used for the calculation. Usually the initial AEP calculation uses the mechanical power curve. For the final real fed-in electricity into a grid the mechanical AEP has to be adjusted for a mechanical-electrical efficiency and an annual availability factor. This is exemplary showed in chapter 5.3.

$$AEP_{mech} = \sum_{i=1}^n P_{mech}(v_i) \cdot Oc(v_i) \quad (3.11)$$

with:

- $P_{mech}(v_i)$ *mechanical power generated at flow speed v_i* [kW]
 $Oc(v_i)$ *time of occurrence of flow speed v_i in one year* [h/year]

Following, the two resources (Itacoatiara and Óbidos) will be illustrated with additional hypothetical histograms for Speed Class 2 and 3 to show what difference it makes for the flow speed distribution and subsequent AEP.

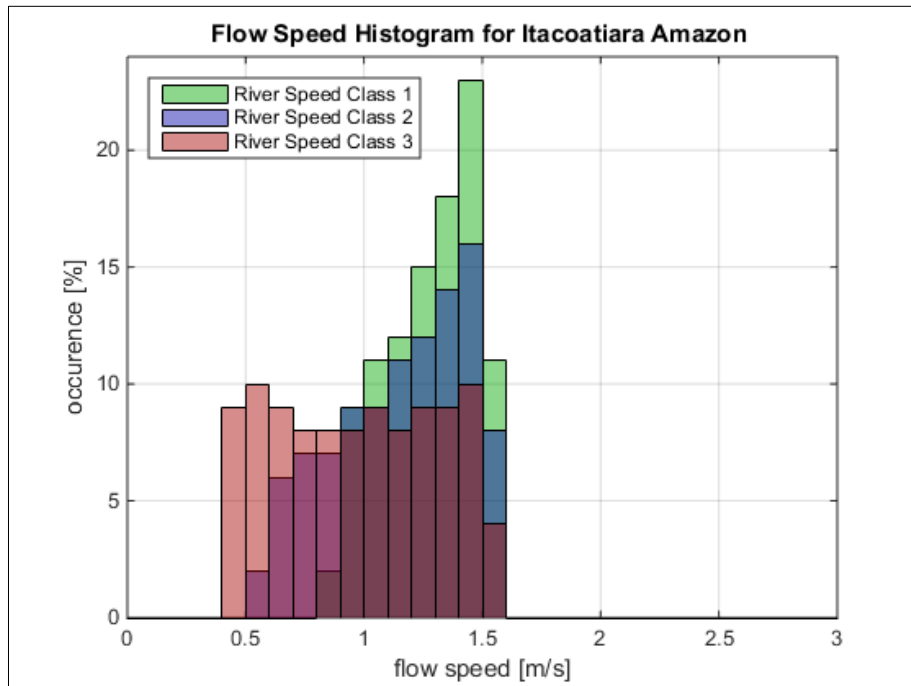


Figure 3.23 Flow Speed Histograms for Itacoatiara, under the assumption that the site could be also a Class 2 or 3 resource (blue and red histogram bars)

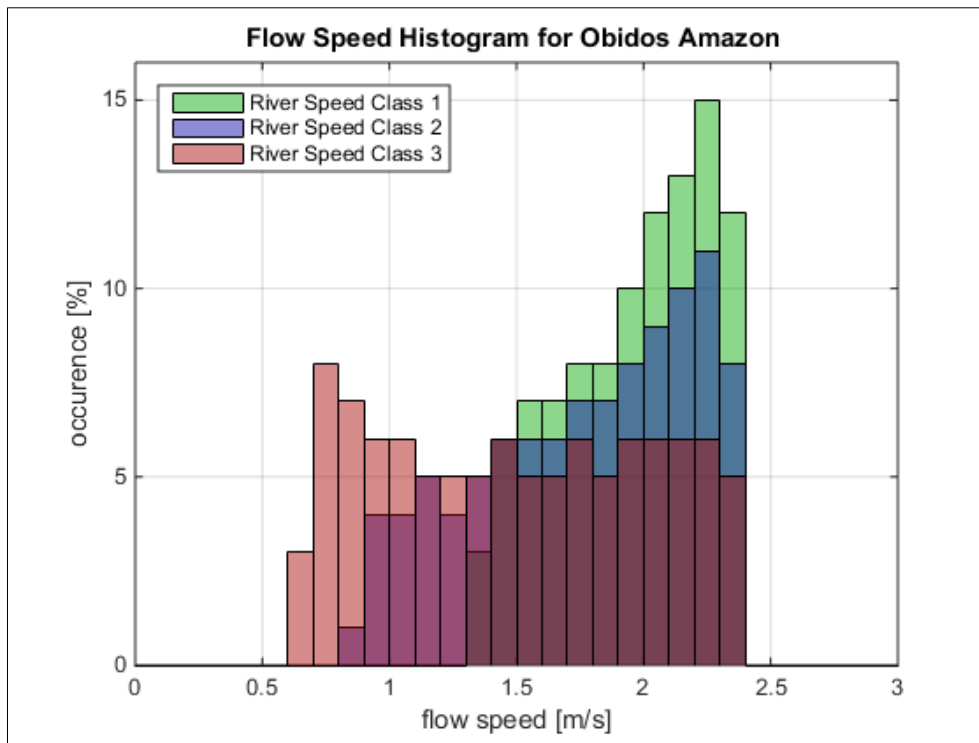


Figure 3.24 Flow Speed Histograms for Óbidos, under the assumption that the site could be also a Class 2 or 3 resource (blue and red histogram bars)

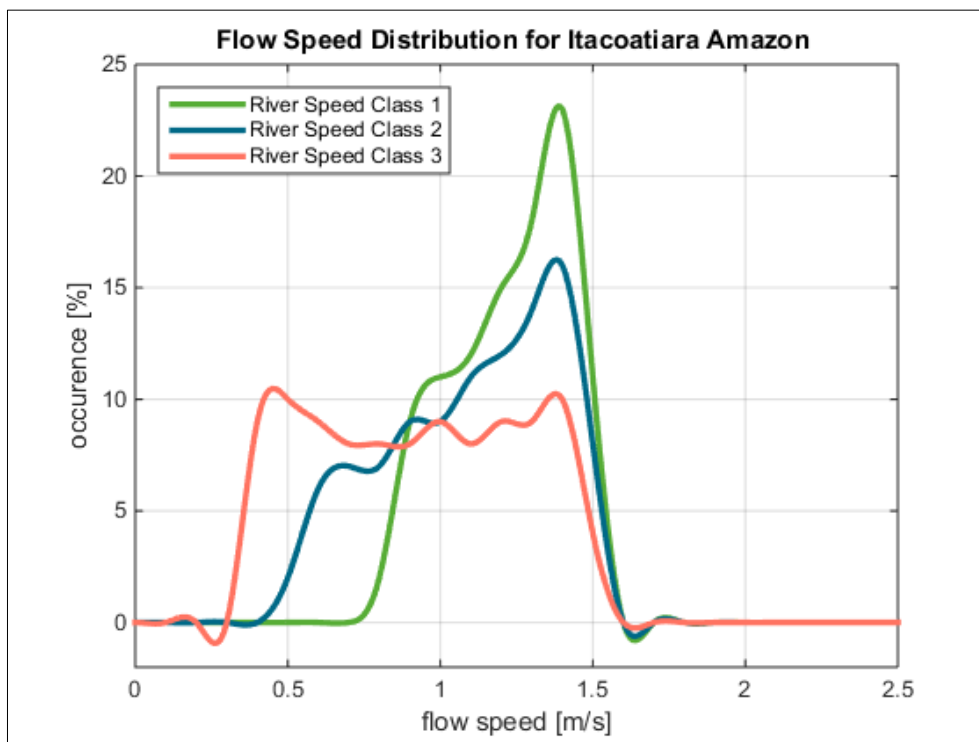


Figure 3.25 Flow Speed Histograms for Itacoatiara, under the assumption that the site could be also a Class 2 or 3 resource (blue and red graphs), as line plot (cubic splines between data points)

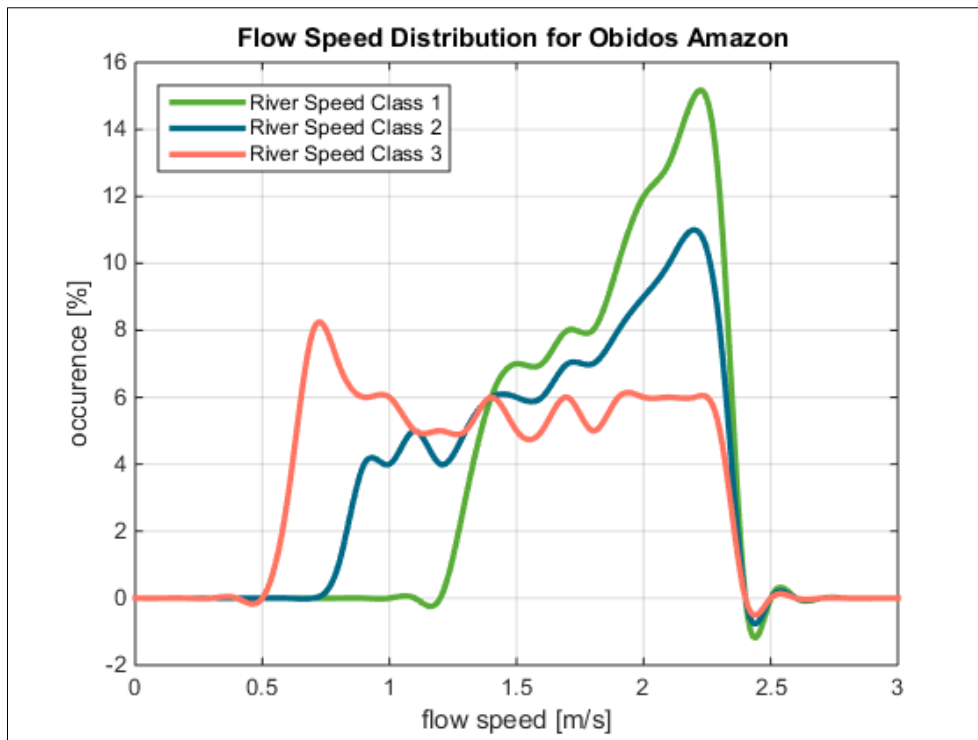


Figure 3.26 Flow Speed Histograms for Óbidos, under the assumption that the site could be also a Class 2 or 3 resource (blue and red graphs), as line plot (cubic splines between data points)

Even if the differences within the three distributions do not appear to be substantially, they are with regards to the annual energy production. This is due to the fact that the overlaying power curve of any turbine grows cubically with the flow speed. So for example if a generator's output at 1,5 m/s is 24 kW, at a flow speed of 2 m/s it is 56 kW. So a supposedly small increase in the flow speed, leads to a substantial change of the produced power by the turbine. This will be demonstrated in chapter 3.4.2.

3.4.2 Calculating mechanical AEPs for different rotor sizes

It is now assumed that four different rotor sizes are applied on the two sites potentially being of resource class 1, 2 or 3. It is further assumed that the generator used for the different rotors is the same for the rotors with a diameter of 6.30 m, 8 m and 10 m, with an electric rated power of 85 kW. For the 4 m rotor a generator with a rated power of 75 kW is used.

The following two figures are illustrating the real flow speed histograms (Speed Class 1) of the two sites together with the mechanical power curves of four different turbines varying in the diameter of the their rotor.

The more of the velocity distribution of the site is placed under the rated power of the turbine (horizontal part of the power curve) the more efficient the system is operating. So ideally it will be chosen a rotor size under which as much as possible of the flow speed distribution of the on hand site lies under the rated power of the power curve.

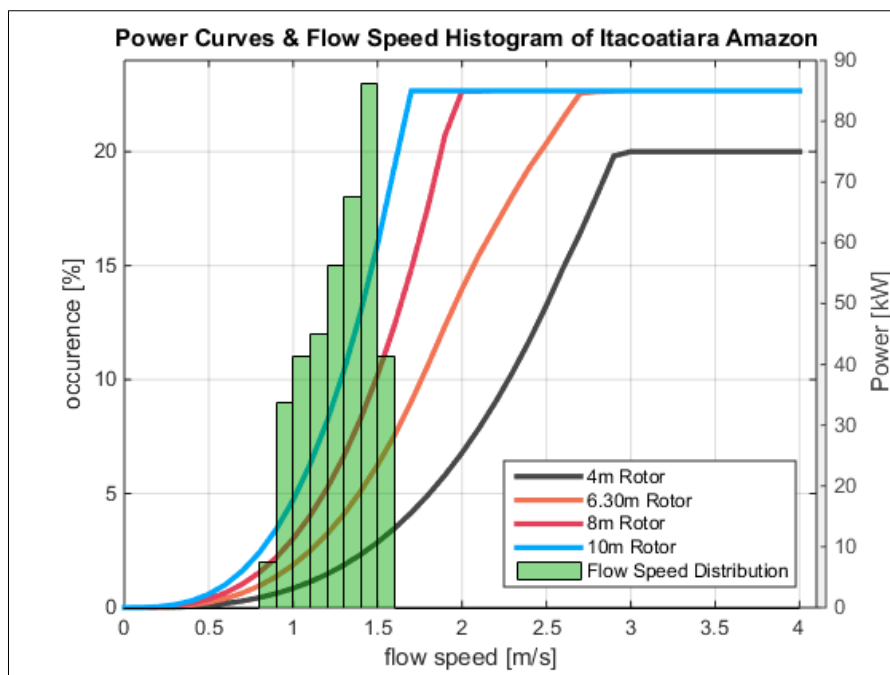


Figure 3.27 Flow Speed Histogram of Itacoatiara with power curves of different rotor sizes

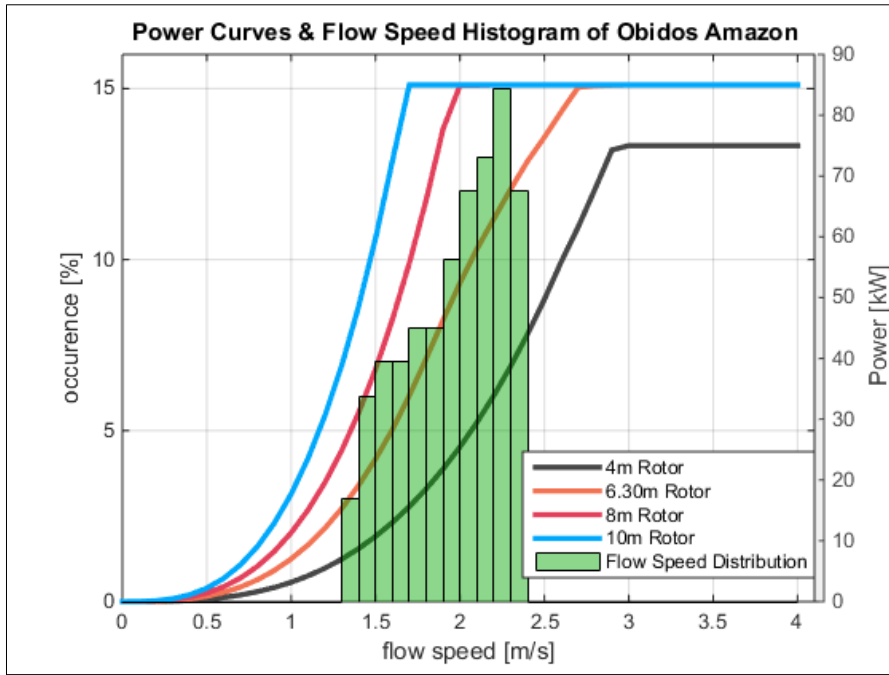


Figure 3.28 Flow Speed Histogram of Óbidos with power curves of different rotor sizes

The following two Figures are illustrating the results for the calculated AEPs of the two sites taking in consideration that both resources could be of Speed Class 1, 2 or 3 and being combined with all four rotor sizes.

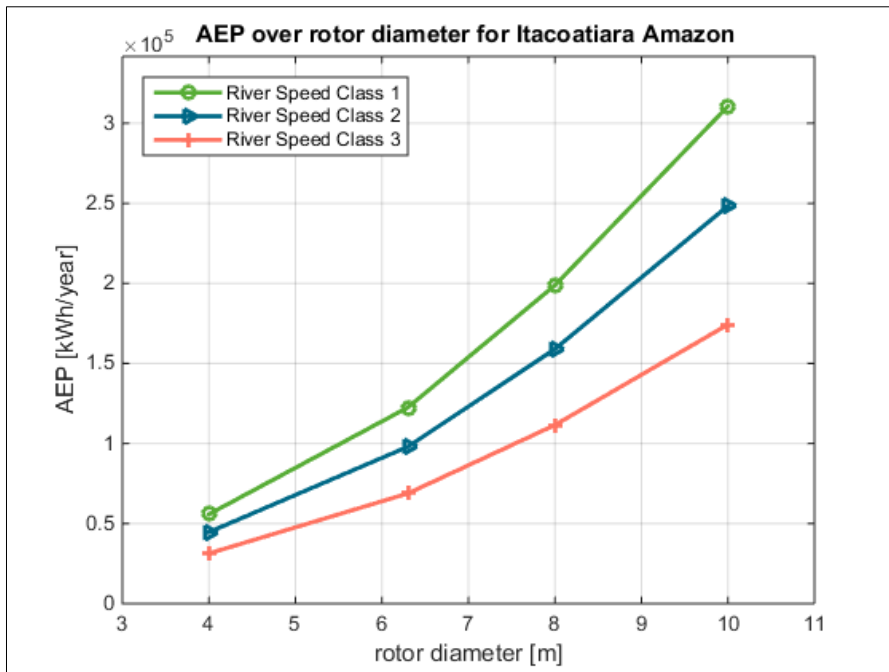


Figure 3.29 AEPs for Itacoatiara under consideration of all Speed Classes (1, 2 and 3) and for different rotor diameters(4 m, 6.30 m, 8 m and 10 m)

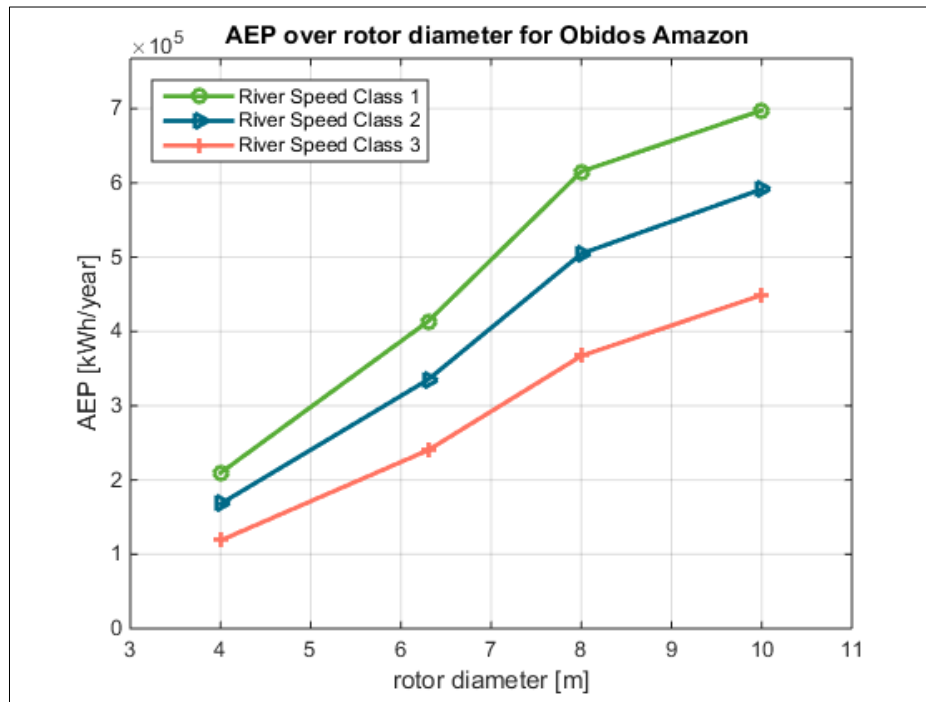


Figure 3.30 AEPs for Óbidos under consideration of all Speed Classes (1, 2 and 3) and for different rotor diameters(4 m, 6.30 m, 8 m and 10 m)

Table 3.10 consists of the AEP calculations for all 15 sites under the same consideration that all four rotor sizes being applied on the resource present at the site.

Table 3.10 AEP Calculations for all 15 sites considering different rotor diameters

Annual Energy Production (AEP)				
Site	D = 4 m [kWh/year]	D = 6.30 m [kWh/year]	D = 8 m [kWh/year]	D = 10 m [kWh/year]
1) Beruri, Rio Purus	6.789,9	14.966,5	24.190,9	37.798,2
2) Caracará, Rio Branco	18.209,9	40.136,5	64.877,3	101.370,8
3) Curicuirari, Rio Negro	19.445,1	42.908,0	69.278,0	108.246,9
4) Foz do Madeira, Rio Madeira	38.566,9	84.803,4	137.404,2	214.694,1
5) Gaviao, Rio Juruá	30.076,9	66.213,4	107.156,5	167.432,0
6) Itacoatiara, Rio Amazonas	55.812,2	122.527,9	198.845,0	310.695,3
7) Manacapuru, Rio Amazonas	56.978,3	125.054,2	202.999,5	317.186,7
8) Manaus, Rio Negro	2.391,5	5.268,8	8.520,4	13.313,1
9) Manicoré, Rio Madeira	101.226,4	218.577,5	360.139,2	492.640,2
10) Óbidos, Rio Amazonas	209.586,6	413.382,0	615.296,0	697.693,6
11) Sao Paulo de Olivenca, Rio Amazonas	110.516,3	239.604,1	393.742,1	564.381,3
12) Tatu, Rio Negro	2.391,5	5.268,8	8.520,4	13.313,1
13) Teresina, Rio Amazonas	74.170,6	162.183,1	264.251,6	412.893,1
14) Downstream UHE Jupia, Rio Paraná	29.270,0	64.449,4	104.281,9	162.940,5
15) Downstream UHE Tucuruí, Rio Tocantins	20.653,2	45.487,2	73.582,4	114.972,5
AEP at Capacity Factor: 1 (constant operation at rated power)	657.000,0	744.600,0	744.600,0	744.600,0

Determining the corresponding Capacity Factors (CFs) to the each AEP:

Capacity Factor (CF):

The Capacity Factor (CF) describes the ratio between the AEP which is achieved at a specific site and the energy extracted at full equivalent hours at rated machine power.

$$CF = \frac{AEP}{FEH} \quad (3.12)$$

with:

<i>AEP</i>	<i>annual energy production at site</i>	[kWh]
<i>FEH</i>	<i>energy extracted at full equivalent hours at rated machine power over one year (e.g.: 85 kW · 8760 h)</i>	[kWh]

The following two figures are illustrating the capacity factor for turbines at Itacoatiara and Óbidos under the same considerations which were used to calculate the AEPs.

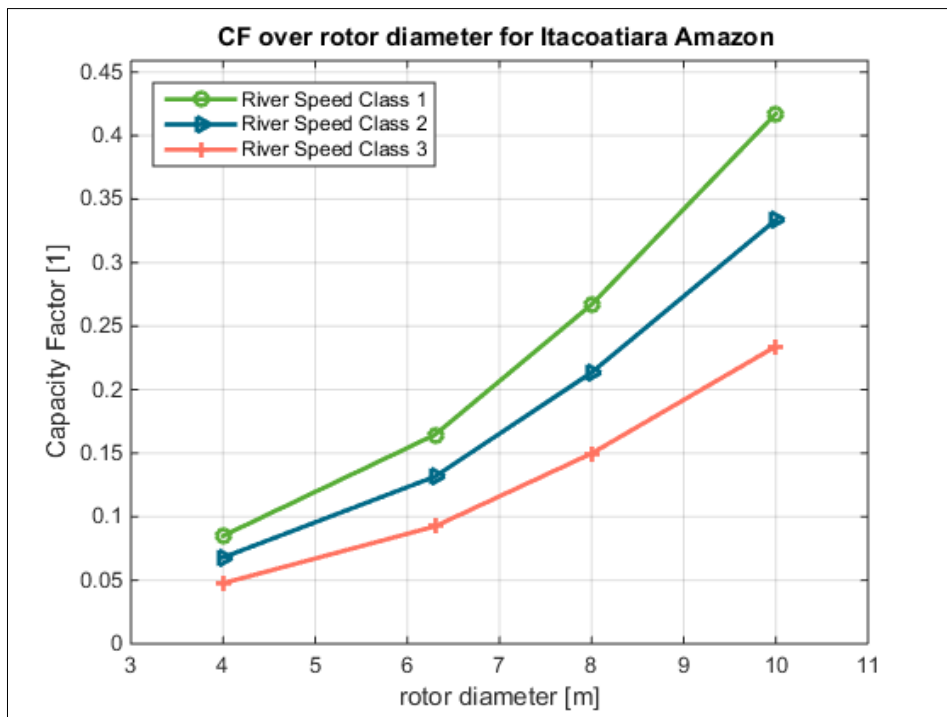


Figure 3.31 Capacity Factors for Itacoatiara under consideration of all Speed Classes (1, 2 and 3) and for different rotor diameters (4 m, 6.30 m, 8 m and 10 m)

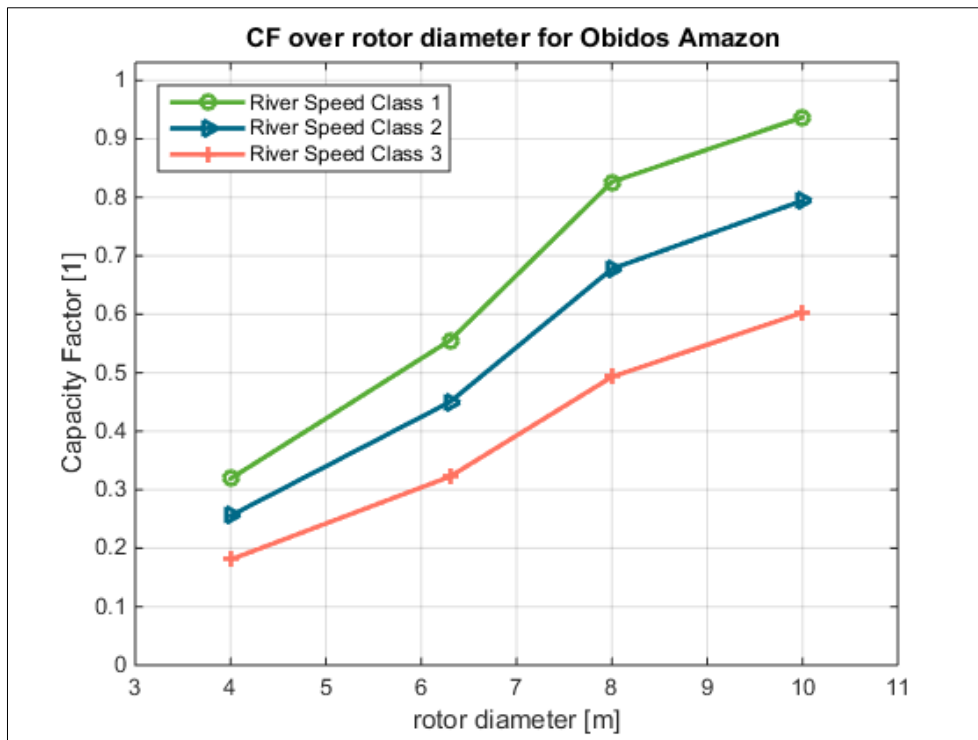


Figure 3.32 Capacity Factors for Óbidos under consideration of all Speed Classes (1, 2 and 3) and for different rotor diameters (4 m, 6.30 m, 8 m and 10 m)

Table 3.11 consists of the CF calculations for all 15 sites under the consideration that all four rotor sizes being applied on the resource present at the site.

Table 3.11 CF Calculations for all 15 sites considering different rotor diameters

Capacity Factor (CF)				
Site	D = 4 m	D = 6.30 m	D = 8 m	D = 10 m
1) Beruri, Rio Purus	0,0103	0,0201	0,0325	0,0508
2) Caracará, Rio Branco	0,0277	0,0539	0,0871	0,1361
3) Curicuirari, Rio Negro	0,0296	0,0576	0,0930	0,1454
4) Foz do Madeira, Rio Madeira	0,0587	0,1139	0,1845	0,2883
5) Gaviao, Rio Juruá	0,0458	0,0889	0,1439	0,2249
6) Itacoatiara, Rio Amazonas	0,0850	0,1646	0,2670	0,4173
7) Manacapuru, Rio Amazonas	0,0867	0,1679	0,2726	0,4260
8) Manaus, Rio Negro	0,0036	0,0071	0,0114	0,0179
9) Manicoré, Rio Madeira	0,1541	0,2936	0,4837	0,6616
10) Óbidos, Rio Amazonas	0,3190	0,5552	0,8263	0,9370
11) Sao Paulo de Olivenca, Rio Amazonas	0,1682	0,3218	0,5288	0,7580
12) Tatu, Rio Negro	0,0036	0,0071	0,0114	0,0179
13) Teresina, Rio Amazonas	0,1129	0,2178	0,3549	0,5545
14) Downstream UHE Jupia, Rio Paraná	0,0446	0,0866	0,1401	0,2188
15) Downstream UHE Tucuruí, Rio Tocantins	0,0314	0,0611	0,0988	0,1544

3.4.3 Thrust as Limiting Factor

From an energetic and economic point of view it is all the time intended to install machines which operate under as high as possible AEPs and CFs, respectively. But there are other factors which may limit an operation under rated generator power, for instance the maximum permitted thrust of the generator. Following, the thrust curves of the various rotors are illustrated over the flow speed distribution of the two sites of closer investigation: Itacoatiara and Óbidos. It can be identified that for Óbidos the 10 m rotor exceeds the maximum permitted thrust for the chosen generator (80 kN).

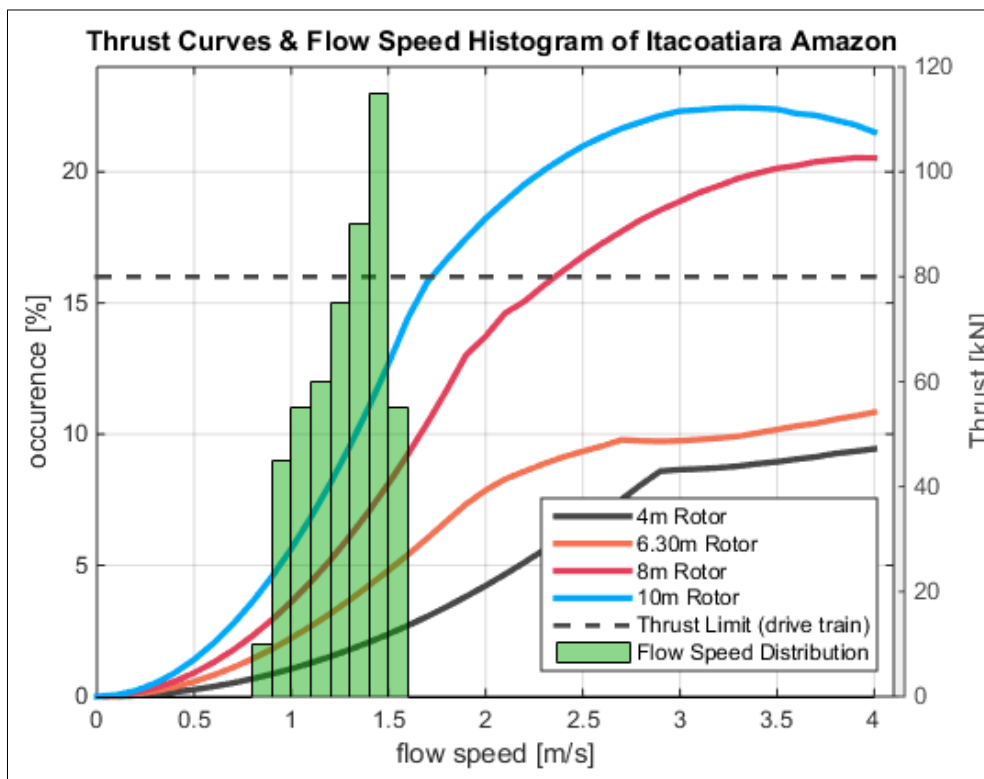


Figure 3.33 Flow Speed Histogram of Itacoatiara with thrust curves of different rotor diameters

Following, a graph with the maximum occurring thrust for three sites under consideration of all four rotor diameters is illustrated. It can be identified that for the two fastest sites, Óbidos and São Paulo de Olivença, the 10 m rotor would exceed the maximum permitted thrust by the generator.

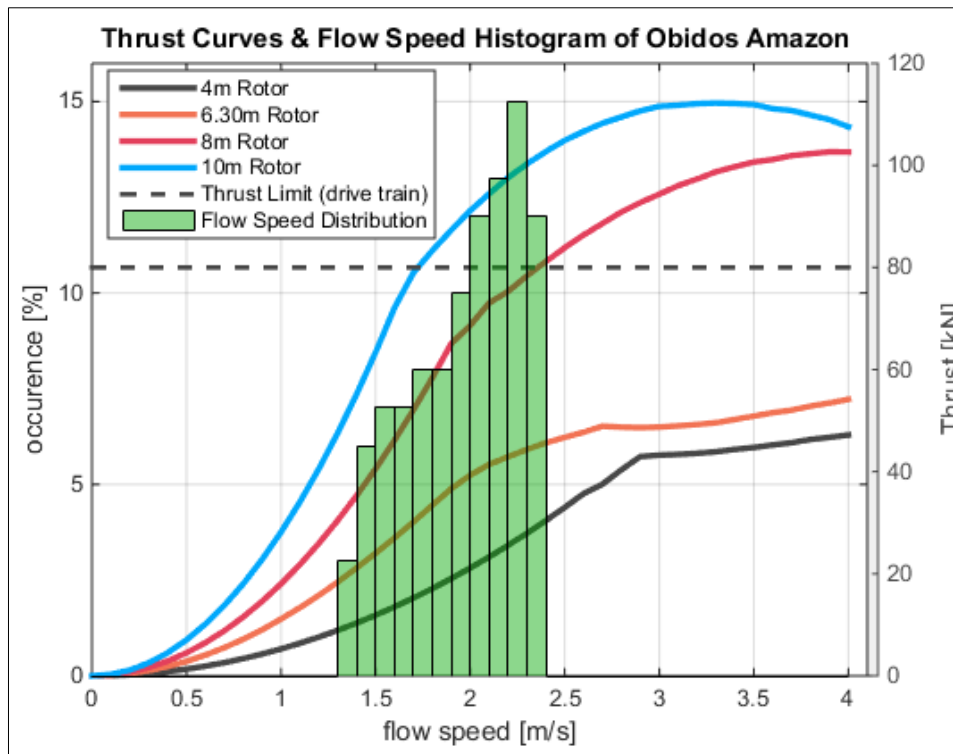


Figure 3.34 Flow Speed Histogram of Óbidos with thrust curves of different rotor diameters

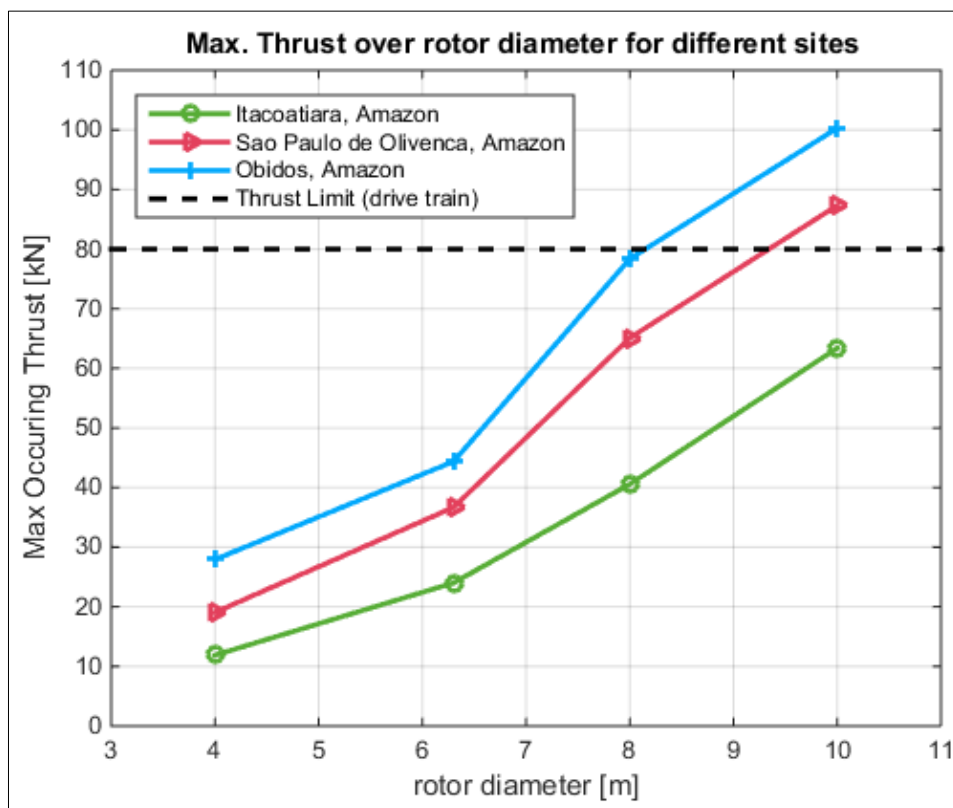


Figure 3.35 Maximum occurring thrust over rotor diameter for three selected sites

4 NUMERICAL ANALYSIS OF OPERATING SIT-250 TURBINES IN RIVER FLOW

After a broad river resource study has been carried out and main characteristics of river resources been described, an on-site CFD simulation aiming the estimation of potential power extraction as well as giving information on efficient turbine spacing and array configuration along a chosen river section is performed.

The numerical study has been performed using a program which has been developed particularly for calculations of tidal flows (ANSYS CFX TideModeller). The CFD Model is fed with power (c_p) and thrust (c_t) data of the particular turbine which itself has been calculated using a Blade-Element-Momentum Theory tool putting in basis data such as pitch angle, lift and drag values. The CFD software then is solving Reynolds-Averaged-Navier-Stokes equations (RANS). See below a schematic illustration of the calculation process of the flow field using an Actuator-Disk-Model.

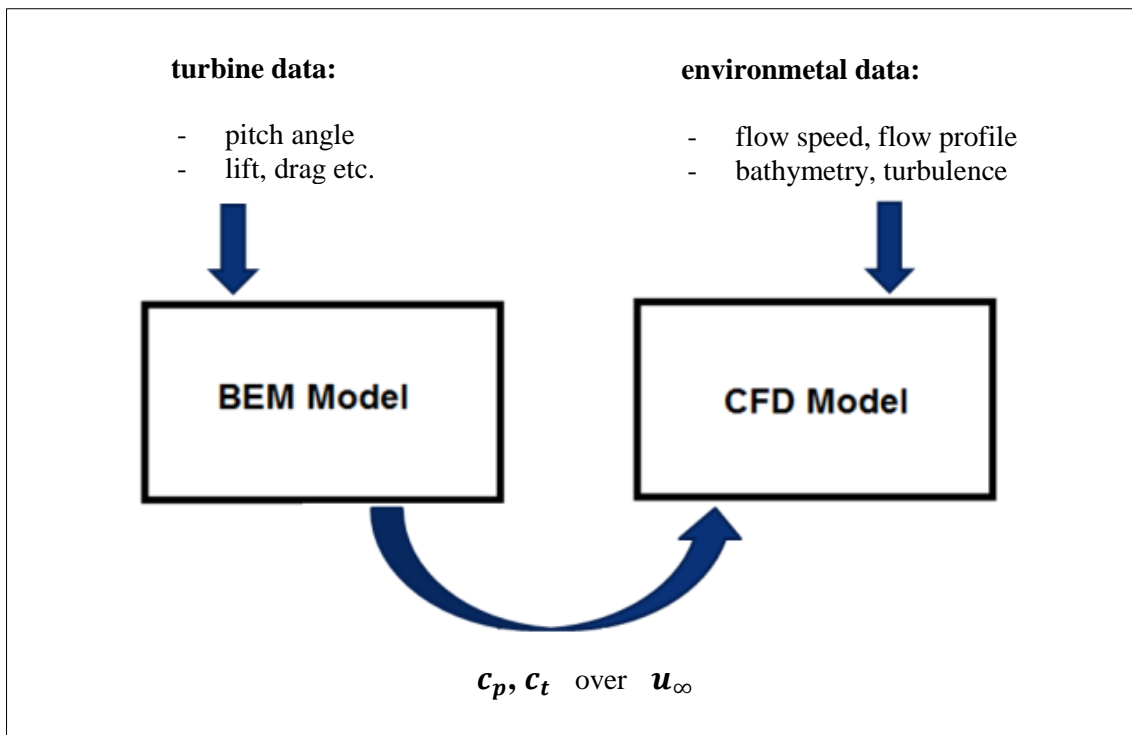


Figure 4.1 Schematic illustration of the calculation process using an actuator disk model

4.1 TIDEMODELLER

TideModeller is an add-on to the commercial ANSYS CFX software and has been developed in particular for flow simulations with tidal turbines. TideModeller can simulate tidal flows at any given location and determines the power and thrust which will be extracted/absorbed by the turbines placed in the flow. In addition its purpose is to layout configurations for entire tidal energy parks. It is using the Actuator-Disk-Theory to determine wake and enables the study of how turbines which are located downstream of another turbine are affected by the wake of the turbines located upstream.

For complex forms of tidal turbine modelling such as the Direct-Rotor-Modelling method (DRM) or the Actuator-Line Model (AL) single turbine blades and their movement over time are simulated. Through such models forces on single blade sections as well as rotational flow of the wake can be determined quite accurately. However, the handicap which those methods lies in the numerical handling – simulations based on DRM or AL models require much finer grids and subsequently higher computational power. Simulation time increases significantly and results do not necessarily provide more accuracy on the general characteristics of the wake.

The Actuator-Disk-Theory on the other hand simplifies the geometry of the turbine significantly by modelling the rotor area as a flat disk. The predominant flow equations still are being solved; only the particular flow around the turbine blades being neglected. The classic AD model simplifies the turbine further by assuming a uniform distribution of the resulting force the turbine exhibits over the entire rotor area. This distribution of the resulting force is described by the thrust coefficient (c_t). The by ANSYS developed computation model is based on the AD-Theory and allows to analyze the behavior of a tidal turbine placed in a tidal flow as well as its implications on the entire surrounding flow field including the wake of the turbine. As input parameters to specify the turbine it is required (1) the rotor diameter, (2) the power coefficient (c_p) over flow speed, and (3) the thrust coefficient (c_t) over flow speed. The AD model will be implemented on a finite volume based Reynolds-Averaged-Navier-Stokes Equations solver for incompressible flow. To represent turbulence, the SST-Turbulence model is used by default but it also can be applied a k- ϵ -model. However,

experiences from wind energy show that those models are not very feasible to represent strong turbulent flow. A k-ε-turbulence model offers better precision in the close wake and the SST-model represents better the far wake. Nevertheless this has not been finally investigated for tidal turbines. The calculation method using the AD theory, as described above, is using some simplifications and therefore the computational possibilities have borders. Concluding, there are three major aspects which are contributing to the inaccuracy to the representation of the wake. Those are:

- (1) *negligence of angular momentum to the flow induced by rotating blades:* as the actuator disk does not rotate in comparison to the real rotor the close wake is not represented as accurate as with an DRM or AL model
- (2) *negligence of the tip vortex:* through missing rotation of turbine blades, tip vortices are not captured with an AD model which in reality occur at the tip of the blades
- (3) *negligence of transient flow characteristics:* through the stationary observation of the AD – RANS method, transient flow characteristics cannot be captured, too.

Nevertheless, under consideration of all disadvantages, the advantages of the AD–RANS method are outweighing the disadvantages and thus the method still is the predominant numerical computation method in the wind and tidal energy industry.

The AD theory will be implemented as sink/source term (S_i) within the RANS equations which are consisting of the momentum and mass conservation equations, see equations (4.1), (4.2). The source term (S_i) simulates the force which the turbine brings into the flow.

$$\frac{\partial(\rho U_i)}{\partial t} + \frac{\partial(\rho U_i U_j)}{\partial x_j} = -\frac{\partial P}{\partial x_i} + \frac{\partial}{\partial x_j} \left[\mu \left(\frac{\partial U_i}{\partial x_j} + \frac{\partial U_j}{\partial x_i} \right) \right] + \frac{\partial}{\partial x_j} \left[\mu_t \left(\frac{\partial U_i}{\partial x_j} + \frac{\partial U_j}{\partial x_i} \right) \right] + \rho g_i + S_i \quad (4.1)$$

$$\frac{\partial U_i}{\partial x_i} = 0 \quad (4.2)$$

with:

U_i	<i>averaged flow speed</i>	[m/s]
ρ	<i>density of water</i>	[kg/m ³]
μ	<i>kinematic viscosity</i>	[m ² /s]
μ_t	<i>turbulent viscosity</i>	[m ² /s]

As discussed above, the AD theory brings in a constant resistance into the flow. This resistance causes thrust on the actuator disk which is equivalent to the turbine's thrust. The source term (S_i) from eq. (4.1) is set to be zero for the whole domain where the actuator disk is not present. For cells which are allocated to the presence of the AD the source term is defined as:

$$S_i = \frac{K}{\Delta x} \frac{\rho}{2} U_i |U_i| \quad (4.3)$$

with:

Δx	<i>thickness of actuator disk</i>	[m]
K	<i>resistance coefficient</i>	[-]

In this work this way of modelling will be applied to analyze the extracted power, exhibited thrust and the wake of the SIT-250 tidal turbine designed by SCHOTTEL HYDRO. The throughout those simulations gained results are assumed to provide reliable information regarding the influence the turbines have on the surrounding flow field as well as on efficient device spacing.

4.2 SIMULATION SET-UP

All CFD simulations carried out in this work aim to provide information on the operation of SCHOTTEL Instream Turbines installed at the "Plat-I" platform designed by Sustainable Marine Energy Ltd. The Plat-I platform is a floating trimaran platform which can mount up to four SCHOTTEL Instream Turbines placed next to each other at its stern. It has a length of 31.658 m and a width of 26.711 m with a maximum floating depth of the turbine blade tip of 7.666 m. The Plat-I platform currently is the first platform system for a commercial application of SCHOTTEL Instream Turbines to generate hydrokinetic ocean energy.

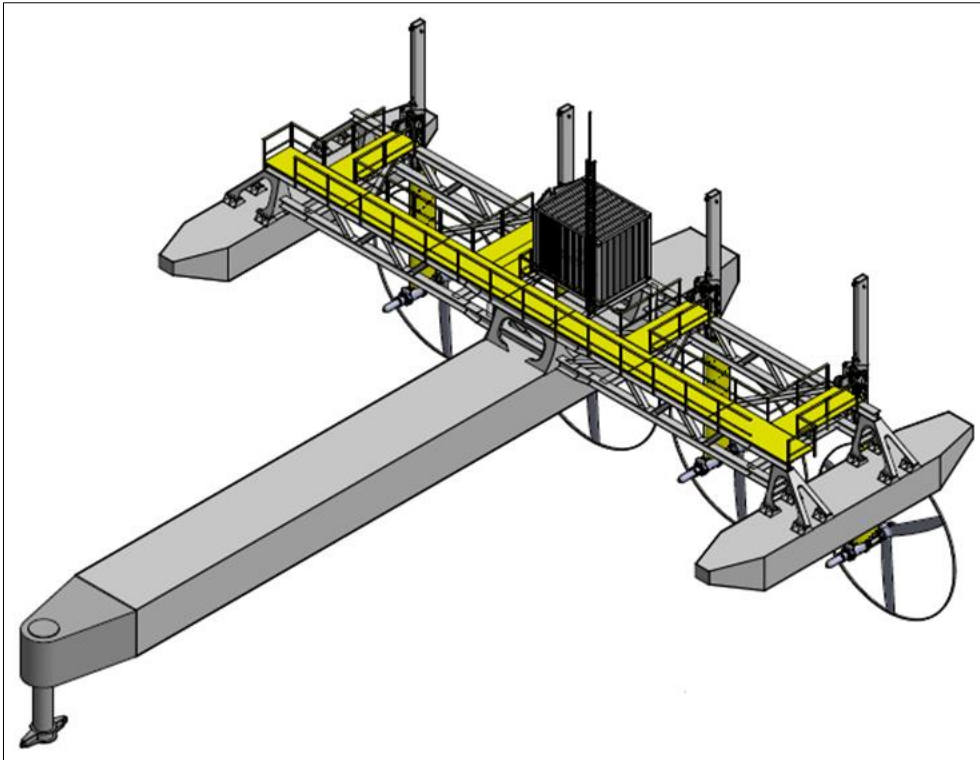


Figure 4.2 Plat-I Platform in operating modus mounting four SCHOTTEL Instream Turbines

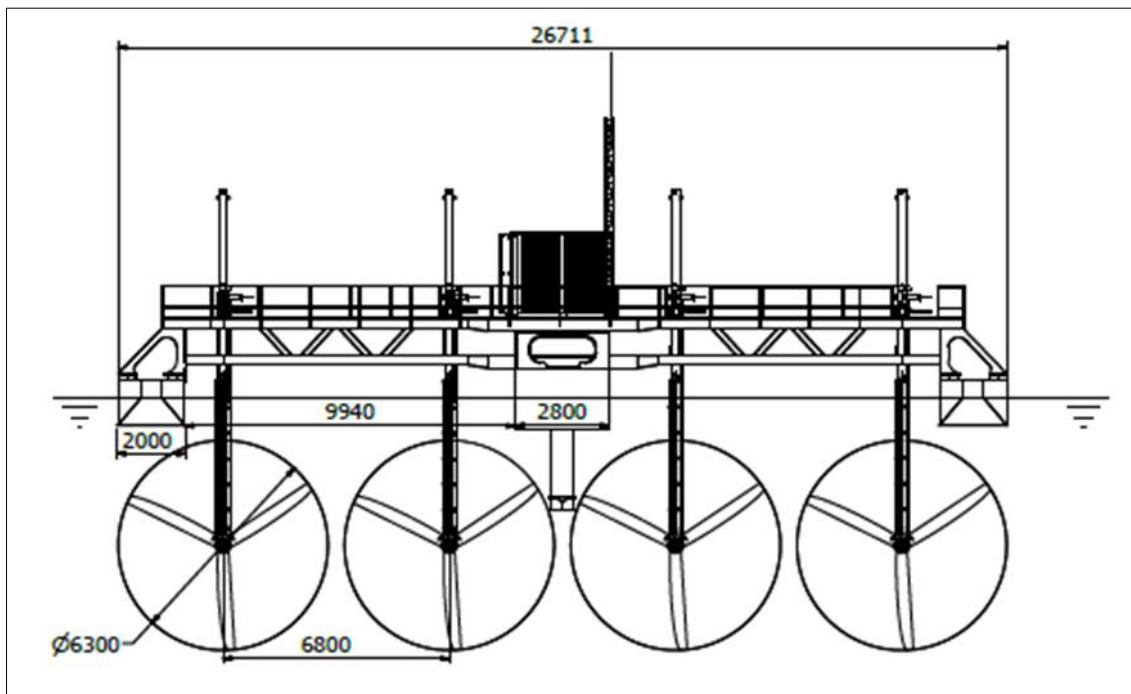


Figure 4.3 Plat-I Platform in operating modus, front view

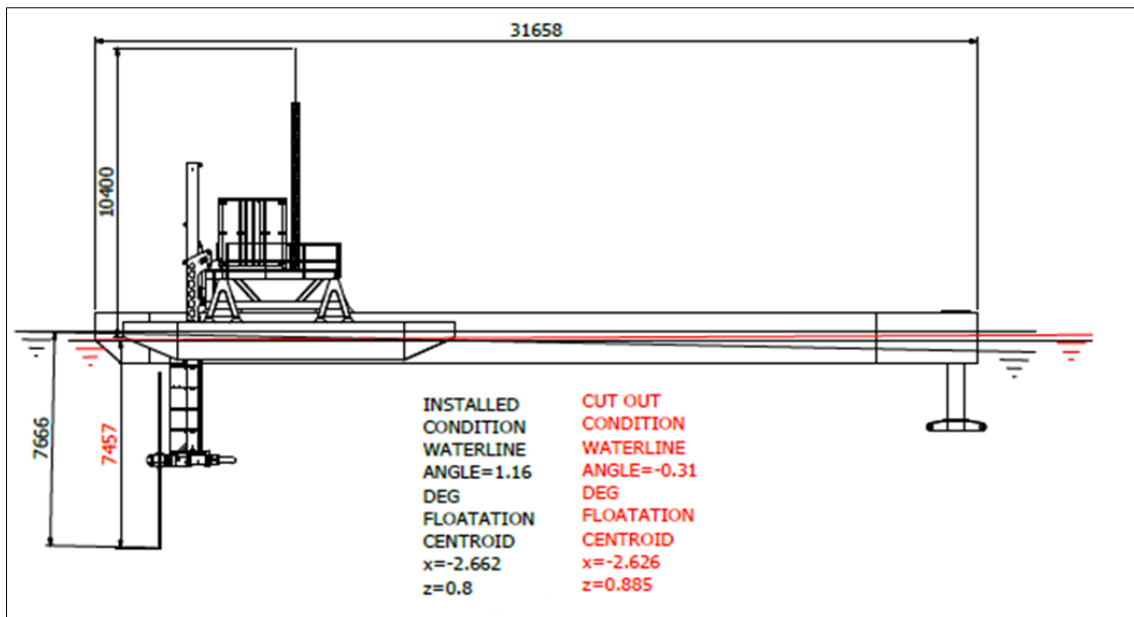


Figure 4.4 Plat-I Platform in operating modus, side view

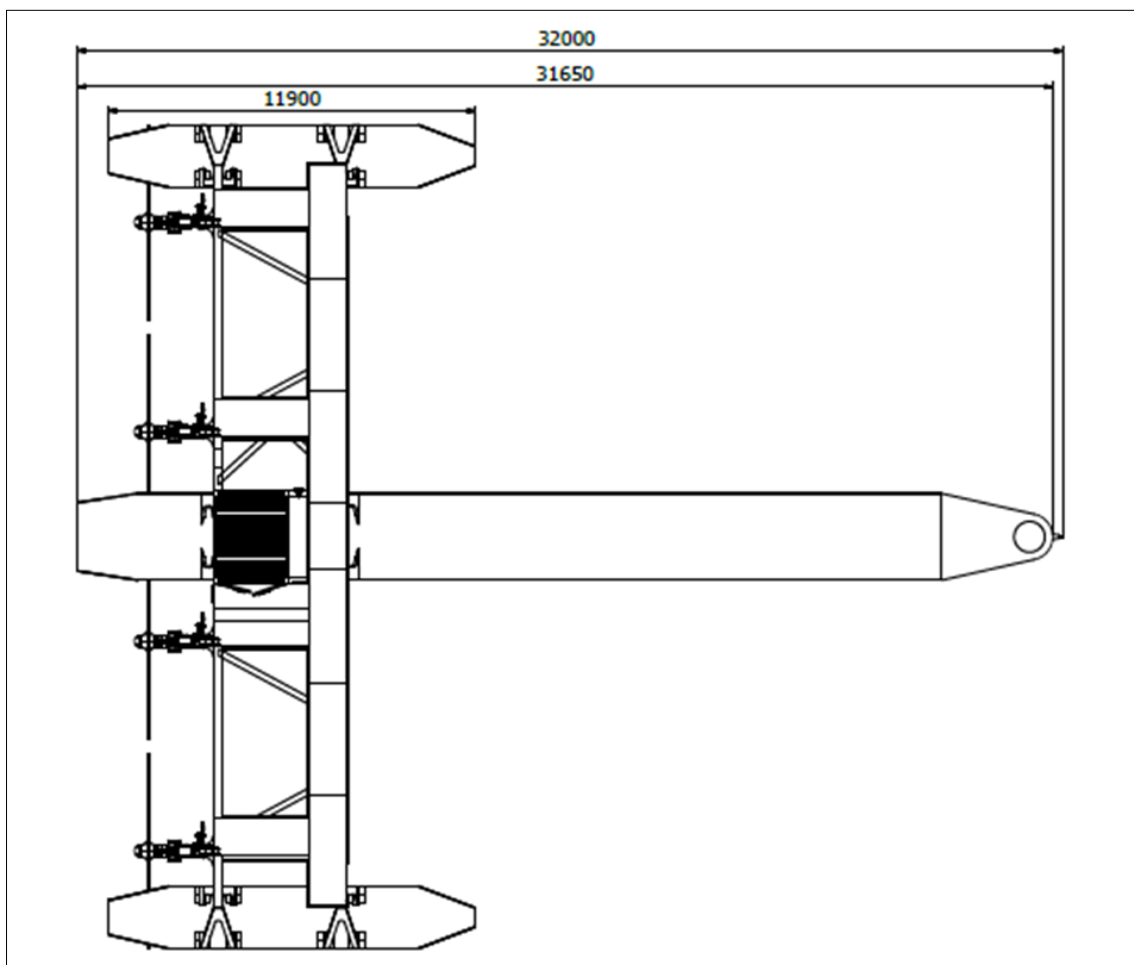


Figure 4.5 Plat-I Platform in operating modus, top view

For the purpose of this work 16 different simulations have been carried out, each aiming to provide information on different details with regards to how the turbines affect the overall flow field. Whereas the first several simulations were aiming to reproduce the river conditions present in the investigated sections (chapter 3) of the Amazon regarding flow speed and flow profile, further simulations focused on the impact of the wake on turbines which are placed downstream of freely streamed turbines. Finally a simulation with 20 turbines configured in a specific array achieving a rated power of 1MW (chapter 5) has been performed with a subsequent feasibility study and overall cost estimation.

Even though various different simulations have been carried out, major settings have not been changed after figuring out an adequate set-up related to the flow conditions at the investigated Amazon sites. This includes the velocity profile, which has been assumed to be of 7th power law (explanation below), the water depth (35 m) and the maximum flow speed of 2 m/s at the surface of the simulation domain.

4.2.1 Simulation Domain and Numerical Grid

The simulation domain is realized using a box-shaped tank with variable lengths X, Y and Z. A second box close around the turbine with a finer mesh can be placed inside the X-Y-Z box. Inside the high resolution box the turbines are placed as actuator disks.

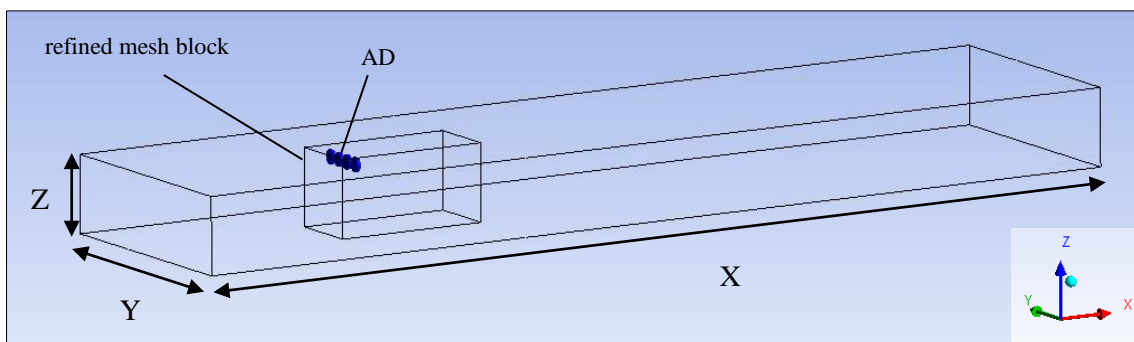


Figure 4.6 Modelled tank

The interconnectedness between the turbines and the entire computational domain is executed automatically by the software which generates a structured mesh. However, in the input script the mesh refinement, position of the refined mesh block, and the

stretching of the meshes can be defined exactly. Following, a schematic setting of the mesh structure is illustrated.

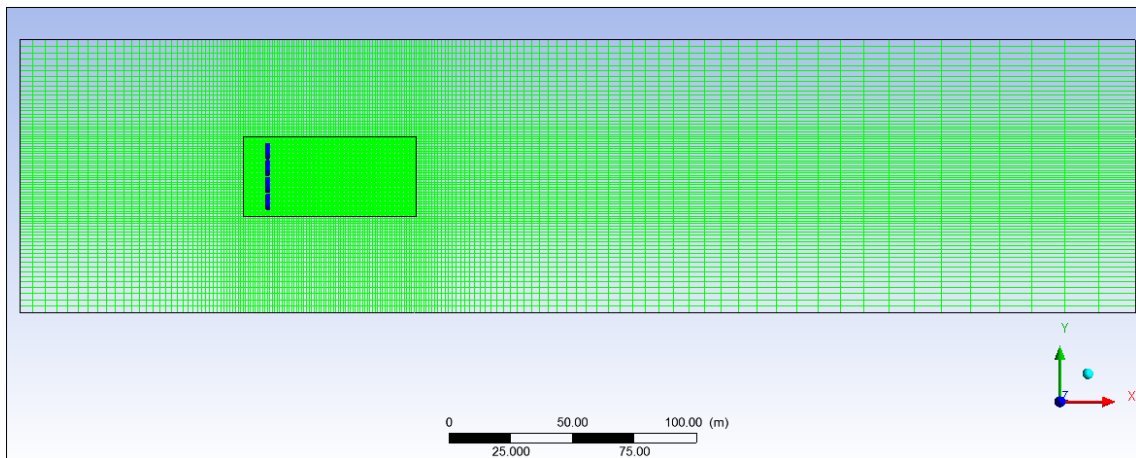


Figure 4.7 Top view simulation domain (X-Y-Plane)

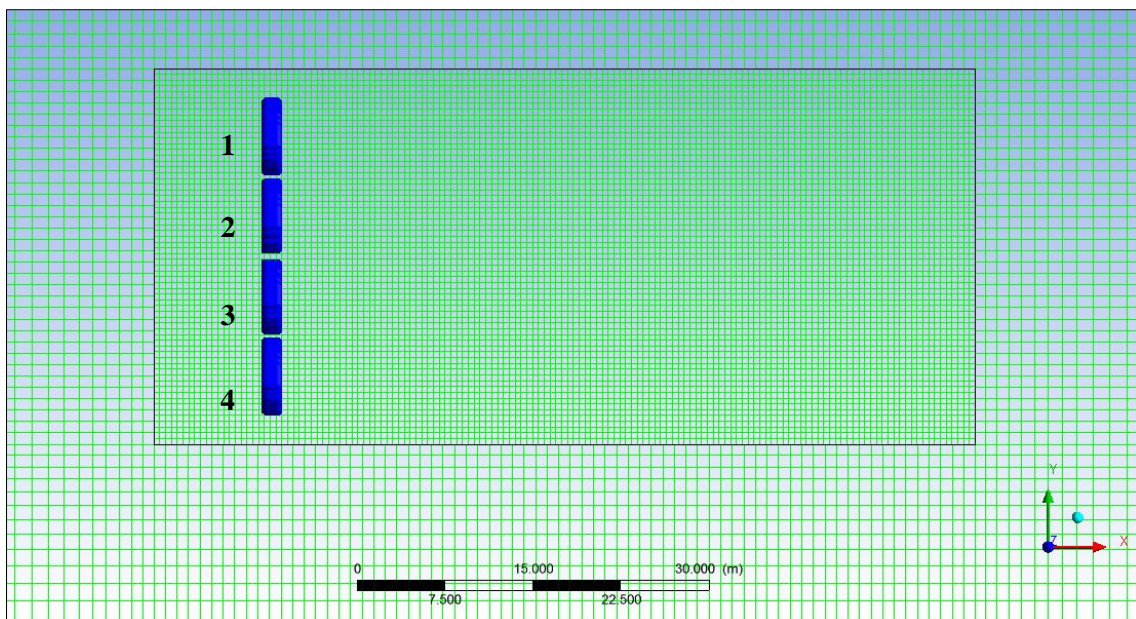


Figure 4.8 Top view (X-Y-Plane), zoomed-in, to illustrate the transition from the coarse mesh to the refined mesh

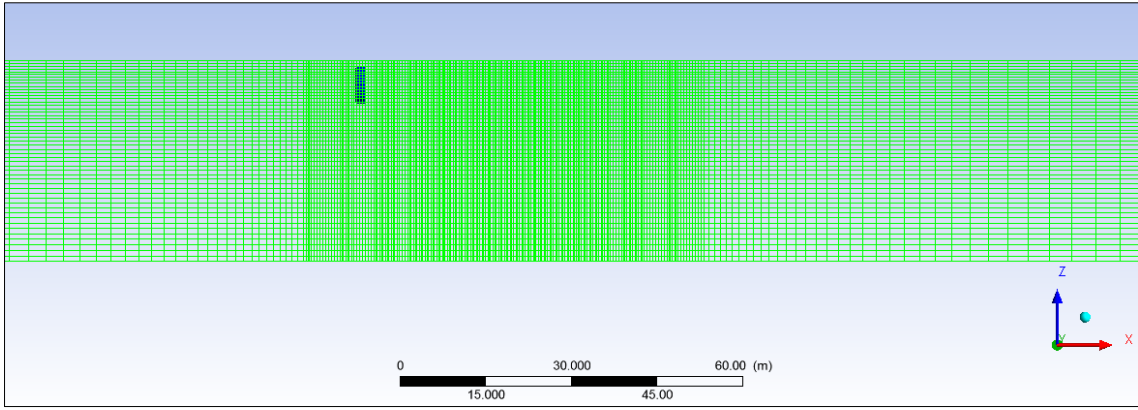


Figure 4.9 Side view on simulation domain (X-Z-Plane), zoomed in

The as actuator disk illustrates turbines are separately being interconnected with the surrounding grid. In the input script it is defined how many cells the each turbine is constructed of. During the simulation process the mesh around the turbine is refined automatically by the software. However, it can be defined how many refinery steps should be performed. The more steps are carried out the more close the turbine is to its geometric ideal configuration (a flat disk).

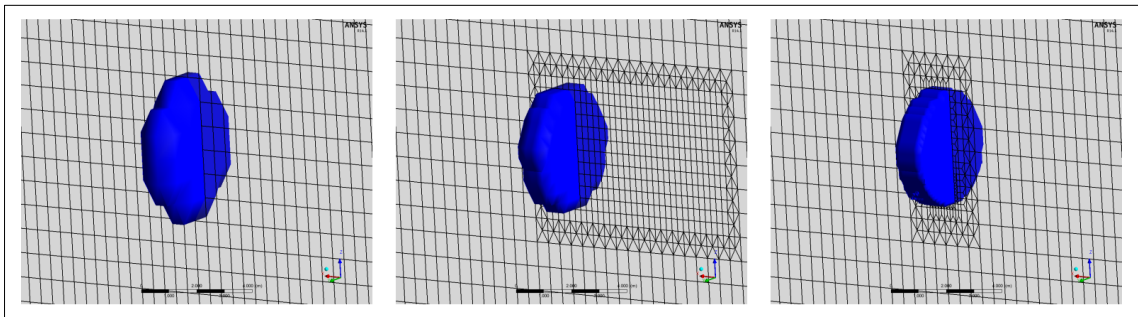


Figure 4.10 Mesh refinement around turbine for one (left), two (middle), and five (right) refinement steps

4.2.2 Boundary Conditions

Before simulating a certain flow, boundary conditions have to be set. Those include the incident flow velocity, the flow profile, the bottom roughness as well as wall definitions. Tidemodeller defines the walls of a tank with “North”, “South”, “East” and “West”, and divides each wall into four sections, see the following figure.

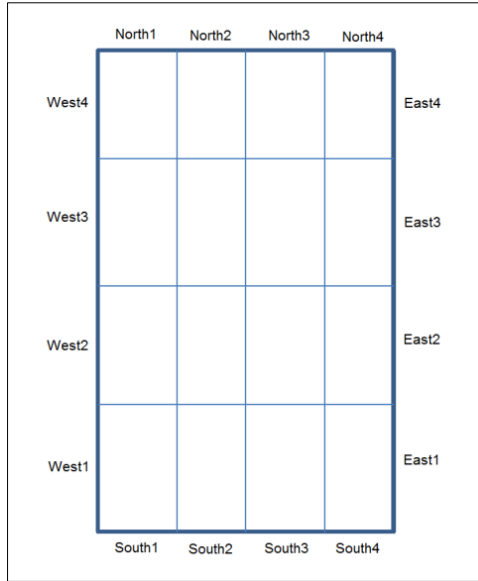


Figure 4.11 Definition of tank walls in Tidemodeller

For all simulations carried out in this work it has been defined that the West-wall functions as inlet side and the East-wall functions as outflow side. The North and South wall are defined as impenetrable. All simulations have been carried out with several characteristics being constant to guarantee comparability between the each simulations: those include (1) the incident flow velocity at the surface, and (2) the velocity profile over the tank depth. The flow speed at the surface was chosen to be 2 m/s (which is present at Óbidos) and the flow profile has been chosen to be of 7th power law characteristic.

7th power law: velocity profile over depth, from free surface to sea/river bed

$$u = u_{ref} \left(\frac{z}{z_{ref}} \right)^{\frac{1}{7}} \quad (4.4)$$

with:

- | | | |
|-----------|---|-------|
| u | flow speed at height z | [m/s] |
| u_{ref} | reference velocity, at free surface | [m/s] |
| z | height z above sea bed | [m] |
| z_{ref} | reference height, (seabed to free surface: e.g. 35 m) | [m] |

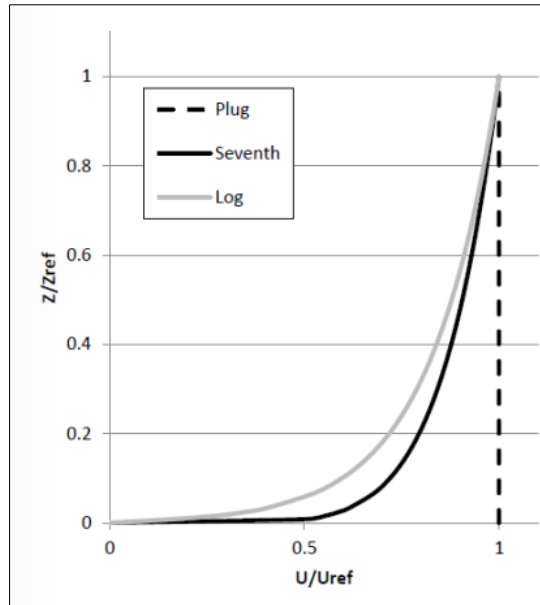


Figure 4.12 Graphical illustration of Plug flow, Seventh Power Law flow and Log Law flow over depth

Table 4.1 Input parameters for simulations (some vary, some are fix), varying are those which figures include ranges

Parameter	value	unit
length of tank: X	350 ... 1500	m
width of tank: Y	80 ... 150	m
depth of tank: Z	35	m
incident flow speed (at free surface)	2.0	m/s
velocity profile	7th power law	-
thrust coefficient (c_t)	0.21 ... 0.72	-
power coefficient (c_p)	0.083 ... 0.44	-
rotor diameter	6.30	m
horizontal coarse mesh resolution	1	m
vertical coarse mesh resolution	50	layers
horizontal fine mesh resolution	0.5	m
vertical fine mesh resolution	50	layers
number of nodes defining turbine	17000	-
number of refinement steps	5	-
roughness length (river bed)	0.03	m

4.3 SIMULATION OF VARIOUS FLOWS USING CFX-TIDEMODELLER

The following figures illustrate the velocity distribution within the simulation domain which forms by the presence of the turbines in the flow. An in depth analysis on the wake and performance of turbines operating in a wake follows in chapter 4.4. This chapter aims to get the reader a first impression of how the flow develops by the presence of turbines and with what dimensions of velocity decrease and wake formation has to be worked later on. It will be illustrated several Plat-I configurations. First, just one platform then two with varying distances between them and finally 5 Plat-I in a 2-1-2 configuration with an output of 1 MW (chapter 5).

4.3.1 One Plat-I

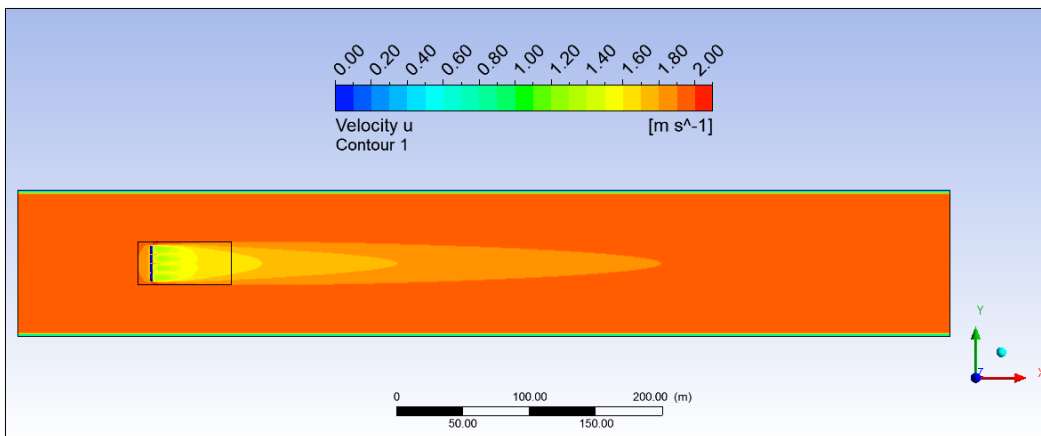


Figure 4.13 1 Plat-I, cut through turbine center X-Y-plane, top view, length of tank: 700 m

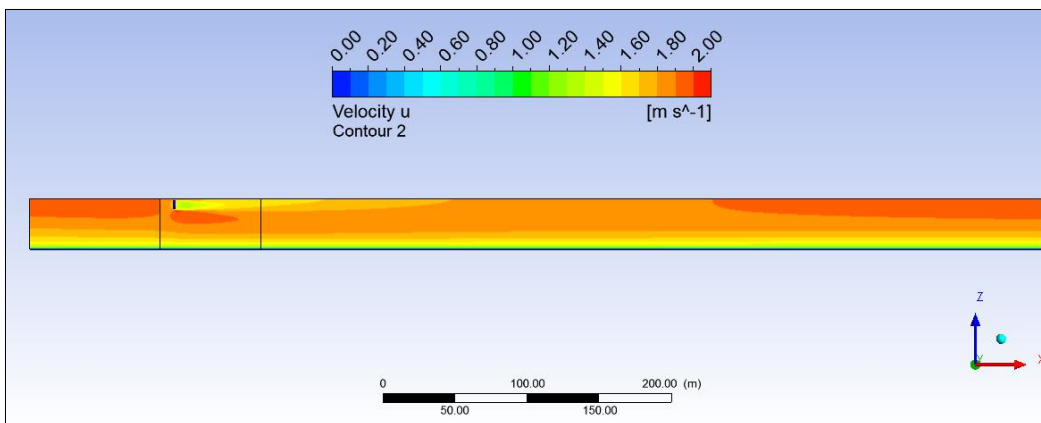


Figure 4.14 1 Plat-I, cut through center of turbine 3, side view, length of tank: 700 m

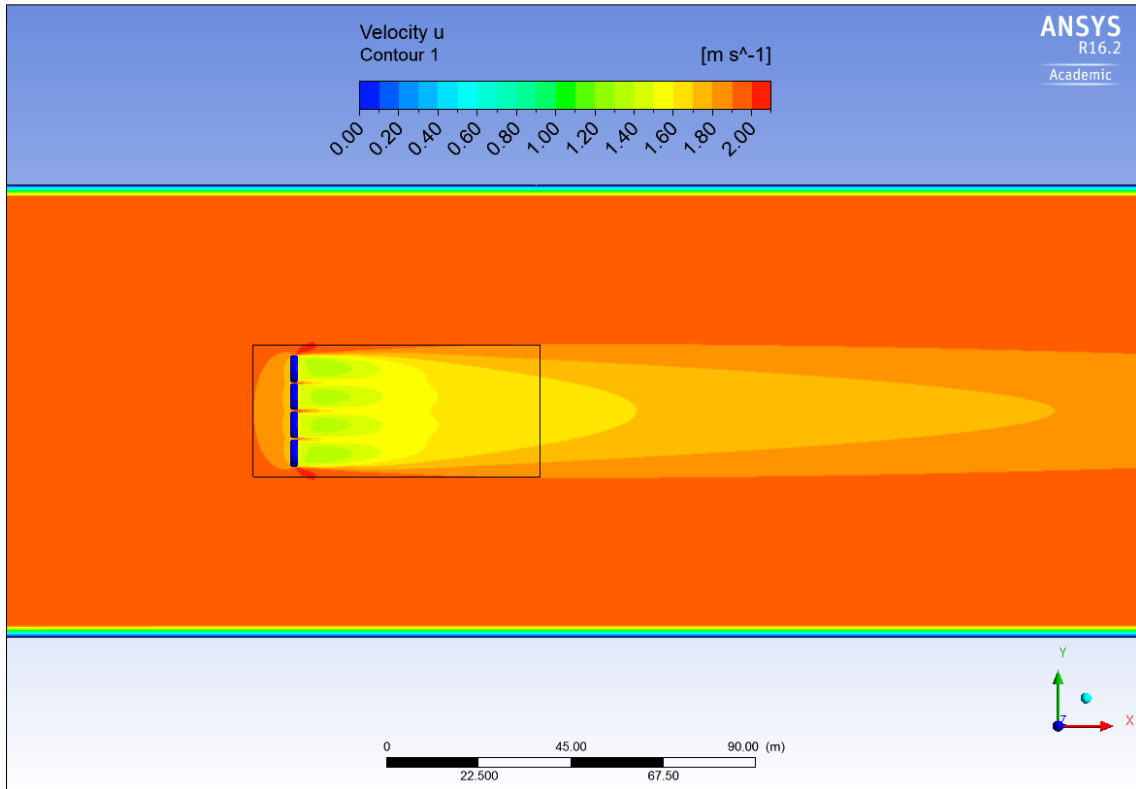


Figure 4.15 1 Plat-I, cut through turbine center X-Y-plane, top view, zoomed, length of tank: 700 m

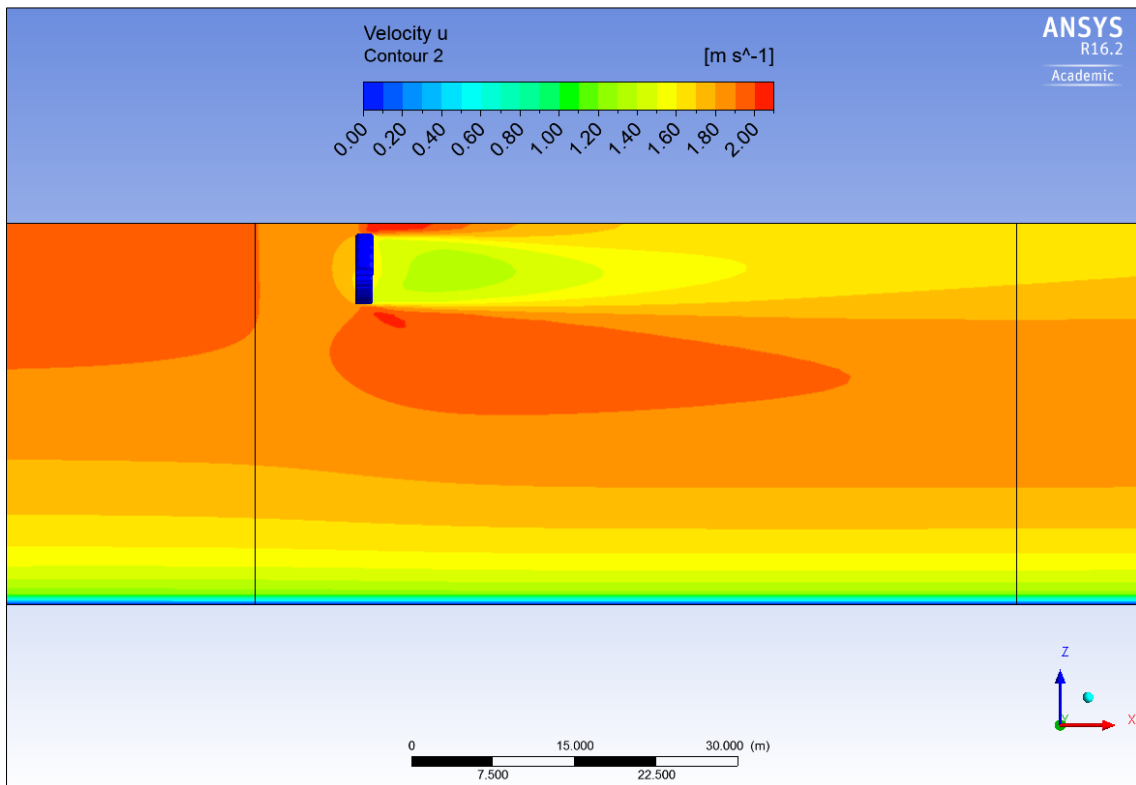


Figure 4.16 1 Plat-I, cut through center of turbine 3, side view, zoomed, length of tank: 700 m

4.3.2 Two Plat-I, Distance: 126 m (20 x D)

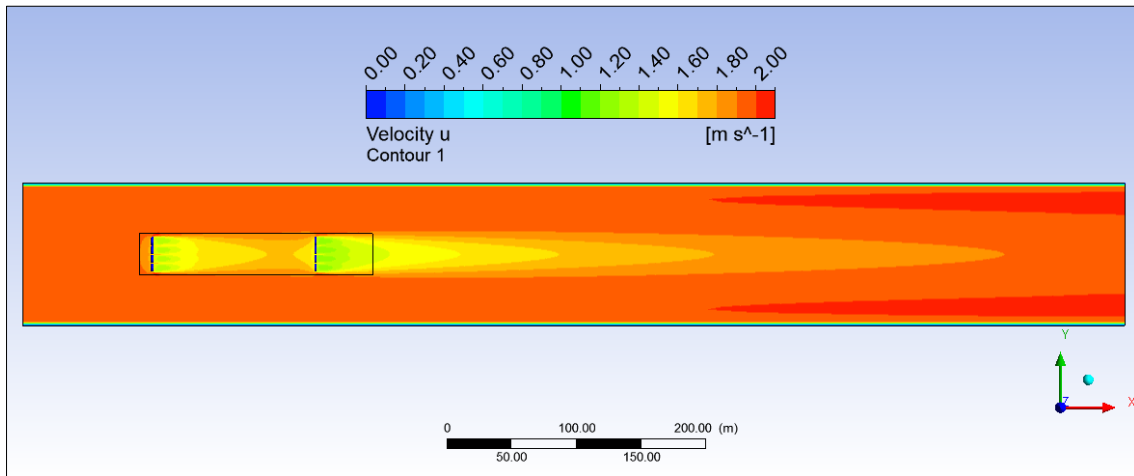


Figure 4.17 2 Plat-I, distance: 20 D, cut through turbine center X-Y-plane, top view, length of tank: 850 m

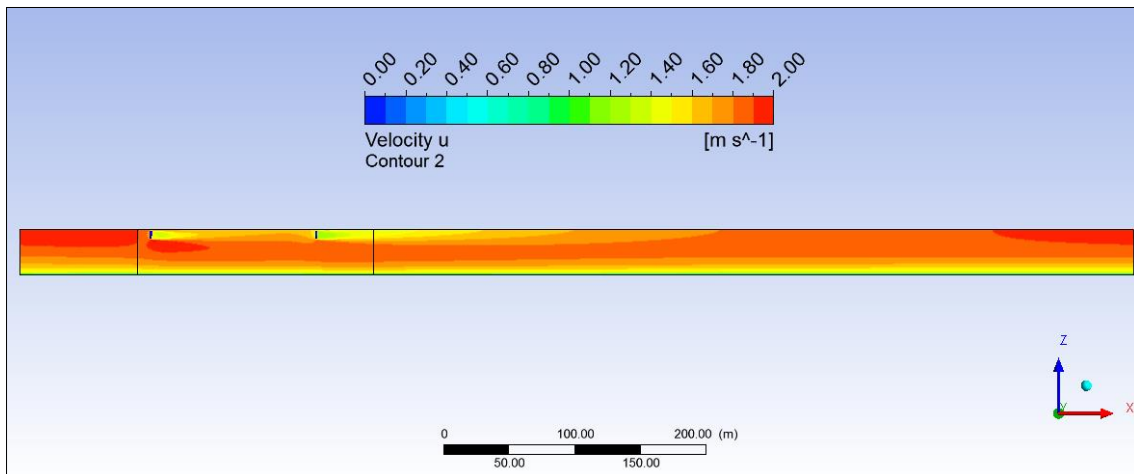


Figure 4.18 2 Plat-I, distance: 20 D, cut through center of turbine 3, side view, length of tank: 850 m

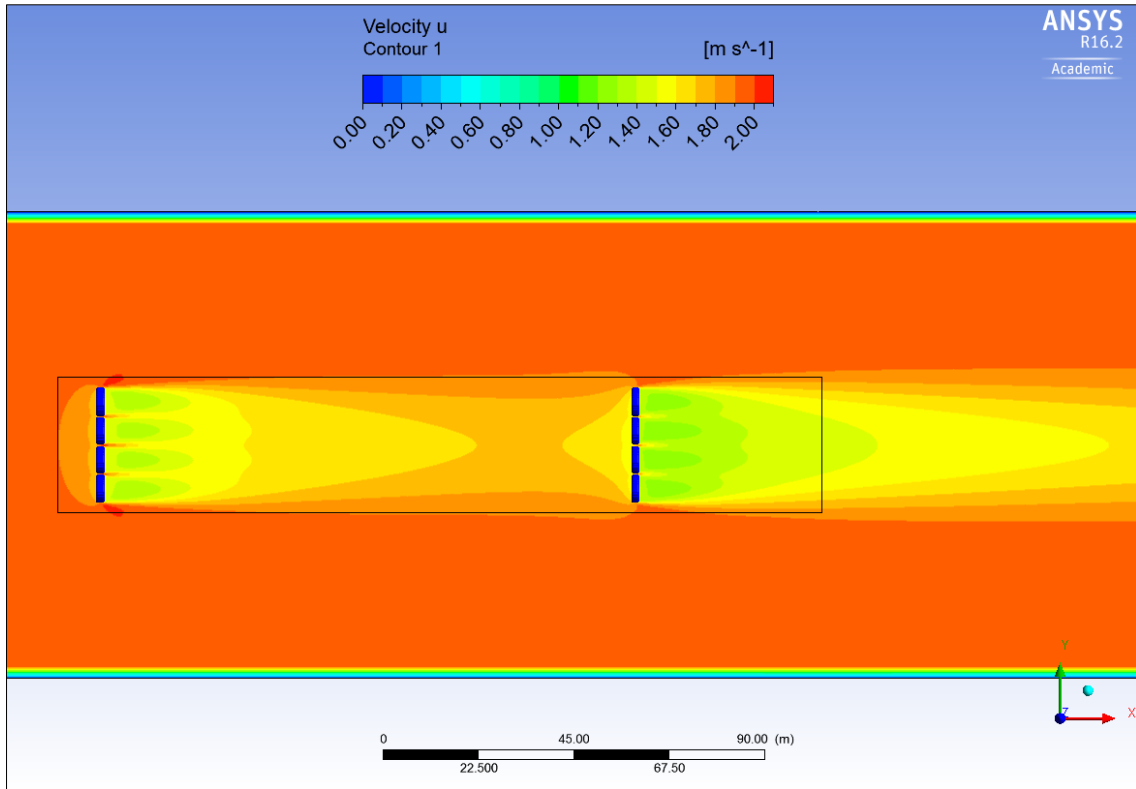


Figure 4.19 2 Plat-I, distance: 20 D, cut through turbine center X-Y-plane, top view, zoomed, length of tank: 850 m

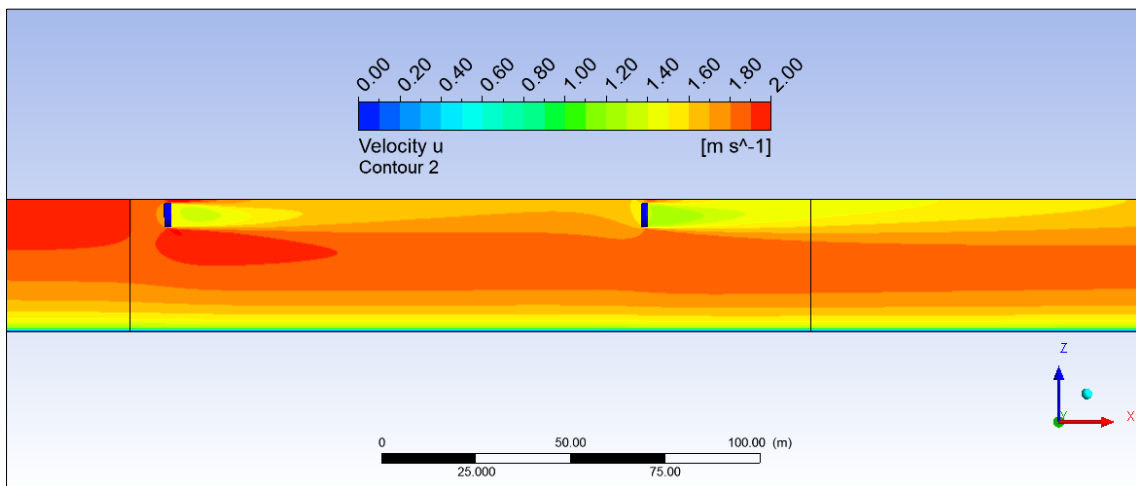


Figure 4.20 2 Plat-I, distance: 20 D, cut through center of turbine 3, side view, zoomed, length of tank: 850 m

4.3.3 Two Plat-I, Distance:441 m (70 x D)

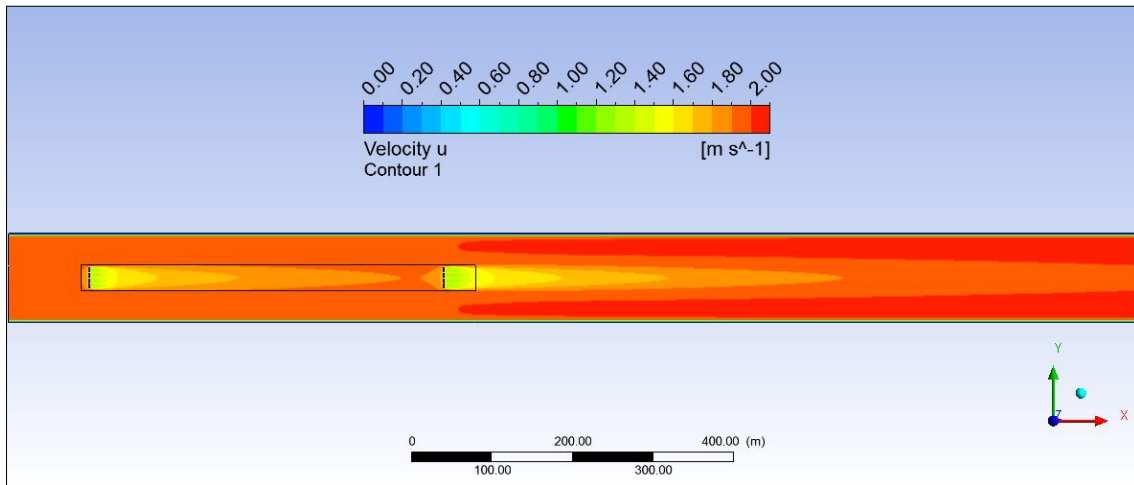


Figure 4.21 2 Plat-I, distance: 70 D, cut through turbine center X-Y-plane, top view, length of tank: 1400 m

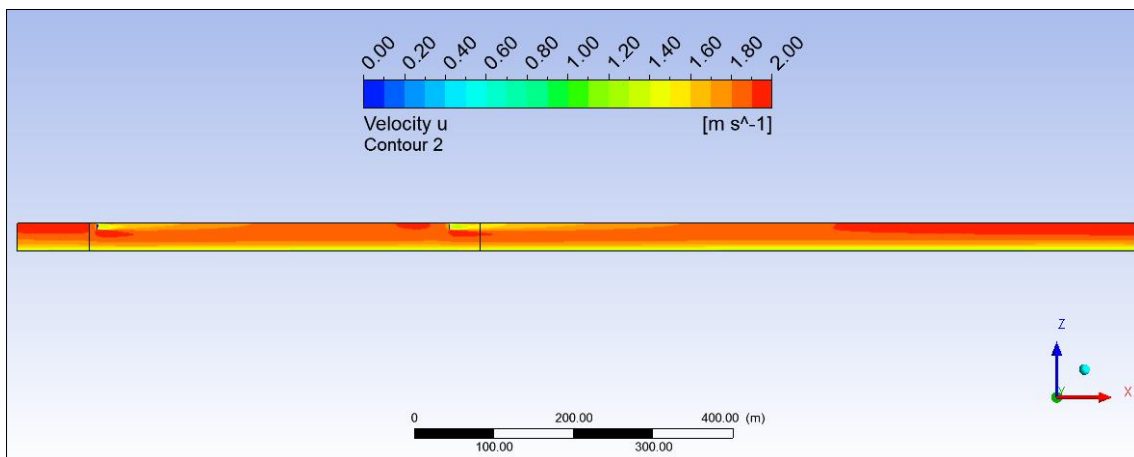


Figure 4.22 2 Plat-I, distance: 70 D, cut through center of turbine 3, side view, length of tank: 1400 m

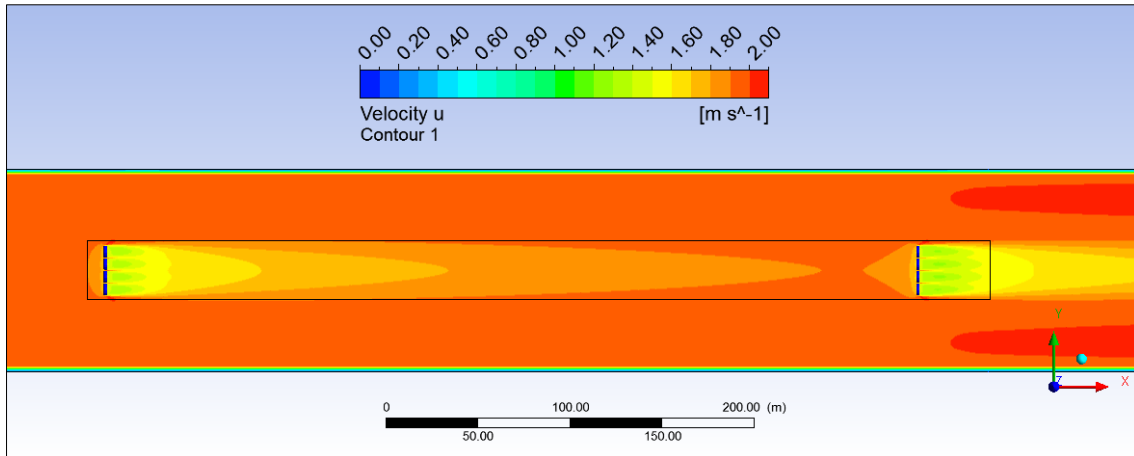


Figure 4.23 2 Plat-I, distance: $70 D$, cut through turbine center X-Y-plane, top view, zoomed, length of tank: 1400 m

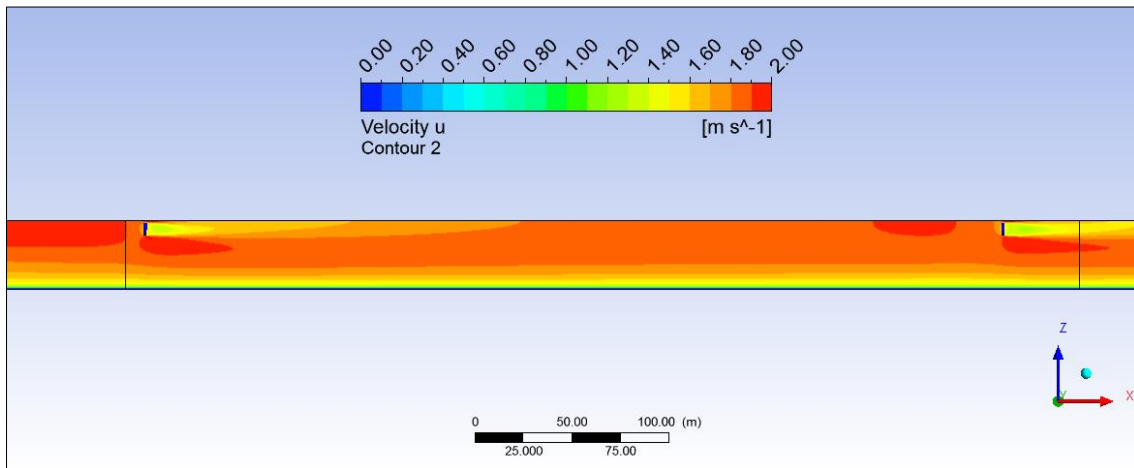


Figure 4.24 2 Plat-I, distance: $70 D$, cut through center of turbine 3, side view, zoomed, length of tank: 1400 m

4.4 CFD POST-PROCESSING

The purpose of any CFD simulation is to extract as much information as possible on the investigated flow to identify/visualize what the flow would look like in reality and if there are occurring phenomena such as vortices, turbulence and velocity or pressure anomalies. If the investigated flow includes turbomachinery operating in it, additional characteristics such as extracted/induced power and thrust as well as wake which the machine induces is targeted to be analyzed.

The simulations carried out in this work include the determination of: (1) the distribution of the flow velocity over the entire domain, (2) the formation of the wakes downstream of the turbines, and (3) the power and thrust absorbed by each turbine from the flow. Therefore data from the CFD results have been extracted and processed to get the intended information.

Flow deficit:

The flow deficit is defined as a deficit of velocity at a specific point within the wake related to the incident velocity of the flow.

$$u_{def} = 1 - \frac{u_{wake}}{u_{\infty}} \quad (4.5)$$

with:

u_{def}	<i>velocity deficit</i>	[m/s]
u_{wake}	<i>velocity at certain point in wake</i>	[m/s]
u_{∞}	<i>incident velocity of the undisturbed flow</i>	[m/s]

Following, flow deficit curves are illustrated representing the drop and subsequent recovery of the flow speed along a turbine’s x-coordinate throughout the entire tank. Velocity is measured at 1000 points of equidistant distance from the entry to the exit of the tank as schematically showed in the following figure.

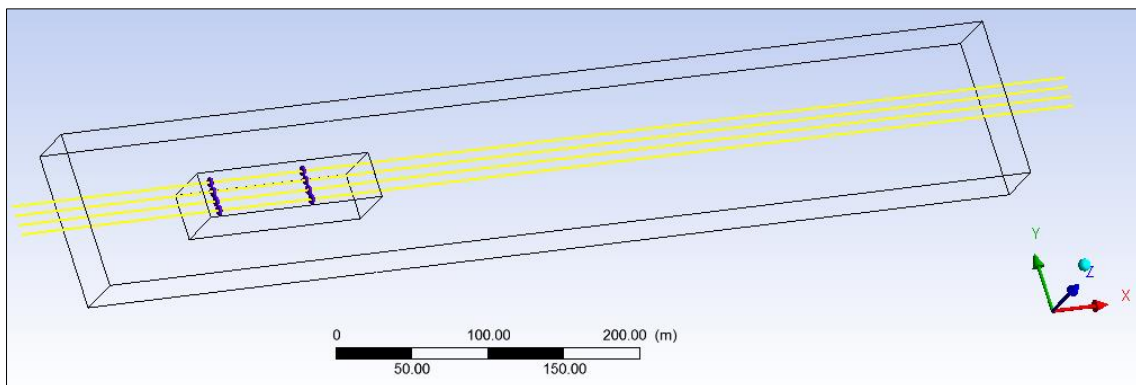


Figure 4.25 Velocity measurement lines throughout tank, height: turbine center, Y and Z-coordinate fix

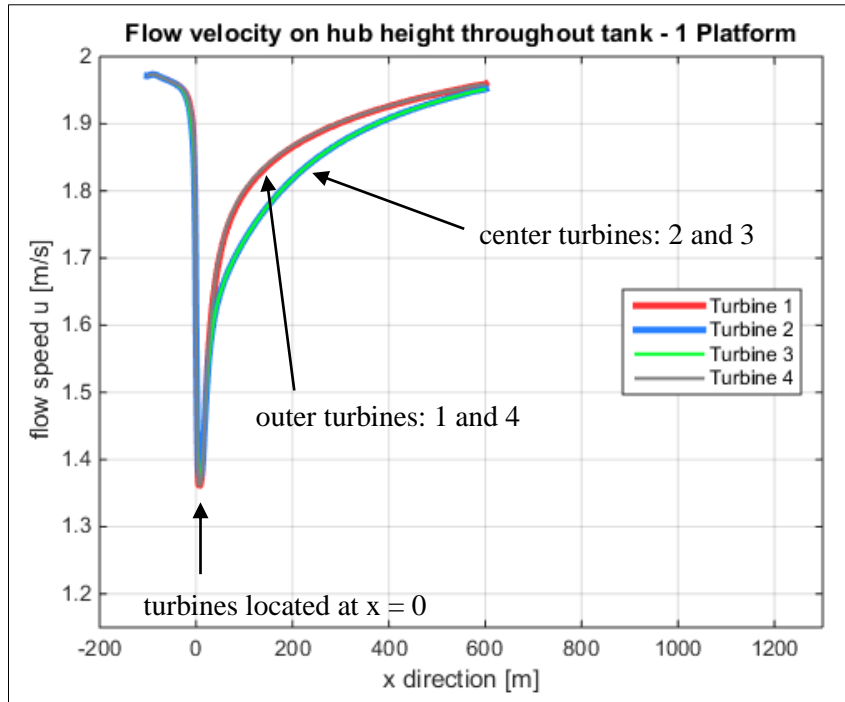


Figure 4.26 Flow velocity throughout tank on hub height of all turbines

The in Figure 4.26 illustrated flow speed reduction due to the presence of the turbine will be transformed in a deficit curve applying equation 4.5, which results in Figure 4.27.

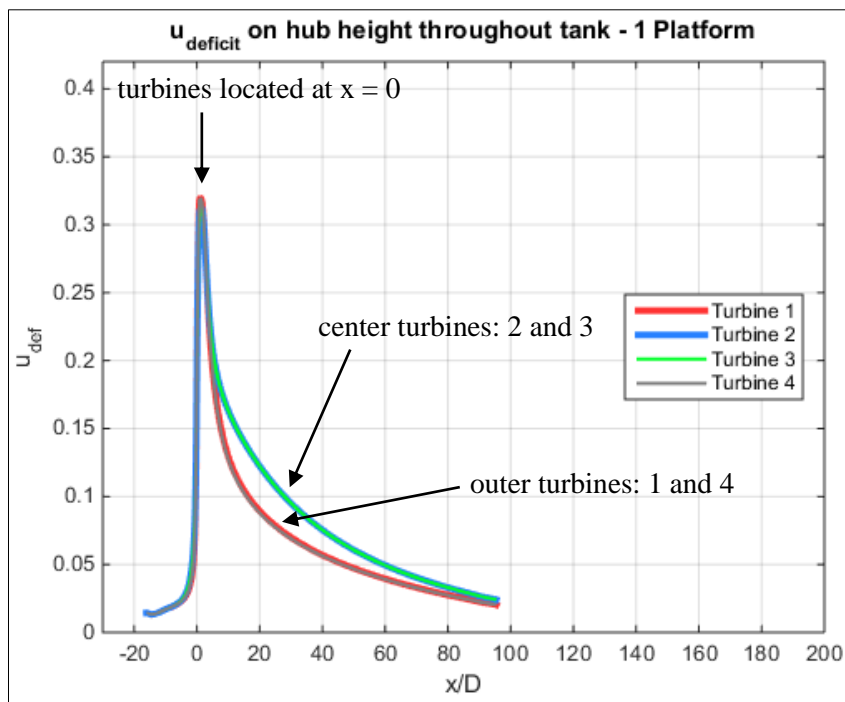


Figure 4.27 Previous figure transformed in non-dimensional illustration: $u_{deficit}$ over x/D

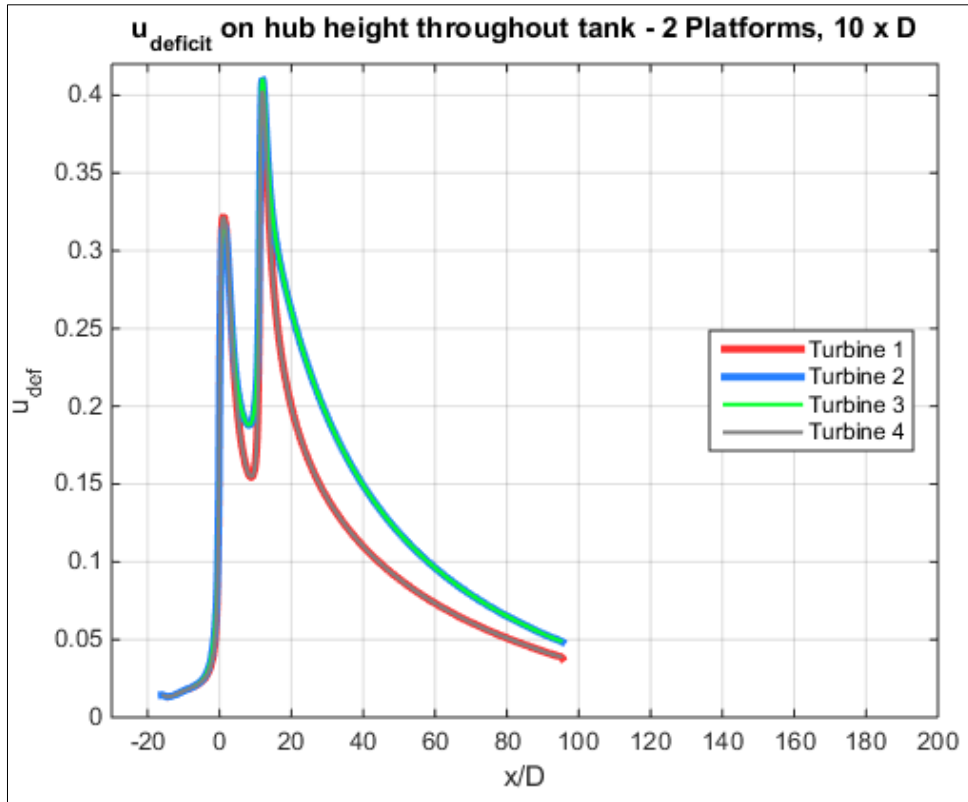


Figure 4.28 u_{deficit} on hub height, 2 platforms, distance: 10 D

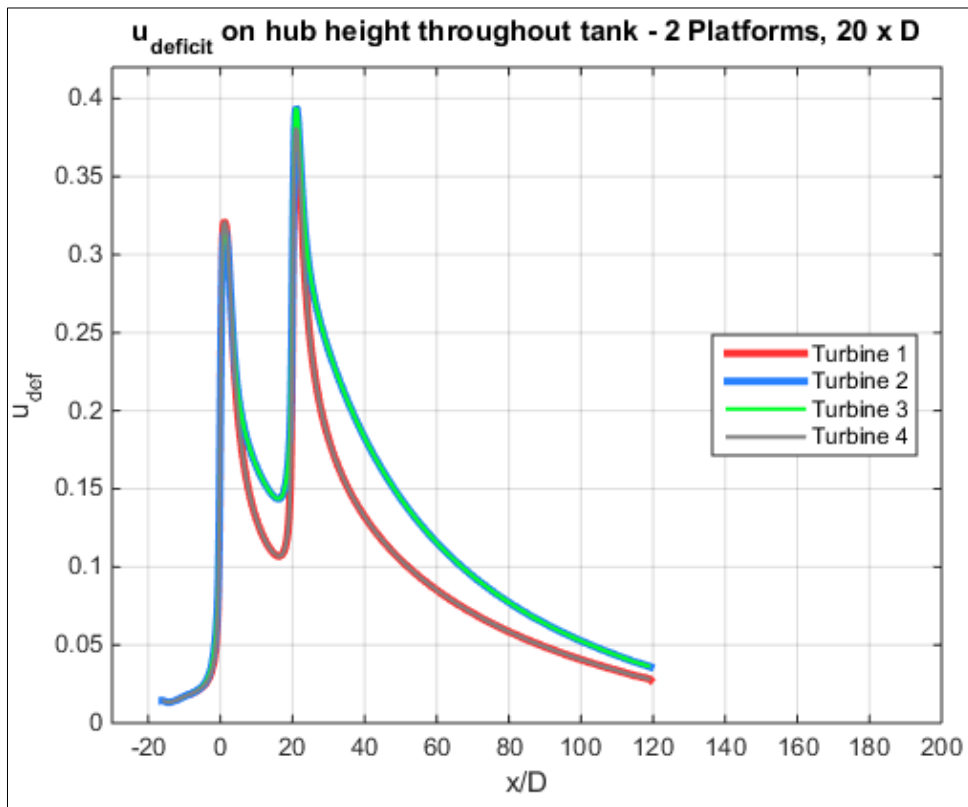


Figure 4.29 u_{deficit} on hub height, 2 platforms, distance: 20 D

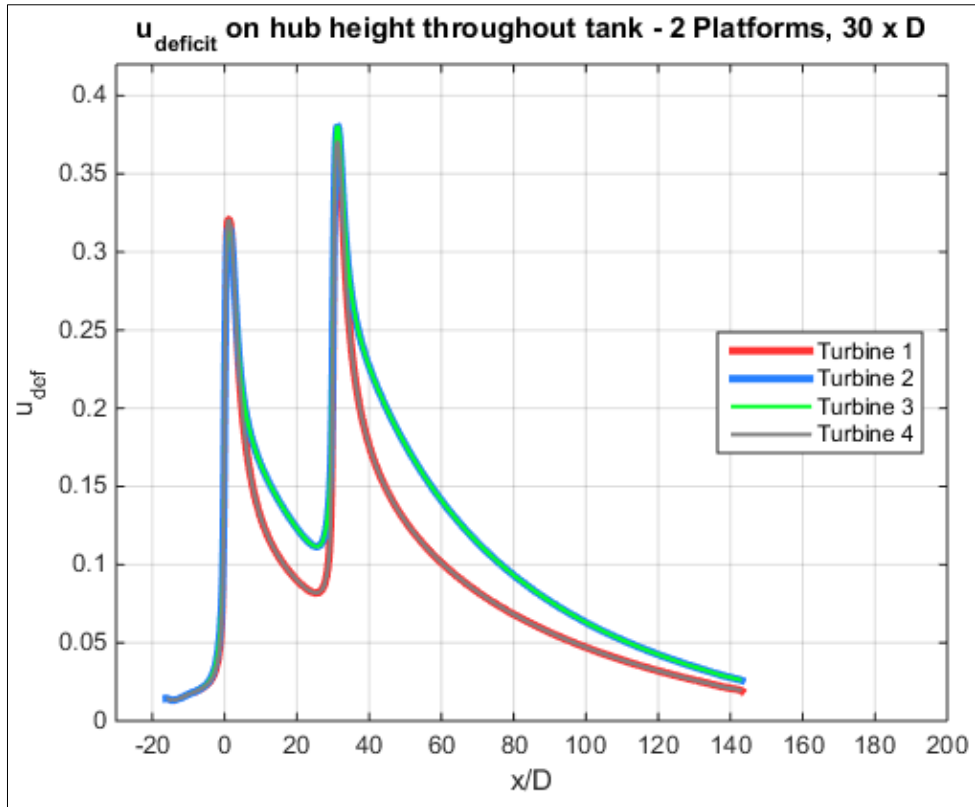


Figure 4.30 $u_{deficit}$ on hub height, 2 platforms, distance: $30 D$

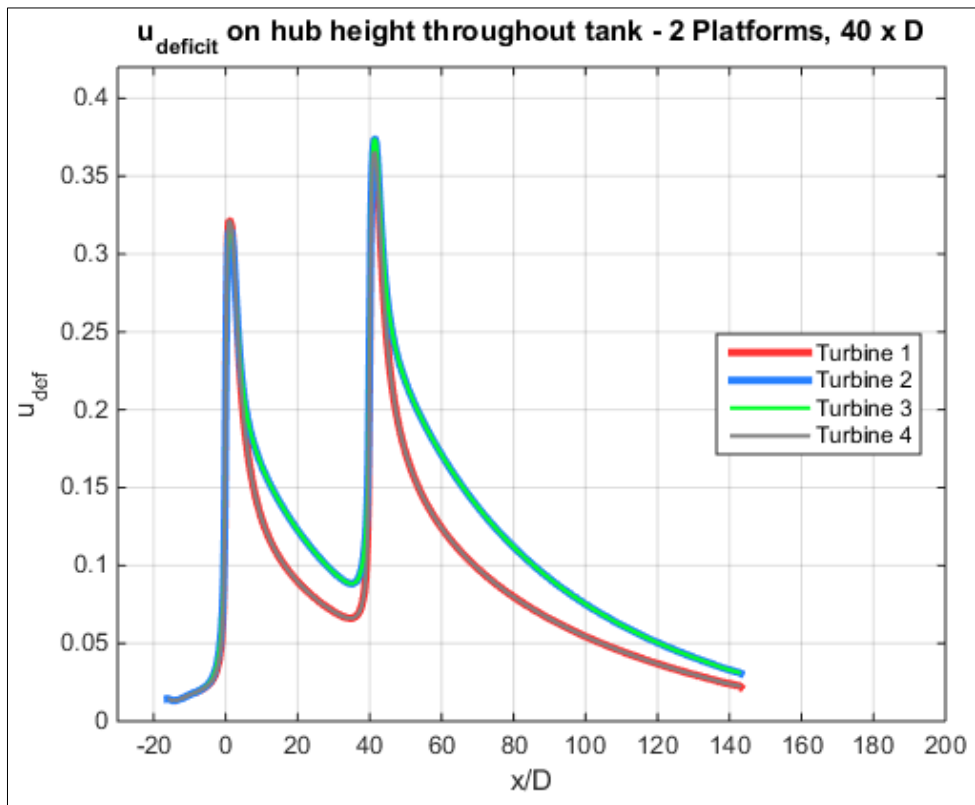


Figure 4.31 $u_{deficit}$ on hub height, 2 platforms, distance: $40 D$

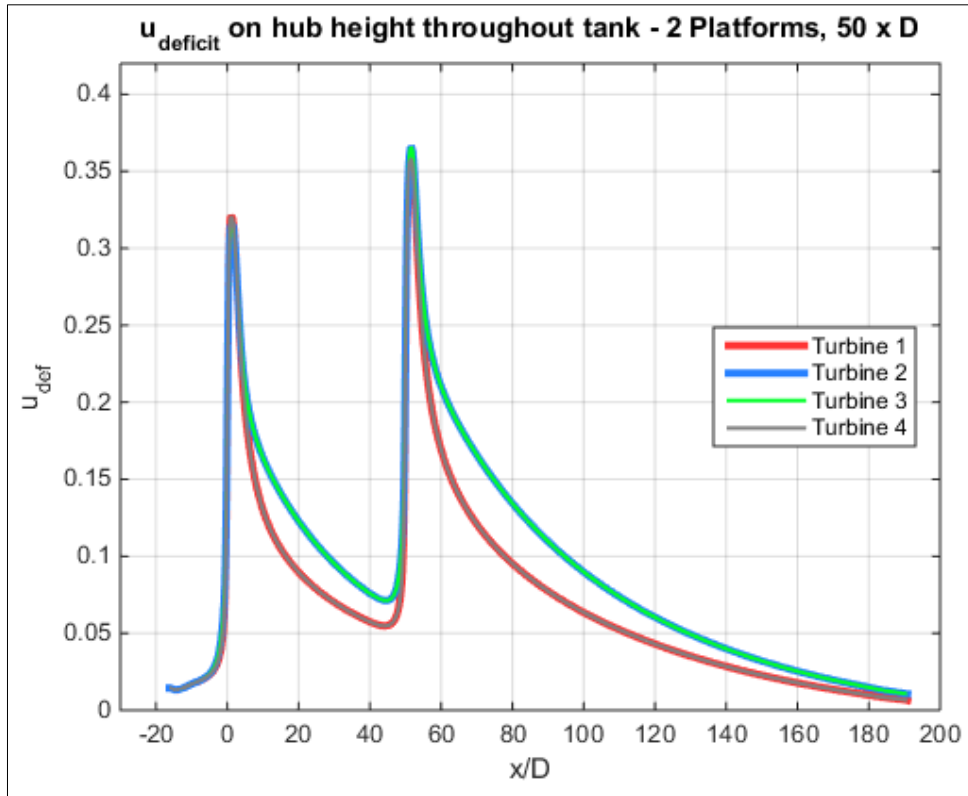


Figure 4.32 $u_{deficit}$ on hub height, 2 platforms, distance: $50 D$

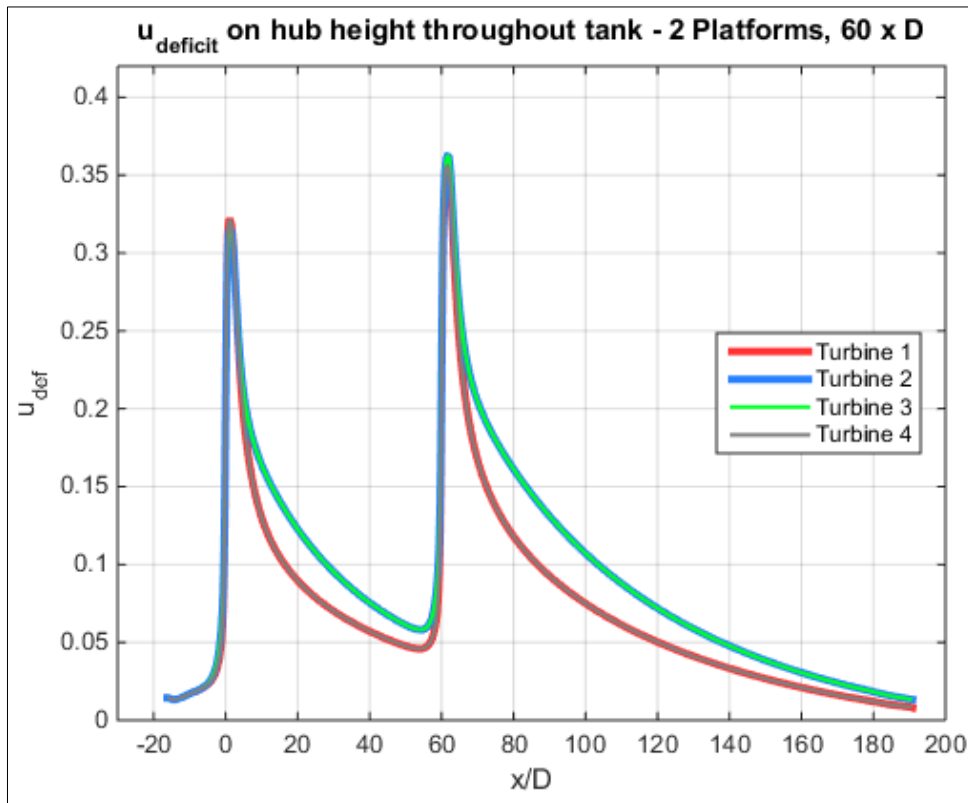


Figure 4.33 $u_{deficit}$ on hub height, 2 platforms, distance: $60 D$

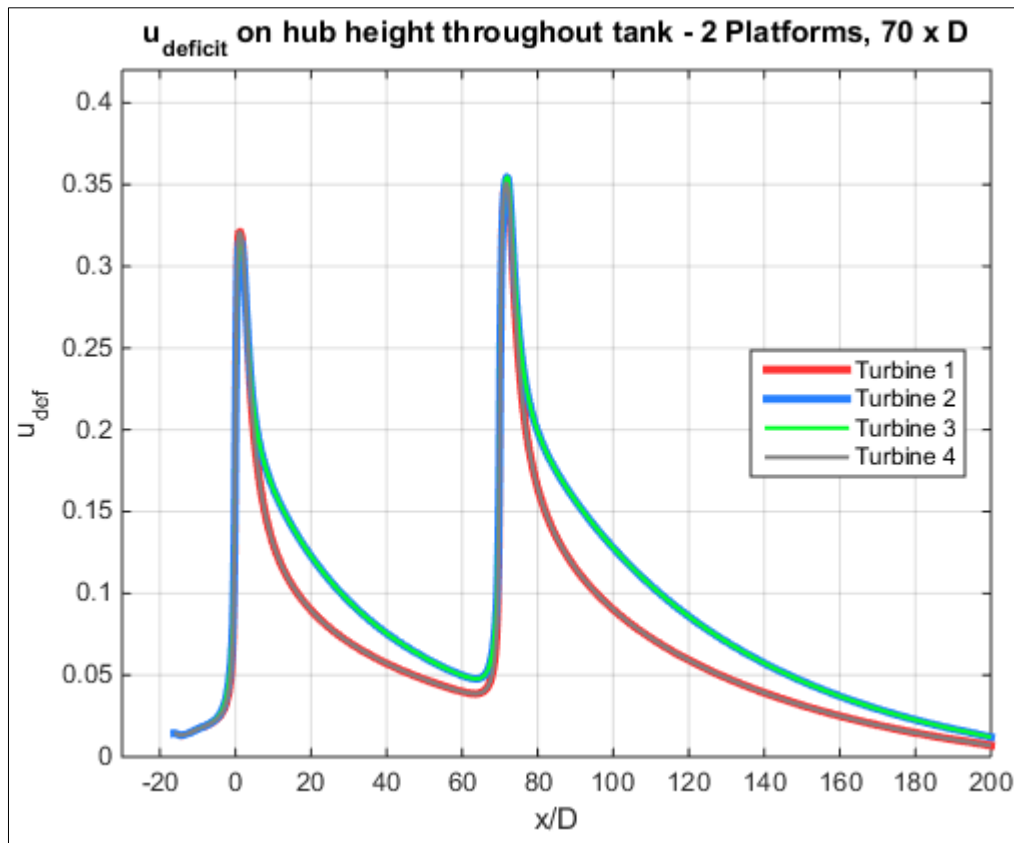


Figure 4.34 $u_{deficit}$ on hub height, 2 platforms, distance: $70 D$

One can see that with increasing distance between the turbine arrays the recovery of the flow speed downstream of the first turbine array improves and subsequently the velocity deficit of the second array diminishes. This flow characteristic has been expected. What also can be identified is the fact that the flow velocity in the wake of the center turbines (two and three) recovers more slowly than the velocity in the wake of the outer turbines (one and four). This is very likely due to the circumstance that in the direct adjacent area of turbine 2 and 3 is the wake area of turbine 1 and 4 respectively. So that viscous effects on surrounding flow does not help the recovery of the flow speed for those two turbines. Whereas half of the adjacent area of turbine 1 and 4 is flow which has not been affected by turbine placement and therefore flow velocity within these two areas is higher so that viscous effects help the recovery of the wake of turbine 1 and 4.

Finally, we are interested in how the wake affects the power extraction of the second turbine array in comparison to the first with varying distance. The investigation revealed following results:

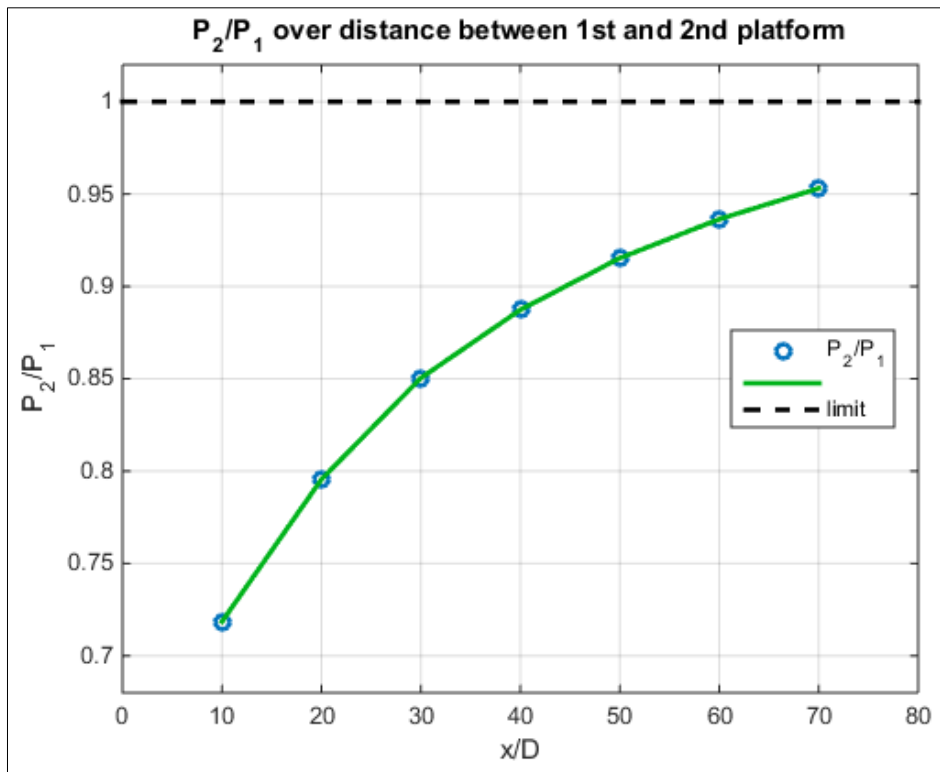


Figure 4.35 Extracted power of second turbine array divided by the first with varying distances between the arrays

We see that the extracted power of the second turbine array increases with increasing distance between the arrays. At a distance of 50 times turbine diameter of the second array to the first, the extracted power is over 90 % of that of the first array. This is considered a feasible distance and would be recommended as a minimum between two Plat-I platforms (where the second platform is placed directly in the wake of the first) if the site allows such space intensive placement.

It is mentioned that the results carried out by the CFD simulation carry some deviations from parts of the expected outcome. In particular the recovery of the flow velocity in the wake is expected to happen faster in reality than the results of the CFD simulations revealed. This is due to mainly two factors. First, the turbulence models which are available in the software kit are not capable to reproduce the complex and highly turbulent river flow which in reality would support a faster recovery of the flow speed in the wake. And second, the use of a RANS model to determine the flow domain which due to its simplifications carry uncertainties with regards to the implementation of viscous effects and turbulence.

5 CASE STUDY: 1 MW RHK POWER PLANT IN THE AMAZON

In this chapter the content discussed previously in this work will be applied to reality conceptualizing a 1MW River Hydrokinetic Energy facility under favorable (real existing) conditions. The site chosen for that proposal is a river section of the Amazon at the city of Óbidos, Pará State, Brazil. This site has been chosen for a variety of reasons:

- (1) the resource present there supports the thesis of a commercial viable generation of hydrokinetic energy,
- (2) flow conditions at Óbidos are extensively documented over decades so that the data recorded there is assumed to be of high reliability, and
- (3) the site is located directly at the city of Óbidos, a town with 10.000+ inhabitants, so that potential energy demand as well as grid infrastructure is assumed to be present close to the generating facility.

It is conceptualized a configuration consisting of five Plat-I platforms each carrying four SCHOTTEL SIT-250 turbines with a rotor diameter of 6.30 m. Even though a larger rotor diameter would lead to a more efficient (higher CF) exploitation of the resource, it is chosen the 6.30 m rotor due to its market readiness, meaning that this turbine already has been successfully tested in open waters and could be applied right away for a commercial power generation project.

5.1 CONDITIONS AT SITE AND PLATFORM POSITIONING

Following, conditions which are necessary to be known to set up a commercial RHK project (at a specific site) will be stated. Those are:

- (1) flow speed distribution at site,
- (2) power curve of turbine, and
- (3) AEP and CF being achieved for chosen power generation unit.

Figure 5.1 combines requirement (1) and (2). The range of the flow speed distribution determined in Figure 5.1 also coincides with the range of the flow speed from an ADCP measurement (Figure 5.2) carried out by the Federal University of Amazonas in July of 2011. This confirms that the assumptions made for the resource seem to be reliable.

As illustrated in Figure 5.2 the flow speed reaches its maximum between approximately 500-1000 m inward from the northern river bank. From an economic point of view it would be suggested to place any energy extraction device within that area. Figure 5.3 and 5.4 are illustrating the site and where platform placement being suggested from a satellite perspective.

Out of the combined flow speed distribution – power curve Figure, the AEP and subsequently the Capacity Factor at which the facility is operating can be calculated as shown in chapter 3.

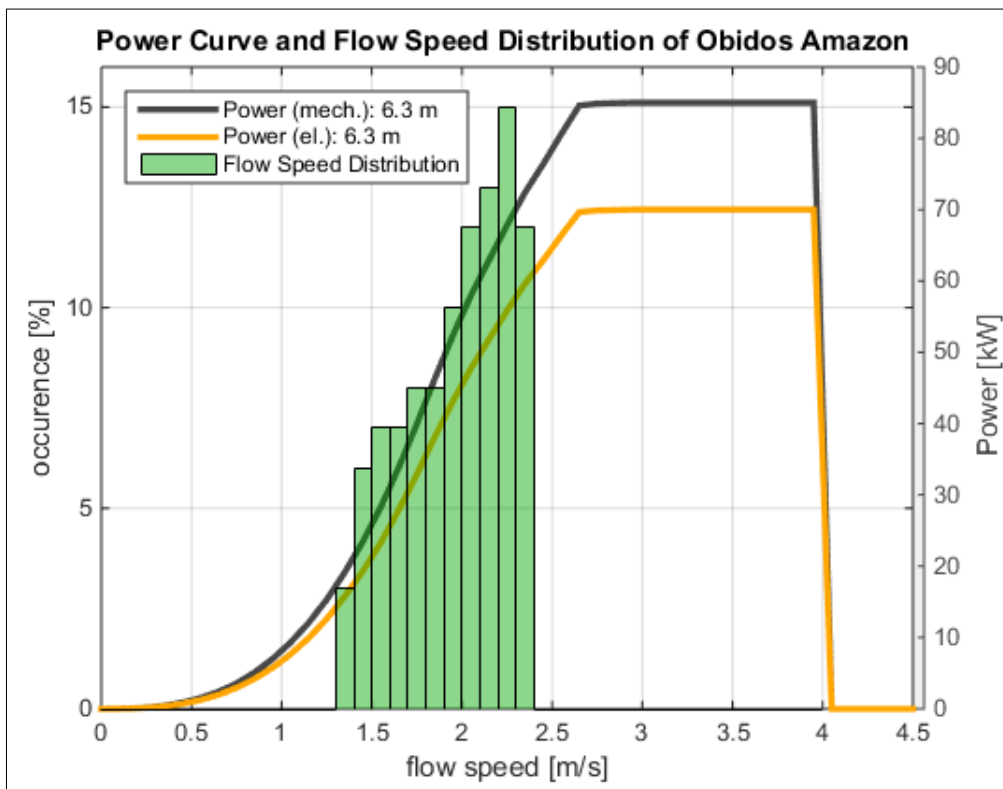


Figure 5.1 Flow Speed Distribution of Amazon at Óbidos and Power Curves (mechanical and electric) of 6.30 m rotor

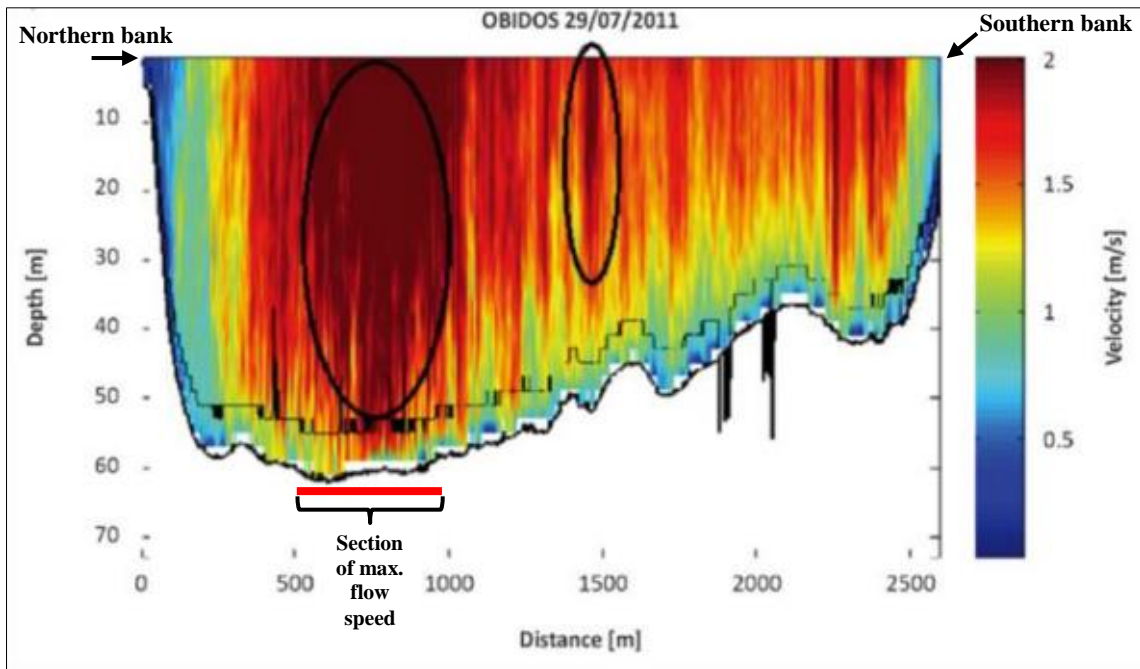


Figure 5.2 ADCP measurement of Amazon river at Óbidos [14], compare flow speeds with that of Figure 5.1

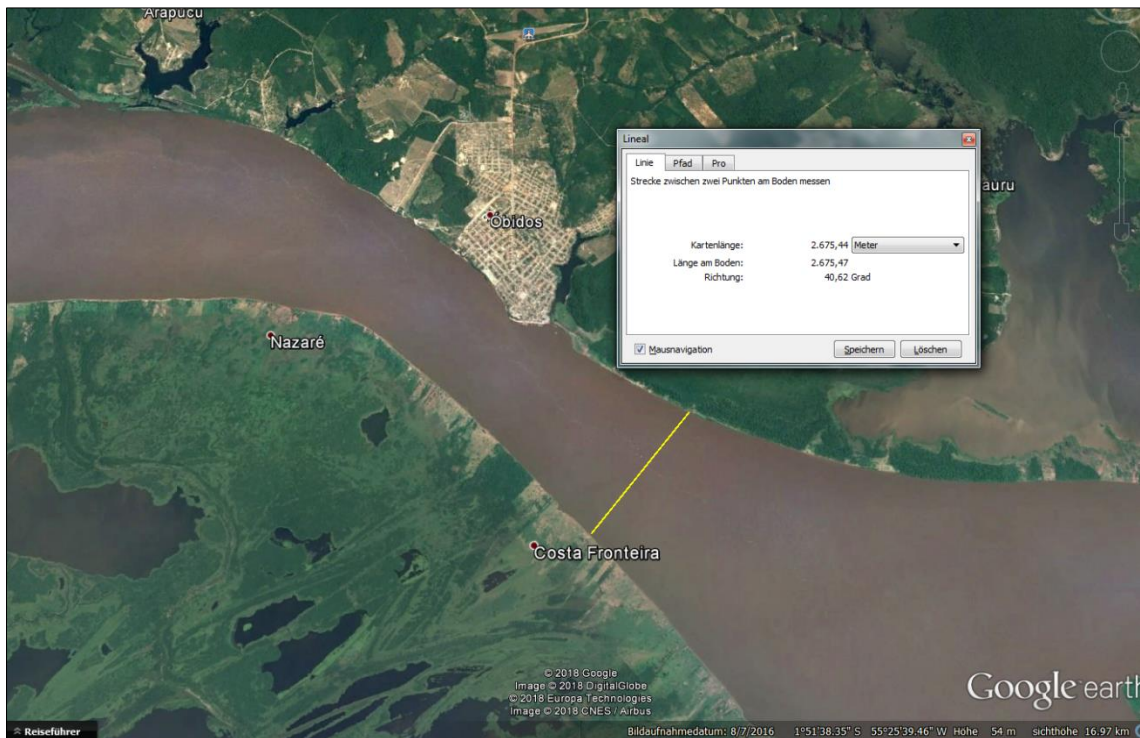


Figure 5.3 Satellite view on site with cross section of ADCP measurement (yellow line), viewing height: 16.97 km

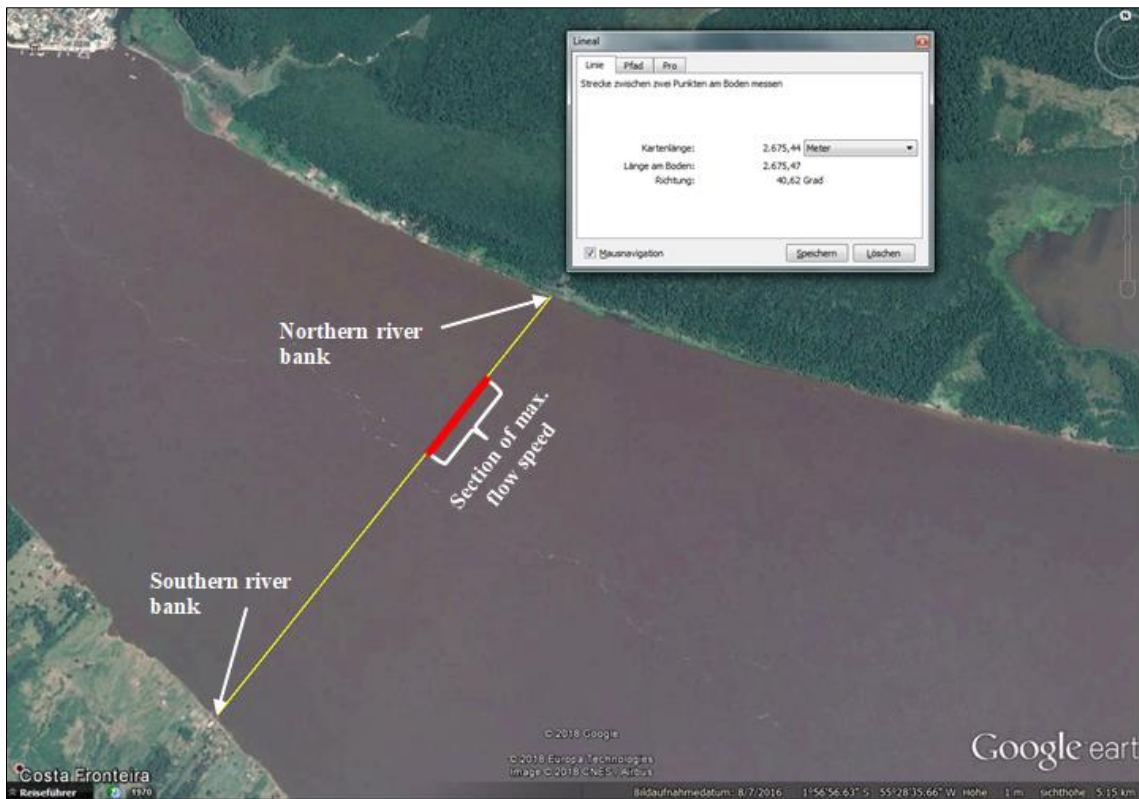


Figure 5.4 Satellite view on site with cross section of ADCP measurement (yellow line), viewing height: 5.15 km

5.2 ARRAY LAYOUT AND YIELD STUDY

The requirement for the array layout is based on the case that for a flow velocity of 2 m/s the total extracted mechanical power is equal or above to 1 MW. Even though this assumption seems overoptimistic according to Figure 5.1 where approximately half of the occurring velocity range is below 2 m/s, it has to be remembered that the flow speed range illustrated in that Figure includes the entire cross sectional area of the river, meaning also the areas of the cross section which are showing velocities below 1 m/s. Figure 5.2 allows the assumption that there exists a section where the flow speed is constantly above 2 m/s. As it is being intended to operate a RHK energy generating facility as economically as possible, it has to be placed where the flow speed is at maximum. At a flow speed of 2 m/s the 6.30 m version of the SIT-250 generates approximately 55 kW of mechanical power measured at the turbine shaft. That means that a configuration of five Plat-I platforms mounting a total of 20 turbines achieves the intended power generation of 1 MW.

The layout aims an efficient use of the river space while achieving the targeted power extraction. As shown in chapter 4, turbines operating in the wake of one another should be placed at a distance of at least $50 \times D$ to each other. A layout which fulfills those requirements is proposed below.

5.2.1 Array Layout

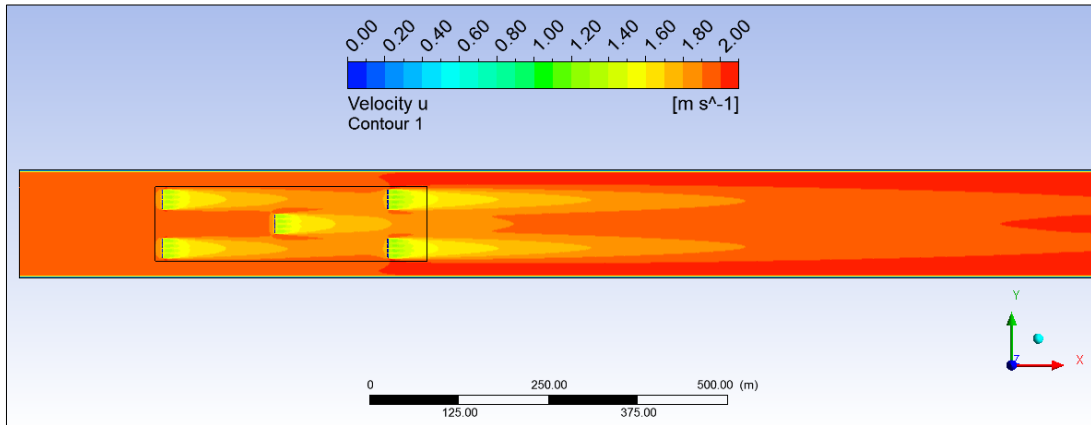


Figure 5.5 5 Plat-I, distance: $2 \times 25 D$, cut through turbine center X-Y-plane, top view, length of tank: 1500 m

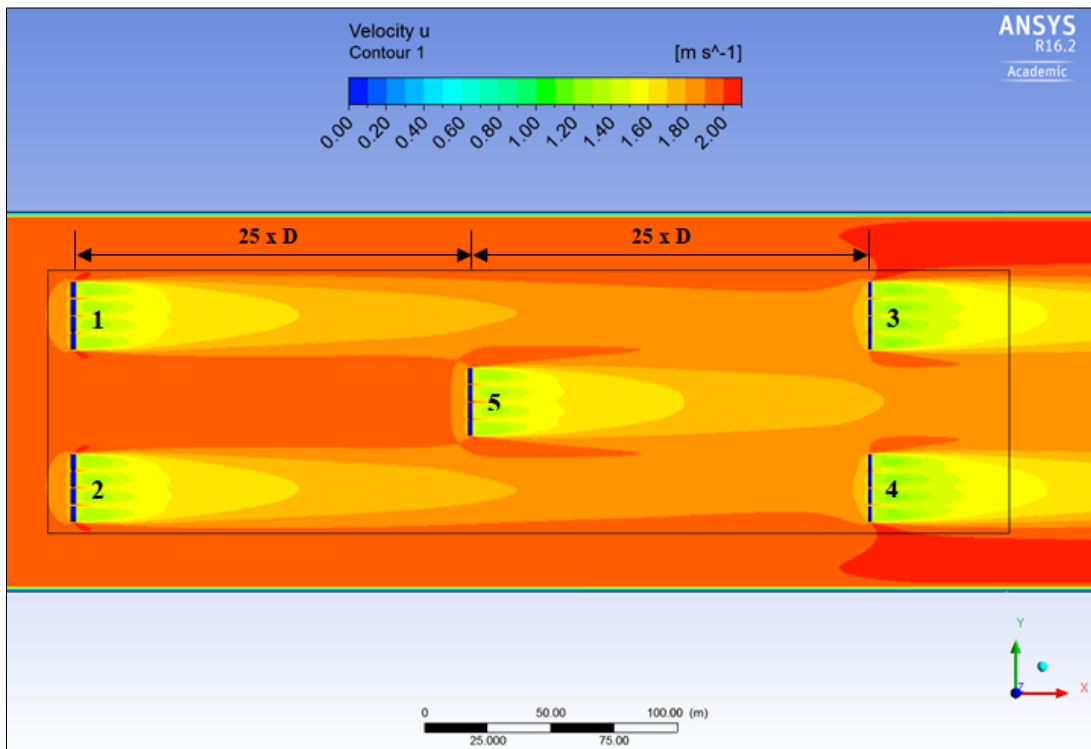


Figure 5.6 5 Plat-I, distance: $2 \times 25 D$, cut through turbine center X-Y-plane, top view, zoomed, length of tank: 1500 m

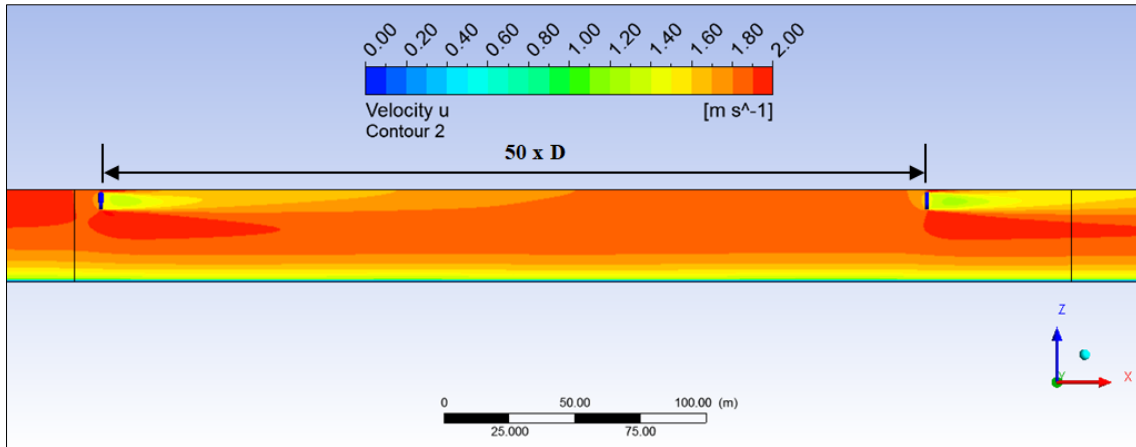


Figure 5.7 5 Plat-I, distance: $2 \times 25 D$, cut through center of turbine 3, side view, zoomed, length of tank: 1500 m

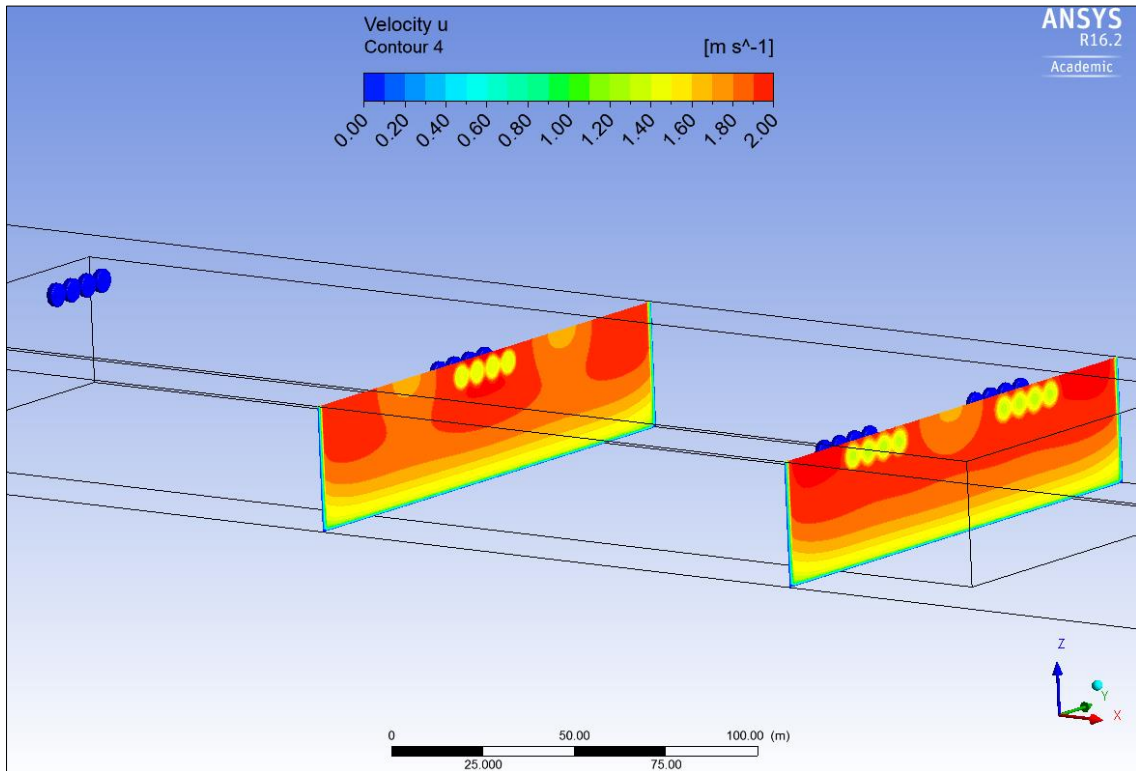


Figure 5.8 5 Plat-I, distance: $2 \times 25 D$, cut through Y-Z-planes 10 m behind turbines, side view, length of tank: 1500 m

The power and thrust determination has been performed by ANSYS CFX POST for each turbine. The summarized result on mechanical power extraction is shown below.

Table 5.1 Mechanical power extracted by each Plat-I platform (rig), calculated by ANSYS CFX POST

Total mechanical power		
rig [#]	mech. power [kW]	average rig power [kW]
1	207,94	
2	207,94	
3	194,12	
4	194,13	
5	210,20	202,86
Total:	1.014,32	kW
Total array efficiency:	97,56	%

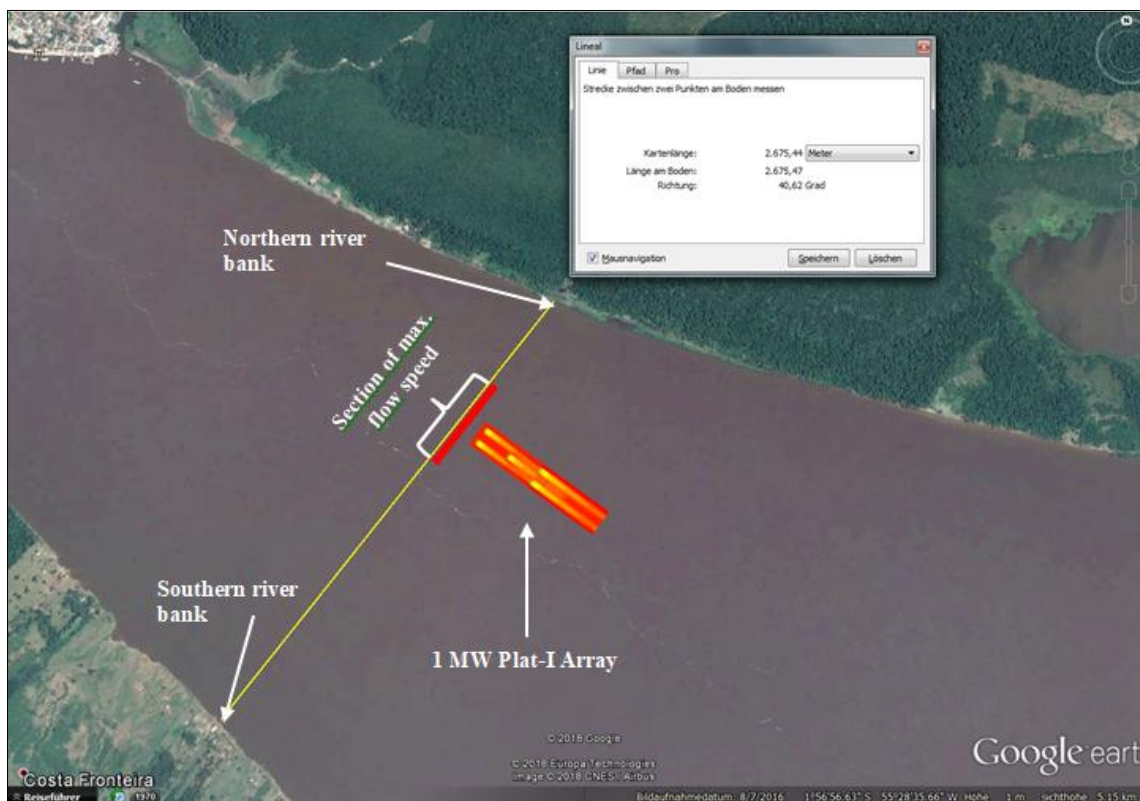


Figure 5.9 Óbidos site with 1 MW Plat-I Array placement, true-to-scale representation

5.2.2 Yield Study

In this section, estimations on the Annual Energy Production (AEP) being made for the case that the above described platform configuration will be operating at the Óbidos site. Two cases will be considered: first, the medium AEP which will be achieved by taking the averaged flow speed distribution of the entire cross sectional area (see Figure 5.1) into account, and second: a high yield AEP which will be achieved by placing the platforms into the “sweet spot” where the flow speed is estimated to be constantly 2 m/s.

For the purpose of estimating the energy which will be fed-in into an electric grid as well as for a subsequent LCoE observation (chapter 5.3) it has to be determined the electric energy which will be generated over a certain period of time. Therefore all previous AEP calculations which determined the mechanical energy produced have to be adjusted for an electromechanical efficiency. This constant for the SIT-250 is set to be 0.8235.

$$AEP_{el} = 0.8235 \cdot AEP_{mech} \quad (5.1)$$

Further, it has to be included an availability of the system operating over the year. This means how many hours of an entire year the system likely being in operation mode instead of for example being halted or in maintenance mode. This factor is set to be 90%. With those properties the AEPs can be determined.

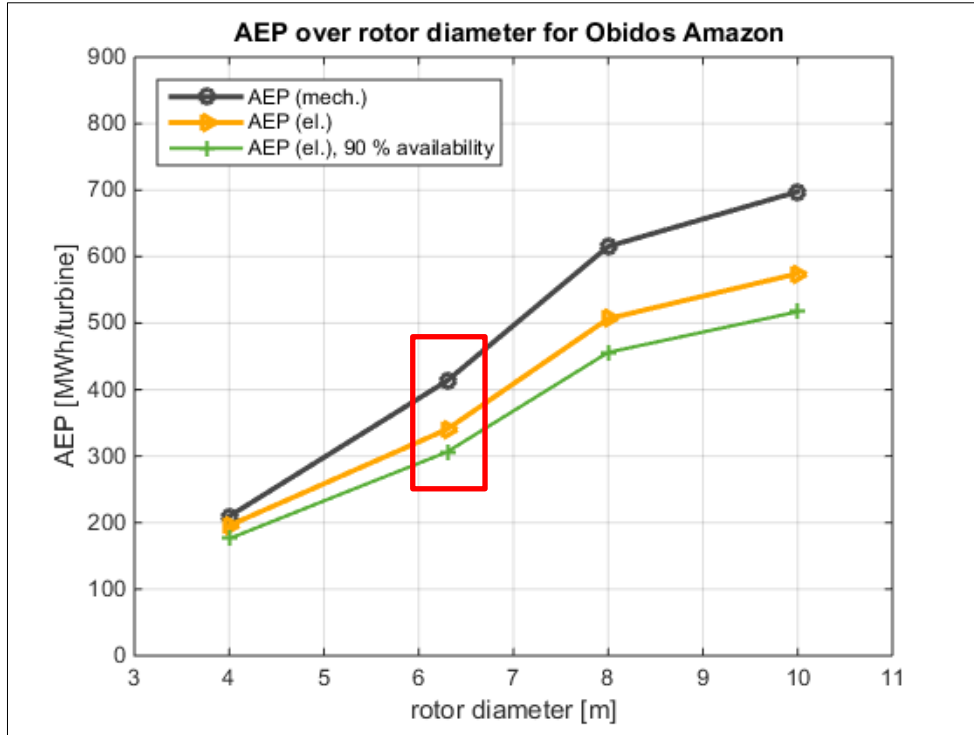


Figure 5.10 Medium AEPs for several rotor diameters

$$AEP_{el,90\%} = 0.8235 \cdot AEP_{mech} \cdot 0.9 \quad (5.2)$$

Figure 5.10 exemplarily illustrates the discounting from the mechanical AEP to the electrical AEP down to the real AEP ($AEP_{el,90\%}$) which ultimately gets fed-in into the grid. It will now be estimated the average AEP and a high yield AEP (constant 2 m/s) for the site.

- (1) Average AEP at site: Basis: Average Flow Speed Distribution (Figure 5.1)

$$AEP_{mech,array} = \left[\sum_{i=1}^n P_{mech}(v_i) \cdot Oc(v_i) \right] \cdot [\# \text{ of turbines}] \quad (5.3)$$

$$AEP_{mech,array} = \left[413.38 \frac{MWh}{year} \right] \cdot [20] = 8267.64 \frac{MWh}{year} \quad (5.4)$$

$$AEP_{el,90\%,array} = 0.8235 \cdot 8267.64 \frac{MWh}{year} \cdot 0.9 = 6128.08 \frac{MWh}{year} \quad (5.5)$$

(2) High Yield AEP at site (a): Basis: Flow Speed constant at 2 m/s

$$AEP_{mech,array} = P_{mech} \left(2 \frac{m}{s}\right) \cdot Oc \left(2 \frac{m}{s}\right) \cdot [\# \text{ of turbines}] \quad (5.6)$$

$$AEP_{mech,array} = 52.36 \text{ kW} \cdot 8760 \frac{h}{year} \cdot 20 = 9173.64 \frac{MWh}{year} \quad (5.7)$$

$$AEP_{el,90\%,array} = 0.8235 \cdot 9173.64 \frac{MWh}{year} \cdot 0.9 = 6799.16 \frac{MWh}{year} \quad (5.8)$$

(3) High Yield AEP at site (b): Basis: ANSYS CFX POST performance summary (Table 5.1)

$$AEP_{mech,array} = 1014.32 \text{ kW} \cdot 8760 \frac{h}{year} = 8885.44 \frac{MWh}{year} \quad (5.9)$$

$$AEP_{el,90\%,array} = 0.8235 \cdot 8885.44 \frac{MWh}{year} \cdot 0.9 = 6585.03 \frac{MWh}{year} \quad (5.10)$$

Table 5.2 Summary of AEP cases with percentage change to base case

Case	$AEP_{el,90\%,array}$ [MWh]	CF [-]	change [%]
(1) Average AEP	6128.08	0.5552	-
(2) High yield AEP (a)	6799.16	0.6160	10.95 %
(3) High yield AEP (b)	6585.03	0.5966	7.46 %

5.3 LCOE CONSIDERATION

In order to compare unit-costs of electricity over the lifetime of different generating facilities and technologies the concept of Levelized Cost of Electricity (LCoE⁴) is used. The LCoE can be represented as the net present value of the unit-cost of electricity over

⁴ sometimes also: Levelized Cost of Energy (LCoE), or in short: Levelized Energy Cost (LEC)

the lifetime of a generating asset. It is often taken as a proxy for the average price that the generating asset must receive in a market to break even over its lifetime. It is a first-order economic assessment of the cost competitiveness of an electricity-generating system that incorporates all costs over its lifetime: initial investment, operations and maintenance, cost of fuel, cost of capital. Equation (5.11) puts the above mentioned in a simple mathematical relation.

$$LCoE = \frac{\textit{sum of all costs over project lifetime}}{\textit{total electrical energy generated over lifetime}} \quad (5.11)$$

The output of eq. (5.11) is a figure of unit [currency/kWh]. There are several LCoE calculation methods in use today. For detailed information on the several methods it is referred to the paper of Foster et al. (2014) “*LCOE models: a comparison of the theoretical frameworks and key assumptions*”.

It is mentioned that the LCoE is not to confound with the price of electricity which is being paid by the end-consumer. The LCoE does not include taxes, profit margins or any other tariffs. It serves just for an economic estimation of when and at what energy price a generating facility will break even (under assumed boundary conditions) to compensate all costs which it accumulated over its lifetime.

The Model used in this work comes from the Department of Energy and Climate Change (DECC), UK Government, and is widely in use for LCoE estimations within the tidal and wind energy industry [25]. It is a model based on discounted cash flows which works with net present values of costs and energy production over a projects’ lifetime.

5.3.1 LCoE Model (DECC – UK)

The LCoE model of the DECC is based on the assumption that both cash flows and the electricity generated being represented using Net Present Values (NPVs) over the project life time. In mathematical formulation:

$$LCoE_{DECC} = \frac{NPV \text{ of Total Costs over project lifetime}}{NPV \text{ of Electricity Generation over project lifetime}} \quad (5.12)$$

$$LCoE_{DECC} = \frac{|\sum_{i=0}^{n=PLT} \text{disc CapEx}_i| + |\sum_{i=0}^{n=PLT} \text{disc OpEx}_i|}{\sum_{i=0}^{n=PLT} \text{disc AEP}_i} \quad (5.13)$$

with:

i	<i>current year (0 ... PLT)</i>	[-]
PLT	<i>Project Life Time of system (e.g. 20 years)</i>	[-]
disc CapEx_i	<i>discounted capital expenditure in year i</i>	[€/US\$/R\$]
disc OpEx_i	<i>discounted operational expenditures in year i</i>	[€/US\$/R\$]
disc AEP_i	<i>discounted Annual Energy Production in year i</i>	[kWh]

The expression “discounted” relates to the fact that the value of any currency unit in the future is less worth than today due to interest and inflation. This fact has to be taken into account when planning a project with cash flows over several years. Usually investors demand an annual interest payment for their capital deployed with a project as well as banks demand interest payments on a loan they draw. Such cost of capital is expressed using a discount rate. In case there are several parties financing a project with different interest rates a so called Weighted Average Cost of Capital (WACC) is applied as discount rate. It combines the shares of capital with the attached interest provided by each party in one number.

$$WACC = \sum_{i=1}^n F_i \cdot cc_i \quad (5.14)$$

with:

$WACC$	<i>Weighted Average Cost of Capital</i>	[-]
i	<i>index for financier (i = 1 ... n)</i>	[-]
n	<i>total number of financiers</i>	[-]
F_i	<i>share of total capital financier i provides</i>	[-]
cc_i	<i>annual interest which financier i demands</i>	[-]

Equation (5.13) is now extended carrying the WACC as discount rate:

$$LCoE_{DECC} = \frac{\left| \sum_{i=0}^{n=PLT} \frac{CapEx_i}{(1 + discount\ rate)^i} \right| + \left| \sum_{i=0}^{n=PLT} \frac{OpEx_i}{(1 + discount\ rate)^i} \right|}{\sum_{i=0}^{n=PLT} disc\ AEP_i} \quad (5.15)$$

with:

discount rate WACC [-]

5.3.2 LCoE Estimation of the 1 MW RHK Case Study

The LCoE model described in the previous section is now applied to the 1MW Plat-I array configuration introduced in chapter 5.2. An Excel spread sheet has been developed to calculate the LCoE for various operation conditions. This chapter will consist of two parts. Part (a) will describe a basis case where the CapEx and OpEx being hold constant and the LCoE being calculated for the three cases introduced in Table 5.2. Part (b) is investigating the sensitivity of a varying CapEx and OpEx to the LCoE.

(a) Base Case:

Table 5.3 Input data for Project Configuration

LCoE Model		INPUT CELLS	
INPUT 1: Project Configuration		Figure	Unit
a)	<u>Platform/Turbines:</u>		
	# of platforms	5	[-]
	rated power of generator	70,00	[kW]
b)	<u>Expenditures:</u>		
	Total CapEx	6.854,26	[k€]
	Total OpEx	342,71	[k€/a]
c)	<u>Installed Power:</u>	1.400,00	[kW]
	Capacity Factor (CF)	0,5552	[-]
	Availability	0,90	[-]
	AEP _{el, 90%, array}	6.128,08	[MWh / a]
d)	<u>Finance:</u>		
	Project lifetime	20	[a]
	Discount rate [WACC]	0,1025	[-]

Table 5.4 Input data for single cost positions

INPUT 2: Cost driver breakdown				
Total CapEx	[k€]	6.854,26	Total OpEx [k€/a]	342,71
Turbine		2.400,00	Option 1: list single expenditures	NO
Platform		2.500,00		
Installation & Foundation		1.050,00	Operations	-
PM & Engineering		250,00	Maint Turbine	-
Transport		400,00	Maint Platform	-
Commissioning		250,00	Other OpEx	-
Other CapEx			Insurance	-
Decomm. (End of PLT)		30,00	Option 2: OpEx as % of CapEx	YES
Disc Decom		4,26		5,00%

Table 5.5 Input data to determine the WACC

INPUT 3: WACC: 10,25%		
	Share	Rate
Equity	0,75	12,00%
Debt capital	0,25	5,00%
Incentives	0	0,00%

With input data from the previous three tables the discounted characteristics (CapEx, OpEx, AEP) could be calculated for each year (Table 5.6).

Table 5.6 Calculation of year by year discounted characteristics

Year	0	1	2	3	4	...	18	19	20
CapEx [k€]	-6850,00	0 k€	0 k€	0 k€	0 k€		0 k€	0 k€	-30,00
OpEx [k€]	0,00	-342,71	-342,71	-342,71	-342,71		-342,71	-342,71	-342,71
disc CapEx [k€]	-6.850,00	0,00	0,00	0,00	0,00		0,00	0,00	-4,26
disc OpEx [k€]	0,00	-310,85	-281,95	-255,74	-231,96		-59,17	-53,67	-48,68
AEP _{et, 90%, array} [MWh]	0,00	6128,08	6128,08	6128,08	6128,08		6128,08	6128,08	6128,08
disc AEP [MWh]	0,00	5.558,35	5.041,58	4.572,86	4.147,72		1.058,06	959,69	870,47

Following, the discounted characteristics being summed up (Table 5.7):

Table 5.7 Summed up discounted characteristic

	Figure	Unit	Comments
$\sum \text{disc CapEx} $	6.854,26	[k€]	initial CapEx + decommissioning at end of PLT
$\sum \text{disc cash out} $	2.868,61	[k€]	only OpEx
$\sum \text{disc AEP}$	51.293,74	[MWh]	

Finally, the discounted summarized figures being put into eq. (5.13):

$$LCoE = \frac{6854.26 \text{ k€} + 2868.61 \text{ k€}}{51293.74 \text{ MWh}} = \mathbf{0.1896} \frac{\text{€}}{\text{kWh}} \quad (5.16)$$

The step performed in eq. (5.16) has been repeated with for the other two cases stated in Table 5.3. Table 5.3 has been extended with an additional column stating the LCoEs of case (2) and (3), see Table 5.8.

Table 5.8 Extention of Table 13 with LCoE column

Case	$AEP_{el,90\%,array}$ [MWh]	CF [-]	change [%]	LCoE [€/kWh]
(1) Average AEP	6128.08	0.5552	-	0.1896
(2) High yield AEP (a)	6799.16	0.6160	10.95 %	0.1708
(3) High yield AEP (b)	6585.03	0.5966	7.46 %	0.1764

(b) Sensitivity of the LCoE to variations in the CapEx and OpEx:

It is investigated how the LCoE reacts to changes in the CapEx and OpEx, respectively. The following procedure is performed:

- (1) the settings from the Base Case (Chapter 5.3.2 (a)) are used as reference values for all further changes in the CapEx and OpEx, this case is described as “100 % CapEx, 5 % OpEx”;
- (2) out of the Base Case, the CapEx is varied and the OpEx is kept constant
- (3) then, the OpEx is varied and the CapEx is kept constant.

Figure 5.11 to 5.14 are illustrating the results of the process described above. It can be concluded that the sensitivity of the LCoE is stronger to changes in the OpEx than to changes in the CapEx. This means that the economic viability of such a project reacts more positive to a reduction in the OpEx than to a reduction in the initial CapEx. It should therefore be a strong incentive to design engineering and project planning to create a system which operates with as little maintenance as possible over its project lifetime. (It should be of higher priority to design a robust product which over its project life time is as minimal as possible exposed to maintenance than to design a cheaper product which will be in maintenance more often.)

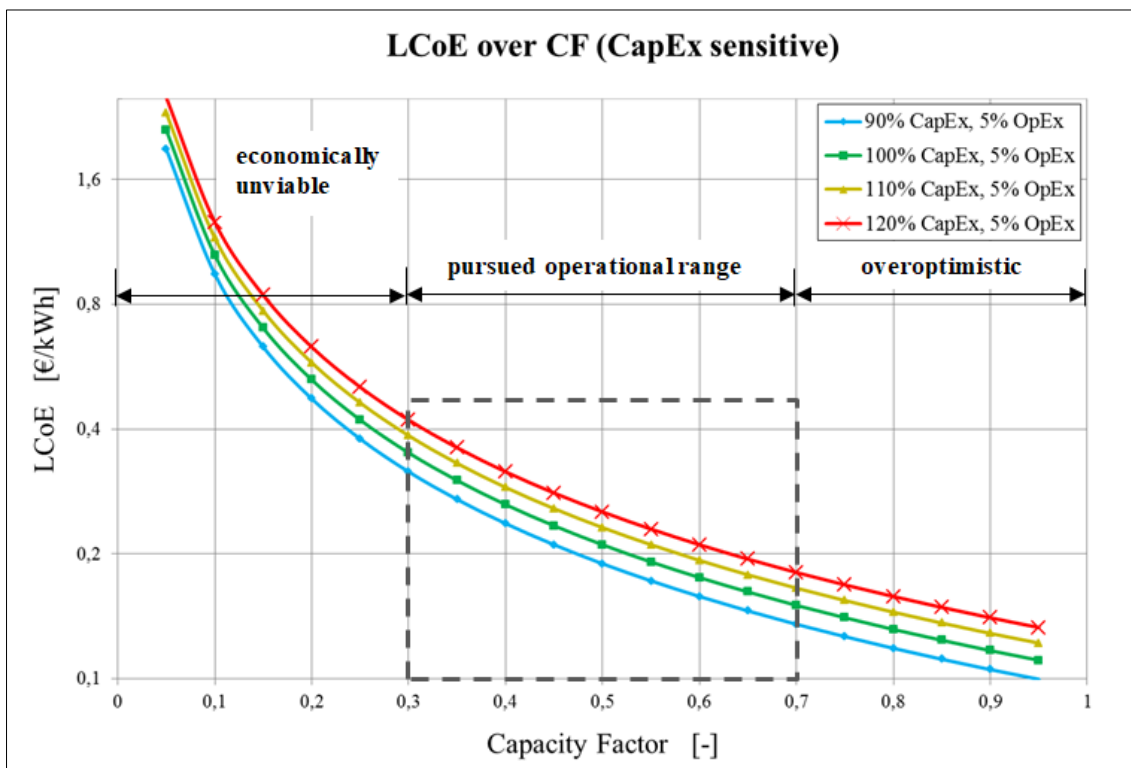


Figure 5.11 Sensitivity of LCoE to changes in CapEx (OpEx const.), note: y-axis logarithmic

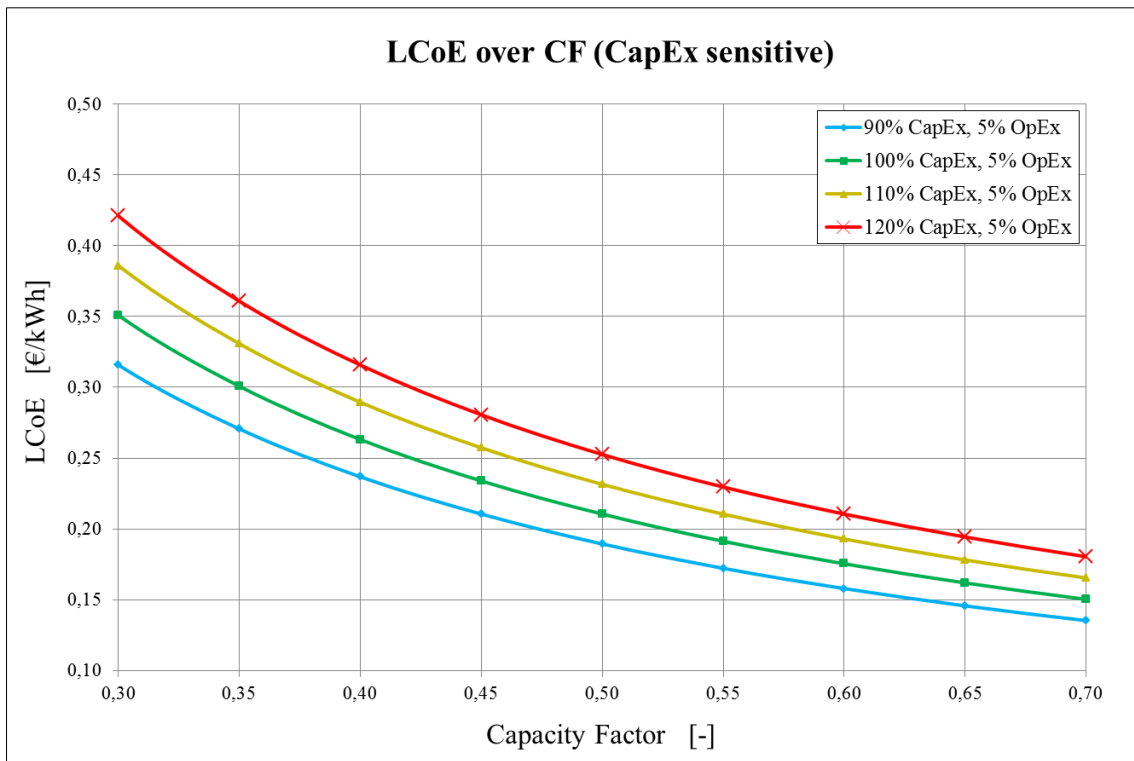


Figure 5.12 Sensitivity of LCoE to Changes in CapEx within pursued operation range

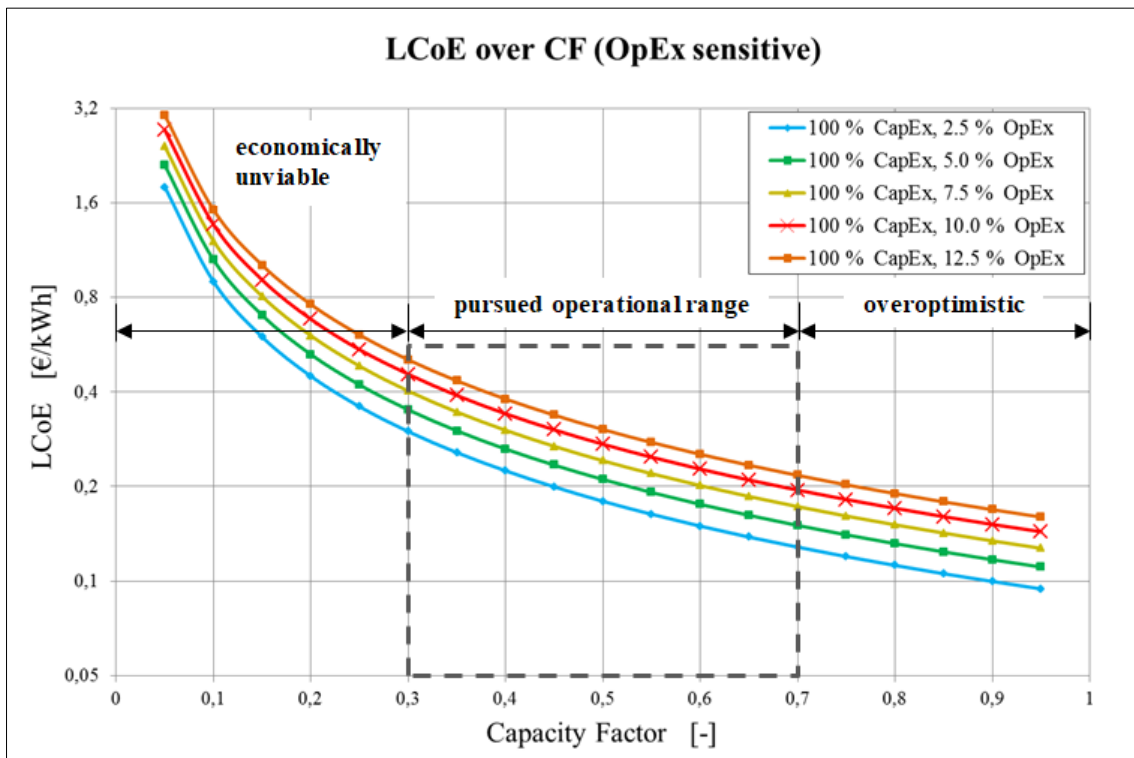


Figure 5.13 Sensitivity of LCoE to changes in OpEx (CapEx const.), note: y-axis logarithmic

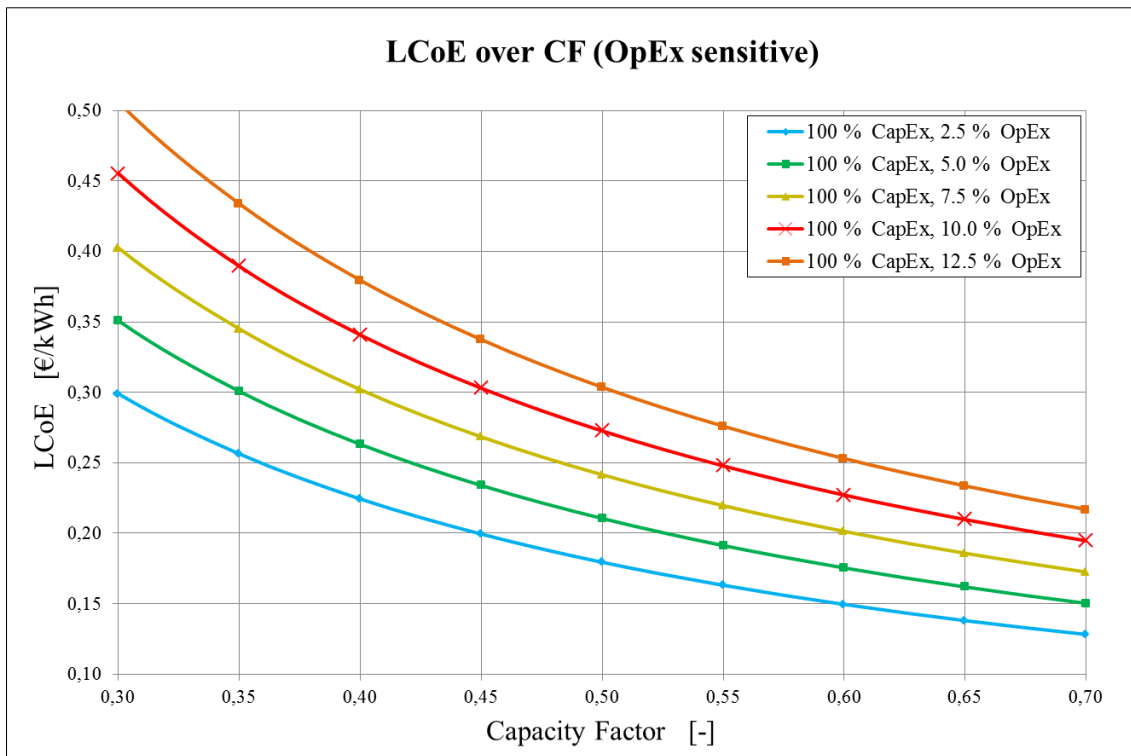


Figure 5.14 Sensitivity of LCoE to Changes in OpEx within pursued operation range

5.3.3 Comparison of LCoEs for several power generating technologies in Brazil

To put the in 5.3.2) determined LCoE figures into perspective to other LCoE numbers which form a nationwide electricity matrix, this section aims to provide a quick overview on actual existing LCoE ranges of different electricity generating technologies in Brazil.

As illustrated in Figure 5.15 the future Brazilian electricity matrix relies on the technologies named there: (1) Large Hydropower (> 30 MW), (2) Thermoelectric Power coming from natural gas, oil and coal, (3) Wind Energy, (4) Biomass, (5) Small Hydropower (1 -30 MW), (6) Solar Energy, and (7) Nuclear Energy.

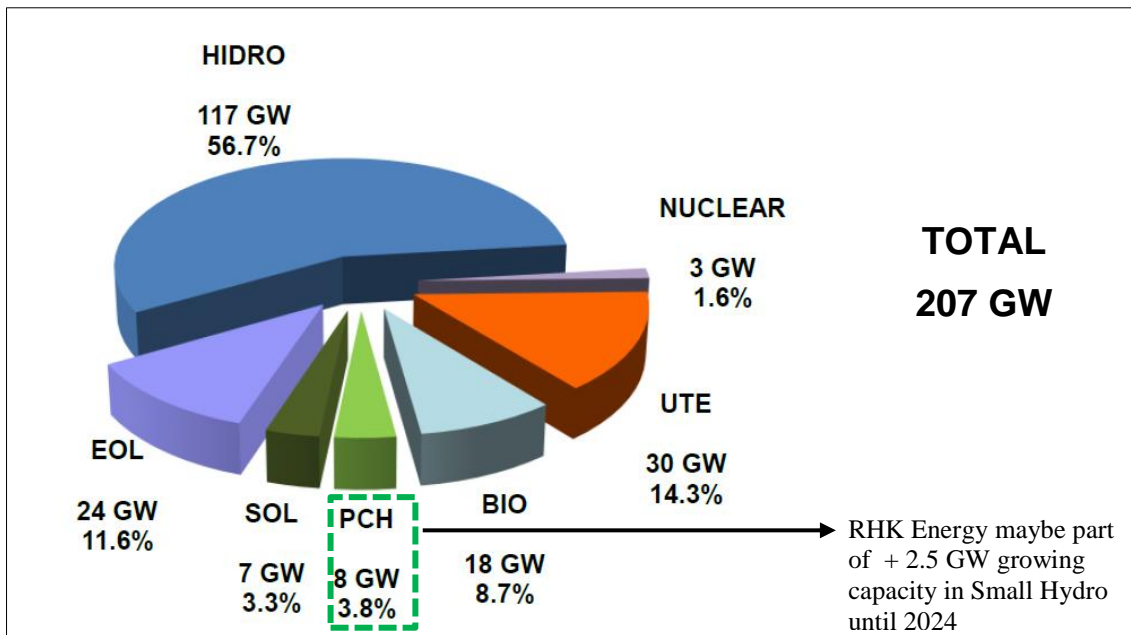


Figure 5.15 Estimated Brazil's Electric Power Generation Capacity by source for 2024 [13]

It is intended to present reliable figures for the each LCoE of the above named technologies generating power in Brazil. The following figure is illustrating the LCoE of various power generating facilities operating currently in Brazil with an adjusted discount rate of 10 %.

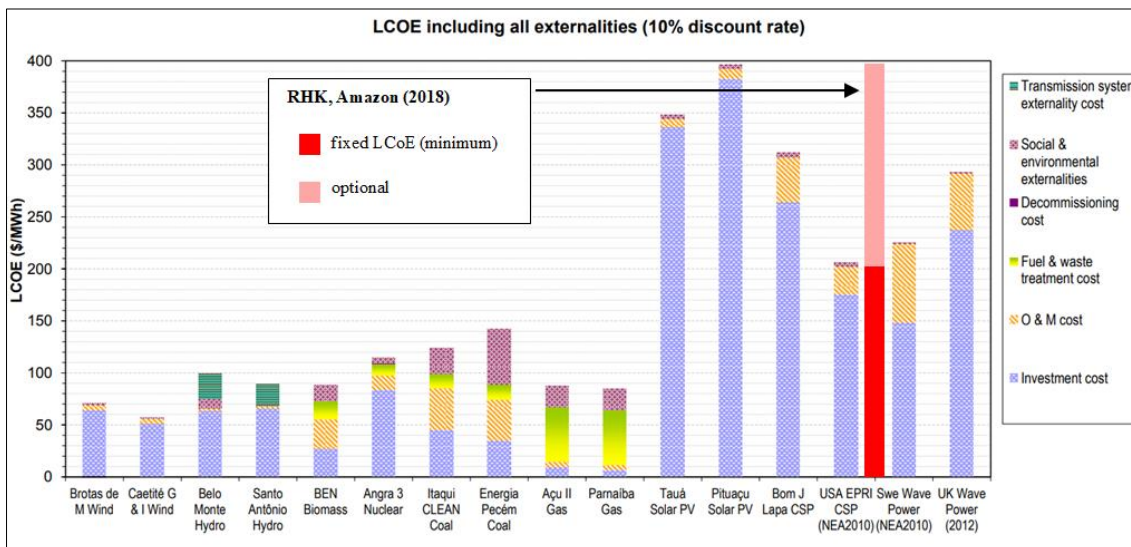


Figure 5.16 LCoE of different generating facilities and technologies including also social, environmental and transmission system costs under the assumption of a discount rate of 10 % [26]

Figure 5.16 gives a quick overview on LCoEs of different technologies and generating facilities, however diesel fueled power facilities which are in common use in rural northern Brazil are not included. Estimated LCoEs for diesel generator operations for several countries are illustrated in Figure 5.17.

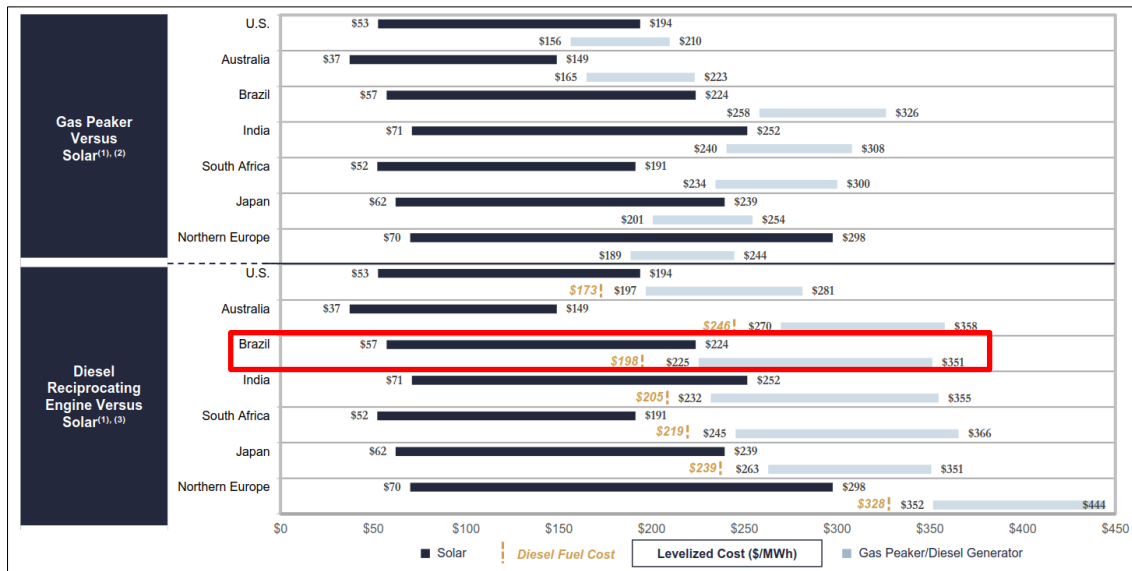


Figure 5.17 Solar versus Peaking Capacity (Global Markets) [27]

It is mentioned that the fuel cost estimations in Figure 5.17 are based on the average oil price of 2017 (54.25 U\$/barrel, BRENT) which can be considered to be comparatively low based on the mean 10-year price of 81,86 U\$/barrel (2008-2017). LCoEs of diesel generating facilities are very sensitive to fuel costs as Figure 5.18 shows. Taking into consideration that the oil price could go back to its 10-year average or beyond that which would mean a price increase of at least 51% the LCoE for diesel fueled power facilities will increase proportional to the increase of fuel costs.



Figure 5.18 LCoE comparison of different alternative and conventional power generating technologies operating in the US with sensitivity to fuel prices: dark areas correspond to $\pm 25\%$ fuel price fluctuation [27]

At the current cost levels for real RHK Energy projects the technology in nowadays seems to be economically competitive to diesel generating facilities. The main advantage of a RHK power plant over a diesel fueled facility is the stability in LCoE. Once a RHK Energy project is set up and the assumptions made are correct, the LCoE will not vary over the entire project lifetime whereas a diesel fueled power plant's LCoE varies continually with the underlying fuel price.

6 CONCLUSION AND OUTLOOK

Conclusion:

In this work the state of the art River Hydrokinetic Energy has been described and applied to real existing river resources in Brazil. With created models for river flow and existing data for hydrokinetic turbines, provided by SCHOTTEL HYDRO, in combination with true data on river flow for particular sites along the Amazon River, provided by the Brazilian Nacional Water Agency, a 1-MW River Hydrokinetic Power Plant has been conceptualized from the positioning of the turbines over the extracted power until the range of the Levelized Cost of Electricity the plant is likely to operate over its project lifetime.

Theory used and concepts applied in this work were:

- | | | |
|-----|---|---|
| (1) | <i>basics in fluid mechanics and hydrology</i> | to capture river flow regimes, |
| (2) | <i>basics in data analysis and processing</i> | to characterize river flow and create new river flow models, |
| (3) | <i>basics in turbo machinery and computational fluid dynamics</i> | to describe power extraction by the turbines and to state annual energy production as well as efficiencies of the extraction devices, |
| (4) | <i>basics in energy economics</i> | to create the LCoE models based on discounted cash flow models. |

As shown in chapter 5, River Hydrokinetic Energy as an additional technology to Conventional Hydropower is capable to make a contribution to a modern grids power

generation technologies. Its advantages of carbon free power generation combined with low civil engineering intervention, low initial capital expenditures, quick project realization and predictable LCoE over a project's lifetime makes the technology a potential future support for baseload power in certain regions. In particular diesel fueled power plants which are often operating in rural off-grid areas potentially could be replaced or at least lowered by operating capacity due to installing hydrokinetic power generating facilities. However, to make any RHK application economically viable the resource present is key. As elaborated in this work river resources can vary significantly regarding their discharge and subsequent flow speed fluctuation over the year. This is why an accurate resource evaluation is of utmost importance within the planning phase of a potential RHK project and has to be carried out at the very beginning of any project proposal.

Resuming the questions presented in chapter 1.2, it is concluded:

- (1) Are rivers principally capable to power hydrokinetic energy extraction devices?
→ Yes, they are. However, comprehensive resource assessment has to be carried out before planning and/or conceptualizing a RHK power plant.

- (2) Which characteristics define a river resource to be suitable for hydrokinetic power generation?
→ Low discharge fluctuation over the hydrologic cycle and high annual mean flow speed (preferably > 1.2 m/s).

- (3) In case of existing feasible resources, what are requirements to the extraction devices for an efficient operation?
→ Suitable rotor diameter, designed for present flow speeds. Turbine system being able to cope with river flow conditions (e.g. floating debris, grasses, sediments etc.).

- (4) How economically viable could a potential river hydrokinetic power plant be operating? Can the technology be cost competitive to peer groups (e.g. wind or solar)?

→ *LCoE at suitable river site: 0.20 – 0.35 U\$/kWh depending on CapEx and OpEx. If range of LCoE gets significantly smaller (e.g. 0.20 -0.23 U\$/kWh), competitive.*

Outlook:

In order to build on the existing work one could face a variety of unanswered questions which within the scope of this work could not have been addressed. Those are, amongst others, the following:

- (1) *design of a suitable mooring system for river bed mounting of a floating platform;*

this includes the study of river bed formations as well as the floating environment to propose an environmentally friendly as well as cost competitive platform anchoring system,

- (2) *commissioning of this type of energy generating facility;*

this includes not only seeking permission from the environmental agencies but also local civil engineering permissions as well as acceptance from the local utility for grid access to feed in the generated electricity

- (3) *evaluation of the occurrence of floating debris and sediments and maybe design of a debris protection system;*

rivers carry objects of various forms and origins, however in the context of this work it is focused on such which could have a negative impact on the operation of the turbines, those include: parts of trees, grasses, and sediments which could erode turbine surfaces

- (4) *on-the-ground resource assessment;*

which consists of ADCP measurements and other flow velocity measurements to figure out what flow speed distribution really is present at a specific site

- (5) *more precise determination of the factors that define the OpEx;*

as shown in chapter 5.3 the LCoE is more sensitive to variations in the OpEx than to variations in the CapEx, it is therefore substantially to the cost structure to determine as precisely as possible all factors that influence the OpEx with their magnitude in currency per kWh

- (6) *investigation of the interference of the turbine rotors to each other;*

analyze how the lateral device spacing is affecting performance and wake development of the each turbines as well as the entire platform.

References

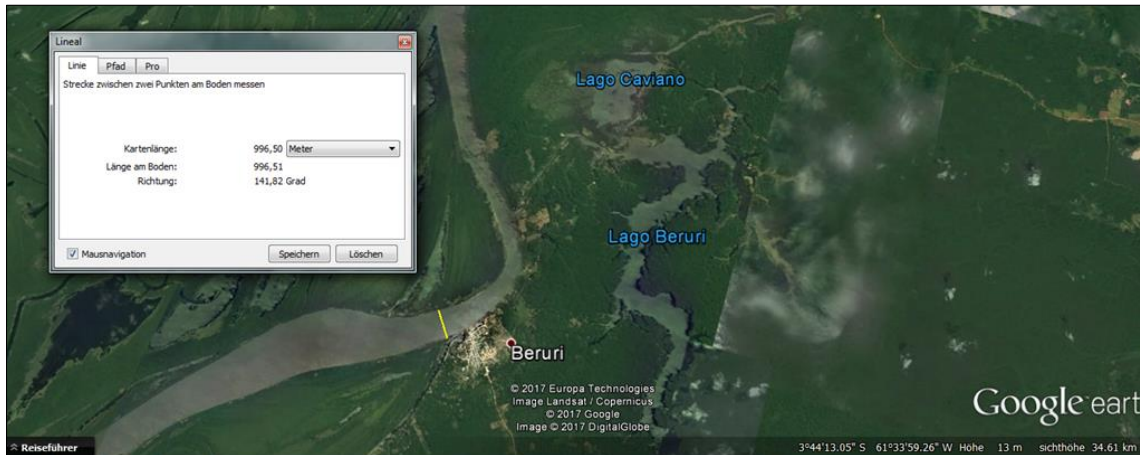
- [1] BP. (2016) www.bp.com/content/dam/pdf/energy-economics/energy-outlook-2016. [Online]. <https://www.bp.com/content/dam/bp/pdf/energy-economics/energy-outlook-2016/bp-energy-outlook-2016.pdf>
- [2] (EIA) U.S. Energy Information Administration. (2016, Juli) www.eia.gov/forecasts/ieo/. [Online]. <https://www.eia.gov/todayinenergy/detail.php?id=26912>
- [3] International Energy Agency (iea). (2017) www.iea.org. [Online]. <https://www.iea.org/publications/renewables2017/>
- [4] R. Gasch and J. Twele, *Wind Power Plants - Fundamentals, Design, Construction and Operation. 2nd Edition*. Berlin Heidelberg: Springer, 2012.
- [5] T. Utsunomiya, *Fundamentals on Wind Turbine Generators*. Kyushu University, Japan: Department of Marine Systems Engineering, 2016.
- [6] J. F. Manwell, J. G. McGowan, and A. L. Rogers, *WIND ENERGY; Theory, Design and Application*. United Kingdom: John Wiley and Sons Ltd, 2009.
- [7] F. M. White, *Fluid mechanics. 4th Edition*. New York, Boston: McGraw-Hill, 2004.
- [8] SCHOTTEL HYDRO GmbH, *Theory on Tidal Turbines*. Spay am Rhein, Germany, 2011.
- [9] SCHOTTEL HYDRO GmbH, *Design of the SIT-250*. Spay am Rhein, Germany, 2017.
- [10] A. C. Fernandes and A. Bakhshandeh Rostami, *Hydrokinetic Energy Harvesting by an innovative vertical axis current turbine.:* Renewable Energy, 2015.
- [11] A. C. Fernandes and A. Bakhshandeh Rostami, *The effect of inertia and flap on autorotation applied for hydrokinetic energy harvesting.:* Applied Energy, 2015.
- [12] A. Bakhshandeh Rostami, *PhD Thesis - Hydrokinetic Energy Harvesting by Autorotation of a plate with hinged axis*. Rio de Janeiro: COPPE, UFRJ, 2015.
- [13] Empresa de Pesquisa Energética (EPE), *Energia Renovável - Hidráulica, Biomassa, Eólica, Solar, Oceânica*. Rio de Janeiro, Maio de 2016.

- [14] Inter-American Development Bank (IADB), *Preliminary Analysis of Potential River Hydrokinetic Energy Technologies in the Amazon Basin.*, November 2015.
- [15] FAO UN. (Rome, 2003) Review of World Water Resources by Country, Water Reports 23. [Online]. <http://www.fao.org/docrep/005/y4473e00.htm>
- [16] P. H. Gleick, *The World's Water, Vol. 8.* Washington Covelo London: Island Press, 2014.
- [17] A. Montanari, *Assessing water resources availability - Inductive methods.*: University of Bologna, 2017.
- [18] T. Ngo-Duc, T. Oki, and S. Kanae, *A variable streamflow velocity method for global river routing model: model description and preliminary results.* University of Tokyo, Japan: Institute of Industrial Science, 2007.
- [19] H. Kling, M. Fuchs, and M. Paulin, *Runoff Conditions in the upper Danube basin under an ensemble of climate change scenarios.*: Journal of Hydrology 424-425, 264-277, 2012.
- [20] A. Pugliese, A. Castellarin, and A. Brath, *Geostatistical prediction of flow-duration curves in an index-flow framework.*: Hydrology and Earth System Sciences, 18, 3801-3816, 2014.
- [21] J. K. Searcy, *Flow-Duration Curves. Manual of Hydrology: Part 2. Low-Flow Techniques.* WASHINGTON: Geological Survey Water-Supply Paper 1542-A. US Department of the Interior. UNITED STATES PRINTING OFFICE, 1959.
- [22] L. B. Leopold and T. Maddock, *The hydraulic geometry of stream channels and some physiographic implications.*, 1953.
- [23] J. Bomhof, *Estimating Flow, Hydraulic Geometry, and Hydrokinetic Power at Ungauged Locations in Canada.* Department of Civil Engineering: University of Ottawa, 2014.
- [24] San Diego State University, *History of the Manning Formula.*: <http://manning.sdsu.edu/>, 2005.
- [25] J. Foster, L. Wagner, and A. Bratanova, *LCOE models: a comparison of the theoretical frameworks and key assumptions.*: The University of Queensland, School of Economics, 2014.
- [26] P. de Jong, *PhD Thesis: Forecasting, integration, and storage of renewable energy generation in the Northeast of Brazil.* UNIVERSIDADE FEDERAL DA BAHIA: Escola Politécnica, Programa de Pós Graduação em Engenharia Industrial, 2017.

- [27] LAZARD Ltd., *LAZARD'S Levelized Cost of Energy Analysis - Version 11.0.*, November 2017.
- [28] John P. Grotzinger and Thomas H. Jordan, *Understanding Earth, 7th Edition.* New York (US): W.H. Freeman and Company, 2014.
- [29] Canadian Hydraulics Center, *Assessment of Canada's Hydrokinetic Power Potential - Phase I Report - Methodology and Data Review.*, March 2010.
- [30] P. H. Gleick, *Water in Crisis: A Guide to the World's Freshwater Resources.*: Island Press, 1993.
- [31] M. S. Güney and K. Kaygusuz, *Hydrokinetic Energy Conversion Systems: A Technology Status Review.*: Renewable Sustainable Energy Rev, 2010.
- [32] T. Divett, R. Vennell, and C. Stevens, *Optimization of multiple turbine arrays in a channel with tidally reversing flow by numerical modelling with adaptive mesh.*: Philosophical Transaction of the Royal Society A, 2013.
- [33] M. J. Kahn and G. Bhujan, *Hydrokinetic Energy Conversion Systems and Assessment of horizontal and vertical axis turbines for river and tidal applications: a technology status review.*: Applied Energy, 2009.
- [34] H. J. Vermaak, K. Kusakana, and S. P. Koko, *Status of micro-hydrokinetic river technology in rural applications: A review of literature.*: Renewable Sustainable Energy Rev., 2014.
- [35] Pacific Institute. (2014) Sustainable Water Management - Peak Water. [Online]. <http://pacinst.org/issues/sustainable-water-management-local-to-global/peak-water/>
- [36] Pacific Institute. (2014) Sustainable Water Management - Soft Path for Water. [Online]. <http://pacinst.org/issues/sustainable-water-management-local-to-global/soft-path-for-water/>

Appendix I – River Sites, Basic Data

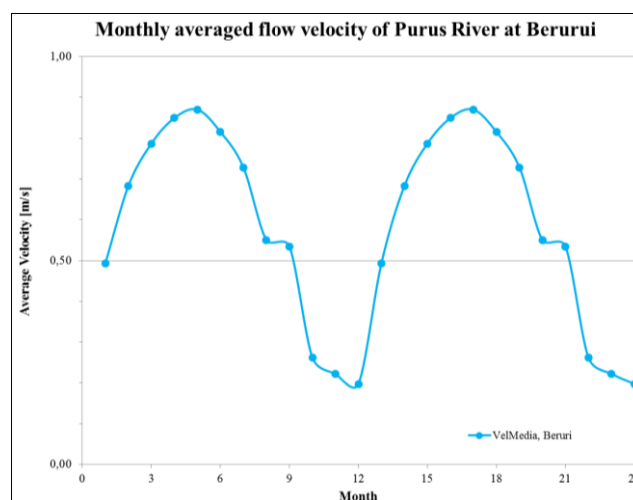
1) Beruri, Rio Purus, AM, Brasil



Satellite picture of site with position where measurements were recorded (yellow), Beruri, AM, Brazil

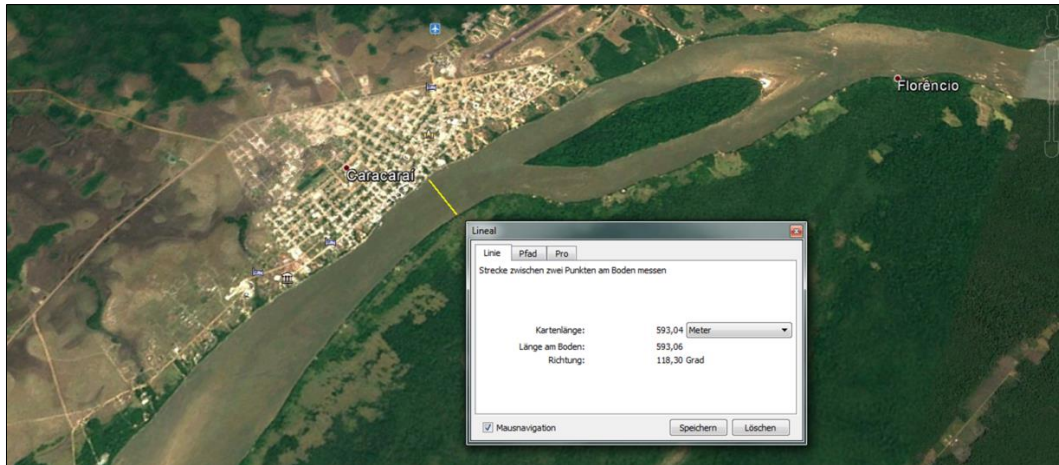
Monthly averaged site data, Beruri, AM, Brazil

month	Monthly Averaged Data (Beruri)				
	Vazao [m ³ /s]	AreaMolhada [m ²]	Largura [m]	VelMedia [m/s]	Profundidade [m]
1	9236,55	18758,00	1085,94	0,49	17,20
2	13189,45	21657,27	1144,00	0,68	19,06
3	16876,92	21042,38	1126,29	0,79	18,69
4	20596,12	24108,60	1159,95	0,85	20,80
5	22480,00	26199,59	1190,92	0,87	22,20
6	21767,85	26574,66	1175,13	0,82	22,65
7	18344,60	24872,56	1090,07	0,73	22,81
8	13530,57	24259,33	1165,44	0,55	20,88
9	11701,94	21889,17	1164,20	0,53	19,02
10	3582,67	13708,32	1034,75	0,26	13,28
11	2801,31	12611,21	1033,92	0,22	12,20
12	2694,13	13667,08	1014,59	0,20	13,47
Average (year)	13066,84	20779,01	1115,43	0,58	18,52



Graphical illustration of the monthly averaged flow velocity at site, Beruri, AM, Brazil

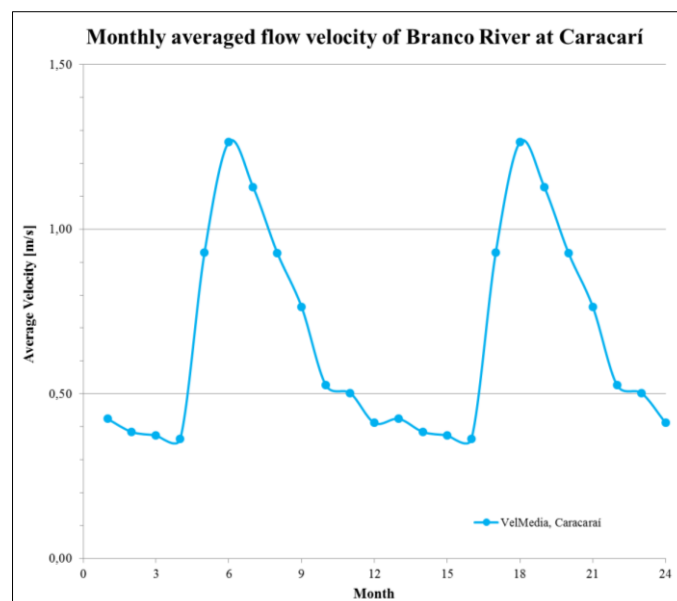
2) Caracará, Rio Branco, RR, Brasil



Satellite picture of site with position where measurements were recorded (yellow), Caracará, RR, Brazil

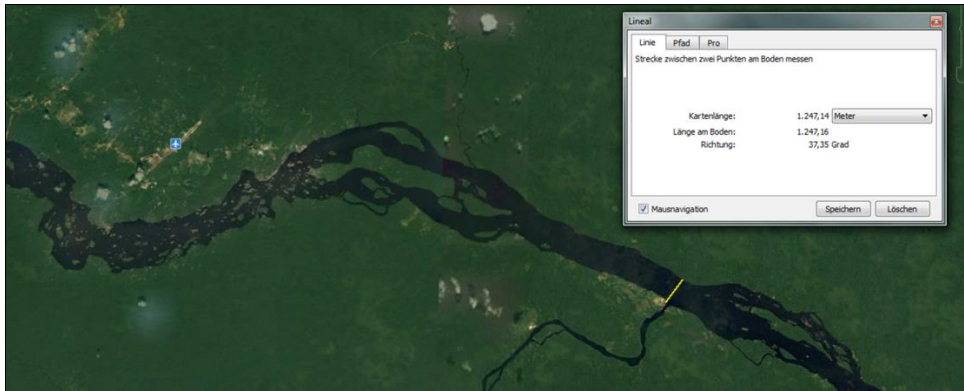
Monthly averaged site data, Caracará, RR, Brazil

Monthly Averaged Data (Caracará)					
month	Vazao [m ³ /s]	AreaMolhada [m ²]	Largura [m]	VelMedia [m/s]	Profundidade [m]
1	1161	2651,93	535,63	0,42	5,06
2	1110	2530,42	558,92	0,38	4,59
3	1155	2878,82	528,64	0,37	5,86
4	1324	3129,68	483,19	0,36	6,78
5	4814	4567,87	529,49	0,93	9,02
6	7416	5706,23	532,24	1,26	11,11
7	6276	4936,44	597,55	1,13	8,49
8	4509	4723,99	612,16	0,93	7,83
9	3156	3937,84	594,35	0,76	6,57
10	1632	3769,68	587,30	0,53	5,15
11	1490	2872,50	584,41	0,50	4,91
12	1175	2823,44	537,76	0,41	5,44
Average (year)	2934,78	3710,73	556,80	0,67	6,73



Graphical illustration of the monthly averaged flow velocity at site, Caracará, RR, Brazil

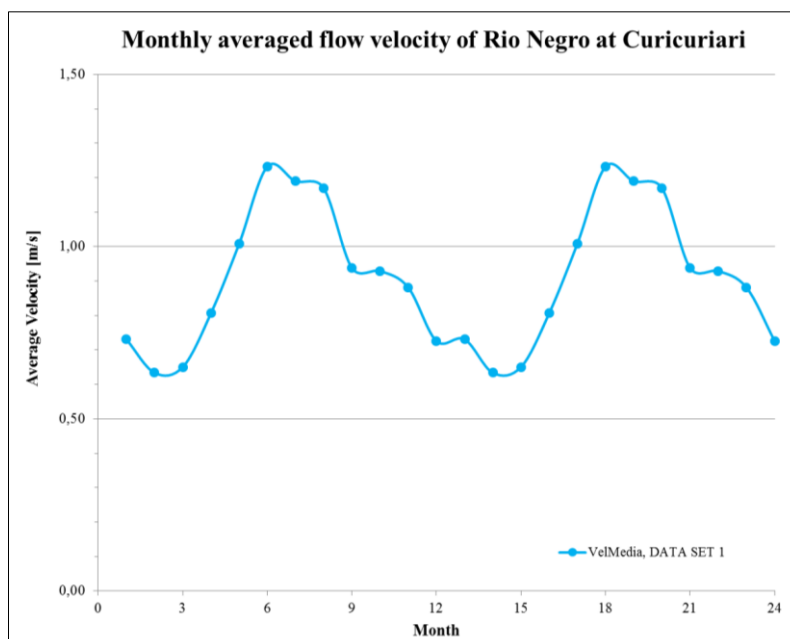
3) Curicuriari, Rio Negro, AM, Brasil



Satellite picture of site with position where measurements were recorded (yellow), Curicuriari, AM, Brazil

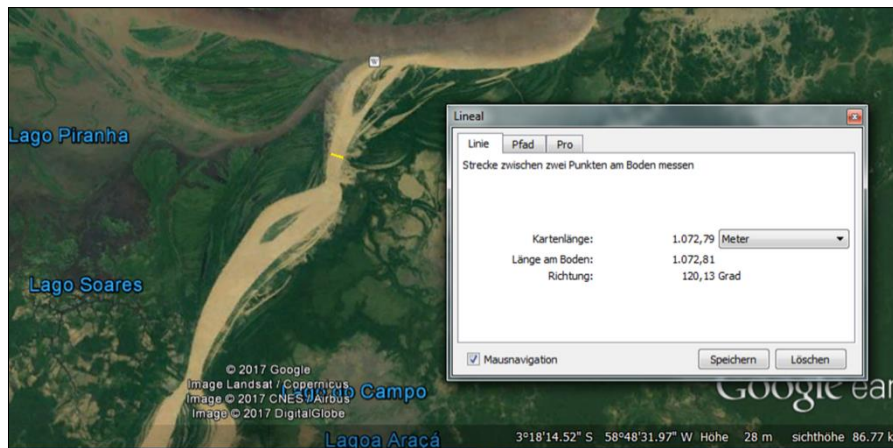
Monthly averaged site data, Curicuriari, AM, Brazil

month	Monthly Average Data (Curicuriari)				
	Vazao [m ³ /s]	AreaMolhada [m ²]	Largura [m]	VelMedia [m/s]	Profundidade [m]
1	7851	10957,80	1268,34	0,73	8,57
2	6943	10136,25	1221,89	0,63	8,23
3	7126	10272,19	1254,03	0,65	8,14
4	9460	11447,71	1292,78	0,81	8,92
5	14808	14156,55	1307,04	1,01	10,82
6	19501	15719,70	1317,44	1,23	12,21
7	18776	16484,57	1314,98	1,19	12,52
8	17444	14865,98	1311,31	1,17	11,33
9	12873	13419,67	1299,18	0,94	10,28
10	11724	12510,21	1298,99	0,93	9,62
11	10393	11223,32	1276,97	0,88	8,95
12	8036	10876,48	1291,12	0,73	8,42
Average (year)	12077,96	12672,54	1287,84	0,91	9,83



Graphical illustration of the monthly averaged flow velocity at site, Curicuriari, AM, Brazil

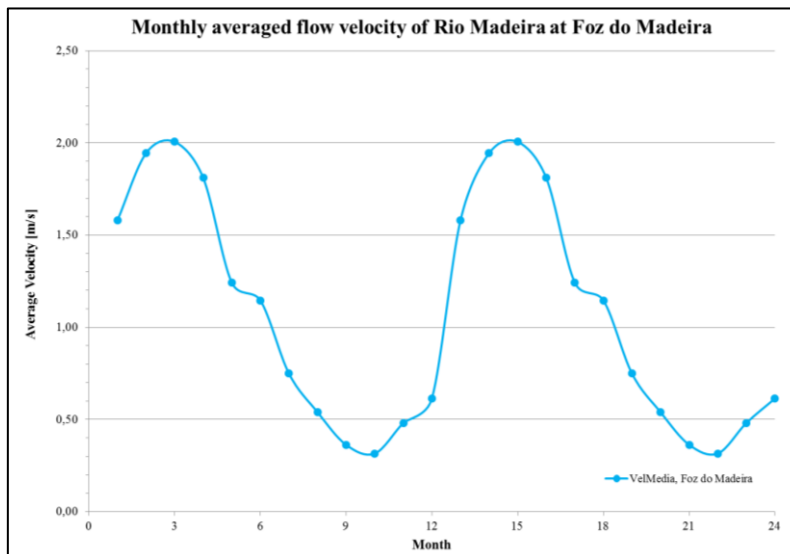
4) Foz do Madeira, Rio Madeira, AM, Brasil



Satellite picture of site with position where measurements were recorded (yellow), Foz do Madeira, AM, Brazil

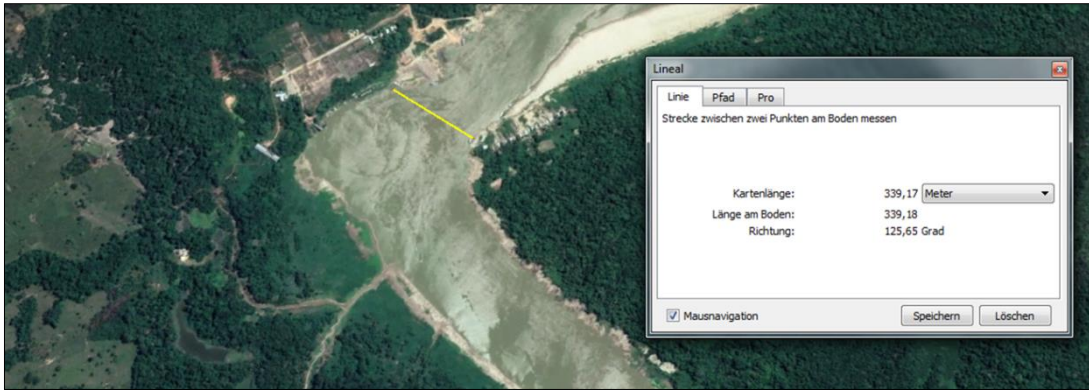
Monthly averaged site data, Foz do Madeira, AM, Brazil

month	Monthly Averaged Data (Foz do Madeira)				
	Vazao [m ³ /s]	AreaMolhada [m ²]	Largura [m]	VelMedia [m/s]	Profundidade [m]
1	35396,29	22698,40	990,57	1,58	22,87
2	42454,86	22898,99	969,61	1,94	23,61
3	51530,78	26024,64	994,74	2,01	26,13
4	51059,84	28279,33	1077,04	1,81	26,20
5	42637,27	34343,33	1418,04	1,24	25,28
6	35950,81	31262,16	1155,88	1,15	27,10
7	26022,88	34745,56	1425,25	0,75	24,38
8	18939,28	35084,36	1581,93	0,54	24,24
9	10585,85	29120,39	1013,59	0,36	28,76
10	7190,97	22675,65	978,32	0,32	23,28
11	28410,38	19941,64	991,77	0,48	20,22
12	13521,59	21664,08	1070,48	0,61	19,68
Average (year)	30308,40	27394,88	1138,93	1,07	24,31



Graphical illustration of the monthly averaged flow velocity at site, Foz do Madeira, AM, Brazil

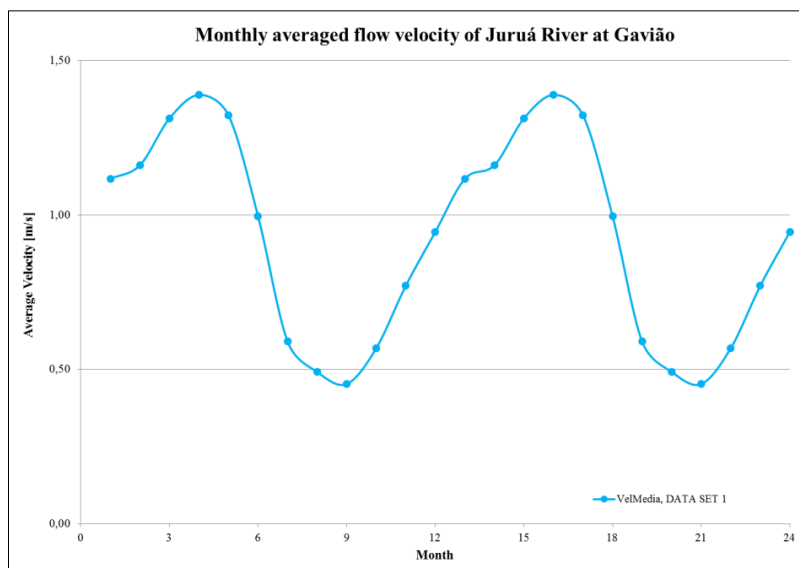
5) Gavião, Rio Juruá, AM, Brasil



Satellite picture of site with position where measurements were recorded (yellow), Gavião, AM, Brazil

Monthly averaged site data, Gavião, AM, Brazil

Monthly Averaged Data (Gavião)					
month	Vazao [m ³ /s]	AreaMolhada [m ²]	Largura [m]	VelMedia [m/s]	Profundidade [m]
1	6150,14	5433,57	369,71	1,12	14,78
2	6771,69	5808,08	362,76	1,16	16,06
3	8413,81	6399,82	385,85	1,31	16,62
4	8665,23	6230,30	384,71	1,39	16,30
5	7995,86	6039,47	361,02	1,32	16,75
6	5644,69	5500,25	363,70	1,00	14,90
7	1957,42	3300,15	302,65	0,59	10,89
8	1262,16	2511,90	270,49	0,49	9,29
9	1071,13	2359,72	282,93	0,45	8,43
10	1589,25	2625,03	278,18	0,57	9,30
11	2938,68	3609,74	307,34	0,77	11,69
12	4541,90	4739,69	350,93	0,95	13,48
Average (year)	4750,16	4546,47	335,02	0,93	13,21



Graphical illustration of the monthly averaged flow velocity at site, Gavião, AM, Brazil

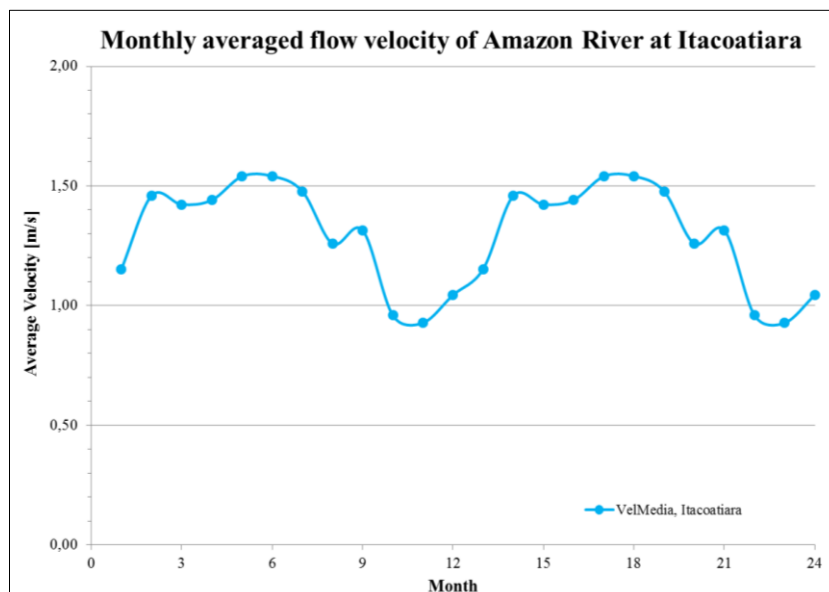
6) Itacoatiara, Rio Amazonas, AM, Brasil



Satellite picture of site with position where measurements were recorded (yellow), Itacoatiara, AM, Brazil

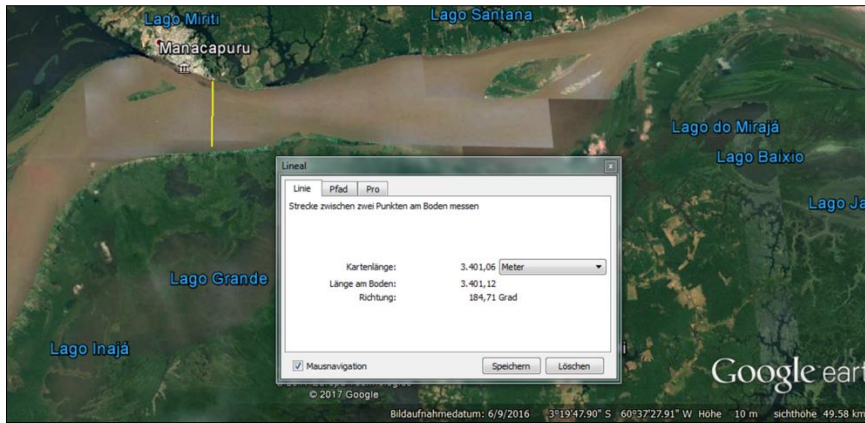
Monthly averaged site data, Itacoatiara, AM, Brazil

Monthly Averaged Data (Itacoatiara)					
month	Vazao [m ³ /s]	AreaMolhada [m ²]	Largura [m]	VelMedia [m/s]	Profundidade [m]
1	123251	106933,60	3311,19	1,15	32,29
2	161793	121011,80	3580,30	1,46	33,79
3	174072	121597,20	3582,51	1,42	33,98
4	174720	121242,50	3547,36	1,44	34,18
5	207934	135183,60	3710,09	1,54	36,45
6	206113	134026,55	3735,52	1,54	34,20
7	194727	131779,03	3878,84	1,48	34,02
8	151899	120252,23	3619,34	1,26	33,22
9	169946	129153,20	3889,74	1,32	33,21
10	95100	100358,28	3377,56	0,96	29,71
11	91968	99318,57	3507,27	0,93	28,35
12	105893	101386,50	3333,86	1,04	30,41
Average (year)	154784,63	118520,26	3589,47	1,29	32,82



Graphical illustration of the monthly averaged flow velocity at site, Itacoatiara, AM, Brazil

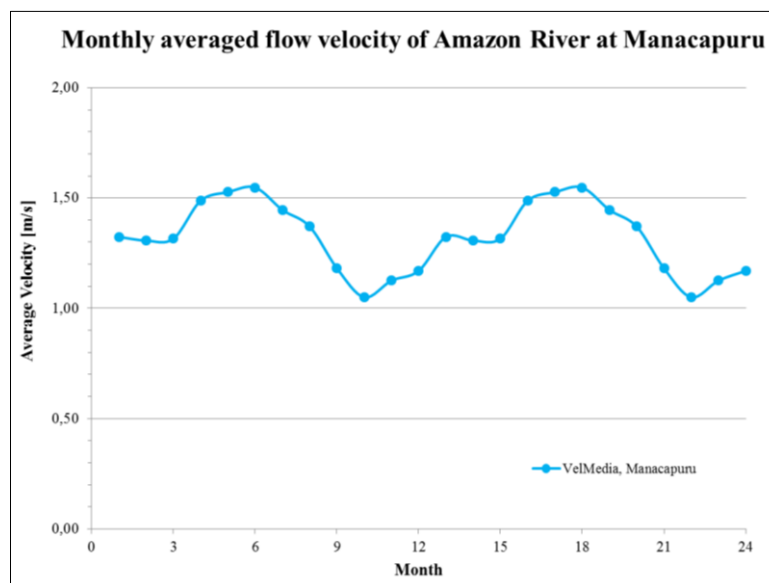
7) Manacapuru, Rio Amazonas, AM, Brasil



Satellite picture of site with position where measurements were recorded (yellow), Manacapuru, AM, Brazil

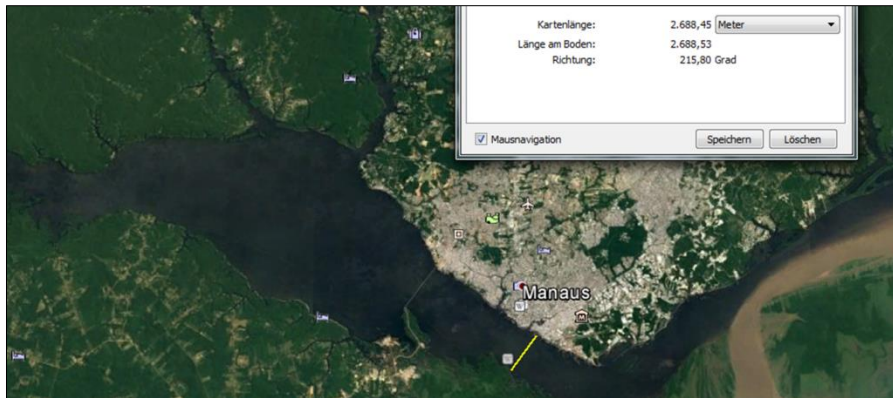
Monthly averaged site data, Manacapuru, AM, Brazil

month	Monthly Averaged Data (Manacapuru)				
	Vazao [m ³ /s]	AreaMolhada [m ²]	Largura [m]	VelMedia [m/s]	Profundidade [m]
1	98765	74417,68	3139,13	1,32	23,70
2	96375	73558,79	3171,78	1,31	23,19
3	101748	76802,41	3146,71	1,32	24,35
4	126098	84893,38	3175,50	1,49	26,76
5	135760	88901,84	3215,42	1,53	27,64
6	142250	91928,85	3335,73	1,55	27,64
7	128455	88678,23	3238,07	1,45	27,35
8	118388	85967,25	3215,28	1,37	26,74
9	90657	75905,13	3156,10	1,18	24,06
10	67046	63251,46	3098,76	1,05	20,35
11	69685	61579,68	3112,20	1,13	19,79
12	78989	64901,72	3113,69	1,17	20,87
Average (year)	104518,12	77565,54	3176,53	1,32	24,37



Graphical illustration of the monthly averaged flow velocity at site, Manacapuru, AM, Brazil

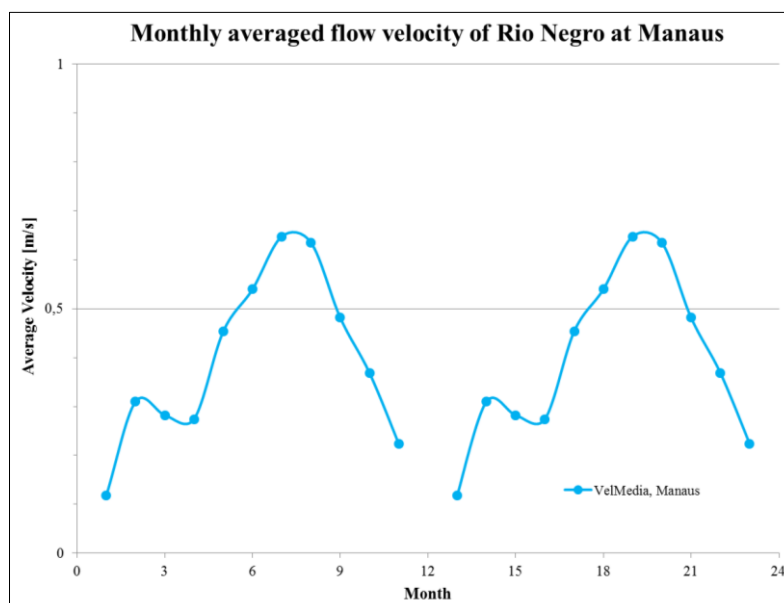
8) Manaus, Rio Negro, AM, Brasil



Satellite picture of site with position where measurements were recorded (yellow), Manaus, AM, Brazil

Monthly averaged site data, Manaus, AM, Brazil

month	Monthly Averaged Data (Manaus)				
	Vazao [m ³ /s]	AreaMolhada [m ²]	Largura [m]	VelMedia [m/s]	Profundidade [m]
1	8685	73782,00	2403,00	0,12	30,70
2	27225	87400,00	2657,00	0,31	32,89
3	25804	91435,35	2647,03	0,28	34,55
4	24605	89507,63	2619,71	0,27	34,18
5	43651	95279,50	2678,83	0,45	35,55
6	52313	97196,33	2657,27	0,54	36,58
7	59844	92383,10	2639,79	0,65	35,01
8	58363	91622,03	2683,54	0,64	34,15
9	38265	80118,50	2590,00	0,48	30,91
10	25631	68449,94	2433,98	0,37	28,12
11	14249	63514,16	2260,19	0,22	28,10
12	-	-	-	-	-
Average (year)	34421,25	84608,05	2570,03	0,39	32,79



Graphical illustration of the monthly averaged flow velocity at site, Manaus, AM, Brazil

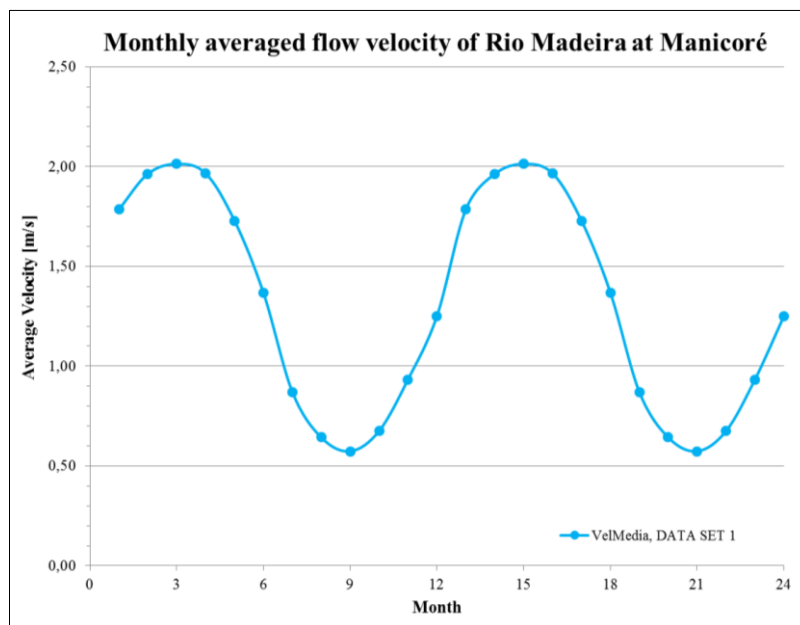
9) Manicoré, Rio Madeira, AM, Brazil



Satellite picture of site with position where measurements were recorded (yellow), Manicoré, AM, Brazil

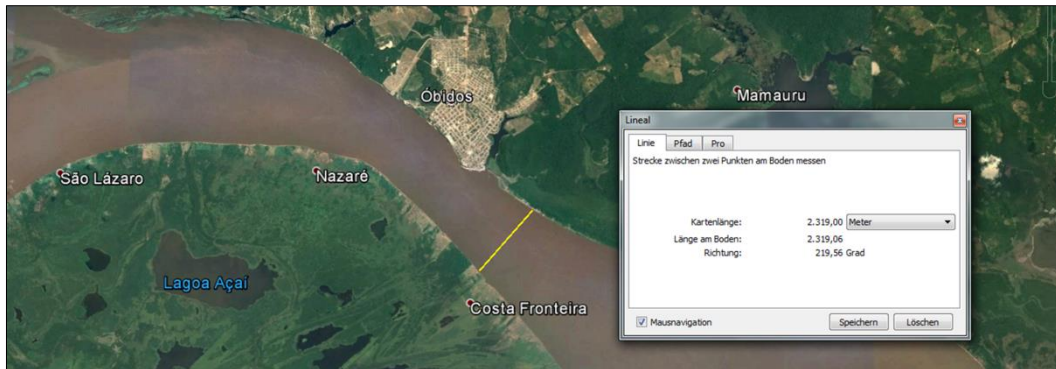
Monthly averaged site data, Manicoré, AM, Brazil

Monthly Averaged Data (Manicoré)					
month	Vazao [m ³ /s]	AreaMolhada [m ²]	Largura [m]	VelMedia [m/s]	Profundidade [m]
1	31902	17878,32	832,60	1,79	21,47
2	39092	19907,88	855,85	1,96	23,25
3	46866	23371,31	949,54	2,01	24,62
4	44611	22701,19	934,49	1,97	24,31
5	37819	21894,93	864,73	1,73	25,44
6	27507	20058,07	834,70	1,37	24,02
7	13601	15498,01	813,22	0,87	19,04
8	8717	13427,50	810,76	0,64	16,60
9	6969	12162,18	790,97	0,57	15,38
10	8470	12109,31	806,96	0,68	14,97
11	11753	12662,02	802,39	0,93	15,37
12	19743	15636,41	846,63	1,25	18,56
Average (year)	24754,21	17275,59	845,24	1,31	20,25



Graphical illustration of the monthly averaged flow velocity at site, Manicoré, AM, Brazil

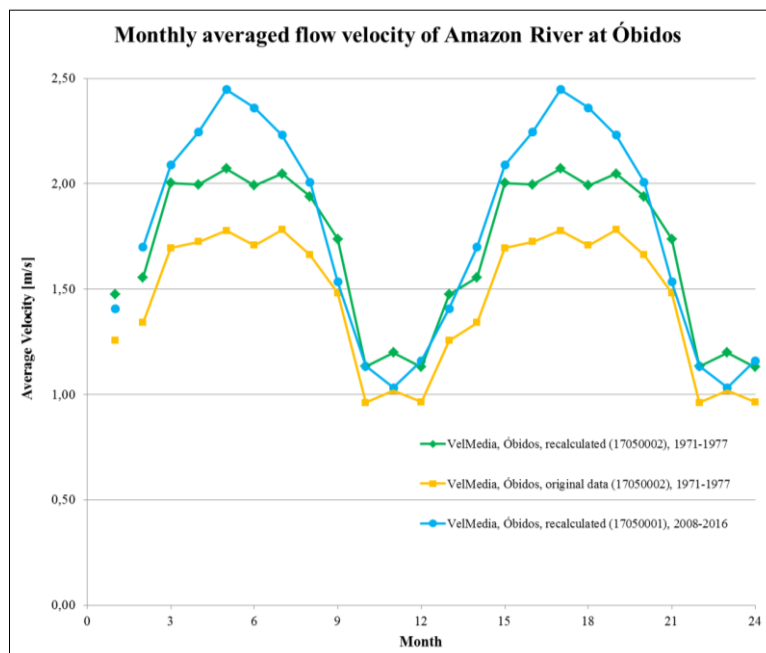
10) Óbidos, Rio Amazonas, PA, Brasil



Satellite picture of site with position where measurements were recorded (yellow), Óbidos, PA, Brazil

Monthly averaged site data, Óbidos, PA, Brazil

Monthly Averaged Data (Óbidos, Data Set 3, 2008-2016)					
month	Vazao [m³/s]	AreaMolhada [m²]	Largura [m]	VelMedia [m/s]	Profundidade [m]
1	140237	99636	2389	1,41	49,3
2	171029	100586	2362	1,70	50,3
3	207513	99346	2368	2,09	49,6
4	238365	106073	2416	2,25	51,9
5	260253	106344	2461	2,45	51,1
6	260815	110506	2545	2,36	51,5
7	245023	109839	2450	2,23	53,0
8	208779	104014	2377	2,01	51,7
9	157778	102845	2363	1,53	51,4
10	110521	97374	2301	1,14	50,0
11	98193	95133	2347	1,03	47,9
12	111094	95726	2298	1,16	49,2
Average (year)	184133,20	102285,11	2389,76	1,78	50,58



Graphical illustration of the monthly averaged flow velocity at site, Óbidos, PA, Brazil

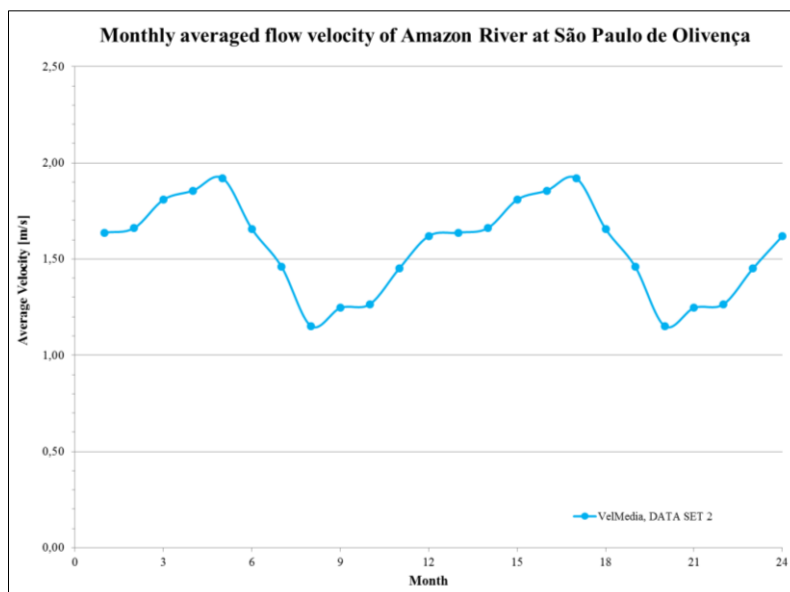
11) São Paulo de Olivença, Rio Amazonas, AM, Brasil



Satellite picture of site with position where measurements were recorded (yellow), São Paulo de Olivença, AM, Brazil

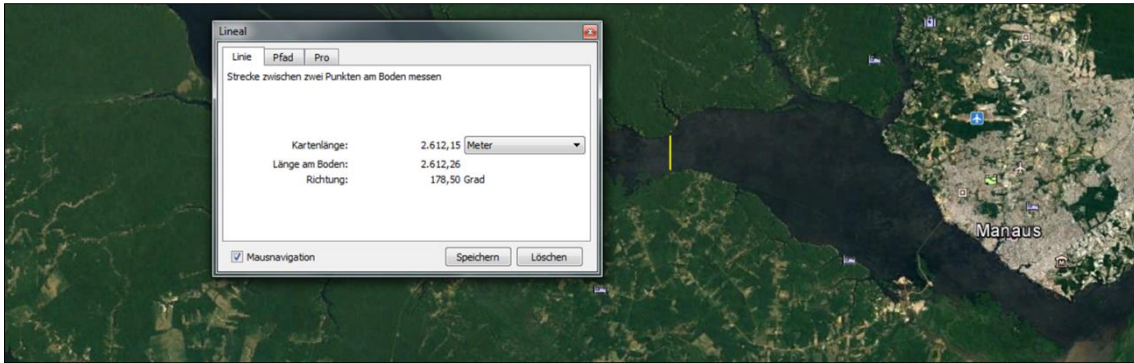
Monthly averaged site data, São Paulo de Olivença, AM, Brazil

Monthly Averaged Data (São Paulo de Olivença)					
month	Vazao [m ³ /s]	AreaMolhada [m ²]	Largura [m]	VelMedia [m/s]	Profundidade [m]
1	47907,08	29032,32	1526,19	1,64	19,07
2	51710,88	30901,56	1502,32	1,66	20,55
3	59214,80	32661,74	1497,17	1,81	21,81
4	64042,23	34572,60	1551,04	1,86	22,32
5	67096,94	34949,91	1517,77	1,92	23,04
6	54297,60	32662,66	1494,82	1,66	21,87
7	46169,15	31325,49	1534,07	1,46	20,45
8	28895,76	24935,08	1482,76	1,15	16,83
9	30366,50	24231,81	1446,33	1,25	16,82
10	30435,52	23775,28	1522,12	1,27	15,70
11	37328,40	26126,96	1496,94	1,45	17,46
12	46488,88	28537,16	1467,83	1,62	19,46
Average (year)	46996,14	29476,05	1503,28	1,56	19,61



Graphical illustration of the monthly averaged flow velocity at site, São Paulo de Olivença, AM, Brazil

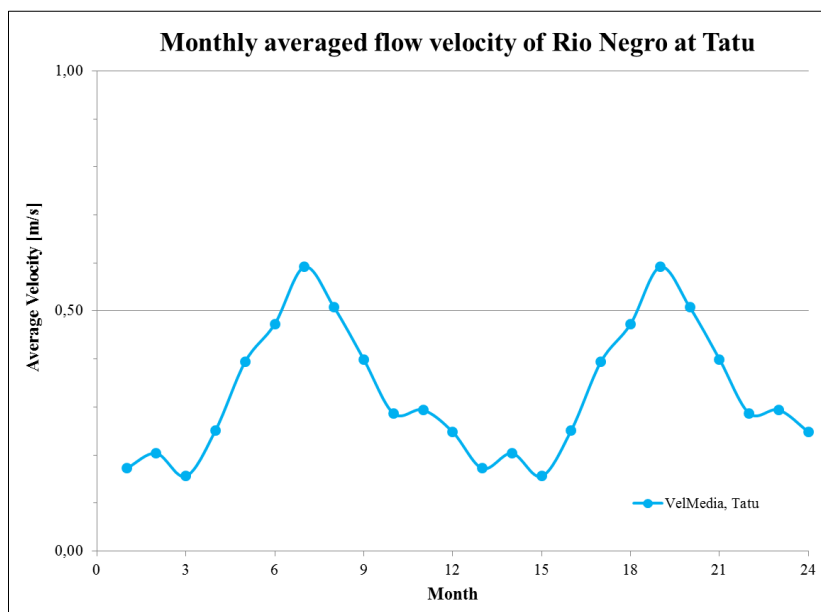
12) Tatu, Rio Negro, AM, Brasil



Satellite picture of site with position where measurements were recorded (yellow), Tatu, AM, Brazil

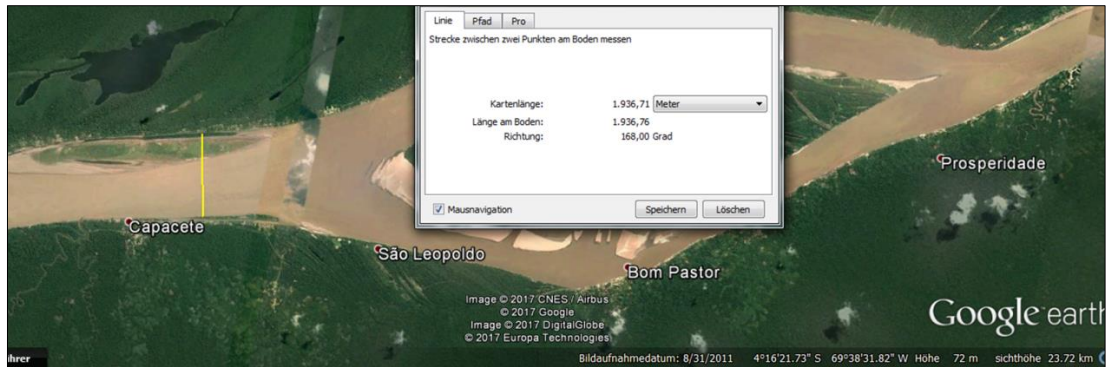
Monthly averaged site data, Tatu, AM, Brazil

month	Monthly Averaged Data (Tatu)				
	Vazao [m ³ /s]	AreaMolhada [m ²]	Largura [m]	VelMedia [m/s]	Profundidade [m]
1	13930	79782,72	2643,62	0,17	30,18
2	17267	81454,79	2654,08	0,20	30,67
3	13523	85838,13	2618,84	0,16	32,80
4	23264	91591,41	2678,42	0,25	34,19
5	37984	95782,96	2696,93	0,39	35,52
6	47254	99792,79	2802,14	0,47	35,62
7	57257	95787,41	2682,50	0,59	35,70
8	47863	94190,67	2688,25	0,51	35,04
9	33297	81850,92	2673,83	0,40	30,57
10	21083	71994,94	2532,73	0,29	28,39
11	19528	65746,24	2501,28	0,29	27,20
12	18547	73716,13	2592,19	0,25	28,44
Average (year)	29233,14	84794,09	2647,07	0,33	32,03



Graphical illustration of the monthly averaged flow velocity at site, Tatu, AM, Brazil

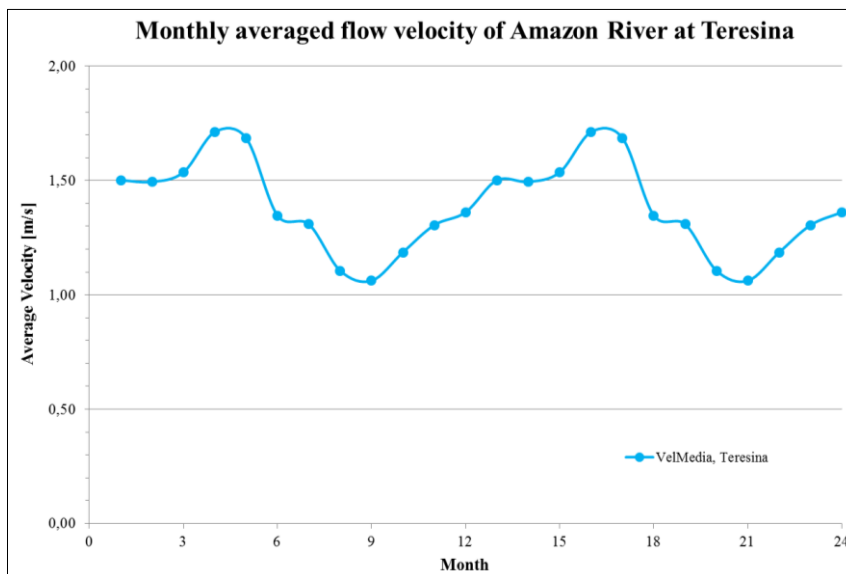
13) Teresina, Rio Amazonas, AM, Brasil



Satellite picture of site with position where measurements were recorded (yellow), Teresina, AM, Brazil

Monthly averaged site data, Teresina, AM, Brazil

month	Monthly Averaged Data (Teresina)				
	Vazao [m ³ /s]	AreaMolhada [m ²]	Largura [m]	VelMedia [m/s]	Profundidade [m]
1	47660,57	31472,29	1985,89	1,50	15,91
2	49421,19	32570,54	2095,33	1,49	15,72
3	55515,63	36110,63	2156,49	1,54	16,74
4	63817,60	37276,10	2129,11	1,71	17,54
5	68584,39	40599,87	2162,15	1,69	18,79
6	42929,50	31849,75	2142,50	1,35	14,86
7	41418,67	31377,89	2051,24	1,31	15,44
8	27301,00	24470,93	2060,55	1,11	11,87
9	24338,00	22925,00	2109,00	1,06	10,86
10	30331,30	25450,50	2028,82	1,19	12,59
11	37977,21	29006,29	2128,16	1,31	13,62
12	40326,14	29381,43	2131,26	1,36	13,78
Average (year)	44135,10	31040,93	2098,38	1,38	14,81



Graphical illustration of the monthly averaged flow velocity at site, Teresina, AM, Brazil

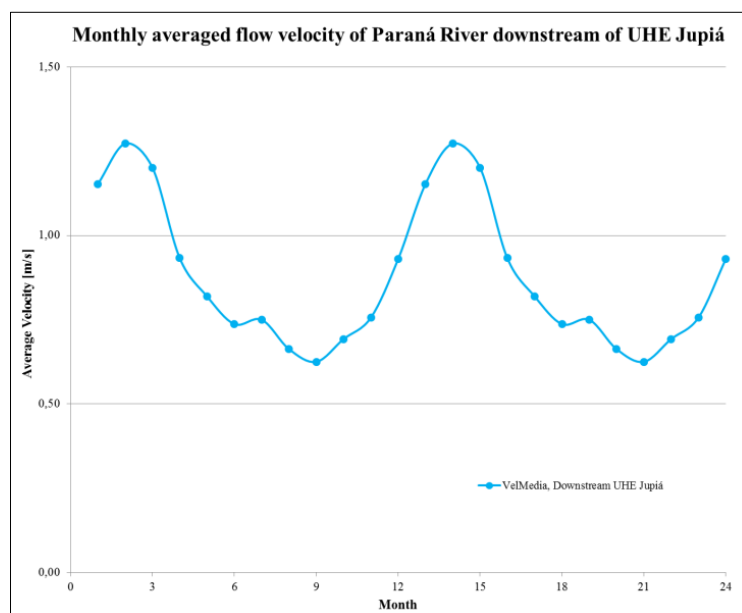
14) Downstream UHE Jupuí, Rio Paraná, MS, Brasil



Satellite picture of site with position where measurements were recorded (yellow), downstream of UHE Jupuí, MS, Brazil

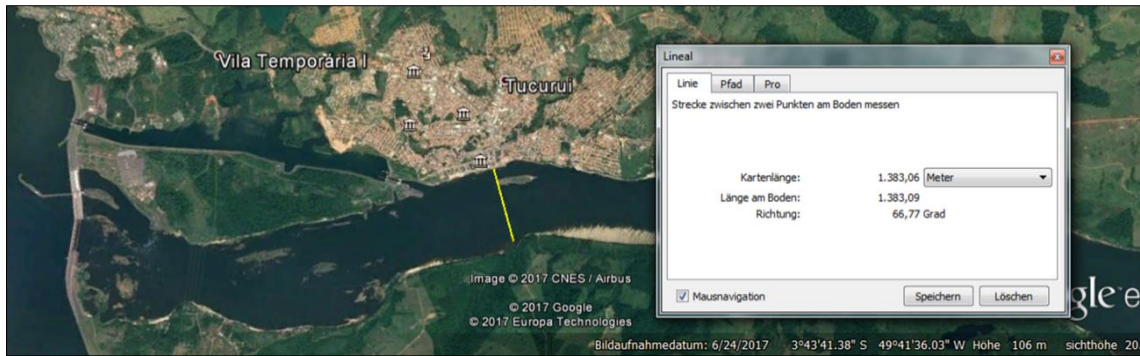
Monthly averaged site data, downstream of UHE Jupuí, MS, Brazil

Monthly Averaged Data (Downstream of UHE Jupuí)					
month	Vazao [m³/s]	AreaMolhada [m²]	Largura [m]	VelMedia [m/s]	Profundidade [m]
1	11121,95	9175,52	881,51	1,15	10,37
2	14512,05	10796,02	893,91	1,27	11,99
3	12552,11	10103,67	833,29	1,20	12,25
4	8045,41	8171,63	874,49	0,93	9,30
5	5400,80	6520,48	868,90	0,82	7,50
6	4684,90	6268,48	864,24	0,74	7,24
7	4759,67	6226,04	861,90	0,75	7,21
8	3539,56	5179,97	859,47	0,66	6,01
9	3483,32	5265,63	859,36	0,63	6,10
10	3941,98	5464,06	862,54	0,69	6,31
11	4586,24	5846,59	866,66	0,76	6,73
12	7326,70	7536,70	872,81	0,93	8,60
Average (year)	6996,22	7212,90	866,59	0,88	8,30



Graphical illustration of the monthly averaged flow velocity at site, downstream of UHE Jupuí, MS, Brazil

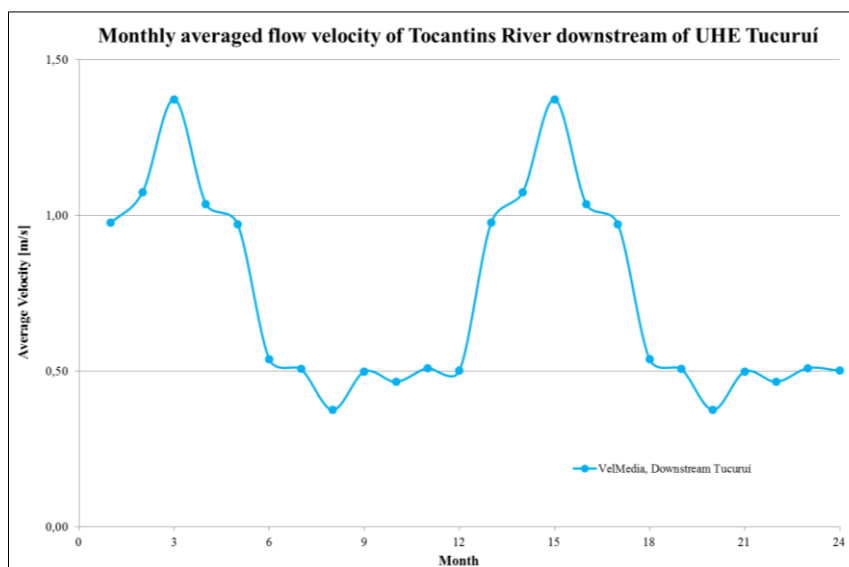
15) Downstream UHE Tucuruí, Rio Tocantins, PA, Brasil



Satellite picture of site with position where measurements were recorded (yellow), downstream of UHE Tucuruí, PA, Brazil

Monthly averaged site data, downstream of UHE Tucuruí, PA, Brazil

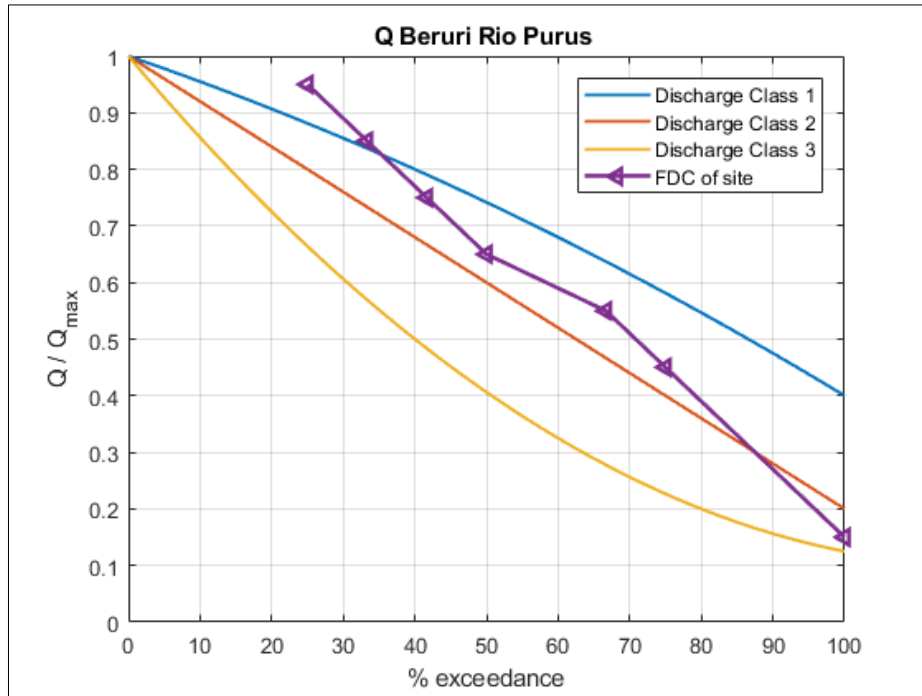
month	Monthly Averaged Data (Tucuruí)				
	Vazao [m ³ /s]	AreaMolhada [m ²]	Largura [m]	VelMedia [m/s]	Profundidade [m]
1	14844,26	14590,42	1415,90	0,98	10,30
2	20288,00	17406,80	1444,70	1,07	11,92
3	26707,92	19178,77	1417,45	1,37	13,57
4	17604,84	16855,92	1410,51	1,04	11,93
5	15295,19	15161,02	1392,45	0,97	10,85
6	5803,83	10691,27	1359,64	0,54	7,87
7	4680,98	9201,88	1348,95	0,51	6,82
8	3388,09	8823,89	1374,69	0,38	6,47
9	4246,43	8347,87	1297,74	0,50	6,41
10	4071,33	8678,90	1345,72	0,47	6,43
11	4684,41	9165,26	1340,21	0,51	6,82
12	5100,68	9514,13	1392,14	0,50	6,83
Average (year)	10559,66	12301,34	1378,34	0,74	8,85



Graphical illustration of the monthly averaged flow velocity at site, downstream of UHE Tucuruí, PA, Brazil

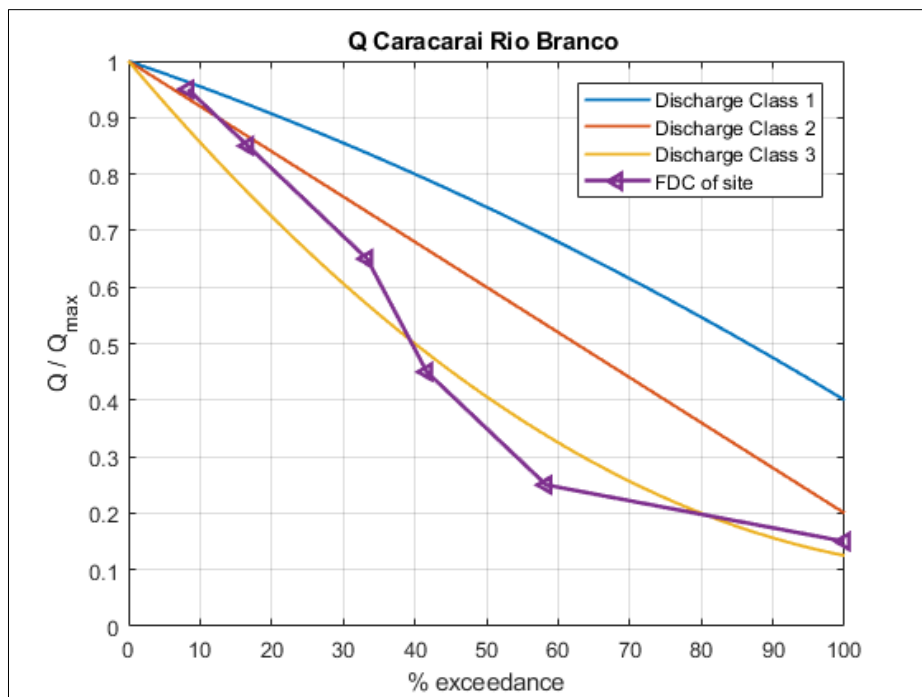
Appendix II – River Sites, Discharge Classification

1) Beruri, Rio Purus, AM, Brasil



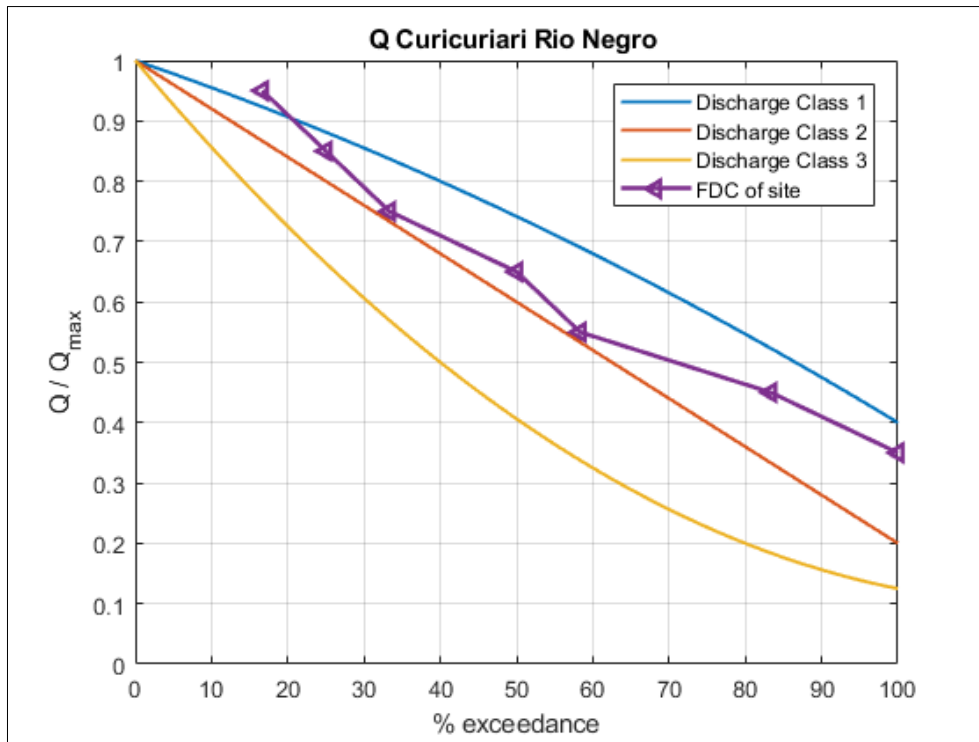
Determined Flow Duration Curve at site on the basis of its monthly averaged discharge data (Appendix I), FDC of site allocated to Discharge Class 2

2) Caracaráí, Rio Branco, RR, Brasil



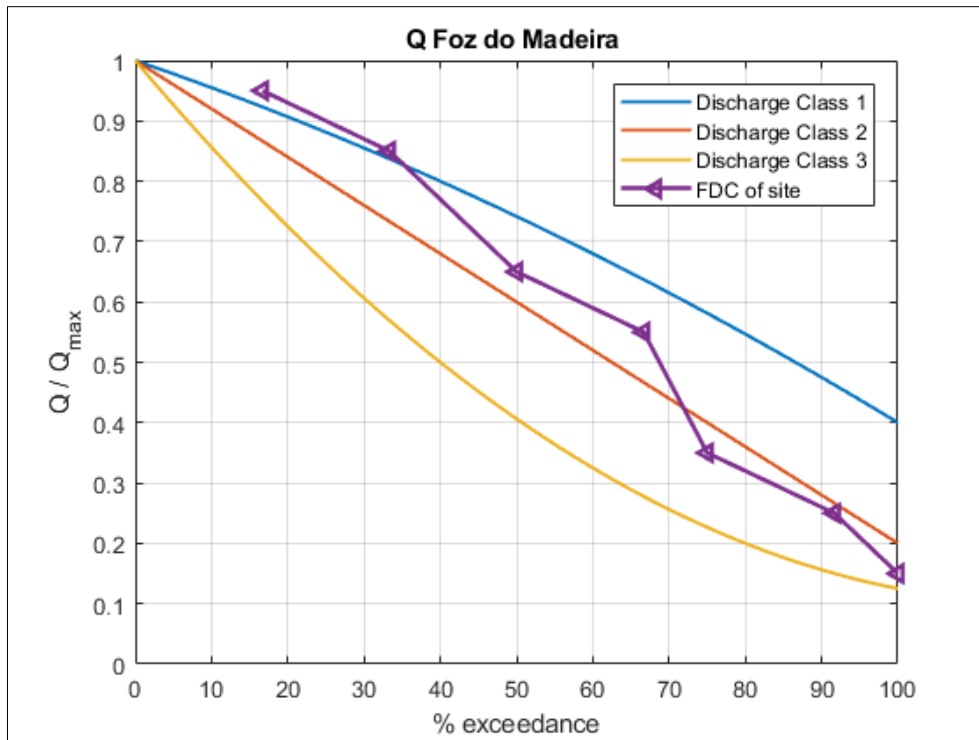
Determined Flow Duration Curve at site on the basis of its monthly averaged discharge data (Appendix I), FDC of site allocated to Discharge Class 3

3) Curicuriari, Rio Negro, AM, Brasil



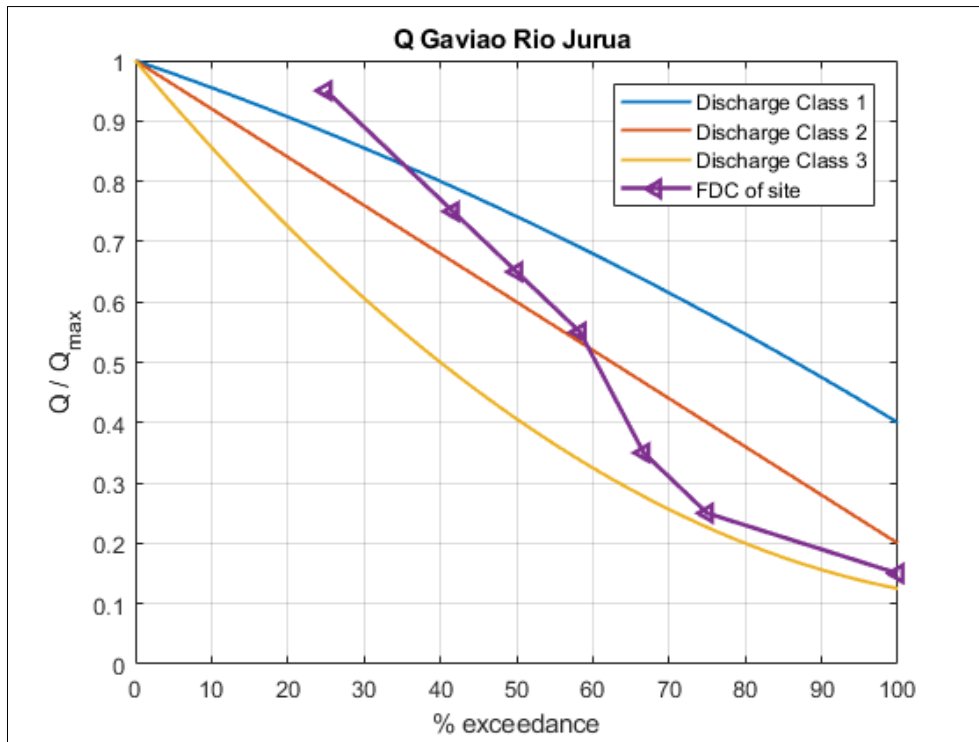
Determined Flow Duration Curve at site on the basis of its monthly averaged discharge data (Appendix I), FDC of site allocated to Discharge Class 2

4) Foz do Madeira, Rio Madeira, AM, Brasil



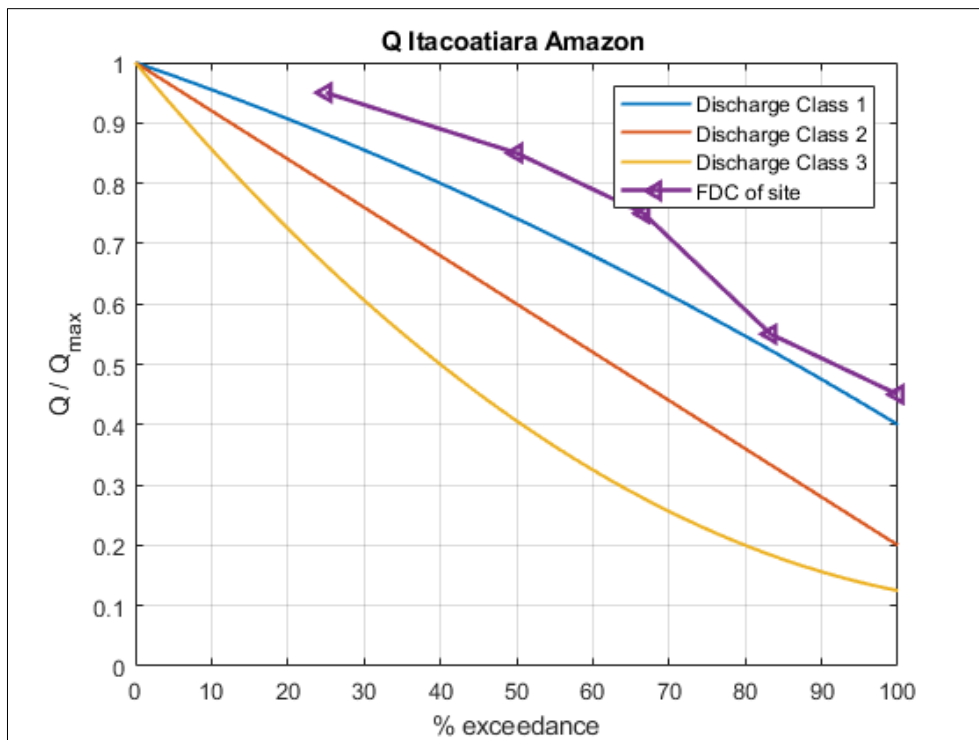
Determined Flow Duration Curve at site on the basis of its monthly averaged discharge data (Appendix I), FDC of site allocated to Discharge Class 2

5) Gavião, Rio Juruá, AM, Brasil



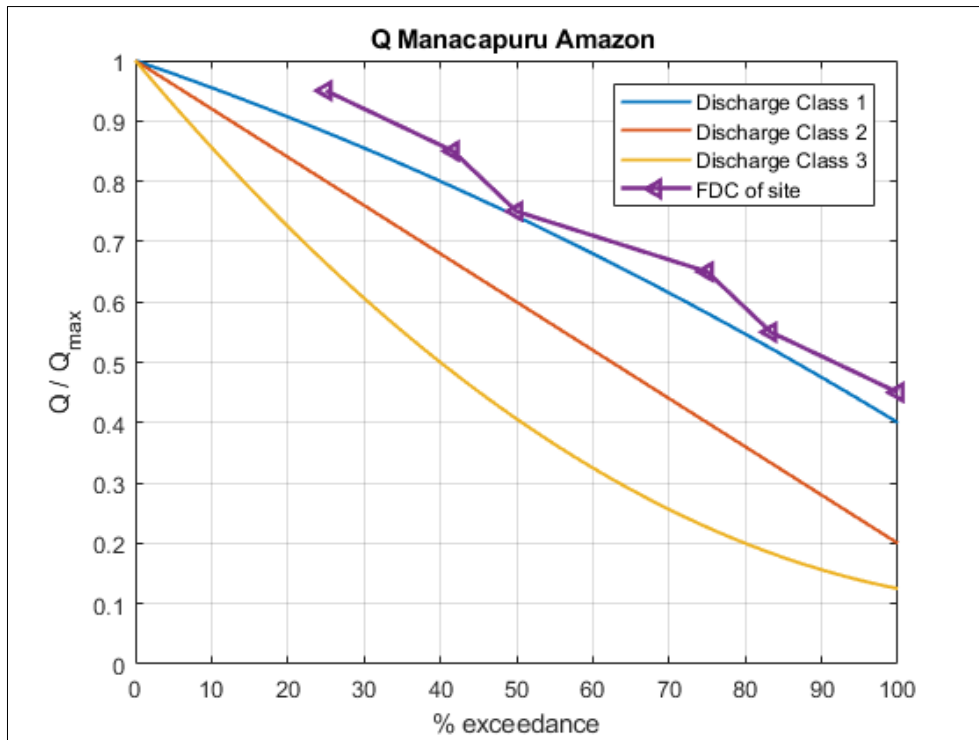
Determined Flow Duration Curve at site on the basis of its monthly averaged discharge data (Appendix I), FDC of site allocated to Discharge Class 2

6) Itacoatiara, Rio Amazonas, AM, Brasil



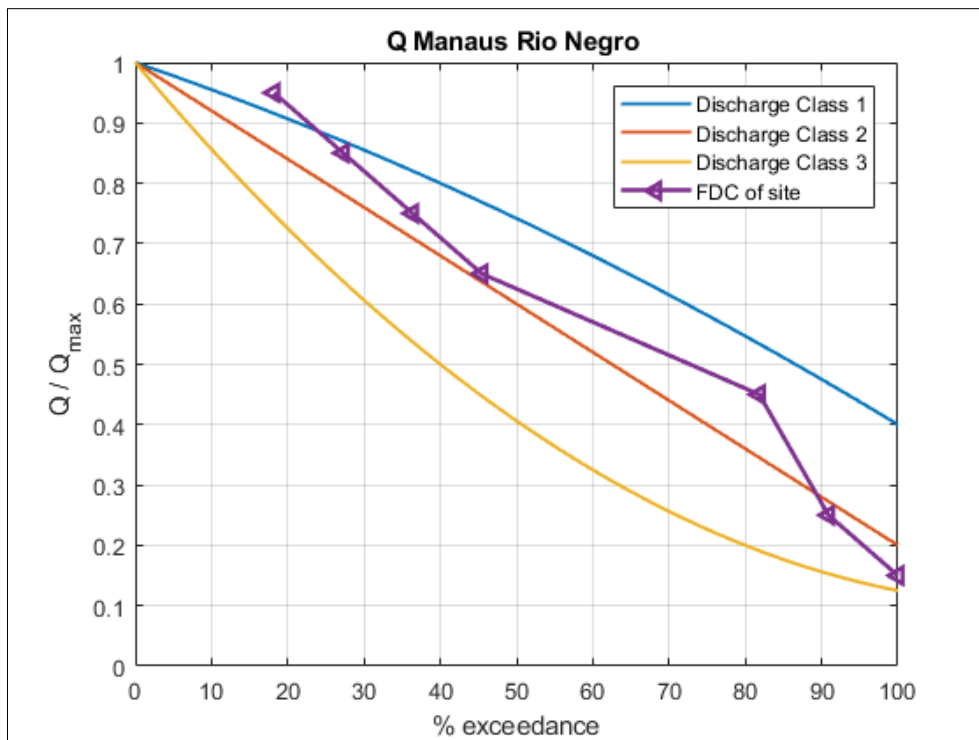
Determined Flow Duration Curve at site on the basis of its monthly averaged discharge data (Appendix I), FDC of site allocated to Discharge Class 1

7) Manacapuru, Rio Amazonas, AM, Brasil



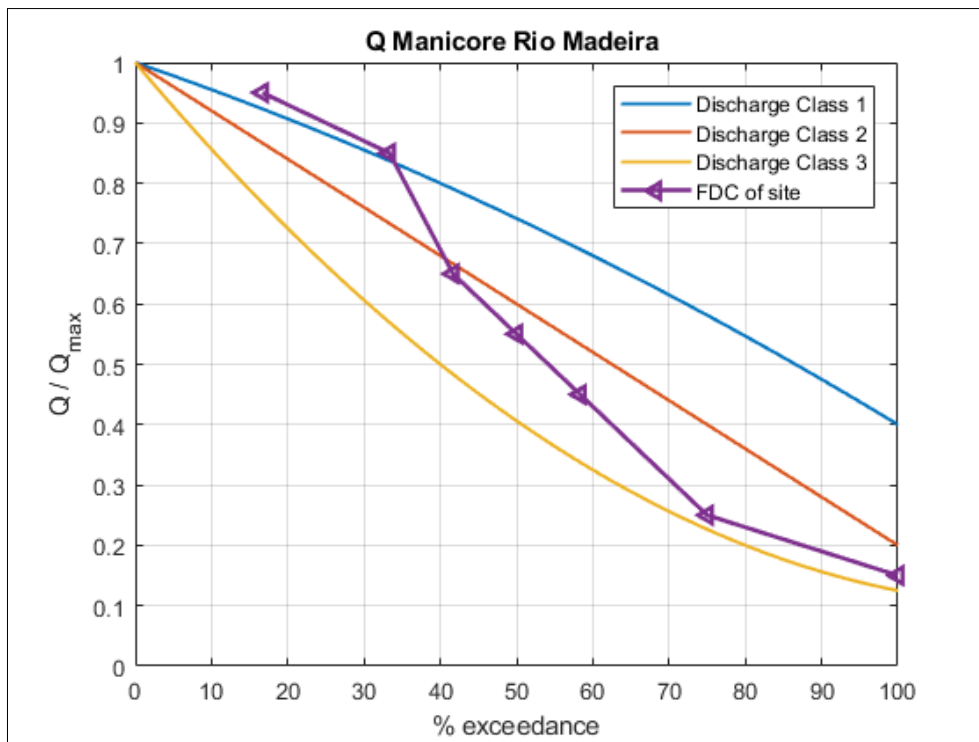
Determined Flow Duration Curve at site on the basis of its monthly averaged discharge data (Appendix I), FDC of site allocated to Discharge Class 1

8) Manaus, Rio Negro, AM, Brasil



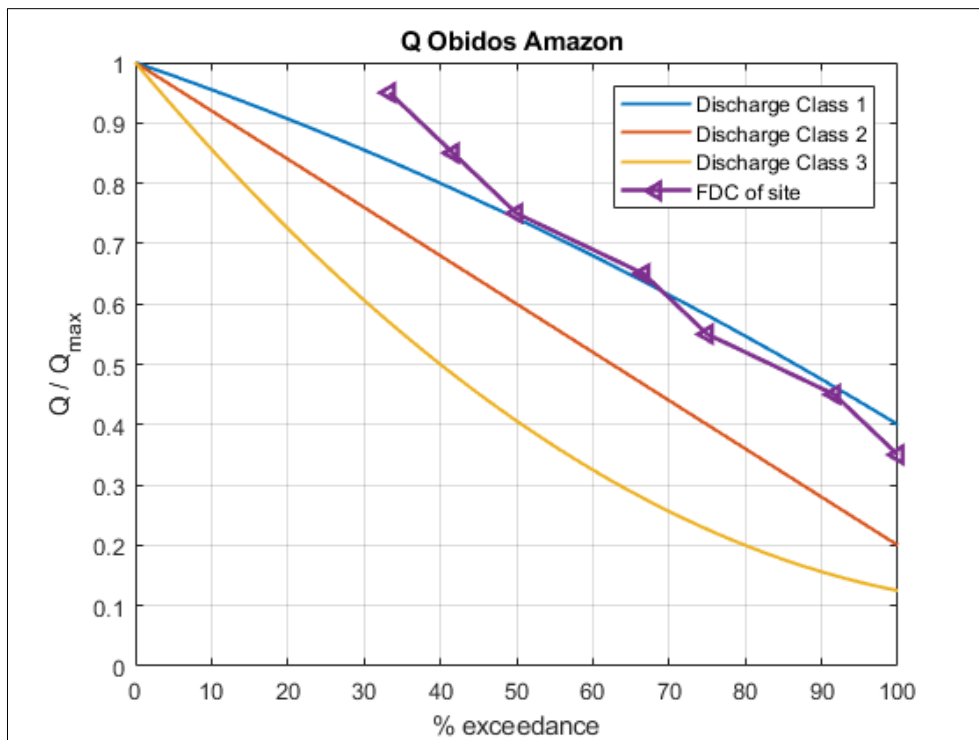
Determined Flow Duration Curve at site on the basis of its monthly averaged discharge data (Appendix I), FDC of site allocated to Discharge Class 2

9) Manicoré, Rio Madeira, AM, Brazil



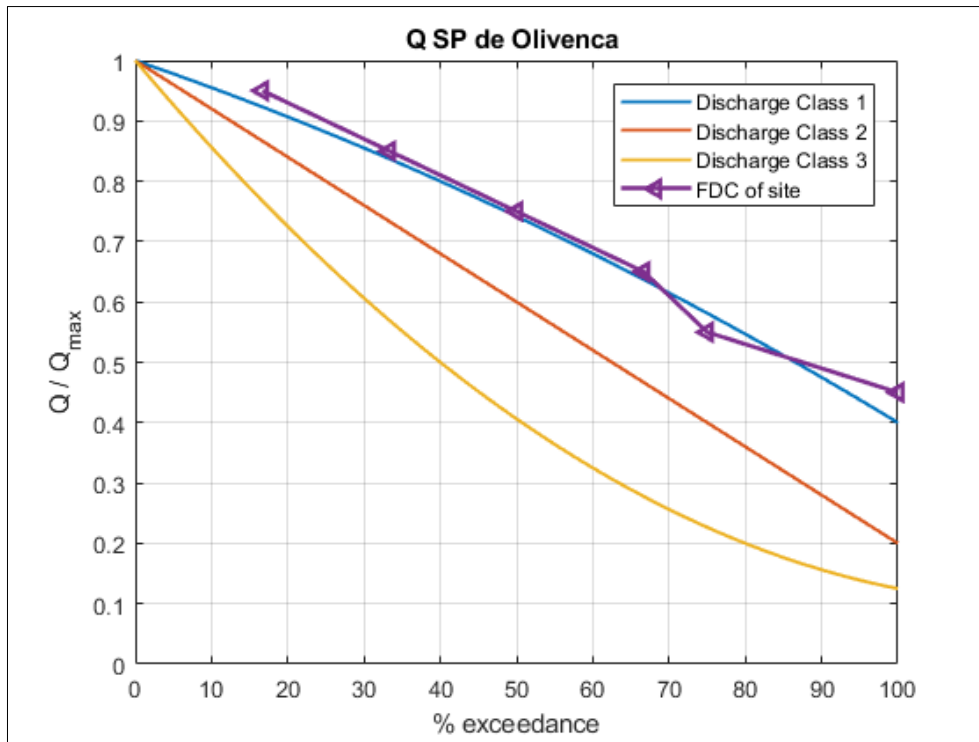
Determined Flow Duration Curve at site on the basis of its monthly averaged discharge data (Appendix I), FDC of site allocated to Discharge Class 2

10) Óbidos, Rio Amazonas, PA, Brasil



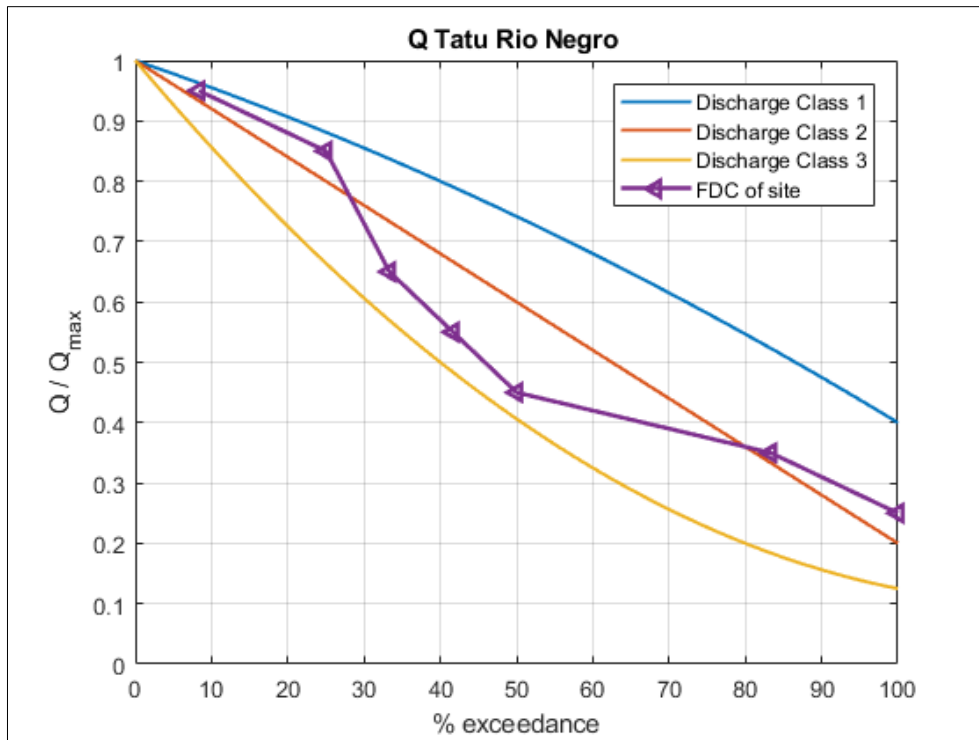
Determined Flow Duration Curve at site on the basis of its monthly averaged discharge data (Appendix I), FDC of site allocated to Discharge Class 1

11) São Paulo de Olivença, Rio Amazonas, AM, Brasil



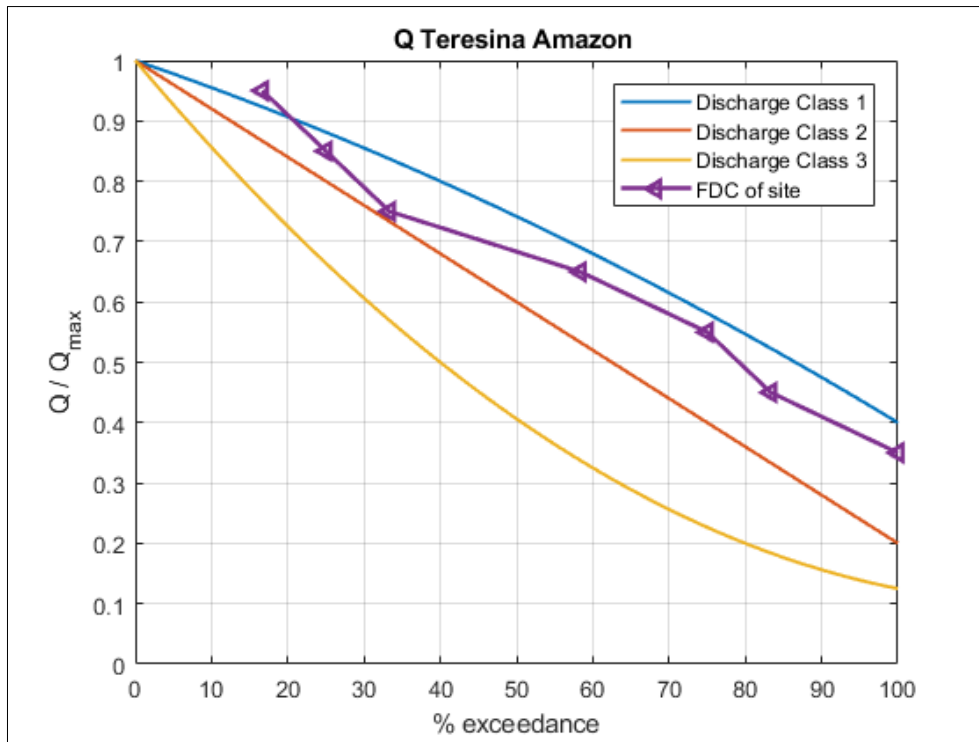
Determined Flow Duration Curve at site on the basis of its monthly averaged discharge data (Appendix I), FDC of site allocated to Discharge Class 1

12) Tatu, Rio Negro, AM, Brasil



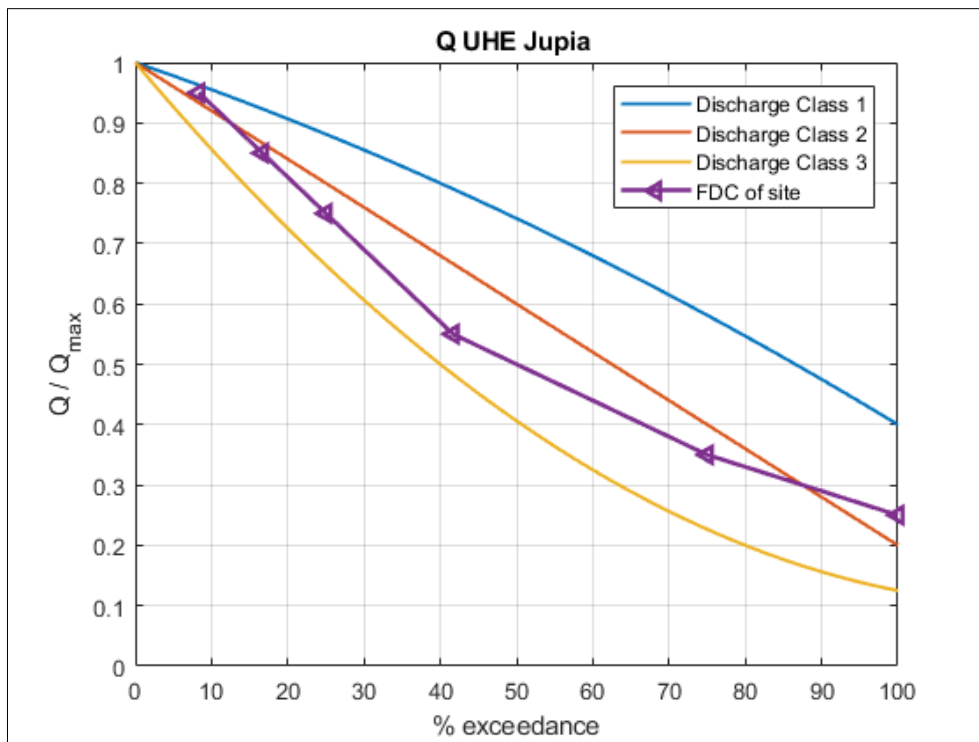
Determined Flow Duration Curve at site on the basis of its monthly averaged discharge data (Appendix I), FDC of site allocated to Discharge Class 2

13) Teresina, Rio Amazonas, AM, Brasil



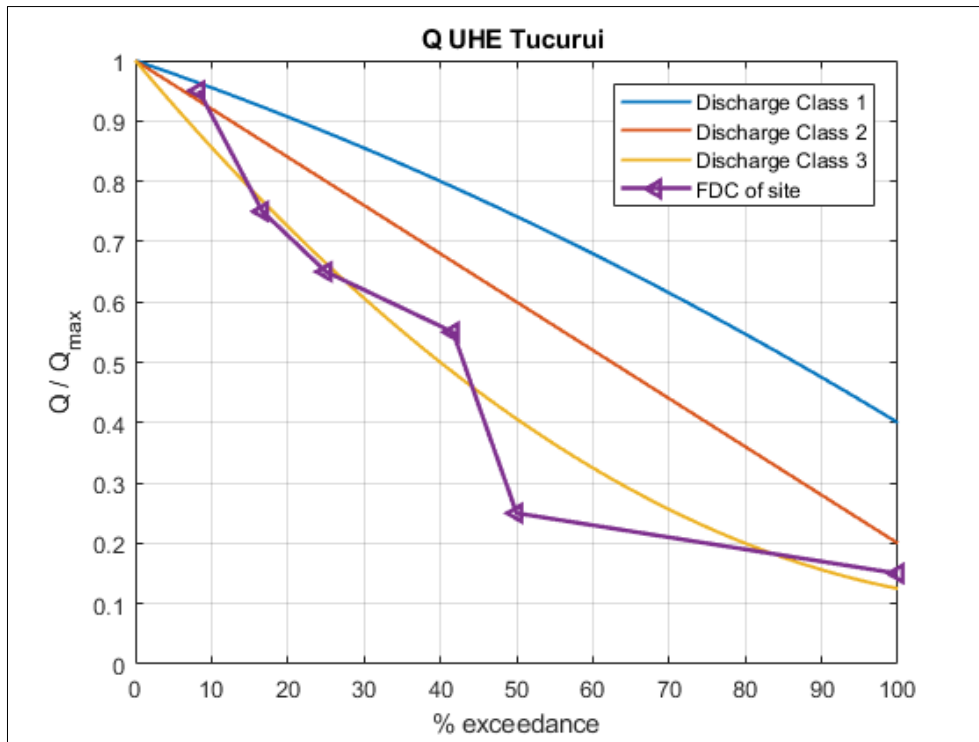
Determined Flow Duration Curve at site on the basis of its monthly averaged discharge data (Appendix I), FDC of site allocated to Discharge Class 1

14) Downstream UHE Jupia, Rio Paraná, MS, Brasil



Determined Flow Duration Curve at site on the basis of its monthly averaged discharge data (Appendix I), FDC of site allocated to Discharge Class 2

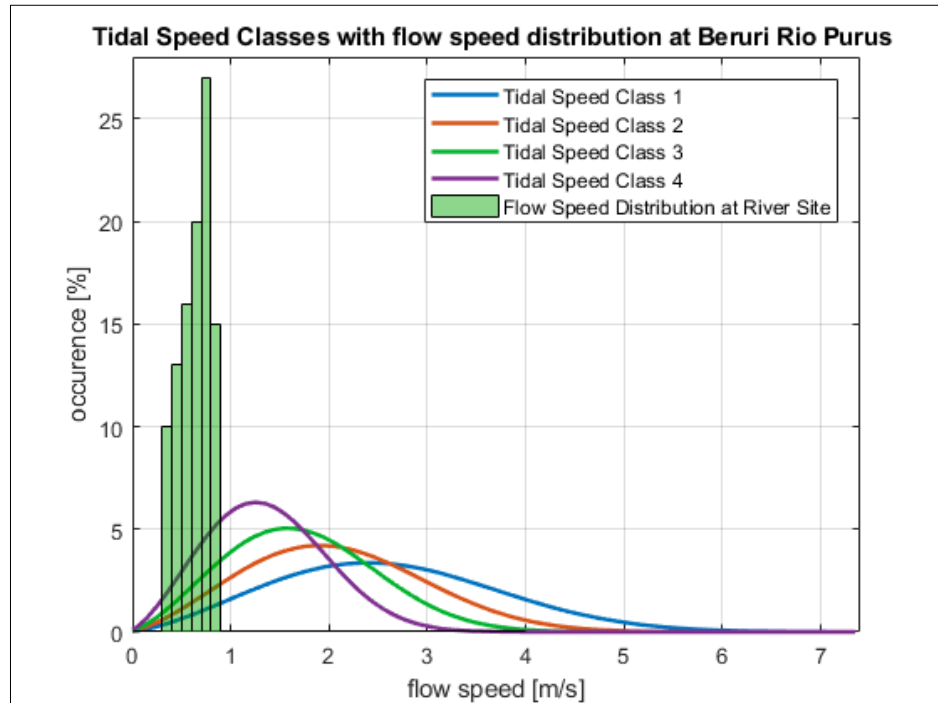
15) Downstream UHE Tucuruí, Rio Tocantins, PA, Brasil



Determined Flow Duration Curve at site on the basis of its monthly averaged discharge data (Appendix I), FDC of site allocated to Discharge Class 3

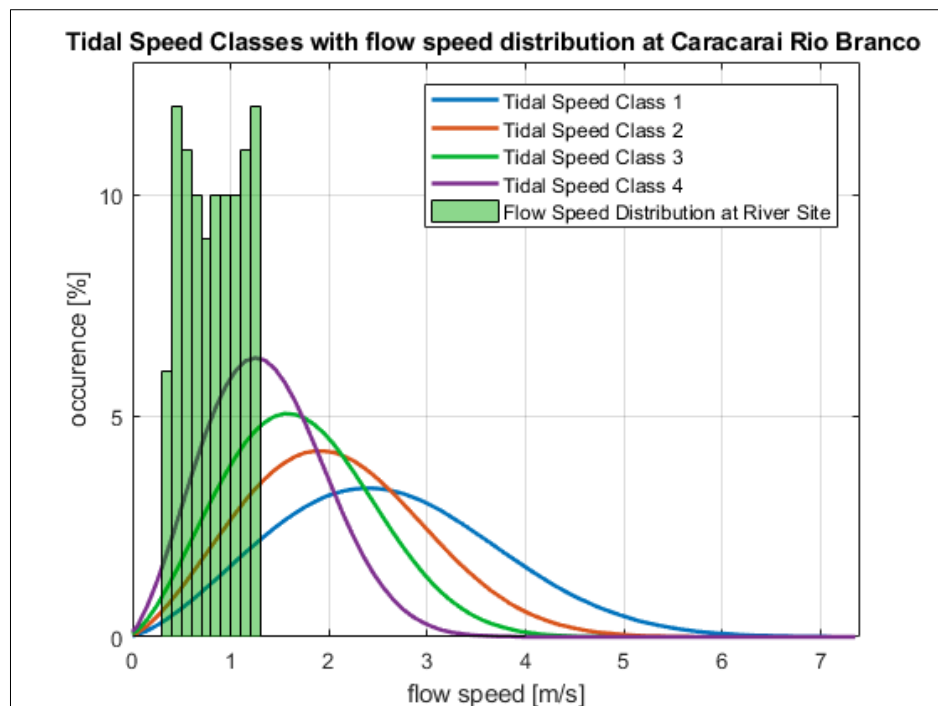
Appendix III – Flow Speed Distribution (1)

1) Beruri, Rio Purus, AM, Brasil



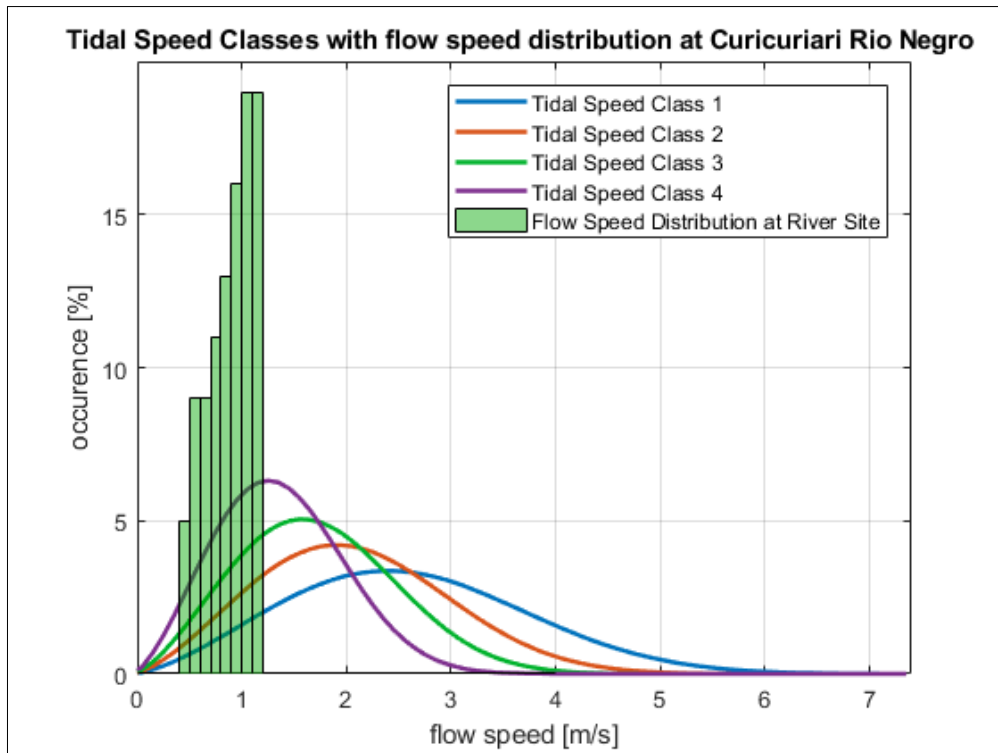
Comparison of river flow speed distribution at site with Tidal Speed Classes

2) Caracaraí, Rio Branco, RR, Brasil



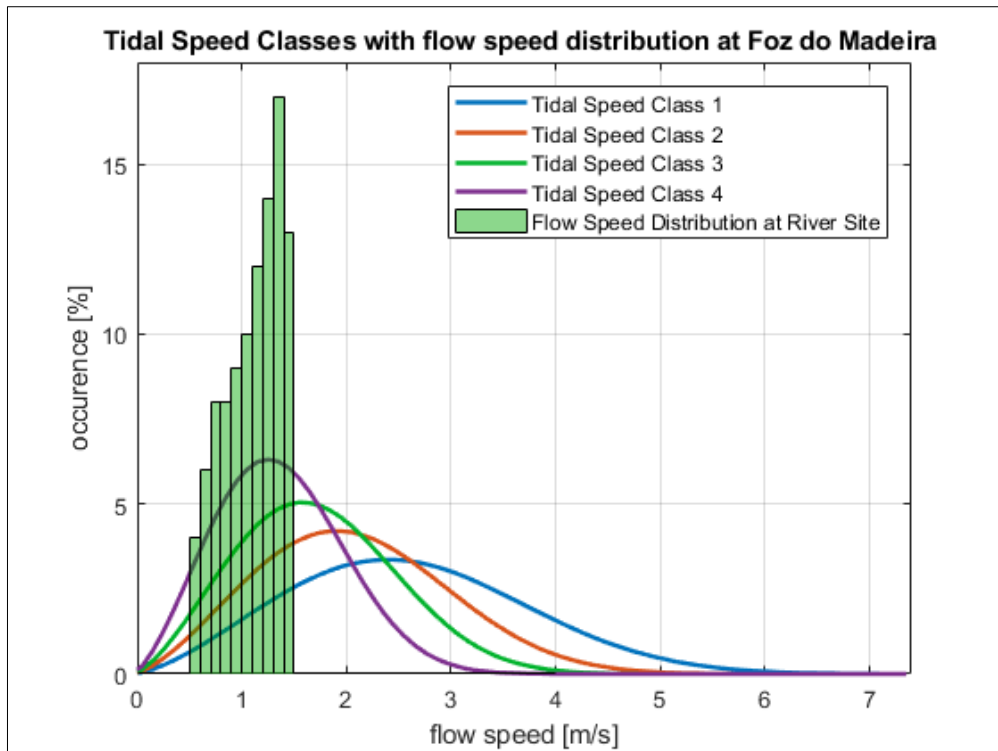
Comparison of river flow speed distribution at site with Tidal Speed Classes

3) Curicuriari, Rio Negro, AM, Brasil



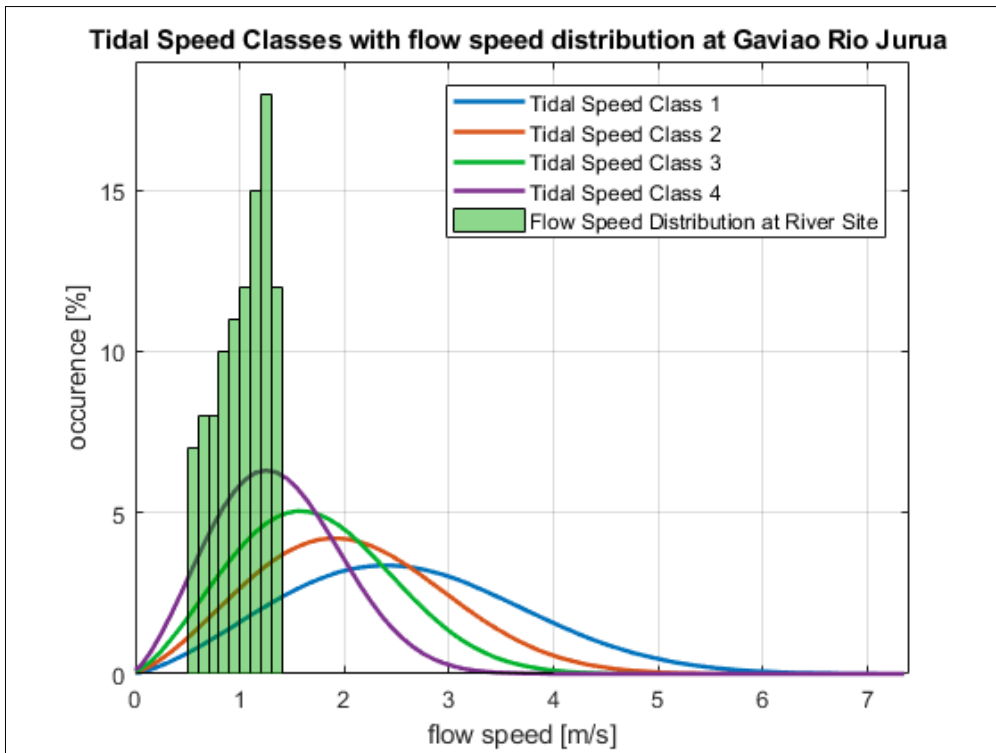
Comparison of river flow speed distribution at site with Tidal Speed Classes

4) Foz do Madeira, Rio Madeira, AM, Brasil



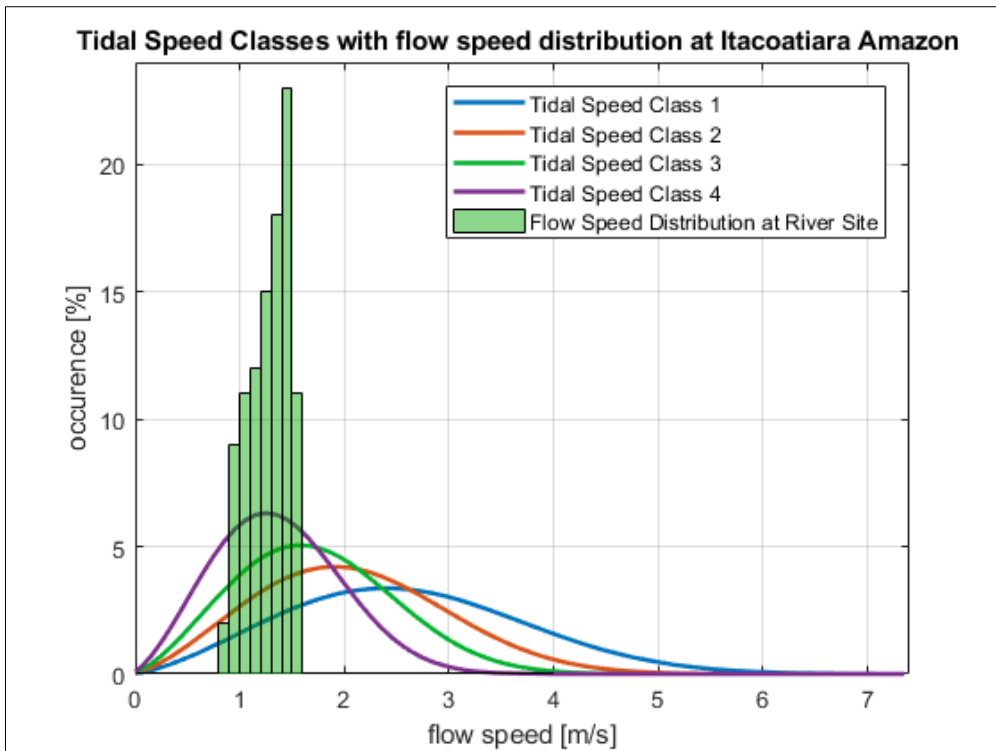
Comparison of river flow speed distribution at site with Tidal Speed Classes

5) Gavião, Rio Juruá, AM, Brasil



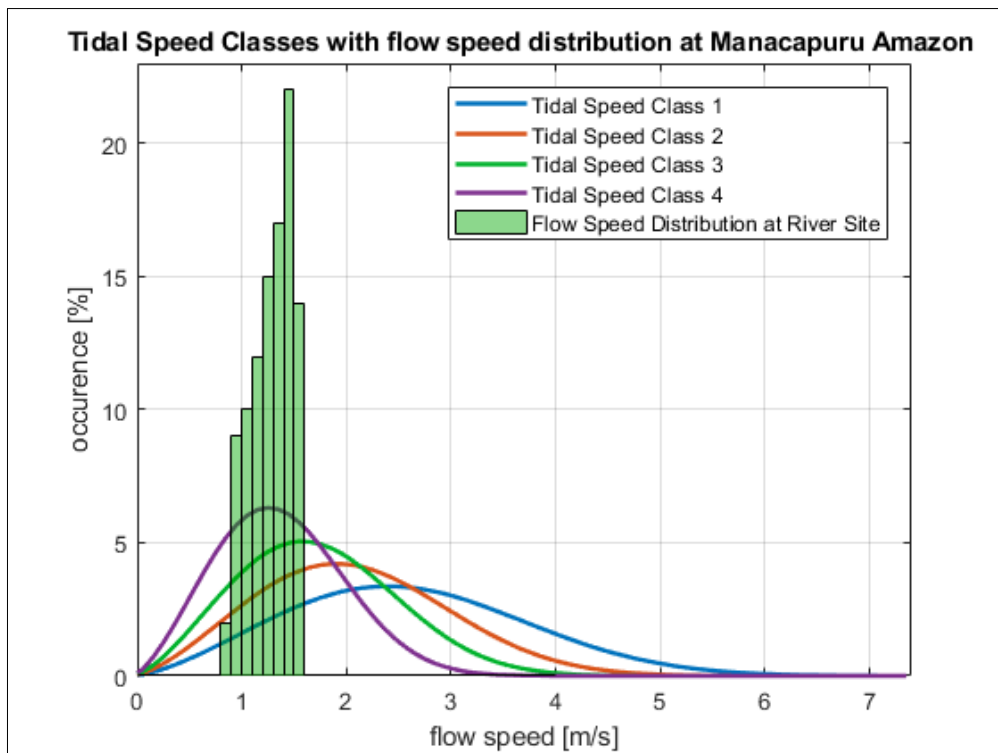
Comparison of river flow speed distribution at site with Tidal Speed Classes

6) Itacoatiara, Rio Amazonas, AM, Brasil



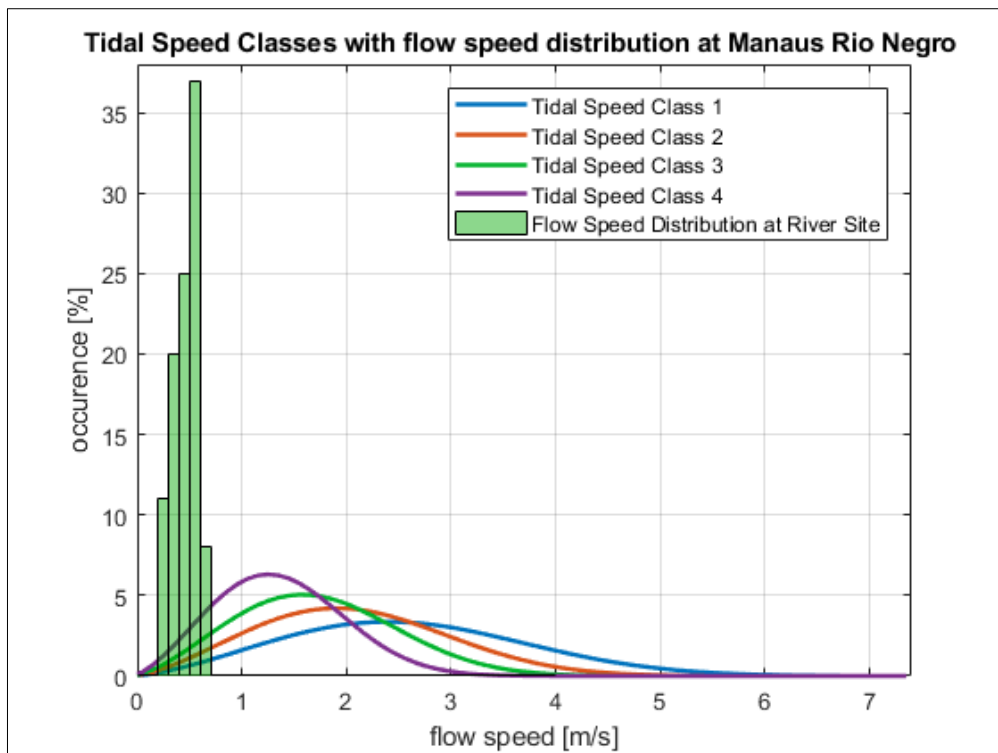
Comparison of river flow speed distribution at site with Tidal Speed Classes

7) Manacapuru, Rio Amazonas, AM, Brasil



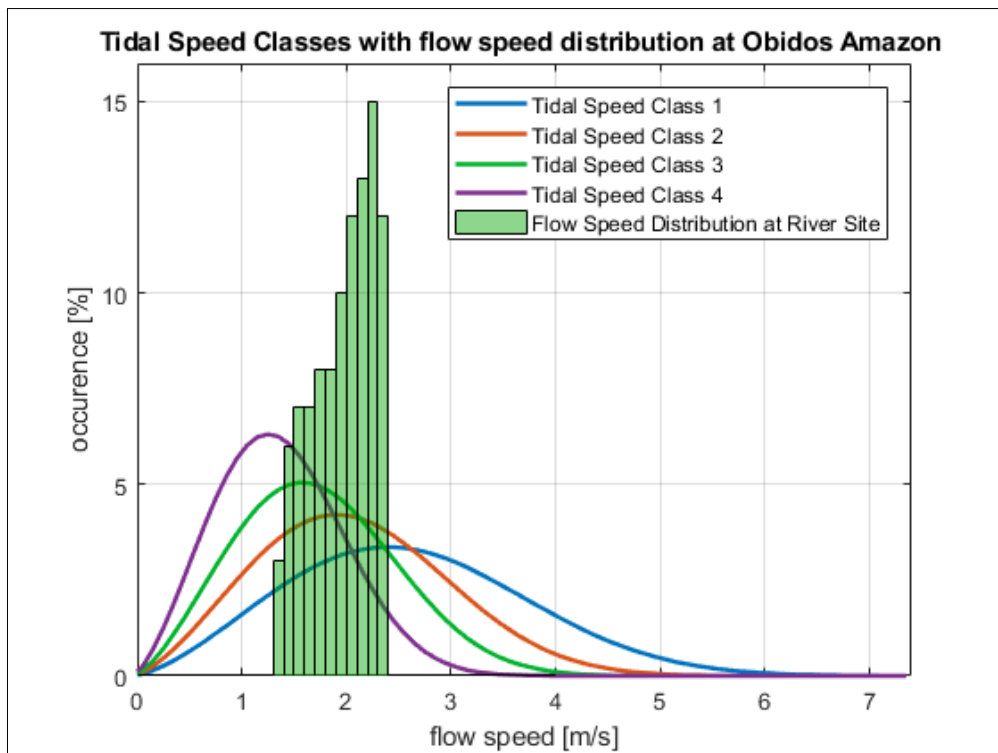
Comparison of river flow speed distribution at site with Tidal Speed Classes

8) Manaus, Rio Negro, AM, Brasil



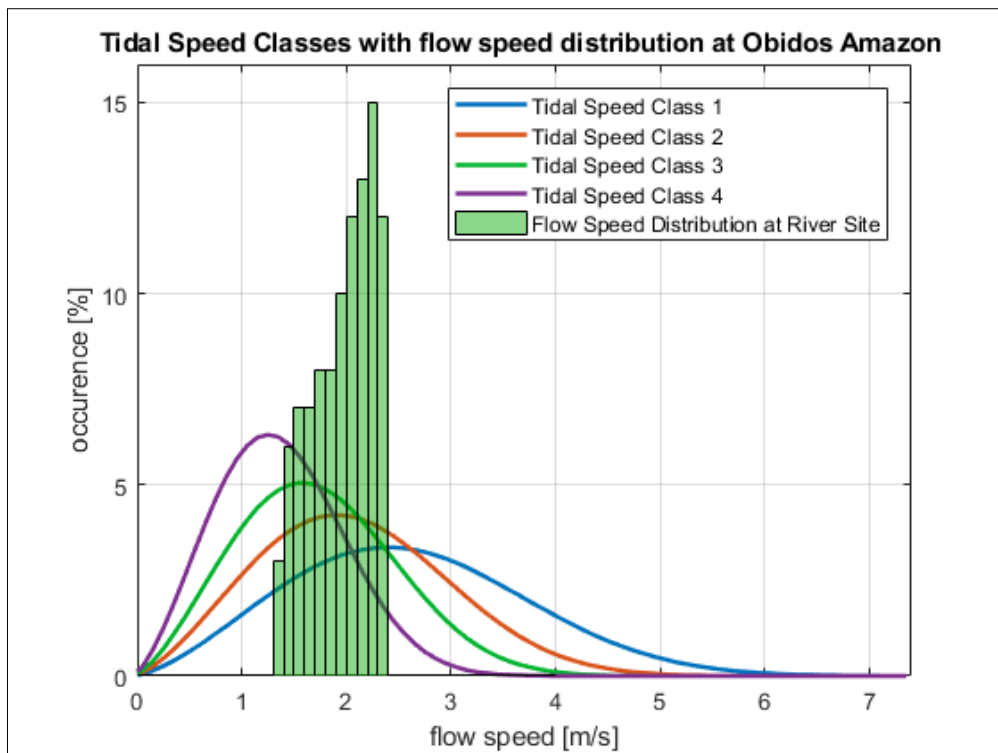
Comparison of river flow speed distribution at site with Tidal Speed Classes

9) Manicoré, Rio Madeira, AM, Brazil



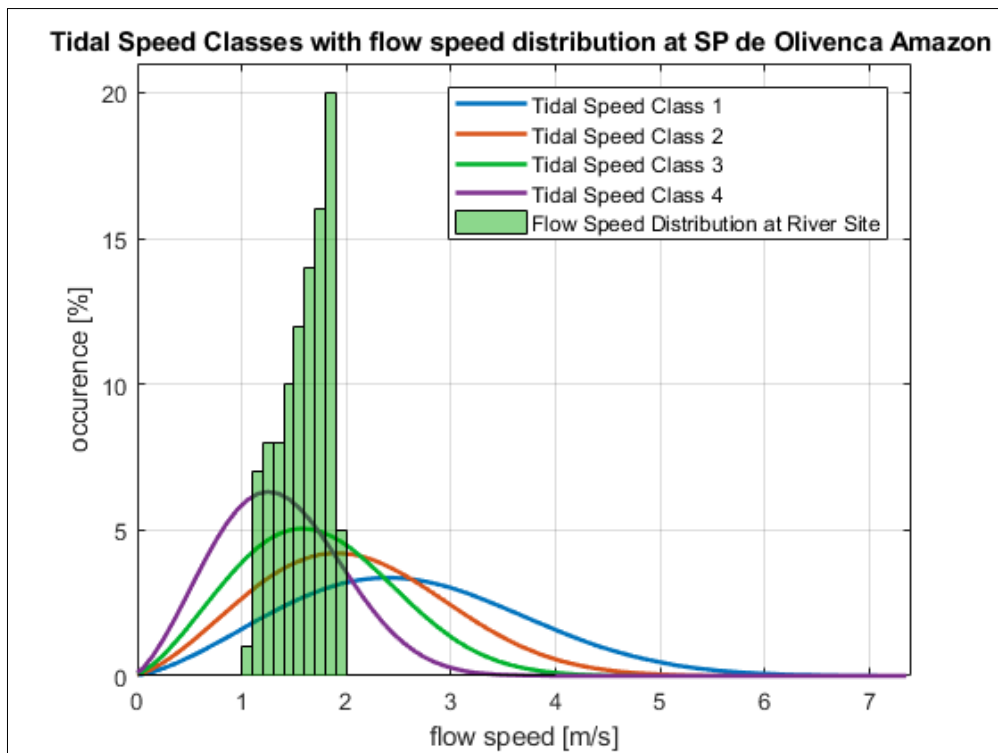
Comparison of river flow speed distribution at site with Tidal Speed Classes

10) Óbidos, Rio Amazonas, PA, Brasil



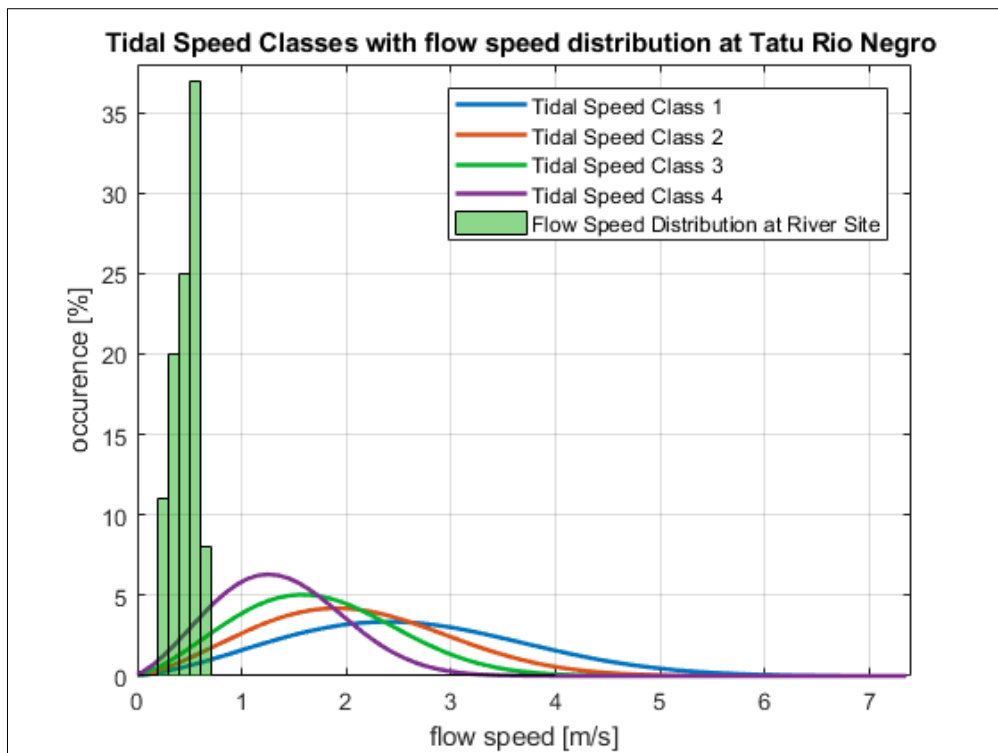
Comparison of river flow speed distribution at site with Tidal Speed Classes

11) São Paulo de Olivença, Rio Amazonas, AM, Brasil



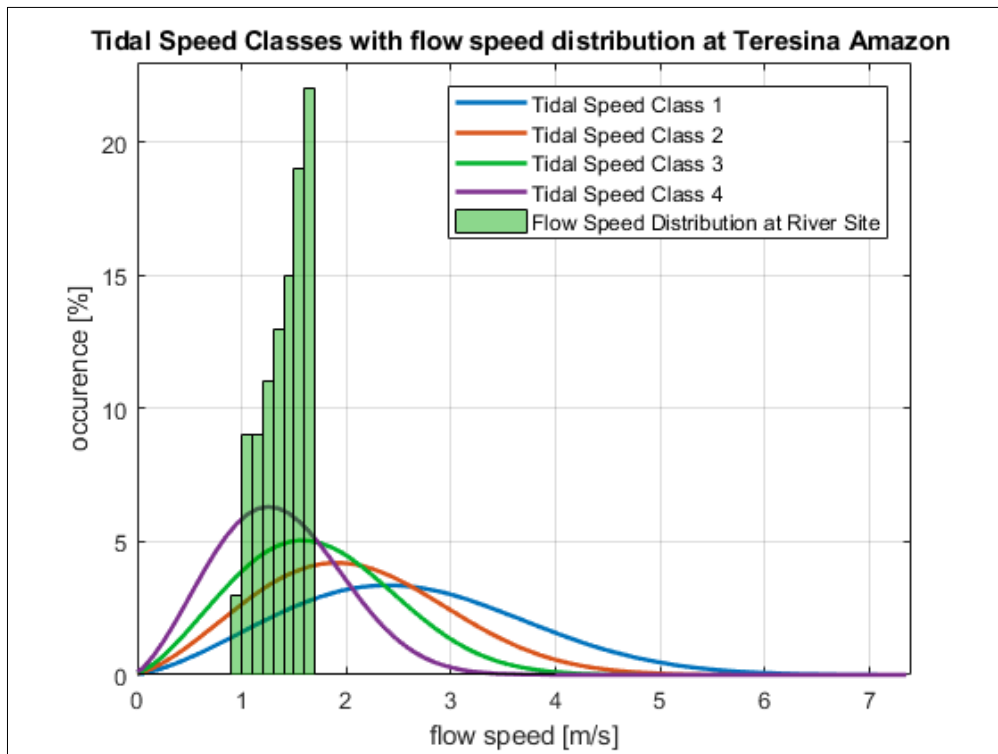
Comparison of river flow speed distribution at site with Tidal Speed Classes

12) Tatu, Rio Negro, AM, Brasil



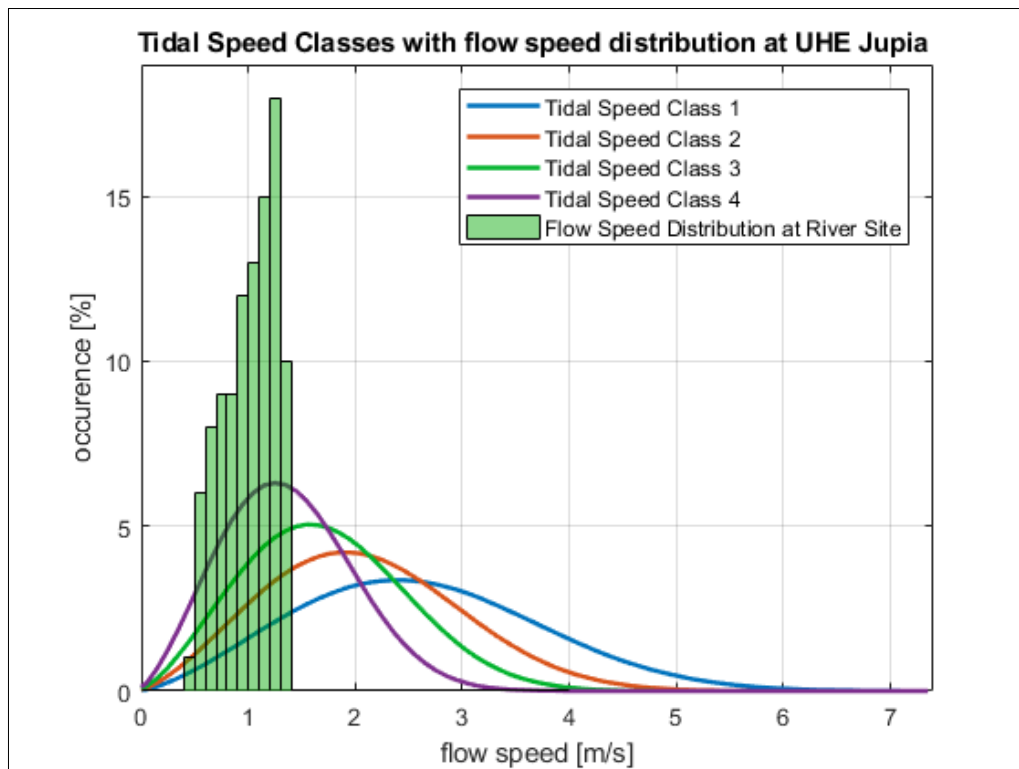
Comparison of river flow speed distribution at site with Tidal Speed Classes

13) Teresina, Rio Amazonas, AM, Brasil



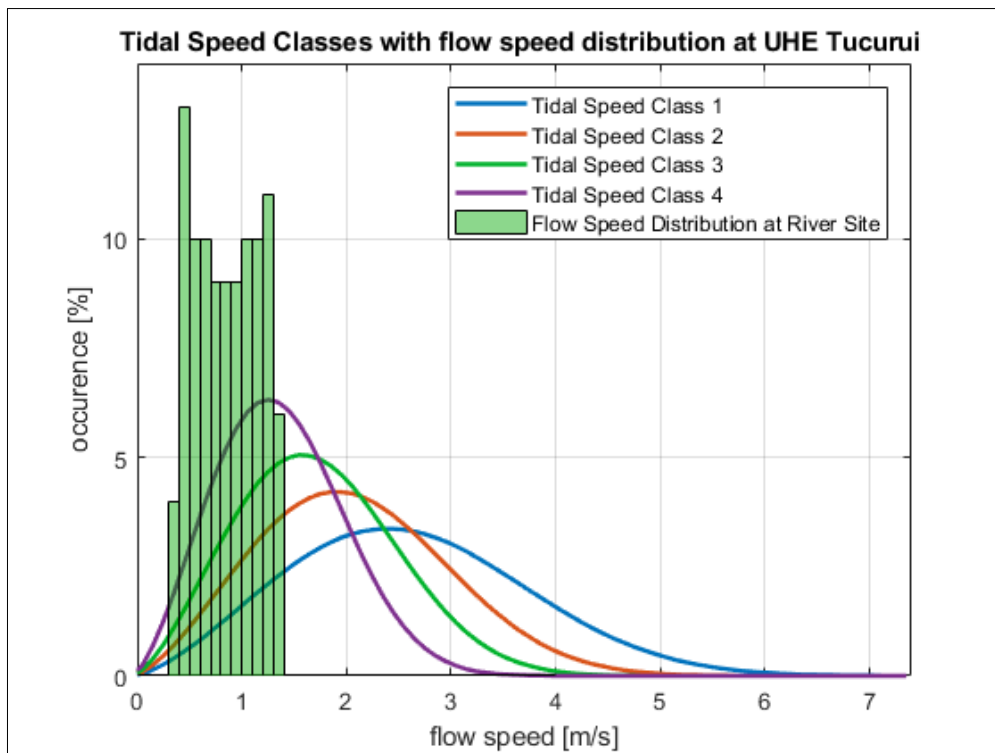
Comparison of river flow speed distribution at site with Tidal Speed Classes

14) Downstream UHE Jupiá, Rio Paraná, MS, Brasil



Comparison of river flow speed distribution at site with Tidal Speed Classes

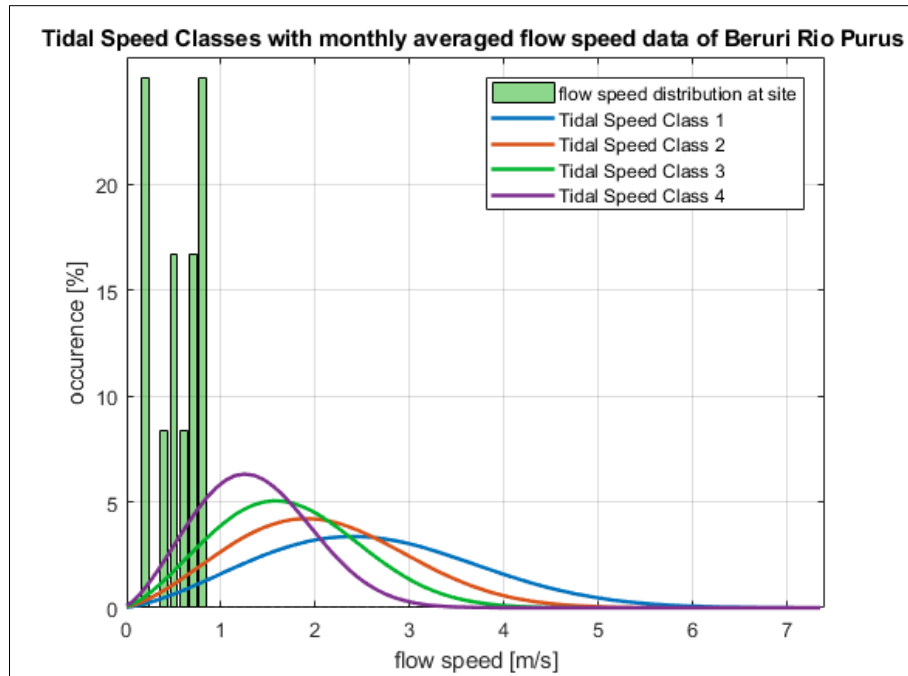
15) Downstream UHE Tucuruí, Rio Tocantins, PA, Brasil



Comparison of river flow speed distribution at site with Tidal Speed Classes

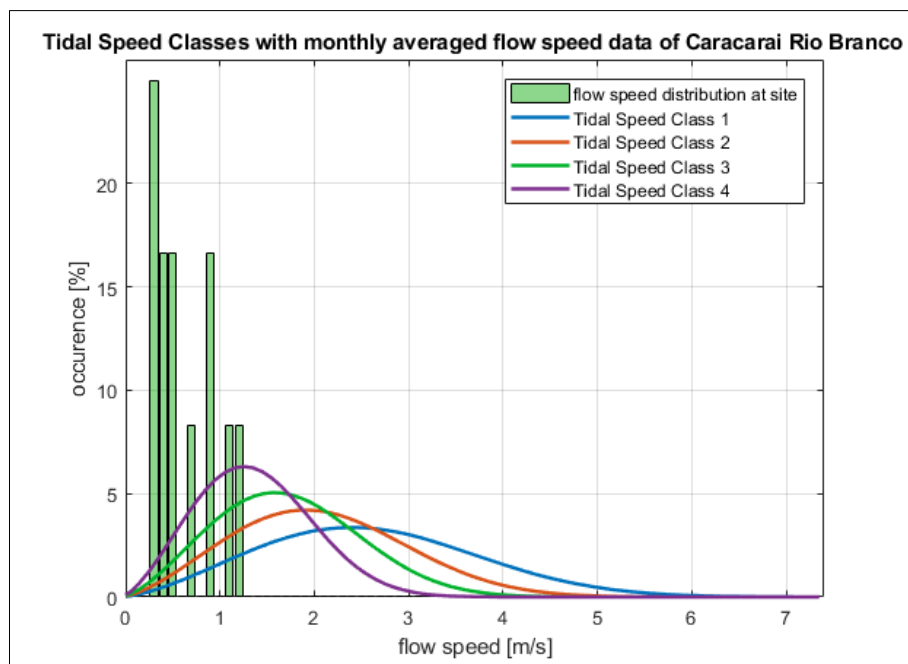
Appendix IV – Flow Speed Distribution (2)

1) Beruri, Rio Purus, AM, Brasil



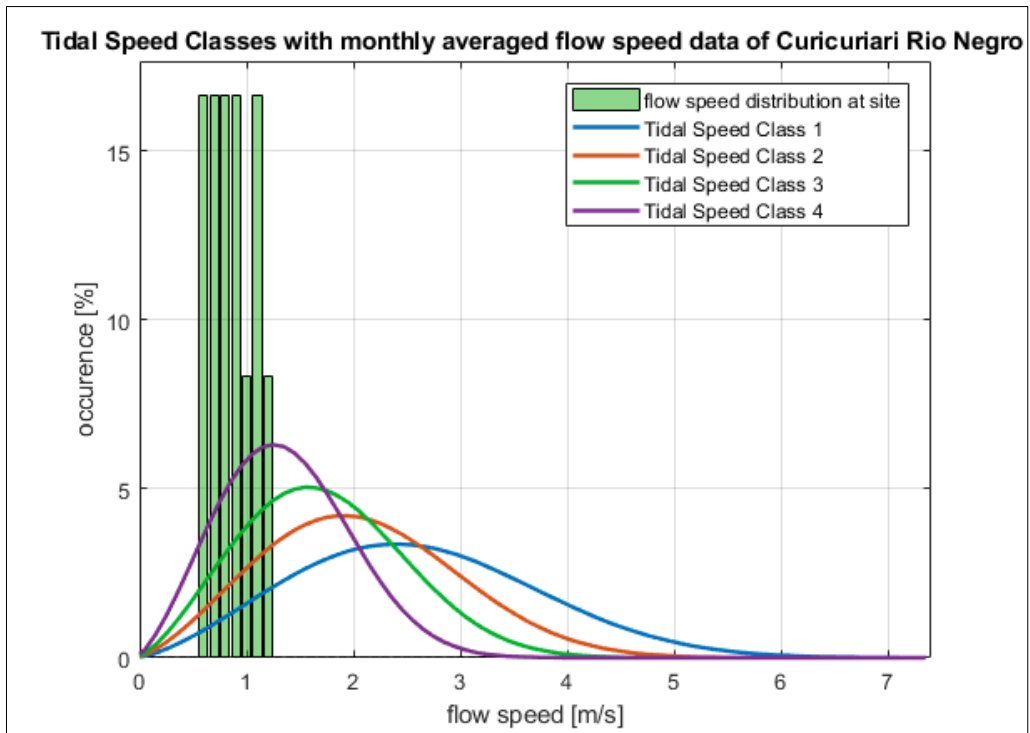
Comparison of river flow speed distribution at site with Tidal Speed Classes using monthly averaged data (Appendix I)

2) Caracarái, Rio Branco, RR, Brasil



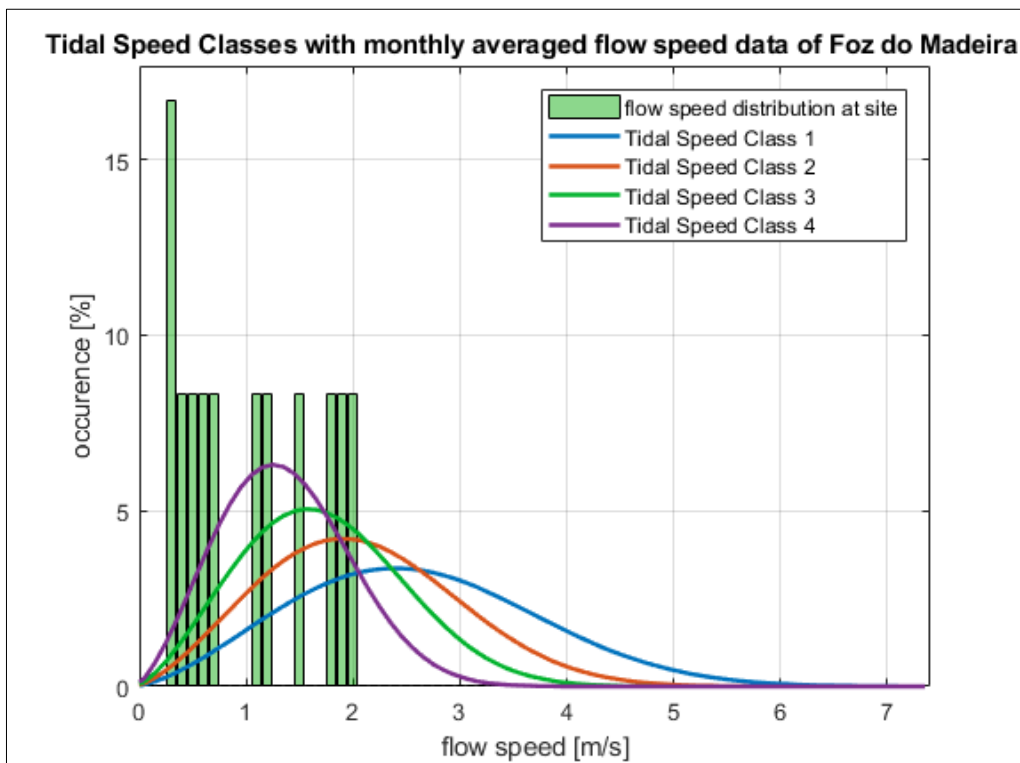
Comparison of river flow speed distribution at site with Tidal Speed Classes using monthly averaged data (Appendix I)

3) Curicuriari, Rio Negro, AM, Brasil



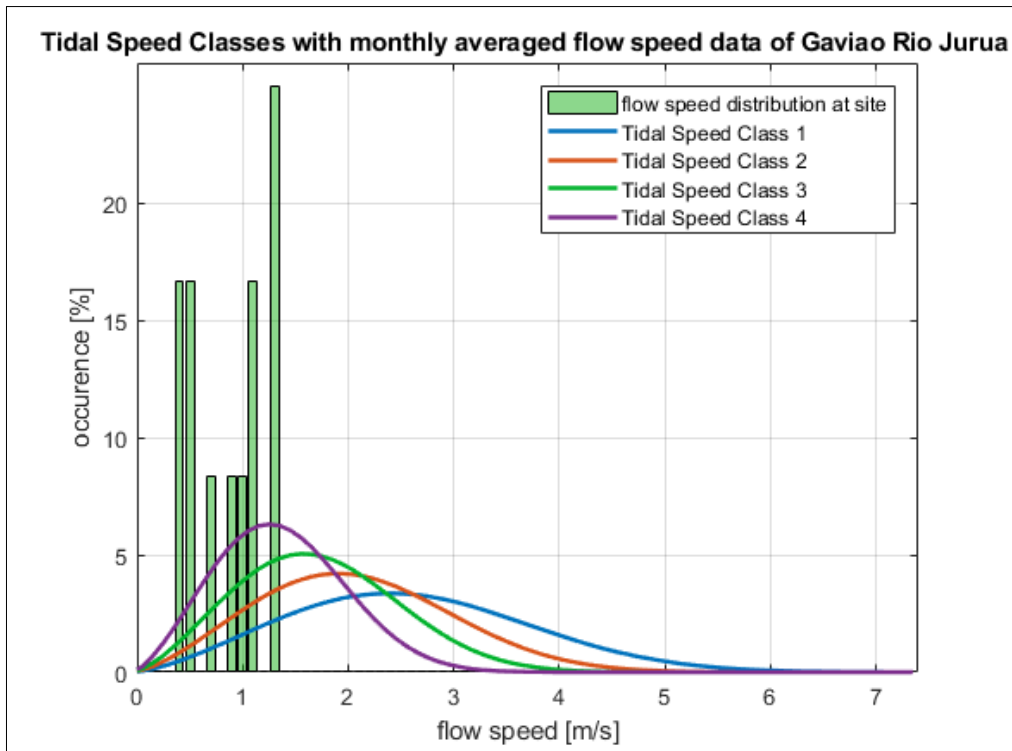
Comparison of river flow speed distribution at site with Tidal Speed Classes using monthly averaged data (Appendix I)

4) Foz do Madeira, Rio Madeira, AM, Brasil



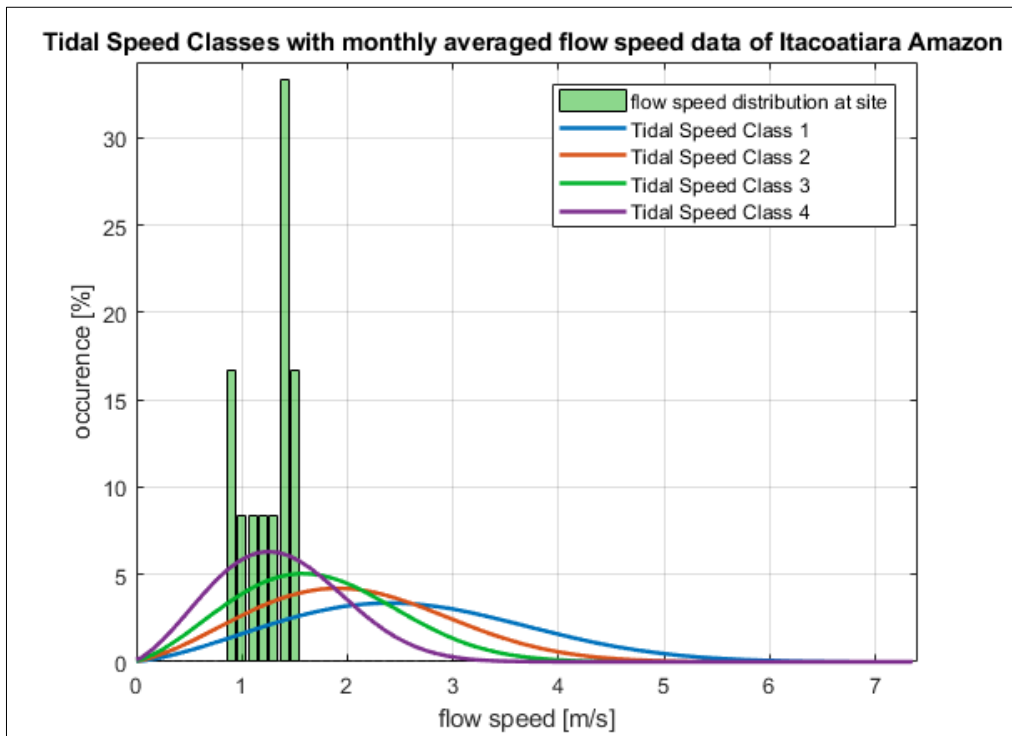
Comparison of river flow speed distribution at site with Tidal Speed Classes using monthly averaged data (Appendix I)

5) Gavião, Rio Juruá, AM, Brasil



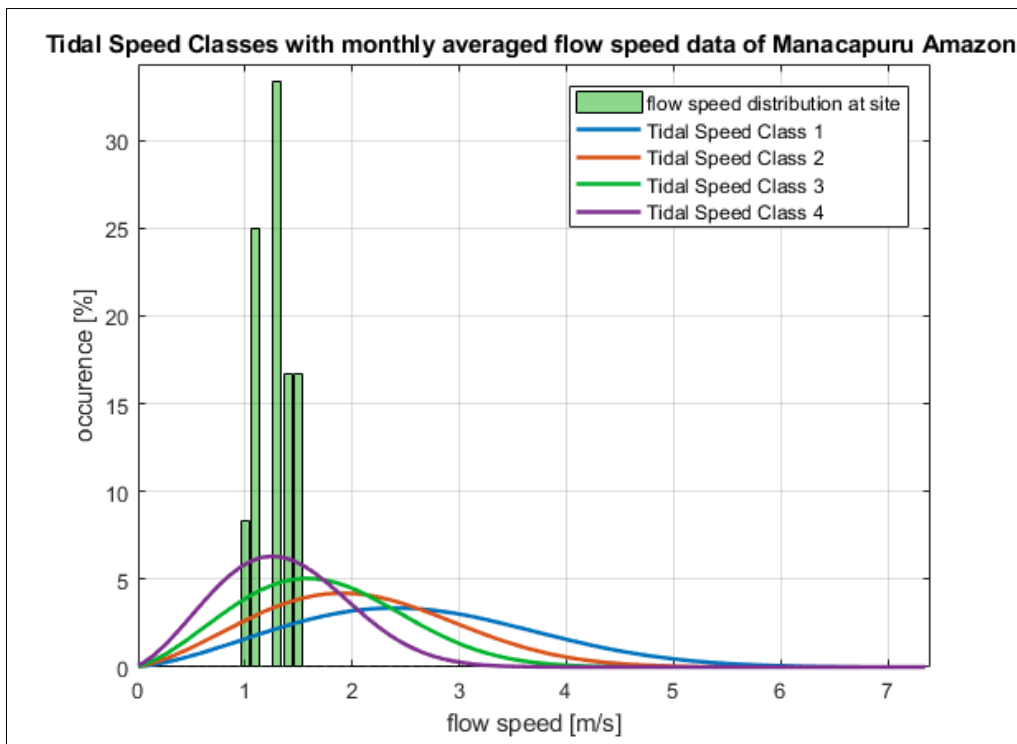
Comparison of river flow speed distribution at site with Tidal Speed Classes using monthly averaged data (Appendix I)

6) Itacoatiara, Rio Amazonas, AM, Brasil



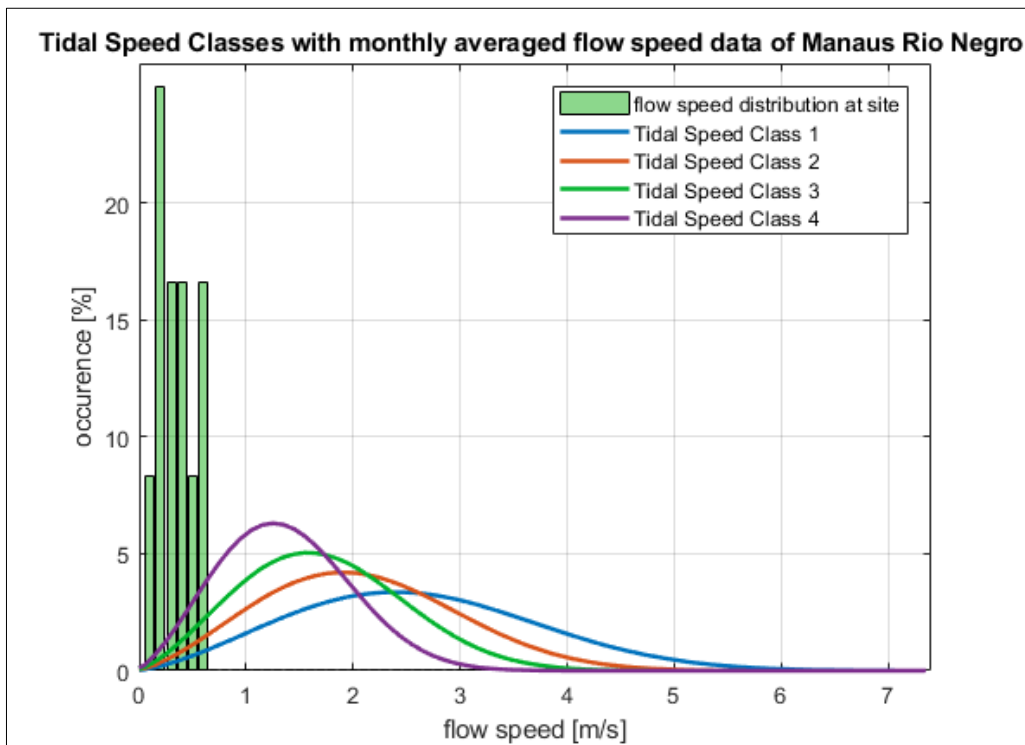
Comparison of river flow speed distribution at site with Tidal Speed Classes using monthly averaged data (Appendix I)

7) Manacapuru, Rio Amazonas, AM, Brasil



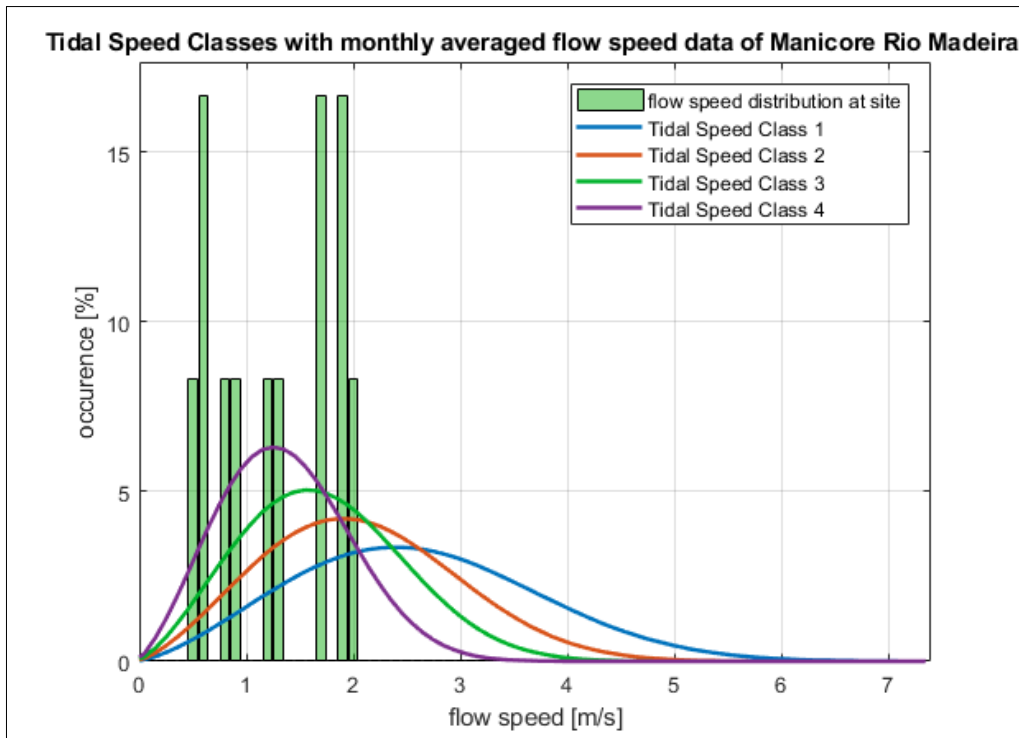
Comparison of river flow speed distribution at site with Tidal Speed Classes using monthly averaged data (Appendix I)

8) Manaus, Rio Negro, AM, Brasil



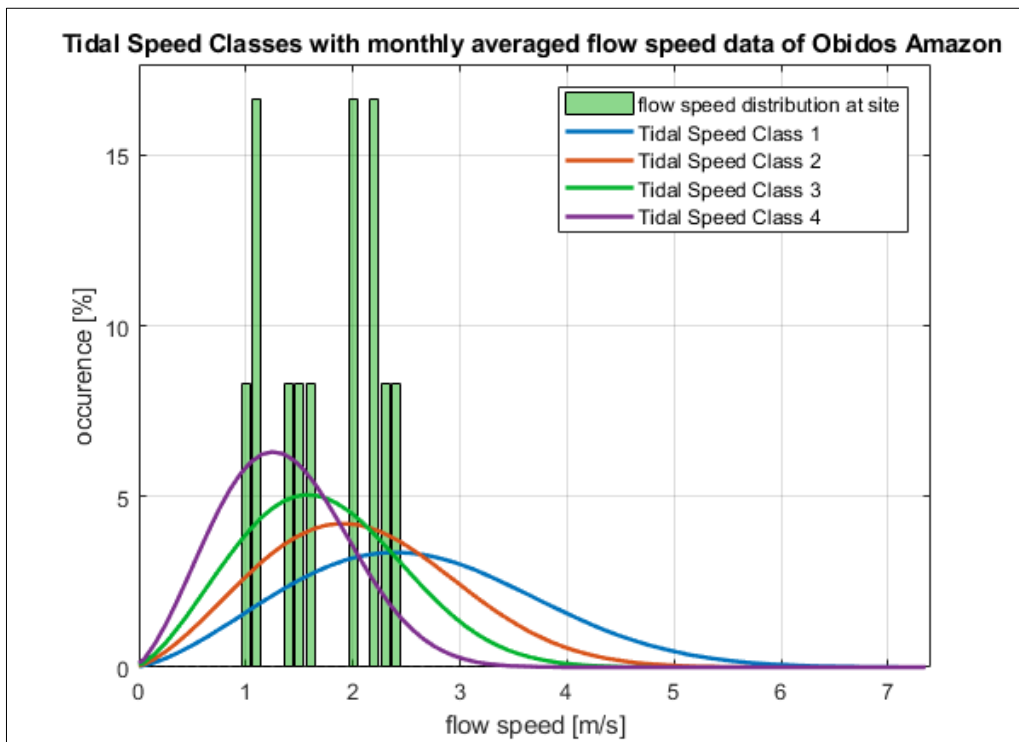
Comparison of river flow speed distribution at site with Tidal Speed Classes using monthly averaged data (Appendix I)

9) Manicoré, Rio Madeira, AM, Brazil



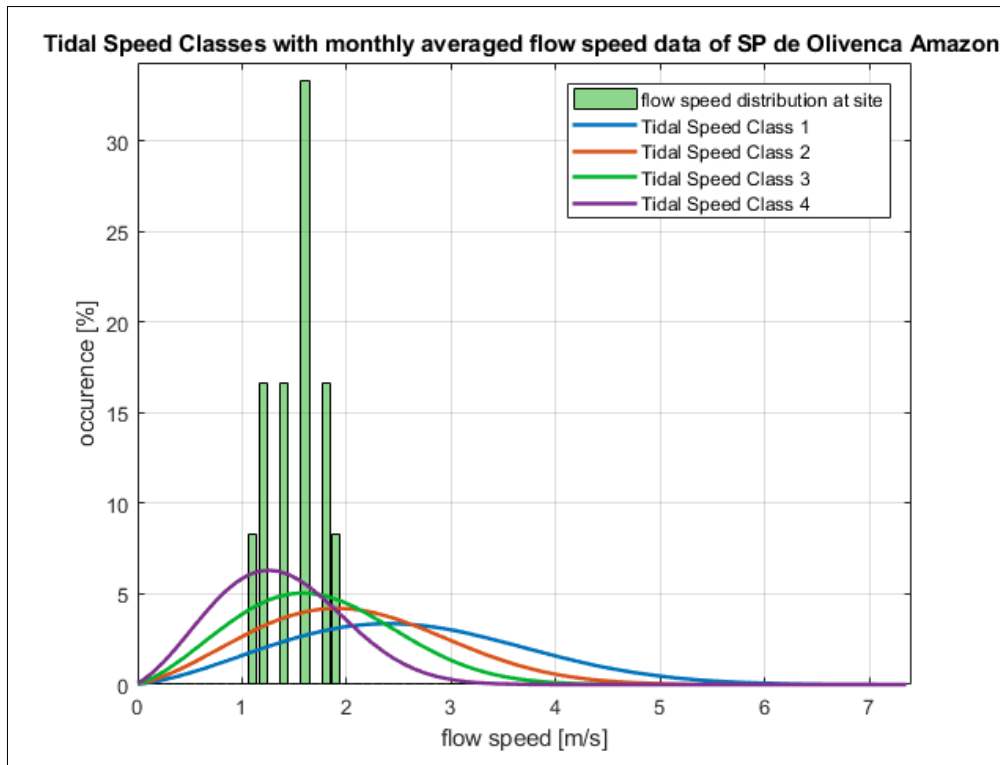
Comparison of river flow speed distribution at site with Tidal Speed Classes using monthly averaged data (Appendix I)

10) Óbidos, Rio Amazonas, PA, Brasil



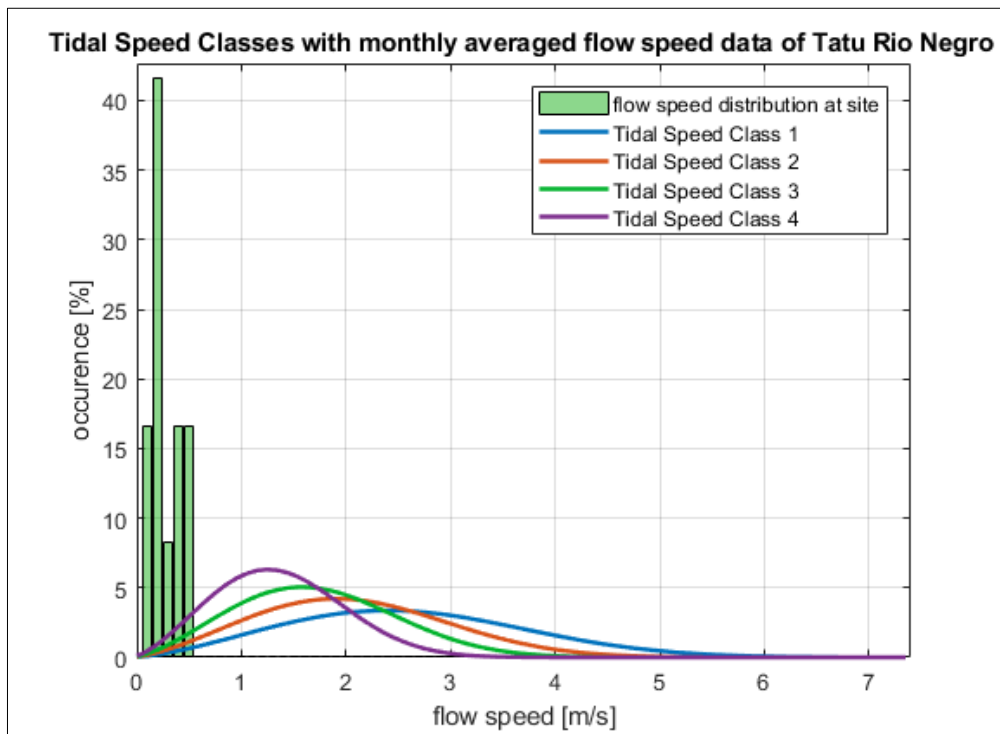
Comparison of river flow speed distribution at site with Tidal Speed Classes using monthly averaged data (Appendix I)

11) São Paulo de Olivença, Rio Amazonas, AM, Brasil



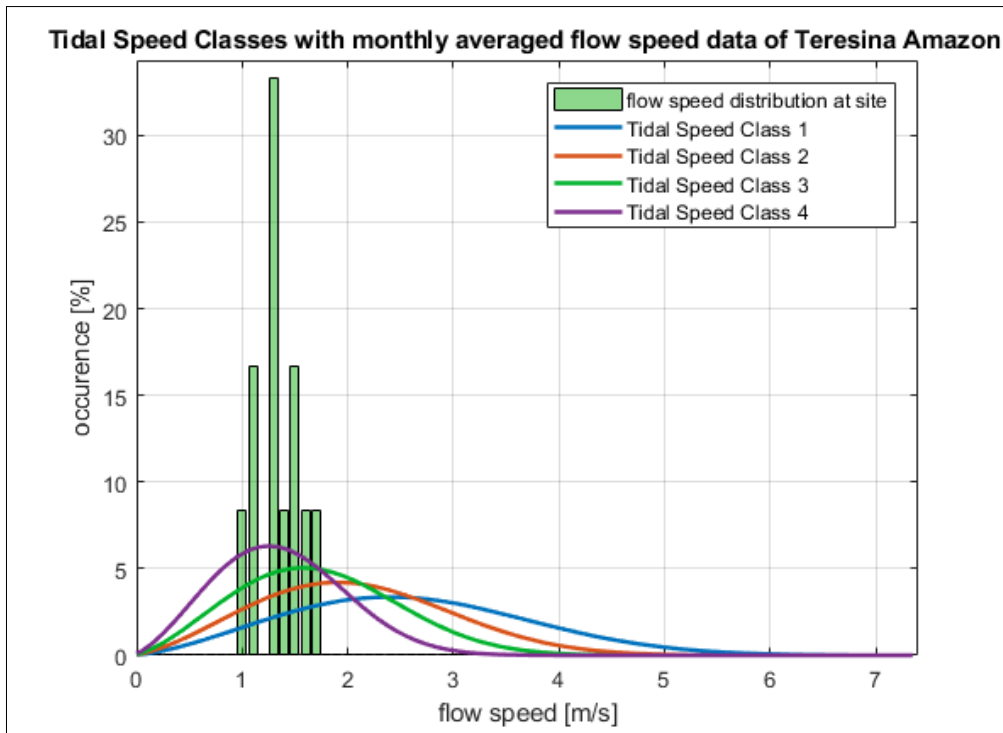
Comparison of river flow speed distribution at site with Tidal Speed Classes using monthly averaged data (Appendix I)

12) Tatu, Rio Negro, AM, Brasil



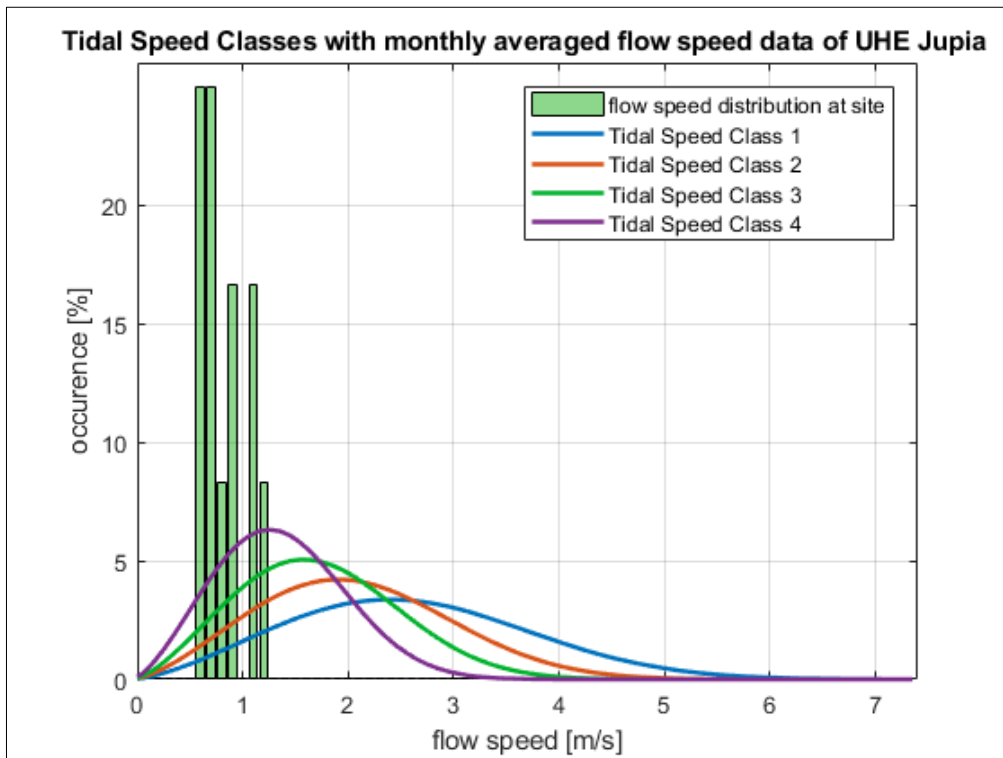
Comparison of river flow speed distribution at site with Tidal Speed Classes using monthly averaged data (Appendix I)

13) Teresina, Rio Amazonas, AM, Brasil



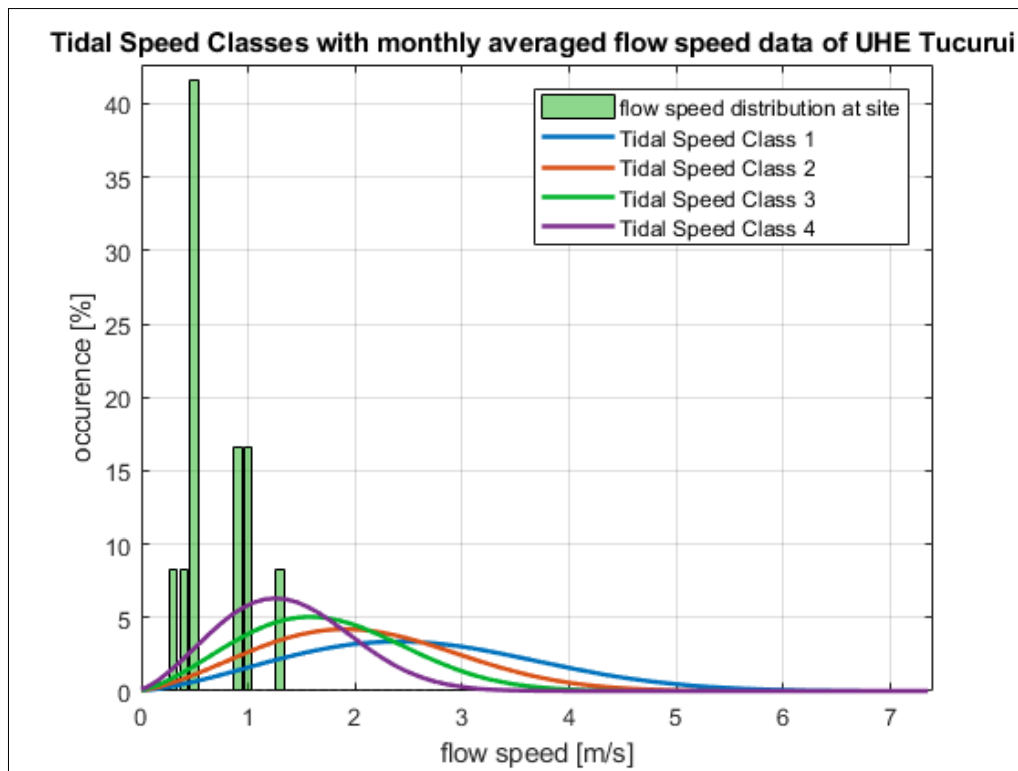
Comparison of river flow speed distribution at site with Tidal Speed Classes using monthly averaged data (Appendix I)

14) Downstream UHE Jupiá, Rio Paraná, MS, Brasil



Comparison of river flow speed distribution at site with Tidal Speed Classes using monthly averaged data (Appendix I)

15) Downstream UHE Tucuruí, Rio Tocantins, PA, Brasil



Comparison of river flow speed distribution at site with Tidal Speed Classes using monthly averaged data (Appendix I)

Appendix V – Code: Main Calculations

```
%%%%%%%%%%%%%%%%%%%%%%%%%%%%%%%%%%%%%%%%%%%%%%%%%%%%%%%%%%%%%%%%%%%%%%%%%
%
%   Comparison of River Resources with established Tidal Speed Classes
%
%                               M. Rupp
%
%%%%%%%%%%%%%%%%%%%%%%%%%%%%%%%%%%%%%%%%%%%%%%%%%%%%%%%%%%%%%%%%%%%%%%%%%
```

%% Conversion from Reference Flow Duration Curves to Flow Speed Histograms

```
% This script aims to make river resources comparable to existing tidal
% speed classes by comparing their distribution and occurrence of the
% flow speed over time. Tidal flow speed distribution is modelled in
% analogy to wind speed distribution (at specific sites) using a Weibull
% distribution model. Rivers (river sites respectively), however, are
% characterized by their annual discharge fluctuation which is reflected
% in a so called "Flow Duration Curve" (discharge over percentage of time
% exceedance per year). The goal is to converse dimensionless FDCs into
% dimensional flow speed histograms and then illustrate them together
% with the existing Tidal Speed Classes.
```

```
% Approach:
```

- 1) define dimensionless RIVER DISCHARGE CLASSES (dimensionless FDCs)
- 2) make dimensionless FDCs dimensional by multiplying them with Q_{max} for each site
- 3) create CROSS-SECTIONAL AREA Duration Curves (dimensionless CDCs) and make them dimensional by multiplying them with A_{max} for each site
- 4) create (FLOW) SPEED Duration Curves (SDCs) and make them dimensional by multiplying them with v_{max} for each site
- 5) build speed flow histograms out of speed duration curves
- 6) create histogram plots of flow speed of river sites together with tidal speed classes

%% load input data

```
clear all
close all
clc
```

```
run input_data.m           % executing an input script which contains
```

```
load site_data.mat        % input data containing the 15 sites with  $Q_{max}$ 
                          %  $A_{max}$ , discharge_class,  $v_{max}$  ...
                          % see: "input_data_for_Comparison_River_Tidal..
                          % _Classes_01.m" (all input data defined)
```

```
names_sites=fieldnames(site_data); % "fieldnames(s)" returns a cell
                                     % array of strings containing the
                                     % names of the fields in structures
```

```

%% Define dimensionless RIVER DISCHARGE CLASSES (continuous curves)

% The study of various river discharge data sets revealed that different
% rivers (at different sites) show similar characteristics regarding
% their annual discharge fluctuation, so that they could be classified in
% so called "discharge classes". These dimensionless curves are
% illustrating Q/Q_max over percentage of time exceedance and thus are
% characterized by the ratio of Q_min to Q_max and the shape of the curve
% between the two points (0|1 and 1|Q_min/Q_max).

% Comparison of river discharge data led to the definition of 3 different
% discharge classes (1..3) in which the investigated sites could be
% categorized

variables.x=linspace(0,1,101); % x-axis for dimensionless FDCs
                                % represents "% exceedance"

Dimensionless_Discharge_Classes.discharge_class_1 = 0.1667.*variables ...
.x.^2-0.4333.*variables.x+1;

Dimensionless_Discharge_Classes.discharge_class_2=-0.8.*variables.x+1;

Dimensionless_Discharge_Classes.discharge_class_3=0.625.*variables ...
.x.^2-1.5.*variables.x+1;

%% make dimensionless DISCHARGE classes dimensional for sites (FDC)

% (multiply Q_max for dimensionless discharge class of site)

for a=1:length(names_sites)

    name_site=names_sites{a};

    if site_data.(name_site).discharge_class == 1

        site_data.(name_site).FDC = Dimensionless_Discharge_Classes. ...
discharge_class_1.*site_data.(name_site).Q_max;

        elseif site_data.(name_site).discharge_class == 2

            site_data.(name_site).FDC = Dimensionless_Discharge_ ...
Classes.discharge_class_2.*site_data.(name_site).Q_max;

        elseif site_data.(name_site).discharge_class == 3

            site_data.(name_site).FDC = Dimensionless_Discharge_ ...
Classes.discharge_class_3.*site_data.(name_site).Q_max;

        end

    end

    variables.a=a;
    clear a;

%% create CROSS-SECTIONAL AREA Duration Curves (CDCs)

% The assumption that discharge variation (over one year) is linear
% proportional to flow speed variation (over one year) is not correct.
% This is due to the variation of the cross sectional area, which is
% significantly smaller than the discharge fluctuation, but which is not
% 0. However this fact has to be considered regarding the creation of
% speed flow duration curves. Therefore the variation of the cross-

```

```

% sectional area of river sites has to be considered. Empirical study of
% river data showed that there could be established three different
% cross-sectional area classes (analogy to discharge classes).

% extend site_data for cross-sectional area variation (cross-section not
% constant, varies over year, weaker than discharge, but VARIES.)

variables.A_min_to_A_max.discharge_class_1=0.7;
variables.A_min_to_A_max.discharge_class_2=0.54;
variables.A_min_to_A_max.discharge_class_3=0.44;

% create dimensionless Cross-Sectional Area Classes

Dimensionless_Cross_Section_Classes.cross_section_class_1 = ...
- 0.0833*variables.x.^2-0.2167*variables.x+1;

Dimensionless_Cross_Section_Classes.cross_section_class_2 = ...
- 0.46.*variables.x+1;

Dimensionless_Cross_Section_Classes.cross_section_class_3 = ...
0.3167*variables.x.^2-0.8767*variables.x+1;

% multiply A_max with dimensionless cross-sectional area class of site

for b=1:length(names_sites)

    name_site=names_sites{b};

    if site_data.(name_site).discharge_class == 1

        site_data.(name_site).CDC=Dimensionless_Cross_Section_Classes. ...
cross_section_class_1.*site_data.(name_site).A_max;

    elseif site_data.(name_site).discharge_class == 2

        site_data.(name_site).CDC=Dimensionless_Cross_Section_Classes. ...
cross_section_class_2.*site_data.(name_site).A_max;

    elseif site_data.(name_site).discharge_class == 3

        site_data.(name_site).CDC=Dimensionless_Cross_Section_Classes. ...
cross_section_class_3.*site_data.(name_site).A_max;
    end

end

variables.b=b;
clear b;
%% create (Flow) SPEED Duration Curves (SDCs)

% after defining the discharge and cross-sectional area development of
% different river (site) classes the flow speed classes are a consequence
% out of the two previous definitions. It is  $v=Q/A$  and thus the
% dimensionless speed classes are defined as discharge class divided by
% cross-sectional area class.

% create dimensionless river speed classes

Dimensionless_Speed_Classes.speed_class_1=Dimensionless_Discharge_Classes.disc
harge_class_1./Dimensionless_Cross_Section_Classes.cross_section_class_1;

```

```

Dimensionless_Speed_Classes.speed_class_2=Dimensionless_Discharge_Classes.disc
harge_class_2./Dimensionless_Cross_Section_Classes.cross_section_class_2;

Dimensionless_Speed_Classes.speed_class_3=Dimensionless_Discharge_Classes.disc
harge_class_3./Dimensionless_Cross_Section_Classes.cross_section_class_3;

% multiply v_max with dimensionless flow speed class of site

for c=1:length(names_sites)

    name_site=names_sites(c);

    if site_data.(name_site).discharge_class == 1

        site_data.(name_site).SDC = Dimensionless_Speed_Classes. ...
speed_class_1.*site_data.(name_site).v_max;

        elseif site_data.(name_site).discharge_class == 2

            site_data.(name_site).SDC = Dimensionless_Speed_Classes. ...
speed_class_2.*site_data.(name_site).v_max;

            elseif site_data.(name_site).discharge_class == 3

                site_data.(name_site).SDC = Dimensionless_Speed_Classes. ...
speed_class_3.*site_data.(name_site).v_max;
            end
        end

% plot dimensional Speed Duration Curve (SDC curve) for each site

    figure(30+c)
    hold all
    grid on
    box on

    plot(variables.x*100, site_data.(name_site).SDC, 'LineWidth', 1.7)

    xlabel('% exceedance')
    ylabel('v [m/s]')
    strspl=strsplit(name_site, '_'); % split string

    if length(strspl)==2
        title(['SDC for ', strspl{1}, ' ', strspl{2}, ' '])
    elseif length(strspl)==3
        title(['SDC for ', strspl{1}, ' ', strspl{2}, ' ', strspl{3}, ' '])
    elseif length(strspl)==4
        title(['SDC for ', strspl{1}, ' ', strspl{2}, ' ', strspl{3}, ' ', ...
            strspl{4}, ' '])
    end

    title(['SDCs for ', (name_site)])
    ylim([0 site_data.(name_site).v_max])
    xlim([0 100])

end

variables.c=c;
clear c;

```

```

%% build speed flow histograms out of speed duration curves

variables.edges_bins=[0:0.1:4];    % define edges (increment) of
                                   % histogram bars (0.1,0.2,0.4)

% include histogram data (rsc = river speed classes), using 'histcounts'
% in site_data (making the SDC in histogram format)

for d=1:length(names_sites)

    name_site=names_sites{d};

    [site_data.(name_site).hist_data_rsc.counts, ...
     site_data.(name_site).hist_data_rsc.edges] = ...
     histcounts(site_data.(name_site).SDC, variables.edges_bins);

% create histogram plot (hist_data_rsc over flow speed) for each site

    figure(d+45)
    hold all
    grid on
    box on

    xlabel('flow speed [m/s]')
    ylabel('occurrence [%]')
    strspl=strsplit(name_site, '_');    % split string

    if length(strspl)==2
        title(['Flow Speed Histogram for ', strspl{1}, ' ', strspl{2}, ' '])

    elseif length(strspl)==3
        title(['Flow Speed Histogram for ', strspl{1}, ' ', strspl{2}, ' ',
              strspl{3}, ' '])

    elseif length(strspl)==4
        title(['Flow Speed Histogram for ', strspl{1}, ' ', strspl{2}, ' ',
              strspl{3}, ' ', strspl{4}, ' '])
    end

    ylim([0 max(site_data.(name_site).hist_data_rsc.counts)+1])
    set(gca, 'YTick', [0:5:max(site_data.(name_site). ...
        hist_data_rsc.counts)]);
    xlim([0 4])

    histogram(site_data.(name_site).SDC, ...
              site_data.(name_site).hist_data_rsc.edges, 'FaceColor', ...
              '[0 0.65 0]', 'FaceAlpha', 0.45);

% add v_mean in site_data

    site_data.(name_site).v_mean=sum(site_data.(name_site).SDC)./100;

end

variables.d=d;
clear d;

%% input tidal speed classes

load tidal_sc.mat    % tidal_sc is containing the speed class data
                    % of the by Schottel defined tidal speed
                    % classes. These Weibull distribution curves
                    % are at hand with different speed increments
                    % (0.4, 0.2, 0.1). Most accurate is 0.1, which

```

```

                                % will be further used.

%% create histogram plots of flow speed of river sites together with tidal
speed classes

for e=1:length(names_sites)

    name_site=names_sites(e);

    figure(200+e)
    hold all
    grid on
    box on

    xlabel('flow speed [m/s]')
    ylabel('occurrence [%]')

    strspl=strsplit(name_site, '_');    % split string

    if length(strspl)==2
        title(['Tidal Speed Classes with flow speed distribution at ', ...
            strspl{1}, ' ', strspl{2}, ' '])

        elseif length(strspl)==3
            title(['Tidal Speed Classes with flow speed distribution at ', ...
                strspl{1}, ' ', strspl{2}, ' ', strspl{3}, ' '])

            elseif length(strspl)==4
                title(['Tidal Speed Classes with flow speed distribution at ', ...
                    strspl{1}, ' ', strspl{2}, ' ', strspl{3}, ' ', strspl{4}, ' '])
    end

    ylim([0 max(site_data.(name_site).hist_data_rsc.counts)+1])

    set(gca, 'YTick', [0:5:max(site_data.(name_site). ...
        hist_data_rsc.counts)]);
    xlim([0 max(tidal_sc.speed_class_1.increment_04.edges+0.4)])

    % to change stepsize (increment) of histograms adjust here for
    % increment. Choose incement 01, 02, or 04.

    plot(tidal_sc.speed_class_1.increment_01.edges, ...
        tidal_sc.speed_class_1.increment_01.counts, 'LineWidth', 1.8);

    plot(tidal_sc.speed_class_2.increment_01.edges, ...
        tidal_sc.speed_class_2.increment_01.counts, 'LineWidth', 1.8);

    plot(tidal_sc.speed_class_3.increment_01.edges, ...
        tidal_sc.speed_class_3.increment_01.counts, 'LineWidth', 1.8, ...
        'Color', [0 0.7 0.1725]);

    plot(tidal_sc.speed_class_4.increment_01.edges, ...
        tidal_sc.speed_class_4.increment_01.counts, 'LineWidth', 1.8);

    histogram(site_data.(name_site).SDC, site_data.(name_site). ...
        hist_data_rsc.edges, 'FaceColor', '[0 0.65 0]', ...
        'FaceAlpha', 0.45);

    legend('Tidal Speed Class 1', 'Tidal Speed Class 2', 'Tidal Speed ...
        Class 3', 'Tidal Speed Class 4', 'Flow Speed Distribution ...
        at River Site');

end

```

```

variables.e=e;
clear e;

%% dimensionless FDC, CDC, SDC plots

% display graph with dimensionless Reference Speed Classes (SDCs)

figure(102)
hold all
grid on
box on

plot(variables.x*100, Dimensionless_Speed_Classes.speed_class_1, ...
      'LineWidth', 2)

plot(variables.x*100, Dimensionless_Speed_Classes.speed_class_2, ...
      'LineWidth', 2)

plot(variables.x*100, Dimensionless_Speed_Classes.speed_class_3, ...
      'LineWidth', 2)

xlabel('% exceedance')
ylabel('v / v_{max}')

title('Reference Flow Speed Duration Curves')

ylim([0 1])
xlim([0 100])
legend('Speed Class 1', 'Speed Class 2', 'Speed Class 3');

% display graph with dimensionless Reference Cross-Sectional Area Classes

figure(101)
hold all
grid on
box on

plot(variables.x*100, Dimensionless_Cross_Section_Classes. ...
      cross_section_class_1, 'LineWidth', 2)

plot(variables.x*100, Dimensionless_Cross_Section_Classes. ...
      cross_section_class_2, 'LineWidth', 2)

plot(variables.x*100, Dimensionless_Cross_Section_Classes. ...
      cross_section_class_3, 'LineWidth', 2)

xlabel('% exceedance')
ylabel('A / A_{max}')

title('Reference Cross-sectional Area Duration Curves')

ylim([0 1])
xlim([0 100])
legend('Cross-sectional Class 1', 'Cross-sectional Class 2', 'Cross- ...
      sectional Class 3');

% display graph with dimensionless discharge classes

figure(100)
hold all
grid on
box on

```

```

plot(variables.x*100, Dimensionless_Discharge_Classes.discharge_class_1,
      'LineWidth', 2)

plot(variables.x*100, Dimensionless_Discharge_Classes.discharge_class_2,
      'LineWidth', 2)

plot(variables.x*100, Dimensionless_Discharge_Classes.discharge_class_3,
      'LineWidth', 2)

xlabel('% exceedance')
ylabel('Q / Q_{max}')

title('Reference Flow Duration Curves')

ylim([0 1])
xlim([0 100])
legend('Discharge Class 1', 'Discharge Class 2', 'Discharge Class 3');

%% create new histograms out of real (Excel-Sheet) flow speed data

run input_data_02.m           % extend site_data with real monthly
                             % averaged flow speed data from each sites

for f=1:length(names_sites)

name_site=names_sites{f};
[site_data.(name_site).hist_data_rsc_02.counts, site_data.(name_site) ...
 hist_data_rsc_02.edges]=histcounts(site_data.(name_site).v_monthly, ...
 variables.edges_bins);

end

variables.f=f;
clear f;

%% create histogram plots of original flow speeds of sites together with
tidal speed classes

for g=1:length(names_sites)

name_site=names_sites{g};

site_data.(name_site).hist_data_rsc_02.new_edges=[0:0.1:3.9];

figure(215+g)
hold all
grid on
box on

xlabel('flow speed [m/s]')
ylabel('occurrence [%]')

strspl=strsplit(name_site, '_');           % split string

if length(strspl)==2
title(['Tidal Speed Classes with monthly averaged flow speed ...
data of ', strspl{1}, ' ', strspl{2}, ' '])

elseif length(strspl)==3
title(['Tidal Speed Classes with monthly averaged flow speed ...
data of ', strspl{1}, ' ', strspl{2}, ' ', strspl{3}, ' '])

elseif length(strspl)==4

```

```

        title(['Tidal Speed Classes with monthly averaged flow speed ...
        data of ',strspl{1},' ',strspl{2},' ',strspl{3},' ',strspl{4}, ...
        ' '])
    end

    ylim([0 max(site_data.(name_site).hist_data_rsc_02. ...
        counts.*8.3333)+1])

    set(gca,'YTick',[0:5:max(site_data.(name_site). ...
        hist_data_rsc_02.counts.*8.3333)]);

    xlim([0 max(tidal_sc.speed_class_1.increment_04.edges+0.4)])

    bar(site_data.(name_site).hist_data_rsc_02.new_edges, ...
        site_data.(name_site).hist_data_rsc_02.counts.*8.3333, ...
        'FaceColor',[0 0.65 0], 'FaceAlpha',0.45)

    plot(tidal_sc.speed_class_1.increment_01.edges,
        tidal_sc.speed_class_1.increment_01.counts,'LineWidth', 1.8);

    plot(tidal_sc.speed_class_2.increment_01.edges,
        tidal_sc.speed_class_2.increment_01.counts,'LineWidth', 1.8);
    plot(tidal_sc.speed_class_3.increment_01.edges,
        tidal_sc.speed_class_3.increment_01.counts,'LineWidth', 1.8, ...
        'Color',[0 0.7 0.1725]);

    plot(tidal_sc.speed_class_4.increment_01.edges,
        tidal_sc.speed_class_4.increment_01.counts,'LineWidth', 1.8);

    legend('flow speed distribution at site','Tidal Speed Class 1', ...
        'Tidal Speed Class 2', 'Tidal Speed Class 3', 'Tidal Speed ...
        Class 4');
end

variables.g=g;
clear g;

%% Putting Power and Thrust Curve over histogram to calculate Annual
Energy Production (AEP)

run turbine_data.m

% This script includes turbine data such as cp, ct, power and thrust
% curves of 4 different rotor diameters (4m, 6.30m, 8m, & 10m)

%% Power Curve with Speed Classes and flow speed histogram of site
for h=1:length(names_sites)
    name_site=names_sites(h);

    figure(300+h)

    hold all
    grid on
    box on

    xlabel('flow speed [m/s]')
    ylabel('occurrence [%]')

    strspl=strsplit(name_site,'_'); % split string

    if length(strspl)==2
        title(['Power Curve and Flow Speed Distribution of ', ...

```

```

    strspl{1},' ',strspl{2},' ')

elseif length(strspl)==3
title(['Power Curve and Flow Speed Distribution of ', ...
strspl{1},' ',strspl{2},' ',strspl{3},' '])

elseif length(strspl)==4
title(['Power Curve and Flow Speed Distribution of ', ...
strspl{1},' ',strspl{2},' ',strspl{3},' ',strspl{4},' '])
end

ylim([0 max(site_data.(name_site).hist_data_rsc.counts)+1])

set(gca,'YTick',[0:5:max(site_data.(name_site). ...
hist_data_rsc.counts)]);

xlim([0 4.5])

% Mechanical Power Curve

addaxis(tidal_sc.speed_class_1.increment_01.edges, ...
Turbines.D_6_30.Power_Curve.y_axis_01,[0 90],'linewidth',2.5, ...
'Color','[0.28 0.28 0.28]');

addaxislabel(2,'Power [kW]')

% Electrical Power Curve

addaxisplot(tidal_sc.speed_class_1.increment_01.edges, ...
Turbines.D_6_30.Power_Curve.y_axis_04,2,'linewidth',2.5, 'Color', ...
'[1.00 0.65 0.00]');

histogram(site_data.(name_site).SDC, site_data.(name_site). ...
hist_data_rsc.edges,'FaceColor','[0 0.65 0]', 'FaceAlpha', 0.45);

legend('Power (mech.): 6.3 m', 'Power (el.): 6.3 m', 'Flow Speed ...
Distribution', 'Location', 'northwest');

end

variables.h=h;
clear h;

%% Annual Energy Production (AEP) of site and Capacity Factor (CF)

% Annual Energy Production (AEP) describes the quantity of Energy being
% extracted at a specific site over one year in [MWh/year]. It can be
% calculated as the product of the sum of all sections of "Power(v) *
% time of occurrence per year of that velocity bin".

% The Capacity Factor (CF) describes the ratio between the AEP and the
% "Energy extracted at full equivalent hours at rated machine power".
% "CF = AEP/FEH at rated machine power"

% Calculating AEP for sites

for i=1:length(names_sites)

name_site=names_sites{i};

site_data.(name_site).AEP.D_4.per_bin = site_data.(name_site). ...
hist_data_rsc.counts.*87.6.*Turbines.D_4.Power_Curve. ...
y_axis_02(1:40);

```

```

site_data.(name_site).AEP.D_4.total =
sum(site_data.(name_site).AEP.D_4.per_bin);

site_data.(name_site).AEP.D_4.el.per_bin =
site_data.(name_site).hist_data_rsc.counts.*87.6.*Turbines. ...
D_4.Power_Curve.y_axis_03(1:40);

site_data.(name_site).AEP.D_4.el.total =
sum(site_data.(name_site).AEP.D_4.el.per_bin);

site_data.(name_site).AEP.D_6_30.per_bin =
site_data.(name_site).hist_data_rsc.counts.*87.6.*Turbines. ...
D_6_30.Power_Curve.y_axis_02(1:40);
site_data.(name_site).AEP.D_6_30.total = ...
sum(site_data.(name_site).AEP.D_6_30.per_bin);

site_data.(name_site).AEP.D_6_30.el.per_bin = site_data. ...
(name_site).hist_data_rsc.counts.*87.6.*Turbines.D_6_30. ...
Power_Curve.y_axis_03(1:40);

site_data.(name_site).AEP.D_6_30.el.total = ...
sum(site_data.(name_site).AEP.D_6_30.el.per_bin);

site_data.(name_site).AEP.D_8.per_bin = ...
site_data.(name_site).hist_data_rsc.counts.*87.6.*Turbines.D_8. ...
Power_Curve.y_axis_02(1:40);

site_data.(name_site).AEP.D_8.total = ...
sum(site_data.(name_site).AEP.D_8.per_bin);

site_data.(name_site).AEP.D_8.el.per_bin = ...
site_data.(name_site).hist_data_rsc.counts.*87.6.*Turbines.D_8. ...
Power_Curve.y_axis_03(1:40);

site_data.(name_site).AEP.D_8.el.total = ...
sum(site_data.(name_site).AEP.D_8.el.per_bin);

site_data.(name_site).AEP.D_10.per_bin =
site_data.(name_site).hist_data_rsc.counts.*87.6.*Turbines.D_10. ...
Power_Curve.y_axis_02(1:40);

site_data.(name_site).AEP.D_10.total = ...
sum(site_data.(name_site).AEP.D_10.per_bin);

site_data.(name_site).AEP.D_10.el.per_bin = ...
site_data.(name_site).hist_data_rsc.counts.*87.6.*Turbines.D_10. ...
Power_Curve.y_axis_03(1:40);

site_data.(name_site).AEP.D_10.el.total = ...
sum(site_data.(name_site).AEP.D_10.el.per_bin);
end

variables.i=i;
clear i;

%% make plot of AEPs of all sites and compare them to each other

% Calculating Capacity Factor (CF) for sites

for j=1:length(names_sites)

name_site=names_sites{j};

site_data.(name_site).CF.D_4 = site_data.(name_site).AEP.D_4. ...
total./(8760.*75);

```

```

    site_data.(name_site).CF.D_6_30 = site_data.(name_site). ...
    AEP.D_6_30. total./(8760.*85);

    site_data.(name_site).CF.D_8 = site_data.(name_site).AEP.D_8. ...
    total./(8760.*85);

    site_data.(name_site).CF.D_10 = site_data.(name_site).AEP. ...
    D_10.total./(8760.*85);
end

variables.j=j;
clear j;

%% CFD Post-Processing

% Various CFD Simulations have been carried out varying the distance
% between platforms placed serial in line. It has been analyzed how the
% distance between the platforms related to the performance of the second
% platform and what is the distance for the second platform operates at
% 0.9 x the performance of the 1st platform.

run post_CFD.m

%% Build all three Speed Duration Curves for each site to show what kind
of difference it makes if a site is Class 1,2 or 3 for the annual
energy production (AEP)

for k = 1:length(names_sites)

    name_site=names_sites{k};

    site_data.(name_site).SDC_varying.Class_1 = ...
    Dimensionless_Speed_Classes.speed_class_1.*site_data. ...
    (name_site).v_max;

    site_data.(name_site).SDC_varying.Class_2 = ...
    Dimensionless_Speed_Classes.speed_class_2.*site_data. ...
    (name_site).v_max;

    site_data.(name_site).SDC_varying.Class_3 = ...
    Dimensionless_Speed_Classes.speed_class_3.*site_data. ...
    (name_site).v_max;
end

variables.k=k;
clear k;

%% Build histograms out of data for Itacoatiara and Óbidos

% Itacoatiara

figure(450)
hold all
grid on
box on

xlabel('flow speed [m/s]')
ylabel('occurrence [%]')

strspl=strsplit('Itacoatiara_Amazon','_'); % split string

```

```

if length(strspl)==2
    title(['Flow Speed Histogram for ', strspl{1}, ' ',strspl{2}, ' '])

    elseif length(strspl)==3
        title(['Flow Speed Histogram for ', strspl{1}, ' ',strspl{2}, ...
            ' ',strspl{3}, ' '])

        elseif length(strspl)==4
            title(['Flow Speed Histogram for ',strspl{1}, ' ',strspl{2}, ...
                ' ',strspl{3}, ' ',strspl{4}, ' '])
        end

ylim([0 max(site_data.Itacoatiara_Amazon.hist_data_rsc.counts)+1])

set(gca, 'YTick', [0:5:max(site_data.Itacoatiara_Amazon. ...
    hist_data_rsc.counts)]);

xlim([0 3])

histogram(site_data.Itacoatiara_Amazon.SDC_varying.Class_1, ...
site_data.Itacoatiara_Amazon.hist_data_rsc.edges, 'FaceColor', ...
'[0 0.65 0]', 'FaceAlpha', 0.45);

histogram(site_data.Itacoatiara_Amazon.SDC_varying.Class_2, ...
site_data.Itacoatiara_Amazon.hist_data_rsc.edges, 'FaceColor', ...
'[0 0 0.65]', 'FaceAlpha', 0.45);

histogram(site_data.Itacoatiara_Amazon.SDC_varying.Class_3, ...
site_data.Itacoatiara_Amazon.hist_data_rsc.edges, 'FaceColor', ...
'[0.65 0 0]', 'FaceAlpha', 0.45);

legend('River Speed Class 1', 'River Speed Class 2', 'River Speed ...
    Class 3', 'Location', 'northwest');

% Obidos

figure(450+1)
hold all
grid on
box on

xlabel('flow speed [m/s]')
ylabel('occurrence [%]')

strspl=strsplit('Obidos_Amazon','_'); % split string

if length(strspl)==2
    title(['Flow Speed Histogram for ', strspl{1}, ' ',strspl{2}, ' '])

    elseif length(strspl)==3
        title(['Flow Speed Histogram for ', strspl{1}, ' ',strspl{2}, ...
            ' ',strspl{3}, ' '])

        elseif length(strspl)==4
            title(['Flow Speed Histogram for ',strspl{1}, ' ',strspl{2}, ...
                ' ',strspl{3}, ' ',strspl{4}, ' '])
        end

ylim([0 max(site_data.Obidos_Amazon.hist_data_rsc.counts)+1])
xlim([0 3])

set(gca, 'YTick', [0:5:max(site_data.Obidos_Amazon.hist_data_rsc. ...
    counts)]);
histogram(site_data.Obidos_Amazon.SDC_varying.Class_1,site_data. ...
Obidos_Amazon.hist_data_rsc.edges, 'FaceColor', '[0 0.65 0]', ...
'FaceAlpha', 0.45);

```

```

    histogram(site_data.Obidos_Amazon.SDC_varying.Class_2, site_data. ...
    Obidos_Amazon.hist_data_rsc.edges, 'FaceColor', '[0 0 0.65]', ...
    'FaceAlpha', 0.45);

    histogram(site_data.Obidos_Amazon.SDC_varying.Class_3, site_data. ...
    Obidos_Amazon.hist_data_rsc.edges, 'FaceColor', '[0.65 0 0]', ...
    'FaceAlpha', 0.45);

    legend('River Speed Class 1', 'River Speed Class 2', 'River Speed ...
    Class 3', 'Location', 'northwest');

%% Build histogram values as plots

for l=1:length(names_sites)

    name_site=names_sites{l};

    site_data.(name_site).SDC_varying.Counts_Class_1 = ...
    histcounts(site_data.(name_site).SDC_varying.Class_1, ...
    site_data.(name_site).hist_data_rsc.edges);

    site_data.(name_site).SDC_varying.Counts_Class_2 = ...
    histcounts(site_data.(name_site).SDC_varying.Class_2, ...
    site_data.(name_site).hist_data_rsc.edges);

    site_data.(name_site).SDC_varying.Counts_Class_3 = ...
    histcounts(site_data.(name_site).SDC_varying.Class_3, ...
    site_data.(name_site).hist_data_rsc.edges);
end

variables.l=l;
clear l;

% create cubic splines between data points

variables.xx = linspace(0,4,401);

for m=1:length(names_sites)

    name_site=names_sites{m};

    site_data.(name_site).splines.cs_1 = ...
    spline(site_data.(name_site).hist_data_rsc_02.new_edges, ...
    [0 site_data.(name_site).SDC_varying.Counts_Class_1 0]);

    site_data.(name_site).splines.cs_2 = ...
    spline(site_data.(name_site).hist_data_rsc_02.new_edges, ...
    [0 site_data.(name_site).SDC_varying.Counts_Class_2 0]);

    site_data.(name_site).splines.cs_3 = ...
    spline(site_data.(name_site).hist_data_rsc_02.new_edges, ...
    [0 site_data.(name_site).SDC_varying.Counts_Class_3 0]);
end

variables.m=m;
clear m;
%% Plot histograms as continuous lines for Itacoatiara and Obidos

% Itacoatiara

figure(450+2)

hold all
grid on
box on

```

```

xlabel('flow speed [m/s]')
ylabel('occurrence [%]')

strspl=strsplit('Itacoatiara_Amazon','_');    % split string

if length(strspl)==2
    title(['Flow Speed Distribution for ', strspl{1}, ' ',strspl{2},...
        ' '])

    elseif length(strspl)==3
    title(['Flow Speed Distribution for ', strspl{1}, ' ',strspl{2},...
        ' ',strspl{3}, ' '])

    elseif length(strspl)==4
    title(['Flow Speed Distribution for ',strspl{1}, ' ',strspl{2},...
        ' ',strspl{3}, ' ',strspl{4}, ' '])
end

xlim([0 2.5]), ylim([-2 25])

plot(variables.xx,ppval(site_data.Itacoatiara_Amazon. ...
splines.cs_1,variables.xx),'-','LineWidth', 2.5, 'Color', ...
'[0.00 0.72 0.00]');

plot(variables.xx,ppval(site_data.Itacoatiara_Amazon. ...
splines.cs_2,variables.xx),'-','LineWidth', 2.5, 'Color', ...
'[0.15 0.50 1.00]');

plot(variables.xx,ppval(site_data.Itacoatiara_Amazon. ...
splines.cs_3,variables.xx),'-','LineWidth', 2.5, 'Color', ...
'[1.00 0.40 0.16]');

legend('River Speed Class 1', 'River Speed Class 2', 'River Speed ...
Class 3', 'Location', 'northwest');

```

```
% Obidos
```

```

figure(450+3)

hold all
grid on
box on

xlabel('flow speed [m/s]')
ylabel('occurrence [%]')

strspl=strsplit('Obidos_Amazon','_');    % split string

if length(strspl)==2
    title(['Flow Speed Distribution for ', strspl{1}, ' ',strspl{2},...
        ' '])

    elseif length(strspl)==3
    title(['Flow Speed Distribution for ', strspl{1}, ' ',strspl{2},...
        ' ',strspl{3}, ' '])

    elseif length(strspl)==4
    title(['Flow Speed Distribution for ',strspl{1}, ' ',strspl{2},...
        ' ',strspl{3}, ' ',strspl{4}, ' '])
end

xlim([0 3])

plot(variables.xx,ppval(site_data.Obidos_Amazon. ...
splines.cs_1,variables.xx),'-','LineWidth', 2.5, 'Color', ...
'[0.00 0.72 0.00]');

```

```

plot(variables.xx,ppval(site_data.Obidos_Amazon. ...
splines.cs_2,variables.xx),'-','LineWidth', 2.5, 'Color', ...
'[0.15 0.50 1.00]');

plot(variables.xx,ppval(site_data.Obidos_Amazon. ...
splines.cs_3,variables.xx),'-','LineWidth', 2.5, 'Color', ...
'[1.00 0.40 0.16]');

legend('River Speed Class 1', 'River Speed Class 2', 'River Speed ...
Class 3', 'Location', 'northwest');

%% Plot all Power Curves

figure (500)

hold all
grid on
box on

xlabel('flow speed [m/s]')
ylabel('Power [kW]')

plot(Turbines.D_4.Power_Curve.x_axis,Turbines.D_4. ...
Power_Curve.y_axis_02,'-','LineWidth', 1.7,'Color', ...
'[0.28 0.28 0.28]');

plot(Turbines.D_6_30.Power_Curve.x_axis,Turbines.D_6_30. ...
Power_Curve.y_axis_02,'-','LineWidth', 1.7, 'Color', ...
'[0.1 0.87 0.21]');

plot(Turbines.D_8.Power_Curve.x_axis,Turbines.D_8. ...
Power_Curve.y_axis_02,'-','LineWidth', 1.7, 'Color', ...
'[1 0.45 0.21]');

plot(Turbines.D_10.Power_Curve.x_axis,Turbines.D_10. ...
Power_Curve.y_axis_02,'-','LineWidth', 1.7, 'Color', ...
'[0 0.66 0.99]');

legend('4m Rotor', '6.30m Rotor', '8m Rotor', '10m Rotor', ...
'Location', 'east');

%% Plot All Power Curves over the site's Histograms

for n=1:length(names_sites)

name_site=names_sites{n};
figure(500+n)
hold all
grid on
box on

xlabel('flow speed [m/s]')
ylabel('occurrence [%]')

strspl=strsplit(name_site,'_'); % split string

if length(strspl)==2
title(['Power Curves & Flow Speed Histogram of ', strspl{1}, ...
' ',strspl{2},' '])

elseif length(strspl)==3
title(['Power Curves & Flow Speed Histogram of ', strspl{1}, ...
' ',strspl{2},' ',strspl{3},' '])

elseif length(strspl)==4

```

```

        title(['Power Curves & Flow Speed Histogram of ', strspl{1}, ...
            ' ', strspl{2}, ' ', strspl{3}, ' ', strspl{4}, ' '])
    end

    xlim([0 4.1])
    ylim([0 max(site_data.(name_site).hist_data_rsc.counts)+1])

    set(gca, 'YTick', [0:5:max(site_data.(name_site). ...
        hist_data_rsc.counts)]);

    addaxis(Turbines.D_4.Power_Curve.x_axis, Turbines.D_4. ...
        Power_Curve.y_axis_02, [0 90], 'linewidth', 2.5, 'Color', ...
        '[0.28 0.28 0.28]');

    addaxisplot(Turbines.D_6_30.Power_Curve.x_axis, Turbines.D_6_30. ...
        Power_Curve.y_axis_02, 2, 'linewidth', 2.5, 'Color', ...
        '[0.95 0.45 0.33]');

    addaxisplot(Turbines.D_8.Power_Curve.x_axis, Turbines.D_8. ...
        Power_Curve.y_axis_02, 2, 'linewidth', 2.5, 'Color', ...
        '[0.89 0.25 0.36]');

    addaxisplot(Turbines.D_10.Power_Curve.x_axis, Turbines.D_10. ...
        Power_Curve.y_axis_02, 2, 'linewidth', 2.5, 'Color', '[0 0.66 0.99]');

    addaxislabel(2, 'Power [kW]')

    histogram(site_data.(name_site).SDC, site_data.(name_site). ...
        hist_data_rsc.edges, 'FaceColor', '[0 0.65 0]', 'FaceAlpha', 0.45);

    legend('4m Rotor', '6.30m Rotor', '8m Rotor', '10m Rotor', 'Flow ...
        Speed Distribution', 'Location', 'southeast');
end

variables.n=n;
clear n;

%% AEPs for all sites with all combinations of speed classes and rotor
diameters

% Calculating AEP for sites
for o=1:length(names_sites)
    name_site=names_sites{o};

    site_data.(name_site).AEP_02.D_4.Speed_Class_1.per_bin = ...
        site_data.(name_site).SDC_varying.Counts_Class_1.*87.6 ...
        .*Turbines.D_4.Power_Curve.y_axis_02(1:40);

    site_data.(name_site).AEP_02.D_4.Speed_Class_1.total = ...
        sum(site_data.(name_site).AEP_02.D_4.Speed_Class_1.per_bin);

    site_data.(name_site).AEP_02.D_4.Speed_Class_2.per_bin = ...
        site_data.(name_site).SDC_varying.Counts_Class_2.*87.6 ...
        .*Turbines.D_4.Power_Curve.y_axis_02(1:40);

    site_data.(name_site).AEP_02.D_4.Speed_Class_2.total = ...
        sum(site_data.(name_site).AEP_02.D_4.Speed_Class_2.per_bin);

    site_data.(name_site).AEP_02.D_4.Speed_Class_3.per_bin = ...
        site_data.(name_site).SDC_varying.Counts_Class_3.*87.6 ...
        .*Turbines.D_4.Power_Curve.y_axis_02(1:40);

    site_data.(name_site).AEP_02.D_4.Speed_Class_3.total = ...
        sum(site_data.(name_site).AEP_02.D_4.Speed_Class_3.per_bin);

    site_data.(name_site).AEP_02.D_6_30.Speed_Class_1.per_bin = ...

```

```

site_data.(name_site).SDC_varying.Counts_Class_1.*87.6 ...
.*Turbines.D_6_30.Power_Curve.y_axis_02(1:40);

site_data.(name_site).AEP_02.D_6_30.Speed_Class_1.total = ...
sum(site_data.(name_site).AEP_02.D_6_30.Speed_Class_1.per_bin);

site_data.(name_site).AEP_02.D_6_30.Speed_Class_2.per_bin = ...
site_data.(name_site).SDC_varying.Counts_Class_2.*87.6 ...
.*Turbines.D_6_30.Power_Curve.y_axis_02(1:40);

site_data.(name_site).AEP_02.D_6_30.Speed_Class_2.total = ...
sum(site_data.(name_site).AEP_02.D_6_30.Speed_Class_2.per_bin);

site_data.(name_site).AEP_02.D_6_30.Speed_Class_3.per_bin = ...
site_data.(name_site).SDC_varying.Counts_Class_3.*87.6 ...
.*Turbines.D_6_30.Power_Curve.y_axis_02(1:40);

site_data.(name_site).AEP_02.D_6_30.Speed_Class_3.total = ...
sum(site_data.(name_site).AEP_02.D_6_30.Speed_Class_3.per_bin);

site_data.(name_site).AEP_02.D_8.Speed_Class_1.per_bin = ...
site_data.(name_site).SDC_varying.Counts_Class_1.*87.6 ...
.*Turbines.D_8.Power_Curve.y_axis_02(1:40);

site_data.(name_site).AEP_02.D_8.Speed_Class_1.total = ...
sum(site_data.(name_site).AEP_02.D_8.Speed_Class_1.per_bin);

site_data.(name_site).AEP_02.D_8.Speed_Class_2.per_bin = ...
site_data.(name_site).SDC_varying.Counts_Class_2.*87.6 ...
.*Turbines.D_8.Power_Curve.y_axis_02(1:40);

site_data.(name_site).AEP_02.D_8.Speed_Class_2.total = ...
sum(site_data.(name_site).AEP_02.D_8.Speed_Class_2.per_bin);

site_data.(name_site).AEP_02.D_8.Speed_Class_3.per_bin = ...
site_data.(name_site).SDC_varying.Counts_Class_3.*87.6 ...
.*Turbines.D_8.Power_Curve.y_axis_02(1:40);

site_data.(name_site).AEP_02.D_8.Speed_Class_3.total = ...
sum(site_data.(name_site).AEP_02.D_8.Speed_Class_3.per_bin);

site_data.(name_site).AEP_02.D_10.Speed_Class_1.per_bin = ...
site_data.(name_site).SDC_varying.Counts_Class_1.*87.6 ...
.*Turbines.D_10.Power_Curve.y_axis_02(1:40);

site_data.(name_site).AEP_02.D_10.Speed_Class_1.total = ...
sum(site_data.(name_site).AEP_02.D_10.Speed_Class_1.per_bin);

site_data.(name_site).AEP_02.D_10.Speed_Class_2.per_bin = ...
site_data.(name_site).SDC_varying.Counts_Class_2.*87.6 ...
.*Turbines.D_10.Power_Curve.y_axis_02(1:40);

site_data.(name_site).AEP_02.D_10.Speed_Class_2.total = ...
sum(site_data.(name_site).AEP_02.D_10.Speed_Class_2.per_bin);

site_data.(name_site).AEP_02.D_10.Speed_Class_3.per_bin = ...
site_data.(name_site).SDC_varying.Counts_Class_3.*87.6 ...
.*Turbines.D_10.Power_Curve.y_axis_02(1:40);

site_data.(name_site).AEP_02.D_10.Speed_Class_3.total = ...
sum(site_data.(name_site).AEP_02.D_10.Speed_Class_3.per_bin);
end

variables.o=0;
clear o;

```

```

%% CFs for all sites with all combinations of speed classes and rotor
diameters

for p=1:length(names_sites)

    name_site=names_sites{p};

    site_data.(name_site).CF_02.D_4.Speed_Class_1 = ...
    site_data.(name_site).AEP_02.D_4.Speed_Class_1.total./(8760.*75);

    site_data.(name_site).CF_02.D_4.Speed_Class_2 = ...
    site_data.(name_site).AEP_02.D_4.Speed_Class_2.total./(8760.*75);

    site_data.(name_site).CF_02.D_4.Speed_Class_3 = ...
    site_data.(name_site).AEP_02.D_4.Speed_Class_3.total./(8760.*75);

    site_data.(name_site).CF_02.D_6_30.Speed_Class_1 = ...
    site_data.(name_site).AEP_02.D_6_30.Speed_Class_1.total./(8760.*85);

    site_data.(name_site).CF_02.D_6_30.Speed_Class_2 = ...
    site_data.(name_site).AEP_02.D_6_30.Speed_Class_2.total./(8760.*85);

    site_data.(name_site).CF_02.D_6_30.Speed_Class_3 = ...
    site_data.(name_site).AEP_02.D_6_30.Speed_Class_3.total./(8760.*85);

    site_data.(name_site).CF_02.D_8.Speed_Class_1 = ...
    site_data.(name_site).AEP_02.D_8.Speed_Class_1.total./(8760.*85);

    site_data.(name_site).CF_02.D_8.Speed_Class_2 = ...
    site_data.(name_site).AEP_02.D_8.Speed_Class_2.total./(8760.*85);

    site_data.(name_site).CF_02.D_8.Speed_Class_3 = ...
    site_data.(name_site).AEP_02.D_8.Speed_Class_3.total./(8760.*85);

    site_data.(name_site).CF_02.D_10.Speed_Class_1 = ...
    site_data.(name_site).AEP_02.D_10.Speed_Class_1.total./(8760.*85);

    site_data.(name_site).CF_02.D_10.Speed_Class_2 = ...
    site_data.(name_site).AEP_02.D_10.Speed_Class_2.total./(8760.*85);

    site_data.(name_site).CF_02.D_10.Speed_Class_3 = ...
    site_data.(name_site).AEP_02.D_10.Speed_Class_3.total./(8760.*85);
end

variables.p=p;
clear p;

%% Graphs for AEPs for Itacoatiara and Obidos with all combinations of
speed classes and rotor diameters

% Itacoatiara

figure(550)
hold all
grid on
box on

xlabel('rotor diameter [m]')
ylabel('AEP [kWh/year]')

strspl=strsplit('Itacoatiara_Amazon','_'); % split string

if length(strspl)==2
    title(['AEP over rotor diameter for ', strspl{1}, ' ', strspl{2}, ...
        ' '])
elseif length(strspl)==3

```

```

title(['AEP over rotor diameter for ', strspl{1}, ' ', strspl{2}, ...
' ', strspl{3}, ' '])

elseif length(strspl)==4
title(['AEP over rotor diameter for ', strspl{1}, ' ', strspl{2}, ...
' ', strspl{3}, ' ', strspl{4}, ' '])
end

xlim([3 11])
ylim([0 1.1.*max(site_data.Itacoatiara_Amazon.AEP_02.D_10. ...
Speed_Class_1.total)])

plot([4 6.30 8 10], ...
[site_data.Itacoatiara_Amazon.AEP_02.D_4.Speed_Class_1.total ...
site_data.Itacoatiara_Amazon.AEP_02.D_6_30.Speed_Class_1.total ...
site_data.Itacoatiara_Amazon.AEP_02.D_8.Speed_Class_1.total ...
site_data.Itacoatiara_Amazon.AEP_02.D_10.Speed_Class_1.total], ...
'o-', 'LineWidth', 2, 'Color', '[0.34 0.68 0.21]');

plot([4 6.30 8 10], ...
[site_data.Itacoatiara_Amazon.AEP_02.D_4.Speed_Class_2.total ...
site_data.Itacoatiara_Amazon.AEP_02.D_6_30.Speed_Class_2.total ...
site_data.Itacoatiara_Amazon.AEP_02.D_8.Speed_Class_2.total ...
site_data.Itacoatiara_Amazon.AEP_02.D_10.Speed_Class_2.total], ...
'>-', 'LineWidth', 2, 'Color', '[0 0.41 0.53]');

plot([4 6.30 8 10], ...
[site_data.Itacoatiara_Amazon.AEP_02.D_4.Speed_Class_3.total ...
site_data.Itacoatiara_Amazon.AEP_02.D_6_30.Speed_Class_3.total ...
site_data.Itacoatiara_Amazon.AEP_02.D_8.Speed_Class_3.total ...
site_data.Itacoatiara_Amazon.AEP_02.D_10.Speed_Class_3.total], ...
'+-', 'LineWidth', 2, 'Color', '[1 0.45 0.38]');

legend('River Speed Class 1', 'River Speed Class 2', 'River Speed ...
Class 3', 'Location', 'northwest');

```

```
% Obidos
```

```

figure(550+1)
hold all
grid on
box on

xlabel('rotor diameter [m]')
ylabel('AEP [MWh/turbine]')
strspl=strsplit('Obidos_Amazon','_'); % split string

if length(strspl)==2
title(['AEP over rotor diameter for ', strspl{1}, ' ', strspl{2}, ...
' '])

elseif length(strspl)==3
title(['AEP over rotor diameter for ', strspl{1}, ' ', strspl{2}, ...
' ', strspl{3}, ' '])

elseif length(strspl)==4
title(['AEP over rotor diameter for ', strspl{1}, ' ', strspl{2}, ...
' ', strspl{3}, ' ', strspl{4}, ' '])
end

ylim([0 9*10^2])
xlim([3 11])

plot([4 6.30 8 10], ...
[site_data.Obidos_Amazon.AEP_02.D_4.Speed_Class_1.total./1000 ...
site_data.Obidos_Amazon.AEP_02.D_6_30.Speed_Class_1.total./1000 ...
site_data.Obidos_Amazon.AEP_02.D_8.Speed_Class_1.total./1000 ...

```

```

site_data.Obidos_Amazon.AEP_02.D_10.Speed_Class_1.total./1000], ...
'o-', 'LineWidth', 2.2, 'Color', '[0.28 0.28 0.28]');

plot([4 6.30 8 10], ...
[site_data.Obidos_Amazon.AEP.D_4.el.total./1000 ...
site_data.Obidos_Amazon.AEP.D_6_30.el.total./1000 ...
site_data.Obidos_Amazon.AEP.D_8.el.total./1000 ...
site_data.Obidos_Amazon.AEP.D_10.el.total./1000], ...
'>-', 'LineWidth', 2.2, 'Color', '[1.00 0.65 0.00]');

plot([4 6.30 8 10], ...
[site_data.Obidos_Amazon.AEP.D_4.el.total.*0.9./1000 ...
site_data.Obidos_Amazon.AEP.D_6_30.el.total.*0.9./1000 ...
site_data.Obidos_Amazon.AEP.D_8.el.total.*0.9./1000 ...
site_data.Obidos_Amazon.AEP.D_10.el.total.*0.9./1000], ...
'+-', 'LineWidth', 1.5, 'Color', '[0.34 0.68 0.21]');

legend('AEP (mech.)','AEP (el.)','AEP (el.), 90 % ...
availability','Location', 'northwest');

%% Capacity Factor Graphs for Itacoatiara and Obidos with all combinations
of speed classes and rotor diameters

% Itacoatiara

figure(550+2)
hold all
grid on
box on

xlabel('rotor diameter [m]')
ylabel('Capacity Factor [-]')

strspl=strsplit('Itacoatiara_Amazon','_'); % split string

if length(strspl)==2
    title(['CF over rotor diameter for ', strspl{1}, ' ',strspl{2}, ...
' '])

elseif length(strspl)==3
    title(['CF over rotor diameter for ', strspl{1}, ' ',strspl{2}, ...
' ',strspl{3}, ' '])

elseif length(strspl)==4
    title(['CF over rotor diameter for ',strspl{1}, ' ',strspl{2}, ...
' ',strspl{3}, ' ',strspl{4}, ' '])
end

xlim([3 11])
ylim([0 1.1.*max(site_data.Itacoatiara_Amazon.CF_02.D_10 ...
.Speed_Class_1)])

plot([4 6.30 8 10], ...
[site_data.Itacoatiara_Amazon.CF_02.D_4.Speed_Class_1 ...
site_data.Itacoatiara_Amazon.CF_02.D_6_30.Speed_Class_1 ...
site_data.Itacoatiara_Amazon.CF_02.D_8.Speed_Class_1 ...
site_data.Itacoatiara_Amazon.CF_02.D_10.Speed_Class_1], ...
'o-', 'LineWidth', 2, 'Color', '[0.34 0.68 0.21]');

plot([4 6.30 8 10], ...
[site_data.Itacoatiara_Amazon.CF_02.D_4.Speed_Class_2 ...
site_data.Itacoatiara_Amazon.CF_02.D_6_30.Speed_Class_2 ...
site_data.Itacoatiara_Amazon.CF_02.D_8.Speed_Class_2 ...
site_data.Itacoatiara_Amazon.CF_02.D_10.Speed_Class_2], ...
'>-', 'LineWidth', 2, 'Color', '[0 0.41 0.53]');

plot([4 6.30 8 10], ...

```

```

[site_data.Itacoatiara_Amazon.CF_02.D_4.Speed_Class_3 ...
site_data.Itacoatiara_Amazon.CF_02.D_6_30.Speed_Class_3 ...
site_data.Itacoatiara_Amazon.CF_02.D_8.Speed_Class_3 ...
site_data.Itacoatiara_Amazon.CF_02.D_10.Speed_Class_3], ...
'+-', 'LineWidth', 2, 'Color', '[1 0.45 0.38]');

legend('River Speed Class 1', 'River Speed Class 2', 'River Speed ...
Class 3', 'Location', 'northwest');

% Obidos

figure(550+3)
hold all
grid on
box on

xlabel('rotor diameter [m]')
ylabel('Capacity Factor [-]')
strspl=strsplit('Obidos_Amazon','_'); % split string

if length(strspl)==2
    title(['CF over rotor diameter for ', strspl{1}, ' ', strspl{2}, ...
        ' '])

    elseif length(strspl)==3
        title(['CF over rotor diameter for ', strspl{1}, ' ', strspl{2}, ...
            ' ', strspl{3}, ' '])

    elseif length(strspl)==4
        title(['CF over rotor diameter for ', strspl{1}, ' ', strspl{2}, ...
            ' ', strspl{3}, ' ', strspl{4}, ' '])
end

xlim([3 11])
ylim([0 1.1.*max(site_data.Obidos_Amazon.CF_02.D_10.Speed_Class_1)])

plot([4 6.30 8 10], ...
[site_data.Obidos_Amazon.CF_02.D_4.Speed_Class_1 ...
site_data.Obidos_Amazon.CF_02.D_6_30.Speed_Class_1 ...
site_data.Obidos_Amazon.CF_02.D_8.Speed_Class_1 ...
site_data.Obidos_Amazon.CF_02.D_10.Speed_Class_1], ...
'o-', 'LineWidth', 2, 'Color', '[0.34 0.68 0.21]');

%% Thrust Curves

for q=1:length(names_sites)

    name_site=names_sites{q};

    figure(600+q)
    hold all
    grid on
    box on

    xlabel('flow speed [m/s]')
    ylabel('occurence [%]')

    strspl=strsplit(name_site,'_'); % split string

    if length(strspl)==2
        title(['Thrust Curves & Flow Speed Histogram of ', strspl{1}, ...
            ' ', strspl{2}, ' '])

        elseif length(strspl)==3
            title(['Thrust Curves & Flow Speed Histogram of ', strspl{1}, ...
                ' ', strspl{2}, ' ', strspl{3}, ' '])

```

```

        elseif length(strspl)==4
            title(['Thrust Curves & Flow Speed Histogram of ', strspl{1}, ...
                ' ',strspl{2}, ' ', strspl{3}, ' ', strspl{4}, ' '])
        end

        xlim([0 4.1])
        ylim([0 max(site_data.(name_site).hist_data_rsc.counts)+1])

        set(gca, 'YTick', [0:5:max(site_data.(name_site). ...
            hist_data_rsc.counts)]);

        addaxis(Turbines.D_4.Thrust_Curve.x_axis, ...
            Turbines.D_4.Thrust_Curve.y_axis, [0 120], 'linewidth', 2.5, ...
            'Color', '[0.28 0.28 0.28]');

        addaxisplot(Turbines.D_6_30.Thrust_Curve.x_axis, ...
            Turbines.D_6_30.Thrust_Curve.y_axis, 2, 'linewidth', 2.5, 'Color', ...
            '[0.95 0.45 0.33]');

        addaxisplot(Turbines.D_8.Thrust_Curve.x_axis, ...
            Turbines.D_8.Thrust_Curve.y_axis, 2, 'linewidth', 2.5, 'Color', ...
            '[0.89 0.25 0.36]');

        addaxisplot(Turbines.D_10.Thrust_Curve.x_axis, ...
            Turbines.D_10.Thrust_Curve.y_axis, 2, 'linewidth', 2.5, 'Color', ...
            '[0 0.66 0.99]');

        addaxisplot(Turbines.D_10.Thrust_Curve.x_axis, ...
            Turbines.Thrust_Limit, 2, '--', 'linewidth', 2);

        addaxislabel(2, 'Thrust [kN]')

        histogram(site_data.(name_site).SDC, site_data.(name_site). ...
            hist_data_rsc.edges, 'FaceColor', '[0 0.65 0]', 'FaceAlpha', 0.45);

        legend('4m Rotor', '6.30m Rotor', '8m Rotor', '10m Rotor', ...
            'Thrust Limit (drive train)', 'Flow Speed Distribution', ...
            'Location', 'southeast');
    end

    variables.q=q;
    clear q;

%% Thrust Curves for Itacoatiara and Obidos with all combinations of speed
classes and rotor diameters

    figure(650+1)
    hold all
    grid on
    box on

    xlabel('rotor diameter [m]')
    ylabel('Max Occuring Thrust [kN]')

    strspl=strsplit('different_sites','_'); % split string

    if length(strspl)==2
        title(['Max. Thrust over rotor diameter for ', strspl{1}, ...
            ' ', strspl{2}, ' '])

        elseif length(strspl)==3
            title(['Max. Thrust over rotor diameter for ', strspl{1}, ...
                ' ', strspl{2}, ' ', strspl{3}, ' '])

```

```

elseif length(strspl)==4
title(['Max. Thrust over rotor diameter for ',strspl{1}, ...
' ',strspl{2}, ' ',strspl{3}, ' ',strspl{4}, ' '])
end

xlim([3 11])
ylim([0 110])

plot([4 6.30 8 10], [Turbines.D_4.Thrust_Curve.y_axis(1,16) ...
Turbines.D_6_30.Thrust_Curve.y_axis(1,16) ...
Turbines.D_8.Thrust_Curve.y_axis(1,16) ...
Turbines.D_10.Thrust_Curve.y_axis(1,16)], ...
'o-', 'LineWidth', 2.0,'Color', '[0.34 0.68 0.21]');

plot([4 6.30 8 10], [Turbines.D_4.Thrust_Curve.y_axis(1,20) ...
Turbines.D_6_30.Thrust_Curve.y_axis(1,20) ...
Turbines.D_8.Thrust_Curve.y_axis(1,20) ...
Turbines.D_10.Thrust_Curve.y_axis(1,20)], ...
'>-', 'LineWidth', 2.0,'Color', '[0.89 0.25 0.36]');

plot([4 6.30 8 10], [Turbines.D_4.Thrust_Curve.y_axis(1,24) ...
Turbines.D_6_30.Thrust_Curve.y_axis(1,24) ...
Turbines.D_8.Thrust_Curve.y_axis(1,24) ...
Turbines.D_10.Thrust_Curve.y_axis(1,24)], ...
'+-', 'Linewidth', 2.0,'Color', '[0 0.66 0.99]');

plot([0 11], [80 80], '--','linewidth',2, 'Color', 'black');

legend('Itacoatiara, Amazon', 'Sao Paulo de Olivenca, Amazon', ...
'Obidos, Amazon', 'Thrust Limit (drive train)', 'Location', ...
'northwest');

```